EXPLOITING MULTI-CELL TYPE CULTURES TO ELUCIDATE TUMOR CELL FEATURES THAT IMPACT MACROPHAGE PHENOTYPE

APPROVED BY SUPERVISORY COMMITTEE

_____
James Kim, MD, PhD (Chair)

_____
John D. Minna MD

_____
Rolf A. Brekken, PhD

_____
Esra Akbay, PhD

_____
James Malter, MD

_____
Lily Huang, PhD

DEDICATION

I dedicate this to my wife, my love and my family.

이 글은 제 아내, 제 가족, 제 사랑인 박 선혜씨를 위한 것 입니다.

EXPLOITING MULTI-CELL TYPE CULTURES TO ELUCIDATE TUMOR CELL FEATURES THAT IMPACT MACROPHAGE PHENOTYPE

by

JOSIAH MALACHI VOTH PARK

DISSERTATION

Presented to the Faculty of the Graduate School of Biomedical Sciences

The University of Texas Southwestern Medical Center at Dallas

In Partial Fulfillment of the Requirements

For the Degree of

DOCTOR OF PHILOSOPHY

The University of Texas Southwestern Medical Center at Dallas

Dallas, Texas

December, 2021

ACKNOWLEDGEMENTS

I have many people to thank for opening my eyes to a world that few know and even fewer understand. For these people, I thank – for not only their commitment of time and effort – but also for their encouragement, because the truth is that I would not have been able to accomplish any of this without them.

I would like to start off by thanking my family. Emily, I am so thankful to have met you during graduate school and now we have a whole life planned together. You have been by my side from almost day one of graduate school. We have spent so many late nights together studying for exams, cramming from journal clubs, and practicing presentations. You have been my confidant and guidance counseling in frustrating times due to bad experimental results or lab environmental issues. Also, by my side from day one and since the beginning of time has been my parents and my siblings. While they had little understanding of what I do, they would ask endless questions about my work. They provided me an escape from everything, being able to go home to the comfort of my family, eat good food, play some video games, and go fishing with Dad. This was the perfect relief from undergrad and graduate studies. My entire family – immediate and extended – have all been my biggest cheerleaders. They constantly support and build me up, and all these actions were desperately needed throughout graduate school.

Second, I would like to thank several important people from The University of Oklahoma. Dr. Gordon taught Introduction to Human Anatomy, a class I took my sophomore year. This was one of the hardest but most exciting classes I have ever taken. Dr. Gordon and I would perform crazy dissections to show off the human body (and she would use this time to talk about her polka group). Dr. Gordon is a great mentor, and I will forever be grateful for her sarcasm and love for teaching. Dr. Sims was my Introduction to Biochemistry professor. Dr. Sims has such an explosive love for biochemistry; it can't help but draw in his students. He taught me to love science and helped me understand that what I truly desired was, not to practice medicine, but to understand it. So naturally I tried to spend as much time with the man that knew everything

about mechanisms of action for medicines. Dr. Sims taught me chemical structure synthesis techniques, DNA ligations, maxi preps, coomassie staining, and x-ray crystallography. He laid the foundations for bench science, which undoubtedly helped get me into graduate school. The final person I would like to thank from OU is the Humphrey Lab. I spent about a 1.5 years in Dr. Humphry's lab. I learned a lot about mice and more about signal transduction pathway signaling, developing a love for macrophages, which evidently became the primary focus of my thesis. She challenged me to be a better scientist and helped me navigate politically through hostile environments. To these professors and many more, I would not be where I am today without you, and I cannot thank you enough.

I would not be able to write this thesis without the help of two groups of people: the Minna and Brekken Laboratories. Due to unforeseen events, I had to change my rotation of choice to Dr. Minna's lab in late 2016, but as expected, the Minna lab is very good at quickly putting together ideas and accommodations, per the request of Dr. Minna. It turned out to be the most influential five weeks of my graduate career. I was placed under Dr. Mike Peyton and Paul Yenerall (now Dr. Yenerall), and both these men taught me techniques that I now use every day: tissue culture, virus packaging, CRISPR, qPCR. You name it; they probably taught me the technique. Both continued to support me through experimental details, reading countless reports and providing playful banter at work. The daily nuances of talking to Kim about family, practicing Korean with Hyunsil and Dr. Long Shan, discussing Indian restaurants with Amit, getting cell lines from Dr. Boning, or trash talking the Longhorns to Dr. Huffman: all these experiences made working in the Minna lab fun and enjoyable. Thank you all for being such a great support.

The Brekken lab is so good at being in the trenches of science. If I ever had issues with an assay, they were there to help me. Dr. Huocong and his infinite knowledge about troubleshooting helped me navigate many experiments. Of course, this help didn't come without a load of sarcasm as well. Dr. Du and Dr. Burton both always provided great advice and helped

me navigate some tough situations. My fellow soldiers – Yuqing, Emily, and Debolina – you all have been great to be in the trenches with, and I appreciate the ability to vent about grad school. Jason, this guy is awesome. If I needed help finding something or doing *In vivo* work, this guy was always there and always did an outstanding job.

This pretty much goes without saying so I will keep it brief. There are two people who I spent the most time with in lab: the first Aiden Nguyen. We shared a bay together. (That says a lot.) This guy has been a great resource for information and a great friend. I wish you luck in your next steps in life. The second is Dr. Raghav Chandra. We did everything together (of course, 6-feet apart from each other due to the pandemic). You will not find someone with more drive and determination than this man. Dr. Chandra is explosively positive about everything, regardless of how tough things get. It was great to finish-up my project with such a great student and friend.

I have been very privileged to have such great world renowned mentors. Aside from the science, I learned from Dr. Minna the art of collaboration and negotiation. Dr. Minna is great at out of the box ideas and dreaming big. These principles are reflected throughout my thesis work and dictate how I approach science. Dr. Brekken has been a science father figure so to speak, he taught me so much about how to approach and be critical of science. He has personally worked with me to improve my writing and presentation skills. In addition to this, he always had an open door policy so I could come ask for personal advice. From day one Dr. Brekken and I have always had a blunt and honest relationship, which I have always appreciated. I am forever grateful for the time, money and effort both these men invested in me.

Finally, I need to reiterate the most important factor in my graduate career: Emily I started this acknowledgement with her, and I must end with her. Here's why: those of you who have a graduate degree understand the psychological and physical stress that graduate studies put on you. I felt that immense weight, yet Emily was and is my rock. When I was falling apart, she was there to patch me up and push me to finish. I am eternally grateful.

DEVELOPMENT OF MULTI-CELL TYPE CULTURES FOR PRECLINICAL THERAPEUTICS IDENTIFIED TO REPOLARIZE MACROPHAGES

JOSIAH M. VOTH PARK, PhD

The University of Texas Southwestern Medical Center at Dallas, 2021

John D. Minna, MD and Rolf A. Brekken, PhD

Lung cancer is expected to kill ~150,000 people this year, encompassing 25% of all cancer related deaths making lung cancer the leading cause of cancer-related mortality in men and women. Lung cancer is divided into non-small cell lung cancer (NSCLC) and small cell lung cancer (SCLC) which represent 80-85% and 15-20% of cases, respectively. My dissertation project focused on understanding how to model the interactions between lung cancer cells, fibroblasts and immune cells. Immune cells are critical components of the tumor microenvironment (TME) that contribute to tumorigenesis, angiogenesis and metastasis. Macrophages are key regulators of the immune landscape within the TME. The plasticity of macrophage phenotypes in the TME correlates with prognosis of NSCLC. Depending on their phenotype, macrophages in the TME can secrete pro-tumor cytokines and chemokines, ultimately suppressing the function of anti-tumor immune cells in the TME. The purpose of my project was to investigate if and how NSCLC cells alter macrophage phenotype in multi-cellular co-cultures and to relate effects on macrophages to the molecular characteristics of different

NSCLCs. The central hypothesis of the project is, tumor cell characteristics drive macrophage polarization in the TME, and this can be captured using a multicellular co-culture model. Given the central importance of macrophages to the TME and the immune landscape of NSCLC, an understanding of the tumor cell characteristics associated with immune suppressive or immune stimulatory macrophage phenotype could be exploited from a therapy perspective in the future. To address this hypothesis, an *in vitro* co-culture system (NSCLC tumor cells, human cancer associated fibroblasts (CAFs), and mouse macrophages) was developed to interrogate cancer cell features driving heterogeneity of macrophage phenotypes across a panel of NSCLCs. We measured: mRNA expression in mouse macrophages with a panel of qPCR probes for genes associated with distinct macrophage phenotypes (*Arg1*, *iNOS*, *Il-1β*, *Il-6*, *Ym-1*, *Socs3*). This system was validated by comparison of macrophage phenotypes represented in the TME of lung cancer xenografts grown in athymic nude mice. Using our platform, we evaluated ~80 NSCLC patient derived lines for their effect on mouse macrophage phenotype. We identified three main macrophage phenotypes across this panel of NSCLCs. To identify cancer cell biomarkers for macrophage polarization, we interrogated molecular characteristics of the cancer lines. Additionally, we expanded the functionality of the platform to assess the effects of pharmacologic agents on macrophage phenotype. As a proof of principle, a small panel of known immune stimulating compounds was tested in the *in vitro* co-culture platform and validated in human tumor xenografts. Finally, we identified a few novel compounds that show selective cancer cell toxicity and reprogram macrophage phenotype. In conclusion, we built a reproducible *in vitro* platform to interrogate macrophage polarization in the TME. We leveraged this platform to identify three dominant macrophage phenotypes induced by NSCLC cells and CAFs. We found that no cancer cell molecular characteristic alone drives macrophage polarization. Finally, we illustrate the significance of this platform for immune stimulating drug identification; we identified two novel chemicals that repolarize macrophages and kill cancer cells simultaneously.

Table of Contents

Prior Publications

1. Chandra R, Karalis JD, Liu C, et al. *The Colorectal Cancer Tumor Microenvironment and Its Impact on Liver and Lung Metastasis.* Cancers 2021;13.
2. Flaming, J., et al., *Abstract PO021: Lung cancer cells and cancer-associated fibroblasts drive macrophage polarization in a co-culture model.* Cancer Immunology Research, 2021. **9**(2 Supplement): p. PO021.
3. Flaming, J., et al., *Abstract 746 Non small-cell lung cancer cells and cancer-associated fibroblasts drive macrophage polarization in a novel co-culture model.* Journal for ImmunoTherapy of Cancer, 2020. **8**: p. A447-A448.
4. Flaming, J., et al., *Abstract B31 Development of multicell type organoid cultures for preclinical studies of immunotherapeutics for lung cancer.* AACR-IASLC, 2021.
5. Yenerall, P., et al., *RUVBL1/RUVBL2 ATPase Activity Drives PAQosome Maturation, DNA Replication and Radioresistance in Lung Cancer.* Cell Chemical Biology, 2020. **27**(1): p. 105-121.e14.
6. Kalaitzoglou, E., et al., *TLR4 Promotes and DAP12 Limits Obesity-Induced Osteoarthritis in Aged Female Mice.* JBMR plus, 2018. **3**(4): p. e10079-e10079.

List of Figures

List of Tables

List of Abbreviations

Small-cell lung cancer (SCLC)

Non-small cell lung cancer (NSCLC)

Tumor protein 53 (TP53 or p53)

Retinoblastoma protein 1 (RB1)

Kirsten rat sarcoma viral oncogene homolog (KRAS)

Epidermal growth factor receptor (EGFR)

B-Raf proto-oncogene (BRAF)

Anaplastic lymphoma kinase (ALK)

RET proto-oncogene (RET)

Cyclin Dependent Kinase Inhibitor 2A (CDKN2A)

Tyrosine kinase inhibitors (TKIs)

Mechanistic target of rapamycin (mTOR)

Mitogen-activated protein kinase (MAPK)

Echinoderm microtubule-associated protein-like 4 (EML4)

Serine/threonine kinase 11 (*STK11*/*LKB1*)

Antigen-presenting cells (APCs)

Major histocompatibility complex (MHC)

T-cell receptor (TCR)

Interleukin (IL)

Interferon-gamma (IFN-γ)

Pattern recognition receptors (PPRs)

Dendritic cells (DCs)

Macrophage colony-stimulating factor (CSF-1)

Lipopolysaccharides (LPS)

Tumor necrosis factor (TNF)

Janus kinases (JAK)

Signal transducer and activator of transcription (STAT)

Toll-like receptor (TLR)

Suppressor of cytokine signaling (SOCS)

Nuclear factor of kappa light polypeptide gene enhancer in B-cells (NFκβ)

Transforming growth factor beta (TGF-β)

Nitric oxide synthase 2 (NOS2)

Arginase (ARG, Arg1)

Mannose receptor 1 (MRC1)

Esistin-like alpha (Retnla)

Chitinase-like protein 3 (Ym1)

Tumor-associated macrophages (TAMs)

Immune Checkpoint Inhibitors (ICIs)

Hypoxia-inducible factor 1α (HIF-1α)

Metalloproteinases (MMPs)

Chemokine (C-C motif) ligand 2/Monocyte chemoattractant protein 1 (CCL2/MCP-1)

Programmed cell death 1 (PD-1)

Programmed death-ligand 1 (PD-L1)

Tumor microenvironment (TME)

Cancer-associated fibroblasts (CAFs)

Cytotoxic T-lymphocyte-associated protein 4 (CTLA4)

Lymphocyte-activation gene 3 (LAG3)

T cell immunoglobulin and mucin domain-containing protein 3 (TIM3)

T cell immunoglobulin and ITIM domain (TIGIT)

B- and T-lymphocyte attenuator (BTLA)

Tyrosine-based switch motif (ITSM)

National Cancer Institute (NCI)

HCC (Hamon Cancer Center at UT Southwestern)

American Type Culture Collection (ATCC)

Short tandem repeat (STR)

Bone marrow-derived monocytes (BMDMs)

Polymerase chain reaction (qPCR)

The Cancer Genome Atlas (TCGA)

Gene set Enrichment Analysis (GSEA)

Mitoxantrone (Mito)

Immunohistochemistry (IHC)

Human Bronchial Epithelial cells (HBECs)

Human Small Airway Epithelial cells (HSEACs)

Cyclin dependent kinase 4 (CDK4)

Human Telomerase reverse transcriptase (hTERT)

Microsatallite instability (MSI)

Interleukin-4 receptor-α (lL-4rα)

C-C Chemokine receptor type (CCR)

Chermerin Chemokine-Like Receptor 1 (CMKLR1)

Extracellular-matrix (ECM)

Inflammatory CAFs (iCAFs)

Myofibroblastic CAFs (myCAFs)

Granulocyte colony-stimulating factor (G-CSF)

Platelet derived growth factor receptor-alpha (PDGFRα)

Granulocyte-macrophage colony-stimulating factor (GM-CSF)

A-smooth muscle actin (α-SMA)

Epithelial cadherins (E-cadherins)

Epithelial-to-mesenchymal transition (EMT)

NSCLC with neuroendocrine features (NSCLC-NE)

Immunogenic cell death (ICD)

Microorganism-associated molecular patterns (MAMPS)

Damage-associated molecular patterns (DAMPS)

Precision oncology probe set (POPS)

Chapter 1: Introduction

1.1 History of lung cancer

Lung cancer was once considered an oddity. It was not until the 18th century that 140 cases of lung cancer were published in a medical journal [5]. German research clinics subsequently devoted extensive resources to the study of this disease. Then, in the 19th century, Hermann Rottmann suggested that tobacco dust was causing lung cancer in German tobacco workers [6]. By that time, tobacco companies had popularized smoking. In 1912, lung carcinogenesis was linked to smoking [7]. Finally, in 1964, the United States Surgeon General declared that smoking causes lung cancer [8]. Despite this declaration of war on tobacco, 6.5 trillion cigarettes are sold each year, which equates to 18 billion cigarettes purchased daily [9]. To combat this, numerous organizations and government agencies have launched initiatives and legislation to educate the public about the deleterious effects of smoking. This has reduced the incidence of lung cancer and related deaths in high-risk populations and minors. Despite these advances, lung cancer remains the leading cause of cancer-related deaths, accounting for ~1.9 million deaths in 2017 [10]. Treatment of lung cancer is challenging and the disease is only curable when treated at early stages. However, most patients are diagnosed at an advanced stage, when the tumor is refractory to traditional chemotherapy. Moreover, the heterogeneity of lung cancer makes its treatment particularly difficult.

1.2 Divisions, types, and classes of lung cancer

Lung cancer is divided into two main subtypes based on histological features and prognostic and therapeutic implications. The first subtype is small-cell lung cancer (SCLC), which represents roughly 15% of all lung cancers and accounts for 30,000 deaths annually in the USA [11]. The vast majority (95%) of patients with SCLC have strong histories of smoke exposure [12]. SCLC is believed to originate from neuroendocrine stem cells within the central airways. These tumors are highly proliferative and commonly have *TP53* and *RB1* mutations

[13]. The second subtype of lung cancer is non-small-cell carcinoma (NSCLC), which accounts for approximately 85% of all lung cancers. The distinction between SCLC and NSCLC is based on histology. With advancements in the molecular characterization and profiling, distinct subtypes of NSCLC have been identified [14-16]. NSCLC cells are larger in size and their mutational burden is considerably more diverse [17] than SCLC cells. Among NSCLC, adenocarcinomas represent ~39% of tumors, while squamous cell carcinomas represent nearly 30% [16, 18]. Adenocarcinomas are typically located in the periphery of the lung, have diverse histological features and can be aggressive in terms of disease progression [19, 20]. More importantly, adenocarcinomas present a diverse mutational burden including mutations in *TP53*, *KRAS*, *EGFR*, *BRAF*, *ALK*, *RET*, and *RB1* [21]. Squamous cell carcinomas are usually found more centrally and originate from the mainstem or lobar bronchi [22]. Squamous cell carcinomas usually exhibit keratinization and inactivating mutations in *TP53* and cyclin dependent kinase inhibitor 2A (*CDKN2A*) [23]. Other classes, such as large-cell lung carcinoma, salivary gland–type tumors, and sarcomatoid carcinomas, represent a small fraction of NSCLC cases [22]. Improvements in molecular techniques have allowed in-depth characterization of oncogenes and tumor suppressors and the development of treatment regimen decisions based on molecular oncogenotype (Figure 1) [24].

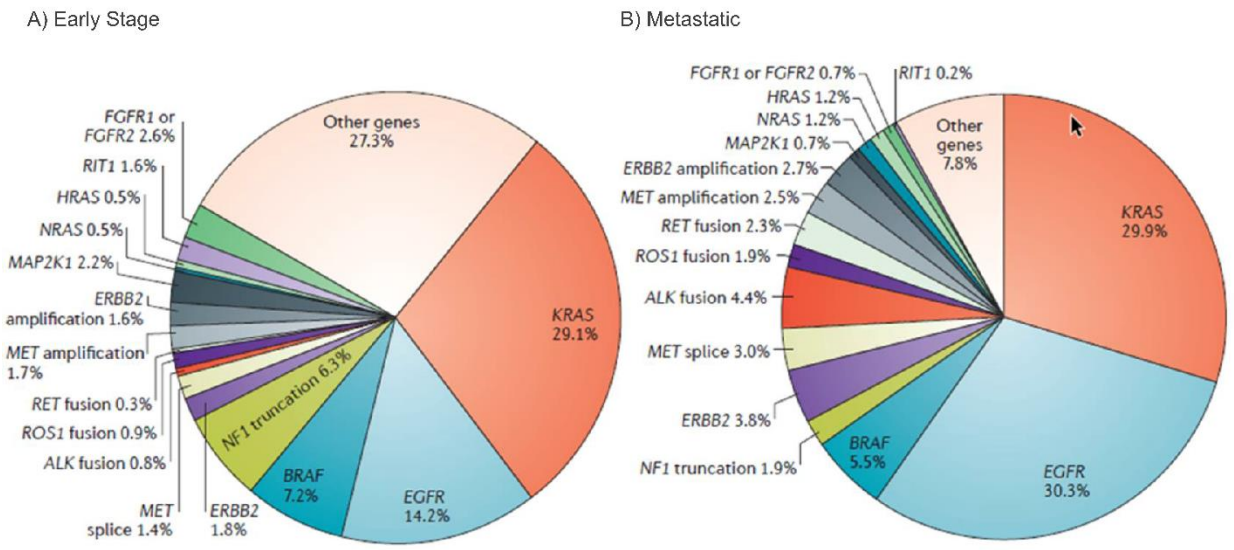

Figure 1: Single oncogenic driver paradigm of lung adenocarcinoma molecular classification. Meta-analysis of genetic alterations most commonly found in lung adenocarcinomas based on status: A) Early-stage, B) Metastatic. Early-stage tumor data were retrieved from the Pan-Cancer Atlas cohort of The Cancer Genome Atlas (TCGA; n = 566) and Kadara et al. (n = 108) [25-29]. Metastatic data were obtained from the MSK-IMPACT and FoundationOne data sets [30, 31]. Figure taken from Skoulidis et al. [24].

1.3 Chemotherapy and precision medicine

Until the 1960s, NSCLC was considered chemoresistant. Therefore, the only options were surgical resection and, in some cases, radiation therapy. For patients with metastatic disease, the only available option was supportive care. Many clinical trials tested novel cytotoxic agents or chemotherapy combinations, but the results were poor, and toxicity was significant—even debilitating [32-36]. In the late 1970s, cisplatin, a newly developed drug, showed promise for advanced-stage disease [37-40]. Furthermore, combining cisplatin with radiation therapy produced response rates of 50–60% [41-44]. These groundbreaking findings galvanized clinicians and researchers and catalyzed an exponential increase in NSCLC-based research. In

the 1980s, cisplatin was combined with alkylating agents, anthracyclines, or vinca alkaloids. Eventually, it was rivaled by its analogue, carboplatin, which was associated with fewer toxic side effects [45]. Later, taxanes (paclitaxel and docetaxel) were used in combination with carboplatin or cisplatin. By the end of the 1990s, numerous types of chemotherapy had been tested clinically in combination with cisplatin or carboplatin [45]. Today, these chemotherapies are still used as major staples in treatment regimens for NSCLC. At the beginning of the 21st century, precision medicine emerged, with the clinical use of oncogene-targeted therapies.

Oncogenes are mutated versions of a group of driver genes called proto-oncogenes that contribute to carcinogenesis. Oncogenes often encode proteins participating in cellular pathways that regulate cell division and growth. Oncogenes typically harbor gain-of-function mutations that confer new activities to the respective proteins.

Tumor suppressor genes suppress tumor development and often undergo loss-of-function mutations that facilitate uncontrolled cell growth. Most patients have a combination of oncogene and tumor suppressor mutations [46].

The most common oncogene found in NSCLC is Kirsten rat sarcoma viral oncogene homolog (*KRAS*). *KRAS* mutants represent roughly 25% of all NSCLCs and are associated with increased RAS/MAPK signaling [47]. Mutant *KRAS* has proven particularly difficult to target directly. Therefore, clinical efforts to inhibit KRAS driven signaling have focused on inhibiting targets upstream or downstream of KRAS. Tyrosine kinase inhibitors (TKIs), MEK inhibitors, and RAS/RAF inhibitors have been used in combination with chemotherapy to treat *KRAS*-mutant tumors. Combinations of docetaxel with selumetinib (MEK inhibitor) or sorafinib (RAS/RAF inhibitor) have shown promising results [48-50]. However, patients with *KRAS*-mutant tumors typically respond poorly to epidermal growth factor receptor (*EGFR*) TKIs [51-53].

Mutation of *EGFR* is the second most common oncogenic alteration in NSCLC. Active EGFR stimulates mechanistic target of rapamycin (mTOR) and mitogen-activated protein kinase

(MAPK) signaling pathways [51, 54]. *EGFR* is usually mutated in exon 19 or exon 21, leading to overexpression, amplification and activation of the receptor [51]. Erlotinib (an *EGFR*-TKI) was one of the first targeted therapies approved and remains a mainline therapy for *EGFR*-mutant NSCLC. It is a reversible *EGFR* inhibitor, as is gefitinib, which was developed soon after erlotinib. Roughly 55–78% of *EGFR*-mutant NSCLC patients respond to these therapies [55]. Resistance is commonly acquired through a new mutation (T790M) [54]. Since the identification of these compensatory mechanisms, second- and third-generation *EGFR*-TKIs have been developed and introduced to clinical practice. Osimertinib, a third generation EGFR TKI approved in 2015, is the most effective EGFR-TKI therapy for T790M mutant tumors. However, resistance to these later generation therapies is also seen.

Anaplastic lymphoma kinase (*ALK*) alterations are the third most common oncogenic driver mutations in NSCLC. The *ALK* gene is rearranged in fusion with the echinoderm microtubule-associated protein-like 4 (*EML4*) gene [51]. This fusion, which encodes a cytoplasmic chimeric protein with constitutive kinase activity, occurs in roughly 7% of NSCLCs [56]. Between 57% and 74% of *ALK*-fusion NSCLC patients respond to crizotinib, an *ALK* inhibitor [57]. Most patients develop resistance to first-line *ALK*-targeted therapy [57-60]. For this reason, clinical trials investigating second-generation *ALK* inhibitors are underway [60].

B-Raf proto-oncogene (*BRAF*) mutations are also commonly identified in NSCLC. These mutations lead to MEK hyperphosphorylation, which promotes cell growth, proliferation, and survival. NSCLC patients with *BRAF*V600E mutations respond poorly to platinum-based chemotherapies [61]. Selective *BRAF* inhibitors vemurafenib and dabrafenib have yielded sizable responses in NSCLC patients harboring the V600E mutation (33% and 42%, respectively) [62, 63]. Clinical trials are currently evaluating the effectiveness of other *BRAF* and MEK pathway inhibitors against *BRAF*-mutant NSCLC patients.

Tumor suppressors are as vital to carcinogenesis as oncogenes. The most common tumor suppressor mutated in NSCLC is *TP53*. Transcription factor p53 (*TP53*) is responsible for

cell cycle checkpoint and cell death responses to DNA damage [64]. When this protein is inactivated, these pathways are dysregulated, and cells evade apoptosis. Roughly 88% of lung cancers harbor a mutation in TP53 [65]. The second most commonly mutated tumor suppressor is Retinoblastoma protein 1 (*RB1*). Like *TP53*, it is a negative regulator of the cell cycle. Inactivation of *RB1* through mutations, deletions, or epigenetic silencing leads to bypassing of the cell cycle G0 checkpoint [66]. *RB1* mutants represent ~20% of lung cancers, and more specifically a large portion of SCLC patients [67]. Another significant tumor suppressor that is mutated in NSCLC is serine/threonine kinase 11 (*STK11*/*LKB1*), which is mutated in ~30% of lung cancers [68]. The STK11 protein is important in the regulation of cellular metabolism and protein synthesis [68-72]. Very few therapeutic approaches to reversing tumor suppressor mutations are currently available.

The course of treatment for NSCLC patients depends on several factors: tumor staging, tumor location, patient health performance status, histological subtype, and molecular characteristics of the tumor. For early-stage patients without metastatic disease, surgical removal of the tumor offers the best chance of survival. When surgery is not an option, radiation can produce the highest cure rates [73]. Late-stage and metastatic patients receive chemotherapy alone or combined with an appropriate targeted therapy, depending on the molecular characteristics of the tumor (e.g., *KRAS*, *EGFR*, or *ALK*). Despite these advancements, surgery and radiation remain the only curative measures for lung cancer patients. In recent years, attempts have been made to leverage the immune system to target tumors.

1.4 Immunotherapies

Antibody therapy has its roots in ancient China. Serum from animals containing antibodies has been used to treat humans with toxins or viruses. In the late 1990s, rituximab was the first antibody approved as a cancer therapeutic (anti-CD20; Non-Hodgkin’s lymphoma).

Antibodies such as bevacizumab (anti-VEGF), cetuximab (anti-EGFR), and trastuzumab (anti-HER2) have now become staples of cancer therapeutics.

The advancements in antibody-based therapies have led drug discovery to the next generation of therapeutics: immunotherapies. Immune-targeting therapies use monoclonal antibodies to block the inhibition mechanisms used by cancer cells to silence the immune system. More specifically, immune checkpoint blockade therapies have significantly impacted the treatment of cancer. In 1991, cytotoxic T-lymphocyte-associated protein 4 (CTLA4) was identified as a negative regulator of T cell activation. In 1992, programmed cell death 1 (PD-1) was identified as a negative regulator of immune responses [74]. In 2001, it was shown that cancer cells express the appropriate ligands to activate these receptors [75]. These discoveries have led to new strategies for treating cancer. As of 2020, 32 different immunotherapies have been approved for cancer patients. These therapeutics are designed to block the inhibitory interactions between cancer cells and adaptive immune cells and are being used in combination with other standards of care (Figure 2).

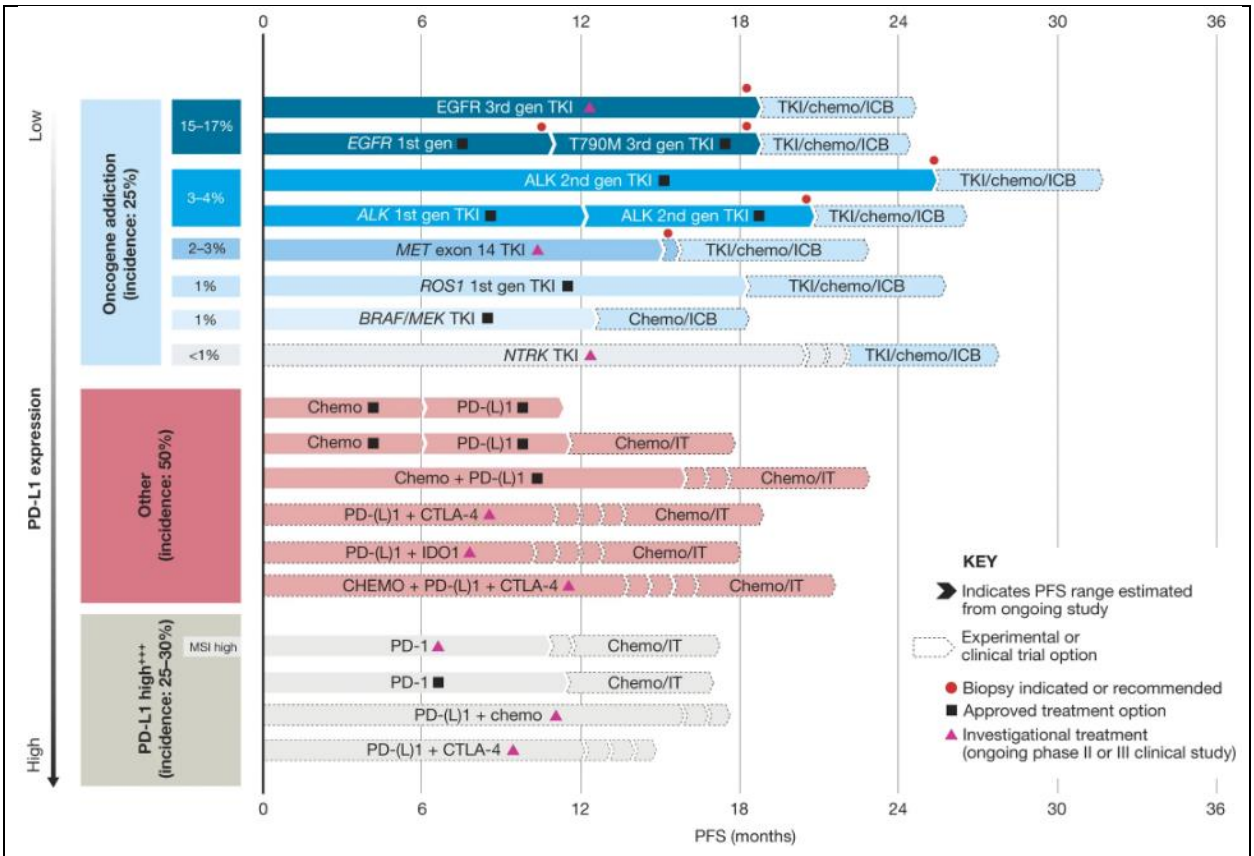

Figure 2: Therapeutics currently used for advanced or metastatic non-small-cell lung carcinoma, their correlations with PD-L1 expression, and associated progression-free survival. PD-L1 expression is used to predict patient response to an immune checkpoint blockade, although it has been found to be a poor predictor. Patients with no or low (<1%) expression are treated with tyrosine kinase inhibitors corresponding to their genomic alterations. Patients with >1% expression are treated with combination therapies that include immune checkpoint blockades. Figure taken from Herbst, et al. [76].

The interplay between the cancer cells, its stromal microenvironment and immune cells modulate tumor progression. Cancer cells can use ligands for immunoreceptors to regulate T cell activity. Studies have identified a series of receptors on cancer cells that can mitigate T cell activity: PD-1, CTLA4, lymphocyte-activation gene 3 (LAG3), T cell immunoglobulin and mucin

domain-containing protein 3 (TIM3), T cell immunoglobulin and ITIM domain (TIGIT), and B- and T-lymphocyte attenuator (BTLA).

PD-L1, the ligand for PD-1 on T cells, can be expressed on tumor cells or on stromal cells, largely myeloid cells, in the TME. PD-L1 can also be found on extracellular vesicles secreted from cells in the TME [77, 78]. Once PD-1 is activated, the immunoreceptor tyrosine-based switch motif (ITSM) is phosphorylated, causing SHP2 sequestration and CD28 inhibition, which leads to the suppression of the PI3K-AKT pathway (cell proliferation) and T-cell receptor (TCR) signaling [79]. Alternatively, T cells can be suppressed through the activation of CTLA-4 by CD80 and CD86 ligands [80] that are expressed on innate immune cells and cancer cells. T cells expressing CTLA4 (Tregs) downregulate the expression of CD80 and CD86 on innate cells and inhibit CD28, which suppresses T cell proliferation [81, 82]. Another checkpoint on T cells is LAG3. T cells are activated by the interaction between CD4 and major histocompatibility complex (MHC) II. However, LAG3 has a higher affinity for MHC II and therefore competes with CD4 binding, thereby preventing T cell activation [83, 84]. TIM3-directed T cell suppression is still under investigation. BTLA suppresses TCR and CD28 signaling [85], and TIGIT suppresses T cells indirectly by increasing interleukin (IL) -10 secretion by natural killer cells [86]. A summation of the ligand-receptor inhibitor and stimulatory interactions between cancer cells, antigen presenting cells (APCs) and T cells is presented below (Figure 3).

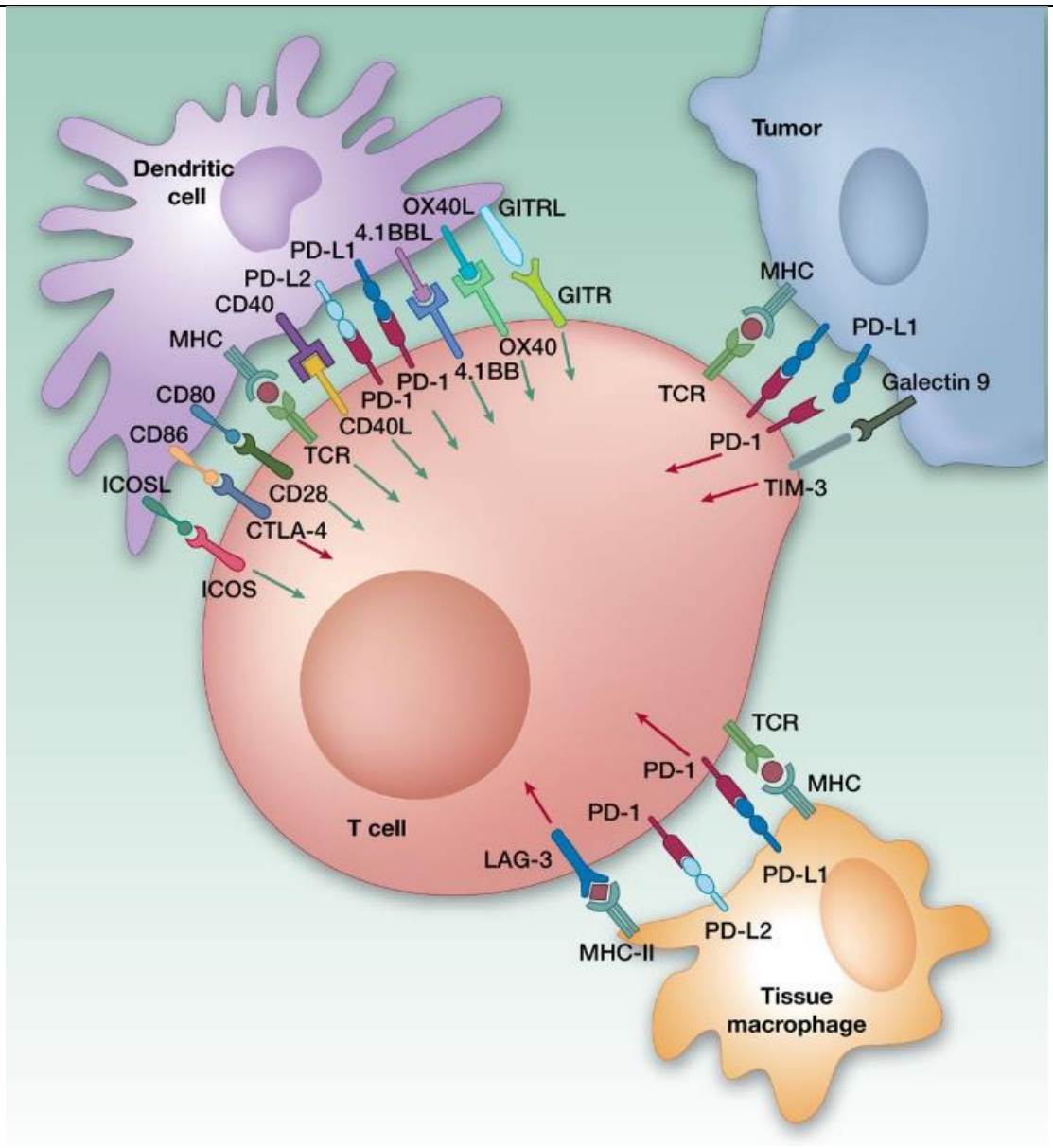

Figure 3: Co-stimulatory and co-inhibitory receptor–ligand interactions between T cells, dendritic cells, cancer cells and macrophages. The green arrows represent cell–cell activation. The red bars represent cell–cell inhibition. This figure illustrates the major receptor–ligand cell–cell pathways of T cell regulation currently known. However, extensive studies in this field are rapidly expanding our knowledge and understanding of such interactions (OriGene poster).

To counteract cancer-driven T cell suppression, immune checkpoint inhibitors (ICIs) are currently used. Lung cancer patients have benefited from these advancements. In the CheckMate 057 study, previously treated non-squamous NSCLC patients treated with nivolumab (PD-1 inhibitor) showed better overall survival than patients treated with docetaxel (12.2 and 9.4 months, respectively; p = 0.002) [87]. In the KEYNOTE-010 trial, overall survival was significantly better with pembrolizumab (PD-L1 inhibitor) than with docetaxel (10.4 and 8.5 months, respectively; p = 0.0008) [14] in the second line setting. Other studies have investigated an array of PD-1, PD-L1, and CTLA4 inhibitors, demonstrating a clinical benefit for a subset of NSCLC patients treated with ICIs (~20%) [14, 87, 88]. Due to these results, PD-1/PD-L1 inhibitors have become the new first- and second-line therapies for NSCLC patients [89-91]. However, it is poorly understood why only a subset of patients respond to PD-1/PD-L1 blockade. PD-L1 expression is currently used as a biomarker for predicting therapeutic effects. However, these are not reliable biomarkers [92]. For this reason, studies have investigated the correlation between immune checkpoint inhibitors (ICIs) response rates and oncogenic driver mutations. Concurrent *KRAS*/*STK11* mutations are less likely to respond to checkpoint blockade therapies [93, 94]. Additionally, studies have shown two main T cell features that contribute to resistance to PD1/PD-L1 blockade: inadequate T cell infiltration due to lack of recruitment by APC cells and T cell exclusion by cancer cells. This argues the importance of innate immune cell phenotype in the TME for response to ICIs. However, these areas are still being investigated. Meanwhile, searching for therapeutics with better predictability is warranted.

Research on the suppression of immune cells by immune checkpoints in the TME is now shifting toward identifying mechanisms of innate immune suppression. New screening platforms focused on the interactions between cancer and innate cells are being tested. Some have tried cytokine-based assays, such as conditioned media strategies [95] and transwell assays [96]. Others have tried co-cultures so that the cells can use cell-cell junctions for communication;

however, these methods are limited to only two cell types at a time [97]. My research focuses on resolving this issue.

1.5 The tumor microenvironment

The TME is composed of malignant and non-transformed cells [98-100]. Cancer cells use extracellular signals to recruit and manipulate epithelial cells, fibroblasts, and immune cells. These extracellular signals include growth factors, extracellular matrix (ECM) remodeling enzymes, and cytokines and chemokines acting through autocrine, paracrine, and endocrine signaling. These signaling molecules influence, angiogenesis, lymphatics, ECM remodeling, and immune evasion. As mentioned above, the TME exhibits a unique and complicated extracellular milieu which have multifaceted functions and pathways that promote tumorigenesis and metastasis. Each extracellular signal can stimulate cell types in different ways, resulting in different processes. Here I will primarily focus on cancer-associated fibroblasts (CAFs), macrophages, and adaptive immune cells. A summary of the interactions between these cell types and the influenced pathways is presented in Figure 4 [99].

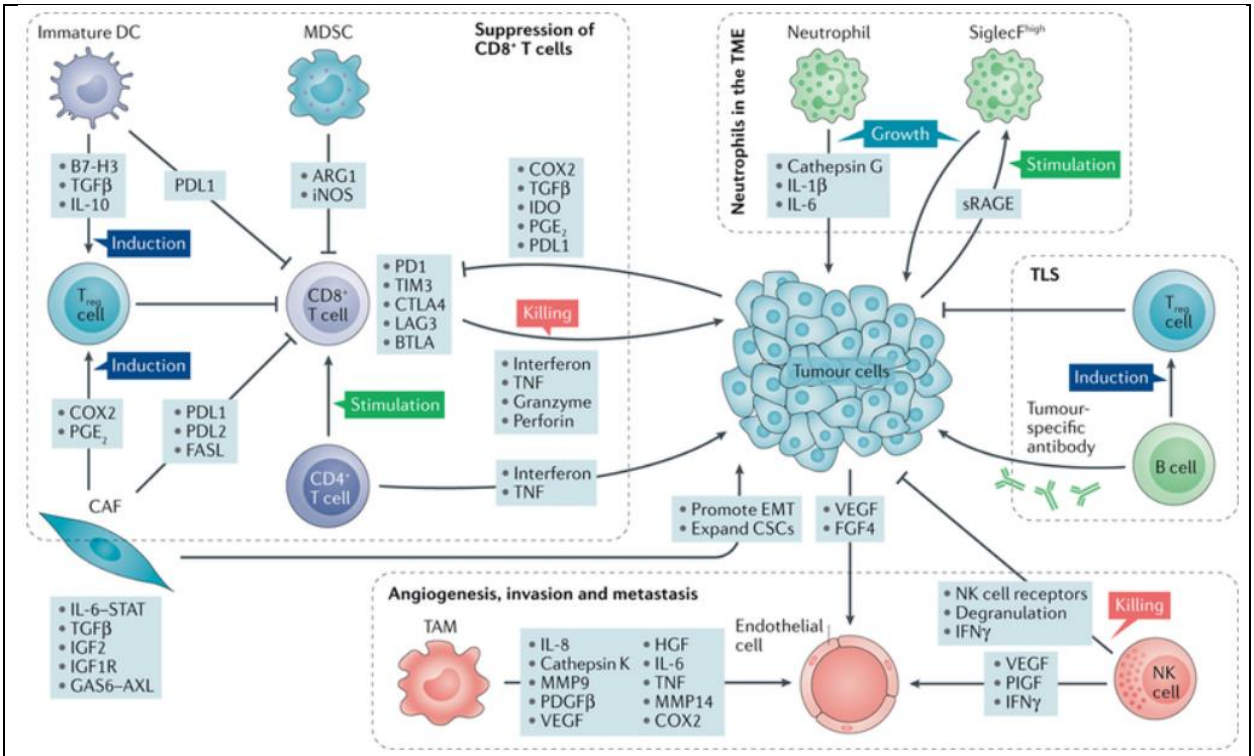

Figure 4: The heterogeneous microenvironment of lung cancer. Lung cancer has a diverse immune composition within the tumor microenvironment. The absence of CD8 cytotoxic T cells and the presence of regulatory T cells are at the cornerstone of tumor immunology. Dendritic cells produce TGF-β, which promotes the regulatory T cell population. Additionally, macrophages suppress T cell activation by reducing L-arginine. Moreover, both dendritic cells and macrophages can suppress activated macrophages by ligand–receptor interactions. Furthermore, neutrophils, natural killer cells, and fibroblasts secrete cytokines, promoting epithelial–mesenchymal transition and angiogenesis. Figure taken from Altorki, et al. [99]

The TME recruits immune-suppressive dendritic cells (DCs) to suppress T cells with the presentation of co-inhibitory molecules [101]. CAFs and DCs secrete TGF-β, which differentiates T cells into regulatory T cells [102, 103]. CAFs also secrete significant amounts of epidermal growth factor (EGF) family proteins, which promote cancer growth and survival, as

well as cytokines CXCL12 and IL-6, which promote cell migration and tumor associated macrophage (TAM) polarization [104-106]. T cells suppressed by DCs secrete considerable amounts of IL-4, IL-5, and IL-13 (which leads to macrophage M2 polarization) [107, 108]. Suppressed T cells also secrete cytokines that promote tumor progression. Furthermore, they can induce a regulatory B cell response, which acts as positive feedback, suppressing T cell–meditated killing and upregulation of IL-10 (which can promote a macrophage M2 phenotype) [107, 109, 110]. These processes result in suppressive macrophage phenotype typically being dominant in the TME. The pathways that TAMs influence to promote tumor growth, angiogenesis, and hypoxia—and ultimately metastasis—are detailed below.

Hypoxia is a condition of low oxygen levels in tissues. In lung cancer hypoxia drives VEGF expression, which enhances M2-like macrophage recruitment and immune suppressive functions of myeloid cells [111-113]. Endothelial cells and macrophages secrete VEGF family proteins, which increase lymphatic vessel sprouting in the TME, providing tumor cells a means for escape [114-116]. To create an escape path for tumor cells, the ECM is broken down and made more elastic. Tumors are stiff, but macrophages and fibroblasts secrete matrix metalloproteinases (MMPs), which degrade the ECM [117-119] in a positive feedback process that promotes angiogenesis [120]. To counteract these processes, many targeted therapies have been created to target specific communication proteins. Macrophages are a critical component to the TME and cancer progression. Therefore, understanding mechanisms of macrophage polarization is paramount.

1.6 Macrophages

Macrophages originate from myeloid progenitor cells. More specifically, hematopoietic stem cells give rise to monocytes in bone marrow. Monocytes then move into the blood and circulate throughout the body until they are recruited to tissues. In the event of an infection or cancer, soluble proteins are used to attract monocytes to the site. Once monocytes enter the

tissue, they differentiate as a result of local signals [121]. Tumors secrete copious amounts of chemokine (C-C motif) ligand 2 and macrophage colony-stimulating factor (MCSF-1/CSF-1) to attract monocytes and induce macrophage differentiation [122]. Macrophages are abundant in most organs, where they control metabolic homeostasis, wound healing, and tissue remodeling [123, 124]. They have glucose- and lipid-sensing receptors that allow them to detect tissue over-nourishment, which changes the macrophage phenotype, resulting in inflammation-induced insulin resistance [124, 125]. Neutrophils respond to bacteria and foreign debris infiltrating open wounds, eventually dying. Macrophages are recruited to the wound to phagocytose the apoptotic neutrophils, remaining bacteria, and debris. Furthermore, anti-inflammatory macrophages produce cytokines and chemokines that promote vascularization and recruitment of endothelial cells, fibroblasts, and keratinocytes to initiate tissue remodeling [124-127]. Macrophages serve different functions depending on the organ in which they reside; for instance, osteoclasts (bone) help break down bones for remodeling, Kupffer cells (liver) remove senescent cells, and microglia (brain) and Langerhans cells (skin) clear cellular debris [128-130].

Macrophages have historically been considered to have only two mutually exclusive phenotypes: M1 (activated, inflammatory, Th1-mediating) and M2 (alternatively activated, anti-inflammatory, Th2-mediating). Naive macrophages can be polarized to the M1 phenotype by stimulation with interferon-gamma (IFN-γ), lipopolysaccharides (LPS), or tumor necrosis factor (TNF) [131, 132]. IFN-γ binds to a heterodimer IFN-γ R1/2, which recruits Janus kinases (JAK) 1 and 2 to activate signal transducer and activator of transcription (STAT) 1 and interferon regulatory factors 1 and 8 [133]. IFN-γ stimulation induces an increase in cytokine receptor expression and several cell adhesion molecules. LPS polarization is mediated by a pattern recognition receptors (PPR) called Toll-like receptor (TLR) 4 [134, 135]. Stimulation of this receptor with LPS induces activation of MyD88 and Mal/Tirap signaling, which leads to the production of pro-inflammatory cytokines IL-1β, IL-6, and several others, including TNF, which

acts as positive feedback for M1 polarization [131-133]. Additionally, M1 polarization leads to increases in the production of nitric oxide (NO) and chemokines, the activity of suppressor of cytokine signaling (SOCS), and the number of antigen-presenting molecules. This inflammatory profile is largely controlled by nuclear factor of kappa light polypeptide gene enhancer in B-cells (NFκβTCGA) signaling.

IL-1β is a strong pro-inflammatory cytokine, produced by only a few cells. When macrophages are polarized to the M1 state, IL-1β is produced in its pyrogenic form. Prior to its release, inflammasome-activated caspase-1 cleaves IL-1β and then releases it into the extracellular milieu via autophagy-induced membrane transporters [136-138]. In the extracellular space, IL-1β competes with IL-1Rα for binding to the IL-1 receptor. IL-1β stimulation of the IL-1 receptor leads to expansion and differentiation of CD4 T cells and prostaglandin secretion and increases the expression of cell adhesion molecules [139, 140]. IL-6 can be either pro-inflammatory (trans-signaling) or anti-inflammatory (classical signaling). It is made in the Golgi and remains there until recycled through endosomes or secreted by tubulovesicular carriers. IL-6 trans-signaling occurs when the soluble IL-6 receptor binds to glycoprotein 130 (expressed by all cells), which prompts monocyte recruitment, promotes maintenance of Th17 cells, activates cytotoxic T cells, and inhibits T cell apoptosis and regulatory T cell development [141-143].

Suppressor of cytokine signaling (SOCS) is a family of seven proteins that regulate the transcription activity linked to M1/M2 macrophage polarization [144]. One of the most characterized proteins from the SOCS family is SOCS3, which regulates IL-6 signaling. Specifically, it inhibits anti-inflammatory IL-6 by directly competing for its receptor [145-147]. Additionally, it inhibits transforming growth factor beta (TGF-β, an M2 marker), promotes TLR signaling by inhibiting TLR suppressive mechanisms, and induces Notch signaling, which has been shown to increase both M1 polarization and antitumor activity [148-150]. Furthermore, it has been implicated in determining the fate of T cells [149, 151].

Inducible nitric oxide synthase 2 (NOS2) is considered one of the main regulators of innate immunity and regulates inflammation with great precision. This enzyme is associated with the M1 phenotype, as it is commonly upregulated to decrease inflammation while increasing the recruitment of innate inflammatory cells [152, 153]. Macrophages exposed to INF-γ, TNF-α, IL-1β, or LPS upregulate NOS2 (iNOS) mRNA expression. NOS2 facilitates the conversion of L-arginine to NO, which leads to an accumulation of HIF-1α, leading to tumor proliferation and differentiation [154-159]. However, as the intrinsic aim of innate immunity is to target hypoxic environments, this process recruits more innate cells to the tumor site [159-161]. NOS2 competes with an enzyme called arginase (ARG) to process L-arginine. ARG facilitates the conversion of L-arginine to urea and ornithine, which is eventually used to increase collagen synthesis and cell proliferation [154, 162]. NOS2 and arginase are competing enzymes that regulate L-arginine metabolism within the urea cycle. L-arginine exists in the extracellular milieu and is used by cytotoxic T cells to maintain the expression of CD3 and CD8 receptors. When arginase is upregulated, macrophages use cationic amino acid transports to collect L-arginine from the extracellular milieu for degradation. L-arginine is broken down by arginase-1 into urea and L-ornithine, which is used to suppress NOS2 function through the polyamine pathway [163]. ARG exists in two isoforms: ARG1 and ARG2. They serve the same function but are found in different locations in the body [164]. ARG1 is present in macrophages and is associated with the M2 macrophage phenotype.

M2 macrophage polarization is induced by stimulation by IL-4 or IL-13. These cytokines bind to multiple receptor heterodimers, activating JAK1 and JAK3 and leading to STAT6 activation. STAT6 regulates the expression of ARG1, mannose receptor 1 (MRC1), resistin-like alpha (Retnla), and chitinase-like protein 3 (Ym-1) [165-169]. The M2 macrophage phenotype has been associated with reduced anti-tumor response, tumor progression, and metastasis. As previously noted, ARG1 is an enzyme that degrades L-arginine and is one of the hallmark M2 markers. Moreover, $MRC1^{+}$ macrophages are associated with increased TGF-β and CCL18

secretion, which leads to fibroblast growth and ultimately tumor metastasis. MRC1 functions as a receptor for the clearance of pro-inflammatory cytokines, such as IL-1β and IL-6 [170-172]. Retnla transcription is suppressed by IFN-γ stimulation. The main function of Retnla is to reduce inflammation. However, it has also been implicated in myofibroblast differentiation, recruitment of bone marrow–derived cells and has been found to exert chemotactic and fibrogenic properties, although the exact mechanism of action is unknown [172-177]. Ym-1 is an M2 marker; like MRC1, stimulation by IL-4 and IL-13 increases its expression, and INF-γ modulates it [177-180]. Ym-1 is thought to exert anti-inflammatory activity by regulating heparan sulfate levels (which regulate M1 polarization) and inhibiting the activation and proliferation of cytotoxic T cells [181, 182].

The M1/M2 dogma is largely represented in homeostatic conditions. However, within the confines of cancer macrophage polarity is perplexing. Technological advancements have allowed closer investigations of macrophage polarity as more phenotypes are being discovered and evaluated. A few M2 subtypes are currently established: M2a, M2b, M2c, and M2d [183-185]. Naive macrophages are polarized into the M2a phenotype by exposure to IL-4 and IL-13 [186, 187]. M2a macrophages are characterized by JAK/STAT3 signaling and increased expression of MRC1, ARG1, and TGF-β [187-191]. This macrophage phenotype has been associated with the production of anti-inflammatory cytokines and wound-healing processes, as well as tumor progression. M2b macrophages are polarized by immune complexes and TLR agonists. These macrophages secrete pro-inflammatory cytokines (IL-1β, IL-6, and TNF-α), as well as anti-inflammatory cytokine IL-10. These macrophages are known as regulatory macrophages due to their roles in blunting immune and inflammatory responses, as well as promoting tumor progression [184, 191-193]. M2c (deactivated) macrophages are induced by IL-10. The IL-10 stimulus leads to STAT3 signaling, which causes the secretion of large amounts of IL-10 and TGF-β. These macrophages are involved in immunosuppression, phagocytosis, and tissue remodeling [190-197]. M2d macrophages, also known as TAMs,

promote angiogenesis, tumor progression, cancer metastasis, and immune evasion. They are characterized by high expression of ARG1, TGF-β, and IL-10. In hypoxic tumors, TAMs increase the expression of HIF-1α, which leads to increased secretion of angiogenic factors, such as VEGF, IL-8, cytochrome C oxidase assembly factor, and matrix metallopeptidase 9, thereby promoting metastasis. They also upregulate programmed death-ligand 1 (PD-L1), which binds to PD-1, inhibiting T cells. Naive macrophages are recruited and polarized to the TAM phenotype by MCSF-1, Chemokine (C-C motif) ligand 2 (CCL2), and IL-6 [191, 194, 198, 199]. Communication networks between macrophages and other immune cells are complex and involve extensive cell-cell and receptor-ligand interactions presented throughout this section (Figure 5).

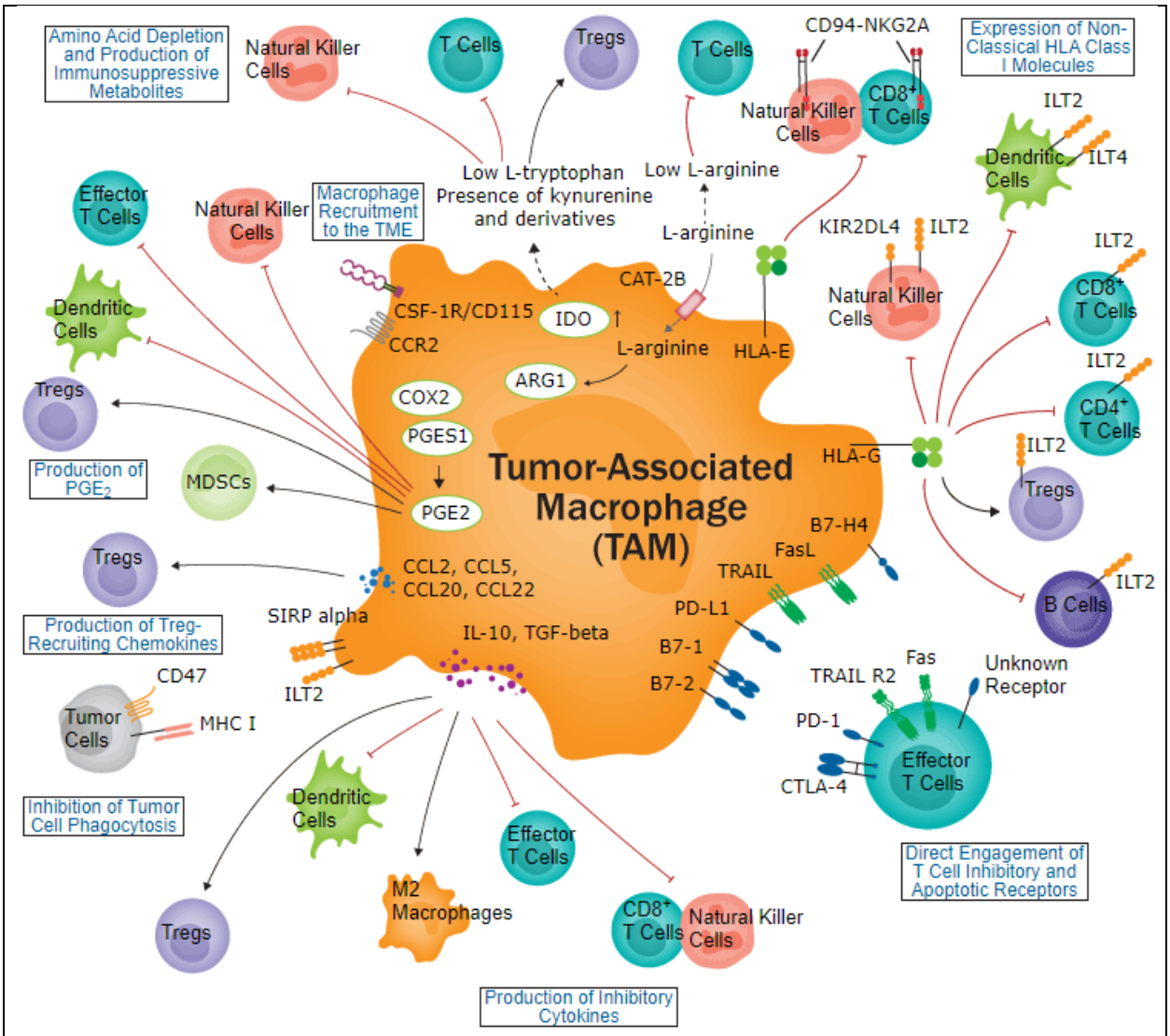

Figure 5: Cancer-immune cytokine signaling. The immune cell milieu within the tumor microenvironment has a complex web of cytokine communications. The solid black arrows represent cell–cell activation. The red bars represent cytokine–cell inhibition. TAMs are polarized by the release of cancer cell cytokines, which act as positive feedback for cancer progression. Moreover, TAM macrophages downregulate immune cells that could attack the tumor (R&D system poster).

It was not until 2000 that the macrophage M1 and M2 phenotypes were accepted. It took another 16 years to realize that macrophage polarization is a spectrum of phenotypes that

constantly change depending on extracellular signals. Few macrophage phenotypes and functions are currently understood. However, single-cell RNA sequencing is revealing many new macrophage subsets in cancer. As macrophages are easily polarized by the extracellular milieu, it is not surprising to find considerable diversification of macrophage polarity states in the tumor microenvironment. Therefore, characterizing macrophage phenotypes within the TME and identifying cancer cell features that dictate macrophage polarization are critical for cancer treatment.

1.7 Aims of this study

Basic science research in cancer biology has made great strides toward improving the quality of care for cancer patients. The five-year survival rate has nearly doubled in the last 30 years (SEER). However, lung cancer remains the leading cause of cancer-related deaths. Chemotherapies can be effective, but often have severe side effects. Most tumors eventually develop resistance to targeted therapies, and immunotherapies only work for a subset of patients. During my time at the University of Texas Southwestern Medical Center, I dedicated my research to developing a platform that could be used to interrogate the phenotype of innate immune cells (macrophages) in response to lung cancer cells and to identify therapeutics that can alter macrophage phenotype. In this study, we developed a novel multicellular co-culture platform to investigate macrophage phenotype in the presence of lung cancer cells and CAFs. We demonstrated our *in vitro* model has *in vivo* and clinical relevance. We profiled macrophage phenotype in co-culture with different human CAFs and 84 patient-derived cancer cell lines. Furthermore, we cross referenced cancer cell line data with macrophage polarity to identify cancer cell characteristic associated with any single macrophage phenotype. Finally, we used the co-culture platform to identify novel small molecules that specifically induce lung cancer cell death and alter macrophage repolarization.

Chapter 2: Materials and Methods

2.1 Cell Lines and cell cultures

Most NSCLC lines used in this study were part of the National Cancer Institute (NCI) and HCC (Hamon Cancer Center at UT Southwestern) series of cell lines, with the exception of A427, A549, Calu-1, Calu-6 (American Type Culture Collection; ATCC), DFCI024 (Dana Farber Cancer Institute, courtesy of Pasi Jänne), EKVX, HOP-62 (NCI-60 panel). Cell lines from these collections were maintained in RPMI 1640 (GIBCO, 2.05 mM L-glutamine, MilliporeSigma, catalog# R8758) supplemented with 5% FBS (GIBCO). Normal bronchiole epithelia-derived cell lines [200] were maintained in Keratinocyte SFM (ThermoFisher Scientific, catalog # 17005042) supplemented with human recombinant epidermal growth factor (rEGF) and bovine pituitary extract (BPE) at the time of use. Oncogenic normal bronchiole epithelia-derived cell lines were previously created and characterized (Sato et al. 2006, Sato et al. 2013). All cell lines were maintained in a humidified environment in the presence of 5% CO2 at 37°C. To split cell lines and/or create single cell suspensions, both cancer cell lines and HBECs were first washed with 1X PBS (Sigma, catalog # P3813-1PAK) then trypsinized using .05% Trypsin-EDTA (Gibco, catalog #2530054). For cancer cell lines, trypsin was neutralized using 2 volumes of R5. For HBECs, trypsin was neutralized using 1 volume of Trypsin Neutralizing Solution (Lifelife CM-0018). Cells were then spun at 1000rpm for 5 minutes and then used for subsequent analyses. Cancer cell lines were frozen in a solution consisting of 10% DMSO, 10% fetal bovine serum and 80% RPMI-1640. HBECs were frozen in a solution consisting of 10% DMSO and 90% KSFM. All cell lines were DNA fingerprinted (PowerPlex Fusion Kit, Promega) and mycoplasma free (myco kit, Boca Scientific).

2.2 Fingerprinting ID

All cell lines were verified by DNA fingerprinting with the Promega Fusion system (Cat# DC2408) which consists of 24 short tandem repeat (STR) markers. These loci collectively provide a genetic profile with a random match probability of 10^-28. Fingerprints were compared against our database of more than 10,000 reference fingerprints that were collected from ATCC (www.atcc.org), DSMZ (www.dsmz.de), JCRB (cellbank.nibiohn.go.jp), RIKEN (en.brc.riken.jp), Cellosaurus (web.expasy.org/cellosaurus), and from our own resources [201]. A match is called between two fingerprints when at least 80% of the alleles are identical according to the shared allele match algorithm defined by the International Cell Line Authentication Committee.

2.3 BMDMs isolation and differentiation

BMDMs isolation and differentiation was done as previously reported [202]. L929 cells were grown in T175 flasks with 30 mL of DMEM (11995040, GIBCO) + 10% FBS. Cells were grown to 100% confluency, media was changed and then incubated for 48 hours. The media was collected and new media was added. This collection cycle was repeated for a total of 4 times. Collection media (1X PBS + 5% FS + 1X penicillin/streptomycin), Macrophage Media (20% L929 condition media + 20% BCS + 0.5X sodium pyruvate + 1X MEM +1X NEAA + 1X Glut Max in DMEM without Glutamine). Tibias and femurs were isolated from C57BL/6J mice and cleaned in 70% ethanol. Bones were cut at ends and syringes were used to flush bones with collection media. Collected bone morrow was spun down (5 min X 1000 rpm @ 4°C). Supernatant was removed, re-suspend in macrophage media and filtered with 70 micron filter. Solution was spun down again (5 min X 1000 rpm @ 4°C). Cells were seeded on perti dishes in 8 mL of macrophage media (3 plates per mouse) or frozen down (90% FBS, 10% DMSO). 3 days later 4 ml/dish fresh macrophage media was added to the existing media. 2 days later cells were collected and used.

2.4 Multicellular co-cultures

Normal: Multicellular co-cultures were composed of mouse bone marrow-derived monocytes (BMDMs), patient-derived CAFs and NSCLC cells at a 1:10:50 ratio, respectively [203]. NSCLC and CAF cell lines were trypsinized and BMDMs were plated into 6-well plates at 1.5 x 10^5 total cells per well. Cells were incubated for 40 hours and harvested for quantitative polymerase chain reaction (qPCR) analysis of *bona fide* macrophage polarization markers (*Arg1*, *Nos2*, *Il6*, *Il-1b*, *Ym1*, *Socs3*). Macrophage were seeded at 1.0 x 10^5 per well and treated with PBS, LPS (20 ng/mL), or IL-4 (40 ng/mL). LPS (4-hour stimulation) and IL-4 (18-hour stimulation) treatments were used as positive controls for macrophage polarization into M1-like and M-2-like phenotypes, respectively.

3D Spheroid cultures: A total of 2,000 cells were plated per well in 96 well u-bottom plates for all Spheroid assays. 3D spheroid co-cultures were composed of mouse bone marrow-derived monocytes (BMDMs), patient-derived CAFs and NSCLC cells at a 1:10:50 ratio, respectively. Cells were incubated for 72 hours and harvested for quantitative polymerase chain reaction (qPCR) analysis of *bona fide* macrophage polarization markers (*Arg1*, *Nos2*, *Il6*, *Il-1b*, *Ym1*, *Socs3*).

Drug Co-cultures: Multicellular co-cultures were composed of mouse bone marrow-derived monocytes (BMDMs), patient-derived CAFs and NSCLC cells at a 1:10:50 ratio, respectively [203]. NSCLC and CAF cell lines were trypsinized and BMDMs were plated into 6-well plates at 1.5 x 10^5 total cells per well. Cells were incubated for 12 hours and then treated with chemical agent for 72 hours. The co-culture was then harvested for quantitative polymerase chain reaction (qPCR) analysis of *bona fide* macrophage polarization markers (*Arg1*, *Nos2*, *Il6*, *Il-1b*, *Ym1*, *Socs3*).

2.5 Transwell assay

Macrophages (100,000 cells/well) were plated in 6 well plates and allowed to adhere overnight. Cancer cells and CAFs were plated on polyester tissue culture-treated inserts (0.4 um) (Fisher

scientific catalog # 07-200-170) (70,000 and 30,000 cells/transwell, respectively) and allowed to adhere overnight in separate 6 well plates from macrophages. Transwell were then transferred to macrophage plated 6 wells and incubated for 40 hours. RNA was isolated from macrophages for RT-qPCR analysis.

2.6 Cytokine arrays

Cytokine arrays were performed by following manufacturer's protocol (Human cytokine array abcam catalog # ab133997, Mouse cytokine array catalog abcam catalog # ab133994). Co-cultures were allowed to incubate for 72 hours, supernatant and cells were harvested for cytokine arrays and RT-qPCR. Supernatant proteins were then concentrated using 15mL Amicon Ultra Centrifugal Filters (Fisher Scientific catalog # UFC905024) centrifuge at 4°C for 20 minutes at max speed. Proteins were then resupeneded in 1mL of excess co-culture media and used for cytokine array. Blots were imaged on LiCor Odyssey Fc and quantified using Image Studio Lite version 5.2 per manufacturer's instructions.

2.7 Immunoflourescence

Cells were plated into glass chamberslides (ThermoFisher Scientific, catalog # 154526) and allowed to adhere overnight. Cells were then treated as indicated, media was aspirated, cells were fixed with 4% paraformaldehyde (Fischer Scientific, catalog # 50-980-487) for 10 minutes, washed 3 times with TBS, then permeabilized with 0.5% Triton-X 100 on ice for 10 minutes. After 3 TBS washes, cells were blocked with 5% BSA (Jackson ImmunoResearch, catalog# 001-000-173) in 0.1% TBST for 1 hour. Following blocking, cells were incubated with primary antibody + 5% BSA overnight in 4°C. Cells were then washed 3 times for 5 minutes with 0.1% PBST and incubated with secondary antibody + 5% BSA, either anti-mouse Alexa Fluor 488 (1:500, ThermoFisher Scientific, catalog # A-11029) or anti-rabbit Alexa Fluor 647 (1:500, ThermoFisher Scientific, catalog # A-32795), for 1 hour protected from light. Chambers were

then washed 3 times for 5 minutes with 0.1% PBST, chambers were removed, and glass coverslips (VWR, catalog # 48404-133) were mounted using Vectashield with DAPI (Vector Laboratories, catalog # H-1200). Images were captured at 40X using a Leica DM5500 or a Keyence BZ-X710 and analyzed with BZ-X Analyzer (v1.3.1.1, Keyence).

Antibody list:

F4/80 Monoclonal Antibdy (BM8), eFLour 570, Fisher Scientific catalog # 50-112-3622, 1:100.

ARG1 Rabbit anti-Human, Mouse, Rat, Polyclonal Fisher Scientific catalog # 50-553-319, 1:100.

HLA-ABC Monoclonal Antibody (W6/32), ThermoFisher Scientific catalog # MA1-19027, 1:100.

CD163 Antibody (M-96) Monoclonal Antibody, Santa Cruz Biotechnology # sc-33650, 1:50.

CD206 Mouse anti-Human, Mouse (2A6A10), Fisher Scientific catalog # 50-173-6262, 1:100

2.7 Dextran Assay

Cells were plated into glass chamberslides (ThermoFisher Scientific, catalog # 154526) and allowed to incubate for 40 hours. Dextran, Alexa Fluor™ 647; 10,000 MW, Anionic, Fixable (ThermoFisher Scientific catalog # D22914) were added to co-cultures at a concentration of 100ug/mL. Hoechst 33342 (Fisher Scientific catalog # H3579, 1ug/mL) and Dextrans were then incubated in culture for 1 hours in normal tissue culture environments per manufacturer's instructions. Dextran-containing media was the removed and cells were washed briefly with PBS and fixed with cold 4% paraformaldyhe for 15 minutes. Chambers were removed, and glass coverslips (VWR, catalog # 48404-133) were mounted using Vectashield with antifade (Vector Laboratories, catalog # H-1400). Images were captured at 40X using a Leica DM5500 or a Keyence BZ-X710 and analyzed with BZ-X Analyzer (v1.3.1.1, Keyence).

2.8 Immunoblots

Cells were washed twice with ice-cold PBS and then scraped on ice. Cells were lysed with a modified RIPA buffer (50 mM Tris, 150 mM NaCl, .1% SDS, 1% IGEPAL CA-630, 1% sodium deoxycholate, 2 mM $MgCl_2$, pH 8) with 1 unit/μL benzonase (MilliporeSigma, catalog # E1014), protease inhibitors (MilliporeSigma, catalog # P8340) and phosphatase inhibitors (MilliporeSigma, catalog # 4906845001) by rotating lysates at 4°C for 2 hours. Lysates were then cleared by spinning at max speed for 10 minutes, quantified using BCA (ThermoFisher Scientific, catalog # 23225), mixed with 4X Laemmli buffer (BioRad, catalog # 1610737EDU) and boiled for 5 minutes immediately prior to loading. 20-25 μg of protein was ran on a 4-20% Mini-PROTEAN TGX gel (BioRad, catalog # 4568095) at 220 V. Samples were transferred to nitrocellulose membranes (Bio-rad), followed by blocking with 5% milk (Biorad, catalog # 1706404XTU) in 0.1% in PBST. Primary antibodies were incubated overnight in 4°C, Rabbit anti- PDGFRα (Abcam catalog # AB21234, 1:1000), Mouse anti-αSMA (Biocare Medical catalog # CM001A, 1:1000) and Rabbit anti-GAPDH (Genetex catalog # GTX100118, 1:5000). Blots were washed with 0.1% in PBST three times and then incubated with Goat anti-Rabbit 800CW (Fisher Scientific catalog # NC0809364) and Goat anti-Mouse 680RD (Fisher Scientific catalog # NC0809365) for 1 hour at RT. Blots were washed with 0.1% in PBST three times and then imaged on LiCor Odyssey Fc.

2.9 GFP-cell line lentivirus generation and transduction

To generate lentiviral particles, 2 million Lenti-X 293T cells (Clonetech, catalog # 632180) were forwarded transfected with 9 μg pCMV-dR8.91, 3 μg pMD2.G and 3 μg of LentiPlasmid-of-interest (pLV-eGFP addgene plasmid # 36083) using FuGene6 (Promega, catalog # E2691) following the manufacturers protocol. After 12 hours, media was changed and viral supernatant was collected every day for 3 days and filtered through a .45micron syringe filter (Corning, catalog #431220). For each infection in each cell line, viral supernatant was titrated onto HCC4210F (human cancer-associated fibroblast cells) and mixed with 6 μg/mL polybrene

(Santa Cruz, catalog # sc-134220) and incubated with cells overnight. Cells were grown to 90% confluency and then trypsinzed, pelleted and resuspen in 1mL of ice-cold PBS+2%FBS. Cells were then filtered into a polystyrene flow tube with a 35 μm strainer (Corning, catalog # 352235) and sorted with a BD LSRFortessa flow cytometer. The top 20% highest expressing cells were taken from the flow sorting and cultured in RPMI media + 5% FBS for further use.

2.10 Real-Time qPCR

Refer to the table below for details regarding primers

RNA was extracted with the RNeasy Mini Kit (QIAGEN) and QIAcube robot (QIAGEN) following the manufacturer's recommended protocol. 1 μg of total RNA was mixed with qScript cDNA SuperMix for cDNA synthesis (BioRad) per the manufacturer's protocol. After reverse transcription, RT-qPCR was performed with SYBR Green (BioRad) following the manufacturer's recommended protocol for marker (*Actin, iNos, Il6, Arg1, Ym-1, Il-1b, Socs3*). Mouse specific primers were used to ensure only macrophage transcripts would be detected. All primers were cross examined for no activity on human RNA. RT-qPCR was performed on a CFX384 Touch Real-Time PCR Detection System (BioRad). The cycling program was 95°C for 10 min, 95°C for 15 s, and 60°C for 40 cycles. Each sample was run in quadruplicate, normalized to the actin probe and then normalized to macrophage baseline, and analyzed by the comparative CT method.

Gene Name	Forward Primer	Reverse Primer
Actin	CTGAGAGGGAAATCGTGCGT	AGGGTGTAAAACGCAGCTCAG
Arginase-1	CTCCAAGCCAAAGTCCTTAGAG	AGGAGCTGTCATTAGGGACATC
iNOS	GTTCAGCTACGCCTTCAACAC	CAAGGCCAAACACAGCATACC
Il-6	CGTGGAAATGAGAAAAGAGTTGTGC	TGGTACTCCAGAAGACCAGAGG

Ym-1	TCTGGGTACAAGATCCCTGAA	TTTCTCCAGTGTAGCCATCCTT
Il-1β	TGCCACCTTTTGACAGTGATG	TTCTTGTGACCCTGAGCGAC
Socs3	CAAAAATCCAGCCCCAACGG	GGCTGGCTCCACTTGAAAGA

2.11 Affinity propagation clustering

Affinity propagation clustering was performed as described using Pearson correlation as a similarity metric [204]. Cell lines in the macrophage qPCR dataset (84 cell lines) were clustered according to the expression profiles of the six macrophage genes. Networks were visualized with Cytoscape (https://cytoscape.org/) with edges defined according to the procedure above and edge lengths drawn proportional to Pearson distance using the built-in spring embedding algorithm.

2.12 DNA/RNA extraction for sequencing

DNA for exome or genome sequencing was purified from frozen cell line pellets using DNeasy reagents and protocols with QIAcube robot (QIAGEN). DNA spectra were quantitated using spectrophotometer (Nanodrop) and samples diluted with nuclease free water (Ambion). Cell lines were grown to approximately 70%–80% confluence, washed 2X with PBS and directly lysed from culture flasks using RLT buffer (QIAGEN). Lysates were snap frozen and stored at -80°C. RNA was purified from lysates using RNeasy kit and QIAcube robot (QIAGEN).

2.13 RNA-sequencing

For mulitcellular co-culture experiments, RNA was harvested 40 hrs after platting. RNA was extracted and genomic DNA discarded using the RNeasy Plus Mini Kit (Qiagen, catalog# 74134). RNA samples isolated from multicellular coculture experiments were submitted to Novogene genome sequencing company (Sacromento, CA) or UT southwestern Next

Generation Sequencing Core. The processing centers performed quantitative and qualitative assessment of the RNA samples including the RNA integrity and contamination. Novogene prepared the libraries using poly-T oliogoattached magnetic beads. UTSW NGSC prepped the libraries with Illumina's TruSeq Stranded mRNA library prep kit (Illumina, catalog # RS-122-2101) following manufacturers protocols. Novogene sequenced the libraries on the their HiSeq/MiSeq Illumina machines with 150 nucleotide paired-end reads for an average of 60 million total reads. UTSW NGSC sequnced the libraries with the Illumina NextSeq 500 using V2 reagents and 75 nucleotide single-end reads for an average of 50 million reads. Reads were aligned to the human reference genome GRCh38 and/or mouse reference genome GRCm38 using STAR-2.7 (https://github.com/alexdobin/STAR) followed by read duplicate removal with MarkDuplicates (gatk-4.1.2.0; https://gatk.broadinstitute.org). For co-culture samples, human reads were removed by comparing alignment scores (AS flags in bam files) in the human and mouse alignments: reads for which the human AS value was higher than the mouse AS value were removed (gatk-4.1.2.0 FilterSamReads). FPKM values were generated with cufflinks-2.2.1 (http://cole-trapnell-lab.github.io/cufflinks/). These were then normalized (upper-quartile normalization: Bullard et al, Bioinformatics 2010, 11:94), and log-transformed.

TCGA Matchup: We compared each lung cancer cell line with each lung tumor from the TCGA NSCLC datasets using RNAseq expression and somatic mutation data. The expression similarity measure was the Pearson correlation on the 2000 most variable genes while the mutation similarity measure used a concordance value on 700 cancer genes (Cancer Gene Census, COSMIC) defined as the number of genes mutated in both samples divided by the number of genes mutated in either sample (with genes weighted by their mutation frequency in the tumor sets). A combined score showed the degree of similarity between these cell lines and TCGA specimens. Bulk RNA sequencing from TCGA matched samples were processed using

CIBERSORT to deconvolute relative immune cell populations within the TME (Newman et al., 2019).

GSEA analysis: For GSEA of RNA-seq data, RPKM values for genes with RPKM >1 between groups indicated in study were fed into GSEA (V 2.2.2). The following gene sets from MSigDB were used in all GSEA analyses: H, C1, C2 (CGP, CP, CP:KEGG, CP:Reactome), C5, and C6.

2.14 Viability-based drug dose-response curves

To determine cytotoxicity of the small molecule compounds, NSCLC cells and HBECs were plated at a density ranging from 2,000 of 5,000 cells per well in white tissue-culture-treated 96-well clear bottom plate (Corning), with the seeding density for each cell line based on growth rate. After culturing the cells in assay plates for 24 hr, compounds were added to each plate at the indicated doses (8 replicates per dose per cell line per biological replicate (2)). After an incubation of 96 hr, 15 uL of CellTiter 96(R) AQueous MTS (Promega) was added to each well and mixed. Plates were incubated for 15 min at 37C and absorbance (490nm) was determined for each well using a SpectraMax Paradigm plate reader (Molecular devices).

2.15 Animal Studies

Mice were housed by the UTSW Animal Resource Center at 68-79°F, 30-70% humidity, in individually ventilated cages, with no more than 5 mice per cage on 12 hour on:off light:dark cycles. Mice were screened for and found free of MHV, Sendai virus, MPV, EDIM, MVM, PVM< TMEV-/GD-7, REO-3 virus, Mycoplasma pulmonis, pinworms, fur mites, LCMV, ECTRO, MAV, and K virus and had unrestricted access to RO chlorinated water and irradiated 2916 Teklab global diet (Envigo, catalog# 2916).

Xenograft panel: A cancer cell line panel consisting of A427, H1666, H2009, H460, Calu-6, H1373, H2073 cell lines were utilized. 1 million cells dissolved in100 µL of ice-cold PBS were injected subcutaneously (27-guage needle) into the right rear flank of ≈8-week-old female

athymic nude mice. Each cell line was injected into 8 mice to provide reasonable power for the experiment. However, not all tumors grew to the appropriate size for the study. Tumor dimensions and volumes were measured weekly. Mice were sacrificed when tumor volumes reached 1000 –1500 mm3. Tumors were harvested for IHC interrogation of macrophage polarization.

Mitoxantrone studies: To investigate the impact of mitoxantrone (Mito) on macrophage polarization *in vivo*, 2 million H441 or H2073 cells in 100 µL ice-cold PBS were injected subcutaneously through a 27g needle into the right rear flank of subcutaneously into the right rear flank of ≈8-week-old female athymic nude mice. Mice were weighed and tumor dimensions and volumes were measured weekly. Once average tumor size of all mice reached ≈ 100-200 mm3, (calculated length x width2 x 0.52, where length corresponds to longest axis), mice were randomized into equal groups (n=8), weighed regularly, and treated with MTX via intraperitoneal injection (2.5 mg/kg/q through 27G needle). On treatment days, mice were given either 100 uL of vehicle (PBS) or MTX (2.5mg/kg). Each treatment group was separated into three different time points (Day 3, 17 and 21). Mice were sacrificed to harvest tumor and organs (lungs, kidneys, spleen, pancreas, liver, and blood) at their respective time points (Day 3, Day 17 and Day 21). Tumor, liver and lung sections were stained with hematoxylin and eosin (H&E). Tumors were further interrogated by IHC to investigate macrophage polarization.

2.16 Immunohistochemistry (IHC) and quantification

Refer to the table below for details regarding antibodies

For IHC, tumors were fixed in 10% Formalin (VWR, catalog # 89370-094) for 72 hours with slight agitation at RT, then embedded in paraffin, sectioned into 4-micron slices and placed onto positively charged slides. Immunohistochemistry (IHC) was performed as previously described (Sorrelle N., et al. 2019). Slides were heated at 60°C for 10 minutes, deparaffinzed and

rehydrated. Antigen retrieval was performed with a Biocare Medical Decloaking Chamber at 110°C for 17 minutes using Antigen Unmasking Solution, TRIS-BASED (Fisher Scientific, catalog # NC9800748) then allowed to cool to room temperature for 30 minutes. Slides were washed for 5 minutes with PBS, incubated in ice-cold 10% methanol for 10 minutes at room temperature, washed with de-ionized H20 for 5 minutes, then tissue was blocked for 30 minutes using appropriate blocking solution. Blocking buffer was removed, then primary antibody diluted in Renaissance Buffer (BioCare Catalog # PD905 L) and added to samples at 4°C overnight with agitation. Samples were washed 3 times with 0.5% PBST for 5 minutes, once with PBS for 5 minutes, then secondary antibody solution was added for 30 minutes with agitation at room temperature. Samples were washed once with 0.2% PBST for 5 minutes, twice with 0.5% PBST for 5 minutes, then a solution of 1:250 with the appropriate opal dye in 1X Plus Amplification Diluent (PerkinElmer, catalog # FP1498) was made and added to samples for 3 minutes. After 3 minutes, the solution was quickly aspirated and washed with .05% PBST 3 times, then washed with PBS + 2 mM EDTA for 10 minutes. Subsequential staining rounds follow the same protocol for each stained marker, apart from Antigen Unmasking Solution, citrate-based (Fisher Scientific, catalog # H-3300) is used instead of Antigen Unmasking Solution, TRIS-BASED (Fisher Scientific, catalog # NC9800748). The final staining round DAPI was added during the secondary incubation at 1 ug/mL concentration. Slides were then mounted with Vectamount AQ Aqeuous Mounting Medium (Fisher Scientific catalog # H550160) and cover slipped (VWR catalog # 48404-133). Images were captured at 40X magnification using Vectra Polaris Slide Scanner (AKOYA Biosciences, Delaware, USA). Images were then deconvoluted and re-stitched using Phenochart and inForm software (Akoya Biosciences). The reconstituted images undewerent multiplex quantitative analysis using HALO software (Akoya Biosciences). Tumor borders, regions of necrosis, and visible stroma were annotated and cross-checked to each tissue's associated H&E stain. For individual macrophage subtype characterization, Arginase-1^{+} macrophages were characterized as F4/80^{+}/Arginase-1^{+}. $SOCS3^{+}$ macrophages were

characterized as F4/80^{+} /SOCS3^{+}. Primary tumor cells were marked as Cytokeratin^{+}. All nuclei were identified with DAPI staining. Cell quantity, distribution in the tumor area, and density of each subtype of macrophage were analyzed for the overall tumor area, areas of necrosis, and stromal regions. Spatial infiltrative analyses into regions of necrosis or stroma were also conducted. Quantitative data were abstracted from analyses from each tumor section and analyzed on GraphPad Prism statistical analysis software (GraphPad Software, CA, USA). Quantitative IHC cell count and density analyses were conducted using Mann-Whitney U non-parametric T-tests.

Tissue was stained with multiple rounds of antigen retrieval.

1st: Blocking buffer = Rodent block (Biocare Medical catalog # RBM961H), Primary = Pan-Cytokeratin (Fisher Scientific # NC0581968, 1:300), Secondary = anti-Mouse HRP (Fisher Scientific # NC0141382), Opal – Opal 520 (Perkin Elmer # FP1487001KT)

2nd: Blocking Buffer = 2.5% Goat Serum (Fisher Scientific # NC0533036), Primary = SOCS3 (Fisher Scientific # PIPA129534, 1:500), Secondary = anti-Rabbit HRP (Fisher Scientific # MP-7451), Opal = Opal 690 (Perkin Elmer # FP1497001KT)

3rd: Blocking Buffer = 2.5% Goat Serum (Fisher Scientific # NC0533036), Primary = Arginase1 (Cell Signaling # 936685, 1:500), Secondary = anti-Rabbit HRP (Fisher Scientific # MP-7451), Opal = Opal 570 (Perkin Elmer # FP1488001KT)

4th: Blocking Buffer = 2.5% Goat Serum (Fisher Scientific # NC0533036), Primary = F480 (Fisher Scientific # NC1397643, 1:500), Secondary = anti-Rabbit HRP (Fisher Scientific # MP-7451), Opal = Opal 620 (Fisher Scientific # NC1612059)

2.17 EMT Staining

Immunohistochemistry (IHC) was performed as previously described (Sorrelle N., et al. 2019). Briefly, slides were warmed in a 60℃ oven for 10 min followed by deparaffinization and rehydration. Before antigen retrieval, slides were fixed in 10% neutral buffered formalin for 30 min followed by a PBS wash. Antigen retrieval was performed in antigen retrieval buffer (10 mM Tris-HCl, 1 mM EDTA with 10% glycerol [pH 9]) at 110℃ for 17 min (~4–5ψ). Slides were then cooled down to room temperature and were washed once with PBS. Tissue sections were blocked with 2.5% goat serum (Vector Laboratories, S-1012) for 30 min followed by incubation with primary antibody overnight E-cadherin (1:500; Cell Signaling, 3195S) and Vimentin (1:500; Cell signaling,5741S). Slides were washed three times for 5 min in PBST (0.05% Tween20 and 2 mM EDTA) and incubated with HRP conjugated secondary anti-rabbit Antibody (ImmPRESS; Vector Laboratories, MP-7401) for 30 min on a shaker. Slides were then washed three times for 5 min in PBST. For developing the chromogen signal, Bentazoid DAB (BDB2004L) was used. Slides were counter-stained with hematoxylin and then cover-slipped using VectaMount (H-5501, Vector Laboratories) and scanned at 20X using the Hamamatsu NanoZoomer 2.0-HT. Slides were processed, analyzed and quantified using Fiji Image J software.

2.18 Nanostring

H2073 and H441 tumor tissues were lysed in RLT lysis buffer and purified according to the manufacturer's instructions (QIAGEN). RNA was sent to the Microarray & Immune Phenotyping Core at UT Southwestern and analyzed using a preassembled nCounter PanCancer Immune Profiling Panel (mouse) and the nCounter system (NanoString Technologies) according to the manufacturer's instructions. Samples were then normalized based on the geometric means of the supplied positive controls and the panel of housekeeping genes, as recommended by the manufacturer.

2.19 Statistical Analysis

All statistical analyses were performed with GraphPad Prism (Version 9) unless otherwise stated. Comparative analysis of features across all three macrophage clusters were evaluated by one-way ANOVA with *post-hoc* Brown-Forsythe correction. Affinity propagation clustering based on oncogenotypes, RNAseq expression profiles, and clinical demographics, with identification of exemplars was done as previously described [204]. Additionally, we compared molecular phenotypes of the tumor cell lines to TCGA patient samples by Pearson correlations of RNA expression and by similarity of somatic mutations.

Chapter 3: Investigating macrophage polarity using multicellular co-culture in lung cancer

3.1 Introduction

The advent of single cell transcriptome analysis of mouse and human lung cancer has revealed a spectrum of macrophage phenotypes beyond the traditionally depicted M1 and M2 phenotype [205]. Additionally, studies have shown macrophage populations will change throughout the progression of cancer [206]. However, a platform to investigate macrophage phenotype *in vitro* under conditions that mimic the lung cancer TME has not been established.

3.2 Establish the system

To address this need, we established a multicellular co-culture model that recapitulates the dominant macrophage phenotype present within any individual lung cancer. This platform was

established using murine bone marrow-derived macrophages (BMDMs), cancer-associated fibroblasts (CAFs), and patient derived lung cancer cells lines. We used BMDMs for two primary reasons: BMDMs are easily accessible in large quantities, and second, we can leverage the difference in species to identify mouse specific gene expression. This allowed the interrogation of macrophage polarity *in vitro* co-cultured with a large panel of lung cancer cells. Furthermore, we utilized CAFs that were isolated from lung cancer patient tumors to capture the contribution of fibroblasts to macrophage phenotype. A few hurdles needed to be overcome before the platform could be exploited.

The first hurdle was to isolate hematopoietic stem cells, differentiate them into macrophages and polarize them in a reproducible fashion. As noted in the methods section the Brekken lab had previously developed a protocol for BMDM isolation and differentiation. We utilized LPS (20 ng/mL) and IL-4 (40 ng/mL) to polarize the macrophages into the M1 and M2 phenotypes, respectively (Figure 6A). Once, we determined that BMDM could be reproducibly polarized we needed to identify additional markers to assess macrophage polarity. To this end, we investigated 46 different genes of interest and screened 134 primer pairs to evaluate macrophage polarity (Table 1).

Table 1: Primer Sequences

Oligo Name	Sequence
Arg-F1	TTTTAGGGTTACGGCCGGTG
Arg-R1	CCTCGAGGCTGTCCTTTTGA
Arg-F2	CAAGACAGGGCTCCTTTCAG
Arg-R2	CGTTGAGTTCCGAAGCAAGC
iNos-F1	GGTGAAGGGACTGAGCTGTT
iNos-R1	GCTACTCCGTGGAGTGAACAA
iNos-F2	ACCTTGGTGAAGGGACTGAG
iNos-R2	ACTCCGTGGAGTGAACAAGAC
iNos-F3	GGTGAAGGGACTGAGCTGTTA
iNos-R3	CAACGTTCTCCGTTCTCTTGC

iNos-F4	CAGGGTCACAACTTTACAGGGA
iNos-R4	AGGAGCCTCAGAAGTGTCTCT
iNos-F5	GGTTTGAAACTTCTCAGCCACC
iNos-R5	GGAGTGAACAAGACCCAAGC
Actb-f1	TGAGCTGCGTTTTACACCCT
Actb-f2	AGGCATTGTGATGGACTCCG
Actb-f3	CTGAGAGGGAAATCGTGCGT
Actb-f4	CCCATCTACGAGGGCTATGC
Actb-r1	AAGTCAGTGTACAGGCCAGC
Actb-r2	AGCTCAGTAACAGTCCGCCTA
Actb-r3	AGGGTGTAAAACGCAGCTCAG
Actb-r4	GGTGTAAAACGCAGCTCAGTA
B-IL-6-F	CGTGGAAATGAGAAAAGAGTTGTGC
B-IL-6-REV	TGGTACTCCAGAAGACCAGAGG
A-TNFalpha-F	ATGAGCACAGAAAGCATGA
A-TNFalpha-REV	AGTAGACAGAAGAGCGTGGT
A-IL-10-F	ATAACTGCACCCACTTCCCA
A-IL-10-REV	GGGCATCACTTCTACCAGGT
A-IL-12-F	GATGACATGGTGAAGACGGC
A-IL-12-REV	AGGCACAGGGTCATCATCAA
CCL2-F	GCTCAGCCAGATGCAGTTAA
CCL2-REV	TCTTGAGCTTGGTGACAAAAACT
B-TNF-alpha-F	GGCAGGTTCTGTCCCTTTCAC
B-TNF-alpha-REV	TTCTGTGCTCATGGTGTCTTTTCT
A-IL-6-F	TTCCATCCAGTTGCCTTCTTG
A-IL-6-REV	GGGAGTGGTATCCTCTGTGAAGTC
B-IL-10-F	CAGCCGGGAAGACAATAACTG
B-IL-10-REV	CCGCAGCTCTAGGAGCATGT
B-IL-12-F	AAGCTCTGCATCCTGCTTCAC
B-IL-12-REV	GATAGCCCATCACCCTGTTGA
A-IL-1b-F	TGCCACCTTTTGACAGTGATG
A-IL-1b-REV	TTCTTGTGACCCTGAGCGAC
Arg-1-F	CTCCAAGCCAAAGTCCTTAGAG
Arg-1-Rev	AGGAGCTGTCATTAGGGACATC
iNOS-F	GTTCAGCTACGCCTTCAACAC
iNOS-Rev	CAAGGCCAAACACAGCATACC

B-IL-1b-F	GCCACCTTTTGACAGTGATGAG
B-IL-1b-REV	TTCTTGTGACCCTGAGCGAC
C-IL-1b-F	TGCCACCTTTTGACAGTGATG
C-IL-1b-REV	TGGGTGTGCCGTCTTTCATT
A-MRC1(CD206)-F	GTCAGAACAGACTGCGTGGA
A-MRC1(CD206)-REV	AGGGATCGCCTGTTTTCCAG
B-MRC1(CD206)-F	GTGGAGTGATGGAACCCCAG
B-MRC1(CD206)-REV	CTGTCCGCCCAGTATCCATC
C-MRC1(CD206)-F	AACCAGTTCCTTGAGCTCGG
C-MRC1(CD206)-REV	CTGATTAGGGCAGCCGGTAG
A-CD163-F	GGATCTCCGGGATGCTTCTG
A-CD163-REV	CGCCTGCCAGACGAATATCT
B-CD163-F	ACGGCTGGAGCATGAATGAA
B-CD163-REV	TTGCCTCATGTCCTTCGCAT
C-CD163-F	TGCTGTCACTAACGCTCCTG
C-CD163-REV	TTCATTCATGCTCCAGCCGT
D-CD163-F	TGGTCAGGTCTGGAGTCACA
D-CD163-REV	TCTTTGTGGGCTTCGTTGGT
B2m-m-f1	TCTCACTGACCGGCCTGTAT
B2m-m-r1	TTGGGCACAGTGACAGACTT
B2m-m-f2	TGACCGGCCTGTATGCTATC
B2m-m-r2	CATTGGGCACAGTGACAGAC
B2m-m-f3	AGTATACTCACGCCACCCAC
B2m-m-r3	CGATCCCAGTAGACGGTCTTG
HPRT-m-1f	GCAGTACAGCCCCAAAATGG
HPRT-m-1r	AAATCGAGAGCTTCAGACTCGT
HPRT-m-2f	AGCCTAAGATGAGCGCAAGT
HPRT-m-2r	GGAAAATACAGCCAACACTGCT
HPRT-m-3f	CCCTCTGGTAGATTGTCGCT
HPRT-m-3r	GAAAATACAGCCAACACTGCTGA
Irf4-m-1f	AACTAGAAGCCCCAAAGCCC
Irf4-m-1r	GGCTCACATTCAGCCTGTCT
Irf4-m-2f	CCCTTGCCTGGTCCTGTATG
Irf4-m-2r	GTTTCAGCAAGGGACGAGGA
Irf4-m-3f	ATGCCGTTGAAGAGGTAGGC
Irf4-m-3r	GTCCAGGACAACGACTGAGG

IL-12b-m-1f	ATGAGGAGCTGGCTTTGGTC
IL-12b-m-1r	TTGCATCCATTTGTGTGGCG
IL-12b-m-2f	TGGAGCACTCCCCATTCCTA
IL-12b-m-2r	GAGCTTGCACGCAGACATTC
IL-12b-m-3f	ATTACTCCGGACGGTTCACG
IL-12b-m-3r	GCCATTCCACATGTCACTGC
IL-10-1f	ACCTGGTAGAAGTGATGCCC
il-10-1r	ACAGGGGAGAAATCGATGACAG
IL-10-2f	GACTTTAAGGGTTACTTGGGTTGC
il-10-2r	GCCTGGGGCATCACTTCTAC
IL-10-3f	AAAGGACCAGCTGGACAACAT
il-10-3r	TGGCAACCCAAGTAACCCTTAAA
MRC-1f	GGCTGATTACGAGCAGTGGA
MRC-1r	CATCACTCCAGGTGAACCCC
MRC-2F	TGGAGGCTGATTACGAGCAG
MRC-2r	TCCAGGTGAACCCCTCTGAA
MRC-3F	GCTGGCGAGCATCAAGAGTA
MRC-3R	AGGAAACGGGAGAACCATCAC
TNF-1F	TTCTATGGCCCAGACCCTCA
TNF-1R	GTGGTTTGCTACGACGTGGG
TNF-2F	CCCACGTCGTAGCAAACCA
TNF-2R	TGTCTTTGAGATCCATGCCGT
TNF-3F	CCACGTCGTAGCAAACCACC
TNF-3R	CTTTGAGATCCATGCCGTTGG
TGFb-MUS-1F	CCCGAAGCGGACTACTATGC
TGFb-MUS-1R	CATAGATGGCGTTGTTGCGG
TGFb-MUS-2F	ACGTCACTGGAGTTGTACGG
TGFb-MUS-2R	GTGAGCGCTGAATCGAAAGC
TGFb-MUS-3F	GCCCGAAGCGGACTACTATG
TGFb-MUS-3R	ATAGATGGCGTTGTTGCGGT
Ym-1-1F	GAAGCTCTCCAGAAGCAATCCT
Ym-1-1R	AGCACATCAGCTGGTAGGAAG
Ym-1-2F	AAGCTCTCCAGAAGCAATCCTG
Ym-1-2R	TCCCTTCTATTGGCCTGTCCT
Ym-1-3F	GAAGCTCTCCAGAAGCAATCCTG
Ym-1-3R	TCTATTGGCCTGTCCTTAGCC

ms-H2-DMB2 F1	CCAACCTTTCTGGGATGTGC
ms-H2-DMB2 R1	TAGAAGCCCCAGACGTAGCA
ms-H2-DMB2 F2	ACCCAACCTTTCTGGGATGTG
ms-H2-DMB2 R2	AGGTGTGGTTTGGGCTACTC
ms-H2-DMB2 F3	CACGTGCGTGCTGAATGATG
ms-H2-DMB2 R3	TGCAAGCGATGAATAAGGCT
ms-Ear2 F1	AGTCGGAGGAGAACACCTTATACC
ms-Ear2 R1	ATCTCGGCAGTAGCAGATGAG
ms-Ear2 F2	GTCGGAGGAGAACACCTTATACCC
ms-Ear2 R2	GCACTGGAGCTAAAATGTCCC
ms-Ear2 F3	TCGGAGGAGAACACCTTATACCCA
ms-Ear2 R3	GAGCAAAGGTGCAAAGTGCTG
ms-Cd44 F1	CACCATTGCCTCAACTGTGC
ms-Cd44 R1	TCTGGGCTTCTTGCCTCTTG
ms-Cd44 F2	GGCTCCACCATCGAGAAGAG
ms-Cd44 R2	GAGCTGCTGCATGGCTTTTT
ms-Cd44 F3	CAACTCAGACTCAGGAGCCC
ms-Cd44 R3	CCGTACCAGGCATCTTCGTT
ms-Lyz2 F1	TCAGCCAACACAATGATCACC
ms-Lyz2 R1	CTCACACGACTGCTGTTTCC
ms-Lyz2 F2	AGACTCTCCTGACTCTGGGAC
ms-Lyz2 R2	TGGCAAACTCACAACGTTCATA
ms-Lyz2 F3	TGTGCTTCTACTGCAGCTCAT
ms-Lyz2 R3	TTAGAGGGGAAATCGAGGGAA
ms-Gpx1 F1	AGTCCACCGTGTATGCCTTC
ms-Gpx1 R1	CCTCAGAGAGACGCGACATT
ms-Gpx1 F2	AAAGCGATGCCACGTGATCT
ms-Gpx1 R2	GAGAAGGCATACACGGTGGAC
ms-Gpx1 F3	ACAGTCCACCGTGTATGCCTT
ms-Gpx1 R3	CGCTTCTGCAGATCGTTCATC
ms-S100a11 F1	ACAGCGGGAAGGATGGAAAC
ms-S100a11 R1	TGGAAATCTAGCTGCCCGTC
ms-S100a11 F2	CACCAAGTCATCACCTCCCC
ms-S100a11 R2	GCGTGGGATACATGTTGTGG
ms-S100a11 F3	TCGCTCCTCAACTTGAAGCAA
ms-S100a11 R3	TGTTTCCATCCTTCCCGCTG

ms-Spp1 F1	AACCAGCCAAGGTAAGCCTG
ms-Spp1 R1	GTTAGTCCCTCAGAATTCAGCCA
ms-Spp1 F2	TTCTCCTGGCTGAATTCTGAGG
ms-Spp1 R2	GCTATAGGATCTGGGTGCAGG
ms-Spp1 F3	TTCTCGGAGGAAACCAGCC
ms-Spp1 R3	AGAATTCAGCCAGGAGAACTGC
ms-Ecm-1 F1	GGAACAAAGAGAAGTGCAGCCC
ms-Ecm-1 R1	CAATATGGACTTGGGGAGGGG
ms-Pla2g1b F1	CACCCCAGTGGACGACTTAG
ms-Pla2g1b R1	CAGCTTCTTGGCCTGACTGT
ms-Pla2g1b F2	GACCACTGCTACAGTCAGGC
ms-Pla2g1b R2	TGCAGATGAAGTCCTCGCAT
ms-Pla2g1b F3	ATCACCTGCAGCGCCAAAAA
ms-Pla2g1b R3	GGGCGCAGGGTGAAATAAGA
ms-MIF F1	TTCCACCTTCGCTTGAGTCC
ms-MIF R1	GCATCGCTACCGGTGGATAA
ms-MIF F2	CAGAGGGGTTTCTGTCGGAG
ms-MIF R2	CGTTCGTGCCGCTAAAAGTC
ms-MIF F3	GACTTTTAGCGGCACGAACG
ms-MIF R3	GCAGCTTACTGTAGTTGCGG
ms-Slc39a1 F1	ATGGAGTGAGACCCTCGGGA
ms-Slc39a1 R1	CAGCTTCACTTCCAGCCCTA
ms-Slc39a1 F2	ATGGAGTGAGACCCTCGGGA
ms-Slc39a1 R2	ACAGGTACCAGGCTGCAGAT
ms-Slc39a1 F3	ATGGAGTGAGACCCTCGGGA
ms-Slc39a1 R3	CTTCACTTCCAGCCCTACTGG
ms-Hbegf F1	CGCAAGGGATCTGCTGTTTG
ms-Hbegf R1	GAGTTCTCGAGCTTGCGGTA
ms-Hbegf F2	ACGCTGGGTCCTATTTGCTC
ms-Hbegf R2	TCGGAACACGAACGGTAGAC
ms-Hbegf F3	CGGACAGTGCCTTAGTGGAA
ms-Hbegf R3	GCAGCGATCACTTTGGATGC
ms-Tnip3 F1	ACACTCTTCCCAGGCCAGTA
ms-Tnip3 R1	TCCAGTGTTTGGCACCTTGT
ms-Tnip3 F2	ACATGTCTGGACTGAGTGCG
ms-Tnip3 R2	TCGGAATTGCTGGTCCCATT

ms-Tnip3 F3	CAATGGGACCAGCAATTCCG
ms-Tnip3 R3	GTCGCCCTCTGTCACACTTT
hum-GRAMD18 F1	GCCCACAGATGAGGATGTGG
hum-GRAMD18 R1	AAGGATGACCAGCAGCACC
hum-GRAMD18 F2	ATGTGGCAGGTTCCACACAG
hum-GRAMD18 R2	ATGACCAGCAGCACCAGAC
hum-NOL8 F1	GGCTTTAGGTGAACGACGTG
hum-NOL8 R1	GCCTCAGAAATGTCCTGGCT
hum-NOL8 F2	GAAGGTGGGAGGACGGAAAA
hum-NOL8 R2	GTCGTTCACCTAAAGCCAGC
hum-CCT2 F1	GAGGGGATTCACTTGTGTGC
hum-CCT2 R1	GTCCCAAGGTGCTCTTTACCA
hum-CCT2 F2	TGAGGGGATTCACTTGTGTGC
hum-CCT2 R2	TCCCAAGGTGCTCTTTACCA
Retnla-F1	CTGATAGTCCCAGGGAACGC
Retnla-R1	GTCTGCCAGAAGACGTGACA
Retnla-F2	GAGCCTAAGACGATCTCCTGC
Retnla-R2	CCGGATATCCCACGATCCAC
Retnla-F3	CTAGTGTCACGTCTTCTGGCA
Retnla-R3	ATATCCCACGATCCACAGCC
PPARG-F1	TTCGCTGATGCACTGCCTAT
PPARG-R1	GGAATGCGAGTGGTCTTCCA
PPARG-F2	CGCTGATGCACTGCCTATGA
PPARG-R2	TGTGGAGCAGAAATGCTGGA
PPARG-F3	TTCGCTGATGCACTGCCTA
PPARG-R3	GCTGATTCCGAAGTTGGTGG
PPARG-F4	TTCGCTGATGCACTGCCTATG
PPARG-R4	GTCTTCCATCACGGAGAGGT
CCL2-F1	GTGAGGCTCTGGTCCCTCTA
CCL2-R1	GGTAAGGCTGGCCTGAATGT
CCL2-F2	CAGACCTCTGATGCAGGTCC
CCL2-R2	GTGACGGATGTAGTCCTGGC
CCL24-F1	CCTCCTTCTCCTGGTAGCCT
CCL24-R1	AAGGACGTGCAGCAAGATGA
CCL24-F2	AGCCGGAGGTGTAACTCAGA
CCL24-R2	GCTATGTAGACCAGGGTGGC

Mgl2-F1	GGAGCTTCCTGCTCATTCGT
Mgl2-R1	CCCGATTCCCGCCGAATAAT
Mgl2-F2	TGGAGCTTCCTGCTCATTCG
Mgl2-R2	CCCGCCGAATAATCTCTGGT
Mgl2-F3	CGACTGAGTTCTCGCCTCTG
Mgl2-R3	TCTCTTCCCGCTCCAAGTTC
SOCS3-F1	CAAAAATCCAGCCCCAACGG
SOCS3-R1	GGCTGGCTCCACTTGAAAGA
SOCS3-F2	GCGAGAAGATTCCGCTGGTA
SOCS3-R2	CCTCTGACCCTTTTGCTCCT
SOCS3-F3	AGATTGGCTTCTTCCTCAGGC
SOCS3-R3	CCCTCAGACGAATTCCAGGTC
CXCL10-F1	TTCTGAAAGGTGACCAGCCG
CXCL10-R1	CCACTTGAGCGAGGACTCAG
CXCL10-F2	TGAGAGACATCCCGAGCCAA
CXCL10-R2	GAGGCAGAAAATGACGGCAG
CPS1-F1	TCGTGTCGAGGTTTCCAAGG
CPS1-R1	CTGCTTCAATCCCACCTCGT
CPS1-F2	GCCAACAGAGGACAGAACCA
CPS1-R2	GGAGTGTGTTGTCCAGAGCA
CCR2-F1	CAAGCACTTAGACCAGGCCA
CCR2-R1	ACTCGATCTGCTGTCTCCCT
CCR2-F2	AGGAGCCTCTTTGCCTTGTG
CCR2-R2	GAGAGCCCTGCTCACTTTCA
CX3CR1-F1	CTGCTCAGGACCTCACCATGTC
CX3CR1-R1	CTGTTGGTGAGAGCGAGGAC
CX3CR1-F2	TCTGGTGGAGTCTGCGTGAG
CX3CR1-R2	TGAGGTCCTGAGCAGATGGGAA
CD72-F1	GAACTCGTCTGCTCTCAGGC
CD72-R2	AGACACCTGCAGATAGCGAAC
CD81-F1	TCCATGAGACGCTCAACTGT
CD81-R1	AGCTACCACAATGGCTGCAA
CD81-F2	AAAGACCAGATCGCCAAGGA
CD81-R2	TAGTCAGTGTGGTCAGTGCG
Rsad2-F1	ATCGCTTCAACGTGGACGAA
Rsad2-R1	GGAAAACCTTCCAGCGCAC

Rsad2-F2	GATGGTTCAAGGACTATGGGGA
Rsad2-R2	CTTGACCACGGCCAATCAGA
CD206-F1	TTCCCTCAGCAAGCGATGTG
CD206-R1	CCACCCTCCTTCCTACAAGC
CD206-F2	CCATTGCACTTTGAGGGAAGC
CD206-R2	CGTGGATCTCCGTGACACTC

These genes were carefully selected from a meta-analysis of genes most significantly upregulated in M1 and M2 polarized macrophages [206-209]. Primers were designed using NIH nBlast tool against genes of interest specific to *Mus musculus* (house mouse) transcriptome. To ensure quality control all primer sets were evaluated by: NIH Primer-BLAST to ensure no reactivity with the *Homo sapiens* transcriptome. Additionally, primer sets were tested with human cell lines to ensure no activity, as well as in polarized macrophages for predicted outcomes (Table 2). From our primer screen six macrophage markers (*Arg1*, *iNOS*, *Il-6*, *Ym-1*, *Il-1β*, *Socs3*) met the requirements and were selected for future studies (Figure 6B). Primers with the best activity in macrophage transcripts, no-activity in human transcripts and minimal/no background activity without enzyme were selected for further use.

Table 2: Primer Testing

N.D. = Not Detected, N/A = Not tested, NTC = No reverse transcriptase control, Human = Tested against human cancer cells

Primer	CTR	LPS	IL-4	Human	NTC
Actin-1	19.54	20.05	19.34	N/A	39.76
Actin-2	19.15	19.38	19.39	N/A	N/A
Actin-3	18.26	17.62	18.05	32.60	N.D.
Arg-1	35.78	36.52	31.25	38.69	N.D.
Arg-2	35.09	N.D.	31.26	37.31	N.D.
Arg-3	28.89	29.67	27.52	38.69	N.D.
b2m-4	18.92	19.22	18.64	N/A	N/A
b2m-1	24.59	20.53	25.62	38.18	N/A
b2m-2	25.99	24.41	20.92	28.53	N/A

b2m-3	19.06	16.23	21.03	34.06	N/A
CCL22-1	36.96	36.90	34.90	36.07	N/A
CCL22-2	33.12	26.17	32.28	35.01	N/A
CCL22-3	32.11	28.55	29.07	34.18	N/A
CCL24-1	30.76	30.26	27.05	34.79	N/A
CCL24-2	32.68	31.79	29.87	35.11	N/A
CCL2-A	27.82	18.24	28.13	N/A	30.22
CCL2-B	27.88	21.85	28.72	N.D.	N.D.
CCL2-C	31.23	19.42	30.78	35.51	32.96
CD163-A	N.D.	N.D.	N.D.	N.D.	35.18
CD163-B	N.D.	N.D.	N.D.	N.D.	N.D.
CD163-C	37.89	38.51	N.D.	N.D.	N.D.
CD163-D	39.60	N.D.	N.D.	N.D.	N.D.
CD68-1	25.14	24.36	25.53	32.74	N.D.
CD68-2	18.33	17.96	19.42	26.03	N.D.
CXCL10-1	22.27	19.39	25.59	28.39	N.D.
CXCL10-2	26.22	19.19	31.85	33.98	N.D.
Ear2-1	30.22	27.83	24.49	36.89	N/A
Ear2-2	30.43	27.70	24.76	36.40	N/A
Ear2-3	30.14	27.43	24.30	36.42	N/A
Ecm	22.38	22.30	22.10	25.50	N/A
GRAND18-1	32.08	31.72	32.74	26.58	N/A
GRAND18-2	24.10	23.77	24.47	22.08	N/A
hbegf-1	29.79	27.76	23.89	33.31	N/A
hbegf-2	29.46	27.35	23.52	33.10	N/A
hbegf-3	32.21	30.61	26.46	35.80	N/A
hprt-1	26.37	23.20	31.40	33.31	N/A
hprt-2	25.03	24.24	25.80	36.06	N/A
hprt-3	21.39	18.89	36.07	N.D.	N/A
IL-10-1	29.11	21.75	27.36	N/A	N/A
IL-10-2	30.72	22.64	28.42	N/A	N/A
Il-10-3	31.20	22.84	28.52	N/A	N/A
IL-10-A	34.53	27.75	35.64	38.90	N.D.
IL-10-B	34.80	29.40	37.61	N.D.	N.D.
IL-12	34.05	33.85	28.58	39.20	34.24
IL-12-A	34.64	39.32	37.72	34.00	N.D.

IL-12-B	36.08	N.D.	36.07	38.51	35.17
IL-12b-1	34.02	32.47	27.83	N.D.	N/A
IL-12b-2	N.D.	32.35	27.84	N.D.	N/A
IL-12b-3	37.61	33.02	N/A	N.D.	N/A
IL-1b	38.24	26.91	32.44	N/A	N/A
IL-6	37.13	24.53	35.54	38.33	37.58
IL-6-A	33.11	21.80	33.93	N.D.	N.D.
IL-6-B	32.82	20.50	33.05	N.D.	N.D.
iNOS	29.53	27.60	29.75	N/A	N.D.
iNOS-1	35.18	26.18	33.97	N.D.	N.D.
Irf4-1	30.90	30.46	N/A	34.64	N/A
Irf4-2	31.29	27.91	N/A	N.D.	N/A
Irf4-3	30.96	27.90	N/A	37.14	N/A
Mgl2-1	25.55	26.78	23.38	29.56	N.D.
Mgl2-2	24.58	26.86	22.15	30.87	N.D.
Mgl2-3	30.45	33.20	23.63	37.11	N.D.
mif-1	17.12	17.21	16.80	20.22	N/A
mif-2	17.67	17.84	17.30	20.52	N/A
mif-3	17.94	18.23	17.76	20.99	N/A
MRC1	21.52	20.34	27.28	N/A	N/A
MRC1-A	22.59	25.82	20.45	N.D.	N.D.
MRC1-B	27.03	30.02	25.21	38.62	N.D.
MRC1-C	27.36	30.17	25.72	N.D.	37.55
Plagin-1	34.76	36.18	35.01	38.10	N/A
Plagin-2	33.94	35.27	34.04	37.22	N/A
Plagin-3	38.61	38.79	38.52	N.D.	N/A
PPARG-1	35.87	36.87	36.48	33.65	N/A
PPARG-2	37.06	37.58	35.35	36.82	N/A
PPARG-3	35.63	36.86	35.76	34.60	N/A
Retnla-1	36.40	35.89	37.85	35.90	N/A
Retnla-2	35.16	36.67	34.46	38.59	N/A
Retnla-3	35.31	35.67	35.77	33.47	N/A
slc39a1-1	22.66	22.59	22.68	26.32	N/A
slc39a1-2	22.24	22.11	22.28	24.91	N/A
slc39a1-3	23.66	23.50	23.75	27.21	N/A
SOCS3-1	32.96	22.32	33.71	33.24	N.D.

SOCS3-2	28.90	21.85	32.83	33.20	N.D.
SOCS3-3	30.94	23.15	32.11	34.08	N.D.
TGFb	31.74	31.15	31.44	30.63	N/A
tgfb-1	30.27	26.41	21.61	30.63	N/A
tgfb-2	33.48	26.46	26.66	38.94	N/A
tgfb-3	28.09	27.35	25.39	37.69	N/A
TNF-1	38.54	28.47	23.94	N/A	N/A
TNF-2	21.87	27.63	23.88	N/A	N/A
TNF-3	16.05	20.50	24.90	N/A	N/A
TNFa	29.43	20.17	30.42	32.80	37.49
tnlp3-1	26.03	22.21	25.49	28.70	N/A
tnlp3-2	21.78	18.00	21.74	24.82	N/A
tnlp3-3	21.28	17.32	20.87	23.72	N/A
Ym-1	35.70	33.00	24.94	N/A	N.D.
Ym-2	29.73	37.52	N.D.	N/A	N/A
Ym-3	30.82	N.D.	38.94	N/A	N/A

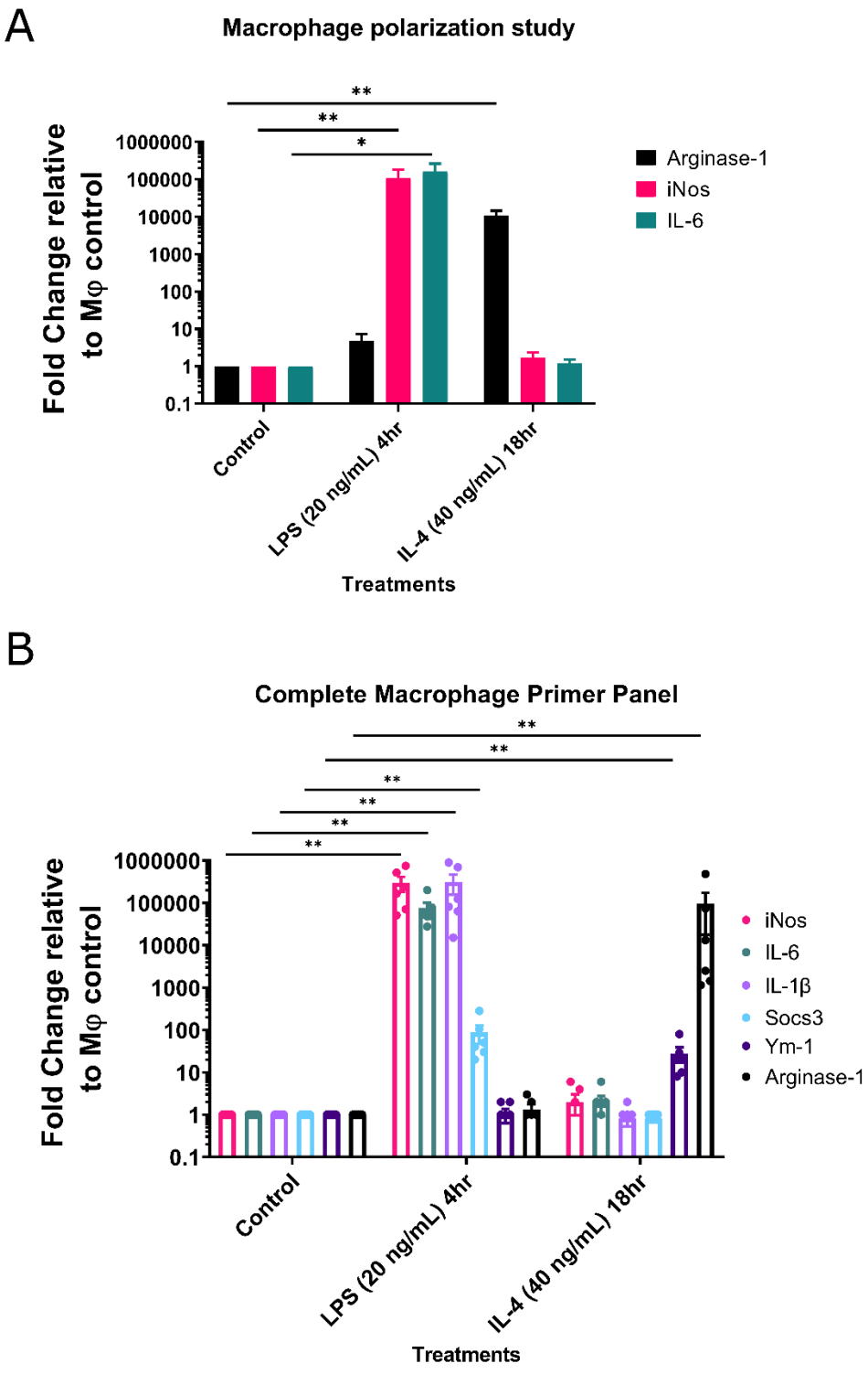

Figure 6: Macrophage polarity studies. Macrophages were stimulated with either LPS or IL-4 to polarize M1/M2 phenotypes, respectively. A) Preliminary studies demonstrating

macrophages can reproducibly be polarized into M1 and M2 phenotypes. B) RT-qPCR of *Arg*, *iNos*, *Il-6, Ym-1, Il-1β, and Socs3* were used to determine macrophage polarity. All results were normalized to baseline macrophages and fold change was calculated using the ΔΔCT method. Treatment groups were analyzed by one-way ANOVA *post-hoc* Kruskal-Wallis test in GraphPad Prism. Mean ± SEM, n = 6, * $p < 0.05$, ** $p < 0.01$, *** $p < 0.001$

Next, we needed to identify the appropriate cell components to include into the co-culture. In addition to macrophages and cancer cells we selected CAFs to represent the stromal component within the TME. CAFs are vital for the paracrine and autocrine cross-talk signaling pathways in NSCLC and are involved in carcinogenesis, cancer progression, extracellular-matrix (ECM) remodeling and metastasis [108]. Furthermore, previous models have forgone this vital component in the context of investigating macrophage polarity in lung cancer. To this end, we sought to build a 3D co-culture model that would incorporate these three cell types. We needed to identify the correct ratio of cell types to use. Previous studies commonly used ratios between 1:1 and 1:5, frequently without justification. However, in our study we relied on studies that demonstrated that fibroblasts typically represent 25% of the cells in the co-culture to be effective as stromal mediators in the TME [210]. Additionally, a previous study interrogated the immune landscape within lung cancer patients by IHC found that in adenocarcinoma, macrophages can represent 5-50% of the tumor structure [203]. We used these findings as a guide for creating our lung cancer 3D co-cultures. Our initial studies investigated the appropriate seeding for macrophages in the co-culture. These studies revealed that ~1:50 ratio of macrophages to cancer cells allowed for effective integration of macrophages into the co-culture system (Figure 7A). We established this model using H2009, but sought to expand this to multiple lung cancer cell lines (Figure 7B). We found that spheroid formation and macrophage integration varied dramatically between different lung cancer cell lines.

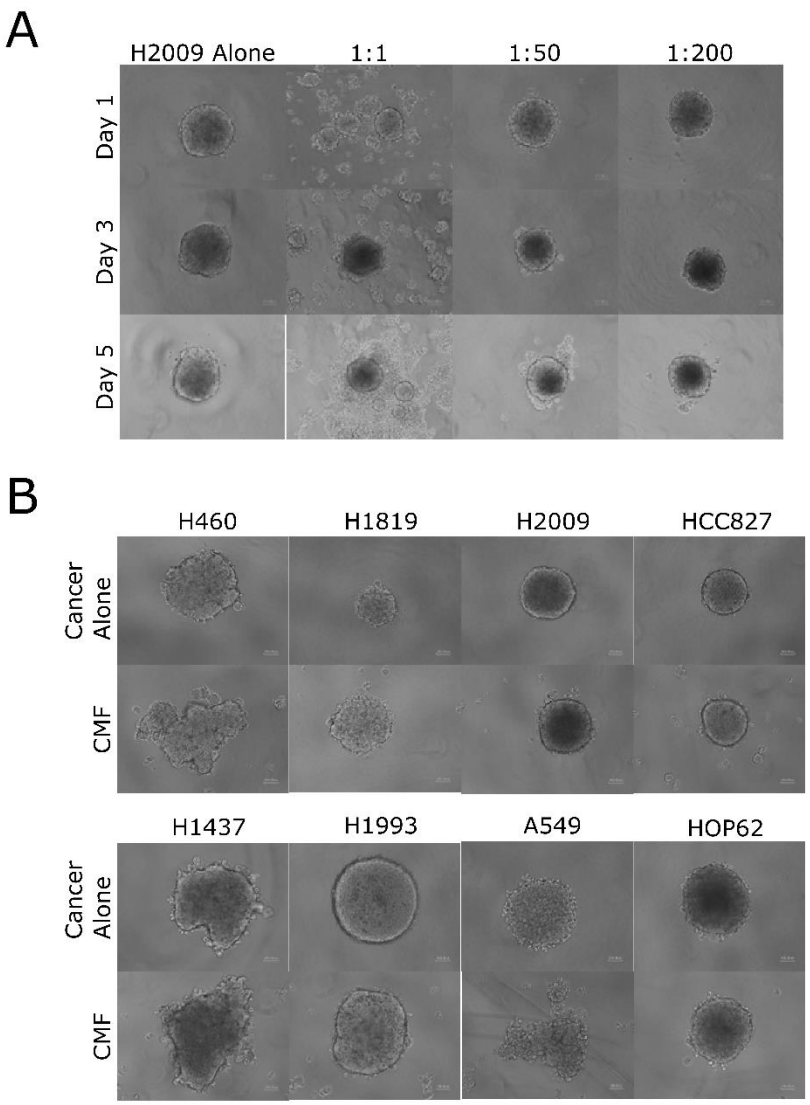

Figure 7: 3D NSCLC Spheroid formation assays. A) H2009 and Raw264.7 macrophages were cultured together in 96 well low-adhesion u-bottom plates and monitored for 5 days. The ratio of cancer cells to macrophages was tested at 1:1, 1: 50, and 1:200. Macrophages out grew biological ratios in culture at the 1:1 ratio. Macrophages were found to be too sparse in the 1:200 ratio cultures. The ratio of 1:50 was found to the most psychological relevant. B) 3D spheroid co-cultures were expanded to multiple NSCLC lines. Extensive heterogeneity was found between cancer cell spheroid formation. (CMF = Cancer cell, Macrophages, Fibroblasts) n = 96.

Due to these inconsistencies, we explored the use of a 2D model, and found that macrophage polarization was similar and the 2D assay was substantially more consistent (Figure 8A). The conclusion was made that spheroid cultures were too labor intensive and inconsistent to provide a robust readout for the project.

Our next assessment was to determine the appropriate timeframe for these co-culture studies. We tested co-cultures employing multiple NSCLC cells for macrophage polarity across multiple time points extending out to 40 hours. We found that at approximately 40 hours, macrophage transcriptional profile was stable (Figure 8C). Additionally, we found that at approximately 80 hours, baseline macrophage transcription begins to vary, and at 96 hours of culture macrophages begin to undergo apoptosis (Figure 8B). Therefore, to preserve macrophage integrity as well as capture polarization within the co-culture, we elected to use 40 hours as the optimal time point to assess macrophage polarity in the co-culture model.

A

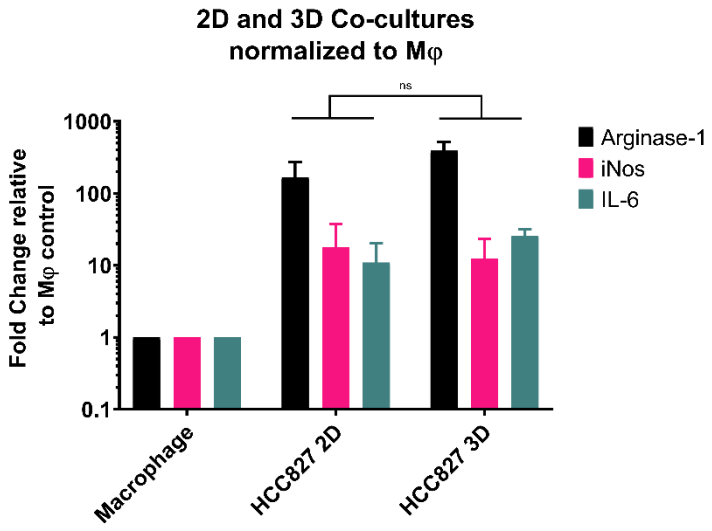
2D and 3D Co-cultures
normalized to Mφ
ns
Fold Change relative
to Mφ control
1000
100
10
1
0.1
Arginase-1
iNos
IL-6
Macrophage
HCC827 2D
HCC827 3D

B

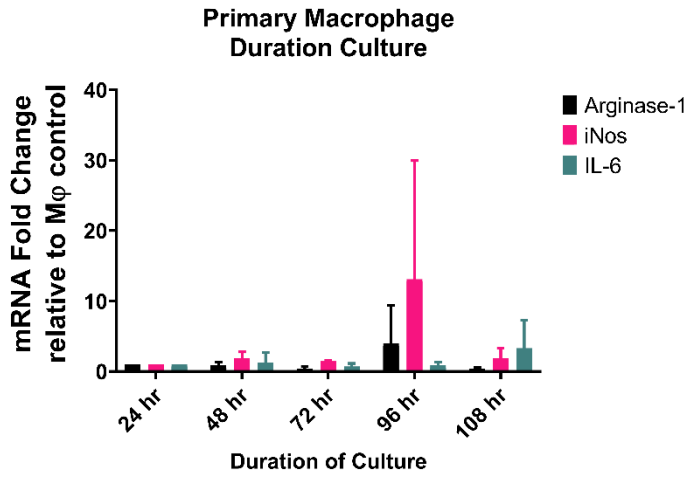
Primary Macrophage
Duration Culture
mRNA Fold Change
relative to Mφ control
40
30
20
10
0
Arginase-1
iNos
IL-6
24 hr
48 hr
72 hr
96 hr
108 hr
Duration of Culture

C

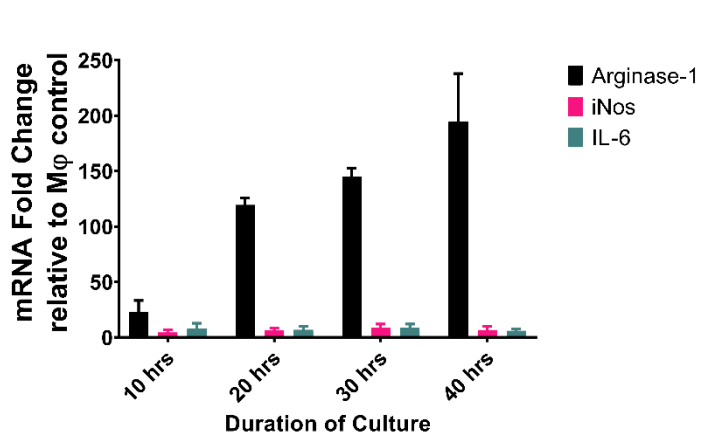
H2009 Co-Culture Timecourse
mRNA Fold Change
relative to Mφ control
250
200
150
100
50
0
Arginase-1
iNos
IL-6
10 hrs
20 hrs
30 hrs
40 hrs
Duration of Culture

Figure 8: *In vitro* co-culture preliminary condition studies. A) HCC827 was used in 3D spheroid and 2D co-cultures and macrophage polarization was compared by RT-qPCR. Two-way ANOVA with a Tukey's *post-hoc* multiple comparison analysis was used to compare 2D and 3D transcripts, n = 2, mean ± SEM. B) Macrophages were cultured in 6 well plates without any stimuli, and harvested at multiple timepoints. Variation in transcription began at 96 hrs. n = 2 C) Macrophages, CAFs and H2009 cells were cultured together in 6 well plates and harvested at multiple timepoints. n = 3, mean ± SEM.

Up until this point in our studies we had relied on macrophages isolated from the bone marrow of C57BL/6J mice in our co-culture model. We wanted to assess whether the genetic background of macrophages could influence the macrophage polarization the co-culture platform. To answer this, we isolated hematopoietic stem cells from FVB and BALB/c mice and differentiated them into macrophages. We found that FVB mouse macrophages used within our co-culture were similar to those seen with C57BL/6J mouse macrophages (Figure 9A-B). Unfortunately, our culture methods were not suitable for BALB/c differentiated macrophages and transcripts from these macrophages in the co-cultures were too poor to quantify. Despite these failures others had reported comparative studies between C57BL/6J and BALB/c macrophages and found that the difference in response to IFN-y stimulation was insignificant between the mouse strains [211]. These data suggest that the phenotypes induced by the co-culture are reproducible across multiple mouse strains.

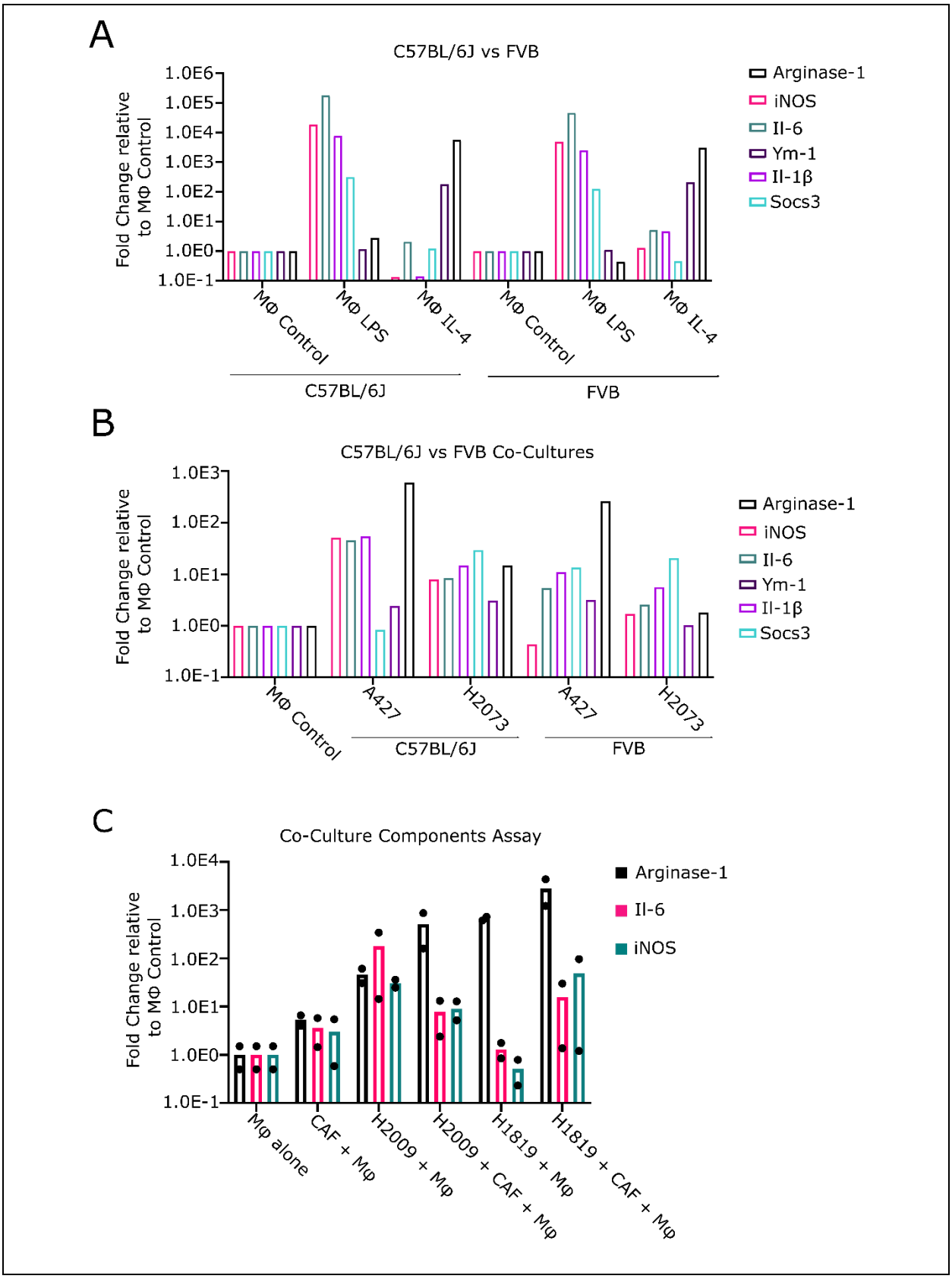
A
C57BL/6J vs FVB
Fold Change relative to MΦ Control
1.0E6
1.0E5
1.0E4
1.0E3
1.0E2
1.0E1
1.0E0
1.0E-1
Arginase-1
iNOS
Il-6
Ym-1
Il-1β
Socs3
MΦ Control
MΦ LPS
MΦ IL-4
MΦ Control
MΦ LPS
MΦ IL-4
C57BL/6J
FVB
B
C57BL/6J vs FVB Co-Cultures
Fold Change relative to MΦ Control
1.0E3
1.0E2
1.0E1
1.0E0
1.0E-1
Arginase-1
iNOS
Il-6
Ym-1
Il-1β
Socs3
MΦ Control
A427
H2073
A427
H2073
C57BL/6J
FVB
C
Co-Culture Components Assay
Fold Change relative to MΦ Control
1.0E4
1.0E3
1.0E2
1.0E1
1.0E0
1.0E-1
Arginase-1
Il-6
iNOS
Mφ alone
CAF + Mφ
H2009 + Mφ
H2009 + CAF + Mφ
H1819 + Mφ
H1819 + CAF + Mφ

Figure 9: Co-culture component assays. A) C57BL/6J and FVB macrophages were polarized with LPS and IL-4 to insure polarization between mouse strain macrophages were comparable, n=1. B) C57BL/6J and FVB macrophages were used in co-culture assays with A427 and H2073 NSCLC lines. Polarization of macrophages by co-culture were comparable between mouse strains, n=1. C) Comparison of dual co-cultures and multicellular co-cultures. RT-qPCR transcriptional analysis of macrophage markers: Arg1, Il-6 and iNos. Cultures are either dual co-cultures (2 cell types) or multicellular co-cultures (3 cell types). n = 2, Mean, p = n.s.

Next, we investigated whether fibroblasts influence macrophage polarization in the context of lung cancer. To address this, we did preliminary studies demonstrating macrophages and fibroblasts cultured together do not influence macrophage polarization, but the combination of lung cancer cells and fibroblasts are vital to establishing the high *Arg* phenotype (Figure 9C). Furthermore, we investigated whether the source of patient derived CAFs can alter the macrophage phenotype. We screened a panel of CAF cell lines, and found the same macrophage phenotype was induced by co-cultures with CAFs from different sources. We found that macrophages cultured with H2009 NSCLC line had equivalent elevation of all three markers. However, the addition of the CAFs polarized the macrophages toward a strong M2 phenotype, dictated by the elevated Arginase expression. Furthermore, we found that macrophages cultured with H1819 NSCLC line presented a strong M2 phenotype and Arginase expression was further promoted with the addition of the CAFs. This demonstrates that macrophage polarity could be modulated depending on the CAF line utilized (Figure 10A). These data suggest that fibroblasts are important to macrophage polarity and the source of fibroblasts can alter macrophage polarization. To investigate this further, we evaluated the phenotype of CAFs used in the co-culture platform. CAFs largely exist in two states:

inflammatory CAFs (iCAFs) and myofibroblastic CAFs (myCAFs). In the context of pancreatic cancer, tumor cells secrete IL-1α, resulting in the generation of iCAFs that secrete IL-6 and granulocyte colony-stimulating factor (G-CSF). These cells propagate inflammation by activating NFκβ and JAK-STAT signaling, leading to activation of immune responses. iCAFs are commonly identified by expression of platelet derived growth factor receptor-alpha (PDGFRα) staining. Alternatively, myCAFs secrete granulocyte-macrophage colony-stimulating factor (GM-CSF) causing polarization of macrophages into an immunosuppressive phenotype, leading to T cell suppression. The predominant marker to identify myCAFs is α-smooth muscle actin (α-SMA) [212]. We used these biomarkers to discern the CAF phenotypes by western blot analysis (Figure 10B). We found that in the CAF lines expression of both myCAF and iCAF proteins were present. Additionally, we submitted these CAF lines for RNA sequencing to interrogate these phenotypes further. We found that iCAF and myCAF gene signatures were present in the CAF lines, but myCAF gene signatures were predominated (Figure 10C). We compared the five CAF lines by performing gene set enrichment analyses (GSEA) and found that extracellular matrix pathways were upregulated in each CAF line (Figure 10D). We then identified genes in the RNA expression data that were differentially expressed (2-fold higher or lower) in any individual CAF line in comparison to the rest of the CAF panel (Table 3). Over-representation analysis of these gene-sets identified several unique pathways upregulated in any one individual CAF lines. However, deeper investigation is needed to decipher larger differences between the CAF lines that could be influencing macrophage phenotypes. The consortium of CAF data argues that CAFs are important in macrophage polarization and can even alter macrophage polarization in the right context of lung cancer.

Table 3: Individual genes of interest for CAF lines

CAF-A

Upregulated: TMEM176B,TMEM176A,GDF10,RPL39P3,A2M,PCSK2,FGL2,ADAMTS8,RP11-307O1.1,PDIA3P2,CFD,HSD17B2,SPON1,PTGDS,CPM,RASL12,TNC,ACKR4,PITX1,CAPG,FGF7,SCUBE1,FBLN1,RARRES1,RASL11A,NKD2,HAAO,KCNF1,KCNJ2,OR7E47P,FGFR4,TMOD1,SERPINF1,SEPP1,RASSF2,MT1M,PSG4,BMP4,TTC28-AS1_3,COX17P1,ADIRF,WFDC1,EDNRB,AKR1C1,C1QTNF9B-

AS1,APOE,USMG5P1,KIAA1644,OLFM1,SLC14A1,GSTM1,ABCA3,ISLR,LRRN4CL,ALDH1A1,DENND2A,PTPRD,SGCD,TCF21,IQSEC3,D4S234E,S100A4,CABLES1,LINC01436,FENDRR,GPX3,TRPA1,NTN1,BDKRB1,TMEM35,CDC37L1-AS1,CYP27A1,PLA2G5,FAM180A,PRKG2,CSDC2,RCAN2,DBNDD1,CYP2S1,FAM131B,DLGAP1,KAZALD1,LINC00578,HR,RENBP,CCL7,LPAR3,PZP,LTBP4,RP11-384F7.2,NR4A2,PDLIM4,RP11-798K23.5,PPAP2C,SHISA3,PLXNC1,C3,USP41,FAM65C,MDK,IL33,RP1-170O19.23,CRLF1,SPTBN4,LINC01140,OLFML2A,RAET1G,GSTM5,CCK,PPAP2B,RSPO2,HOXA6,GALNT15,PLAT,BACE2,ABCG1,MIPEP,GPNMB,ALDH1A3,DCHS1,AQP3,ALDH2,TBX4,ATOH8,OSR2,IQGAP2,SOX9,CXCL6,COLEC12,FOXQ1,CYGB,CECR1,NNAT,FMO2,TNFRSF19,CLDN23,SMAD9,RP4-765C7.2,ST6GALNAC2,KCNJ2-AS1,CLU,BAIAP2L2,CCL13,PF4V1,FAM107B,FAM65B,CDKN1C,MST1R,PLAU,ANO4,SLC40A1,SLC51B,C10orf10,PGF,KCNG2,MYOC,RP11-318C24.1,OLFML2B,SSX2IP,ZFP36L2,ADAM33,RP11-649E7.5,C1QTNF5,EYA4,FAM92A1,MAN1C1,CTC-507E2.2,PPARG,TSPAN2,DIRAS1,SFRP1,CTD-2033D15.2,GALNT18,ANKRD29,SLC38A5,HLA-DMA,STIM2,CPPED1,TMEM150C,ID1,LSAMP,C1QL1,CTSK,RP11-270C12.3,MAF,GRIK4,PEG3,RP11-423H2.3,CXCL12,ITGA7,UCP2,CHST15,PCOLCE2,GPM6B,MAPK10,MT2P1,PALD1,TLCD2,PRCD,RP3-509I19.1,APOC1,EPB41L3,MYOCD,RP11-2N1.2,RP11-206L10.5,LINC00856,RP11-352E6.2,BDKRB2,AKR1C2,ACSL4,ATP6V0E2,GAL3ST4,SLC43A2,CD82,TBC1D19,ADAMTS14,PCDHGB2,BRICD5,AC009403.2,LYNX1,AC109642.1,SLC25A29,FIBIN,RAMP1,MFSD6,DHRS3,FAM150A,AMPD3,NDN,ABCC4,PVT1_1,KCNH2,RAET1E,MFI2-AS1,AC093627.8,PTGES,IL6R,PGD,DTX4,SOX15,FOXF2,DLL4,DKK1,CDH6,LRRC20,CPZ,RP11-1100L3.8,CEP55,MPHOSPH6,MTATP8P1,CRIP1,CAND2,F11R,CORO6,AKR1C3,RP11-90D4.4,RRM2,TM4SF1,ZNF367,FGF9,IL1R1,TNXB,SVEP1,LIF,PRUNE2,LAMA3,QSOX1,PTGER2,FAM47E-STBD1,MASP1,DNM3,SESN3,GPR153,PHYH,GPER1,PGM5,HHEX,CREB5,MARC1,MMD,PALM,METTL13,ABCC6,JUP,MYH11,RN7SL3,RP11-347C12.3,SAMHD1,C1QTNF2,SCARA3,PDE3B,SNN,LXN,PTGS2,CASS4,TYMS,IL15RA,BTBD3,KREMEN1,PTGER3,ACTG2,PCBD1,TOR4A,CYS1,CHI3L2,FHOD3,OR2A1-AS1,PCBP3,ZDHHC14,COL14A1,KNDC1,KLHL13,APBA1,RILP,ABAT,USP18,P4HA3,ABCA8,ZWINT,MANSC1,CPNE7,ASF1B,FAM46C,RPS6KA2,FAM124A,AGT,S1PR1,UPK1A-AS1,PLEKHH2,RP11-404P21.8,SDC1,ANXA2R,ABCC3,RND3,SQRDL,C2,SAMD5,SLC29A1,AP001062.8,MEGF9,C5orf66,LAMA5,CLEC3B,MT1L,TNFSF10,LRRC17,HMGCLL1,TLN2,RNF112,ZNF385A,RP11-597M12.1,PLTP,PTPRN,SYNGR3,SHC2,PIANP,GNG2,SLC16A14,ETV1,MECOM,PKMYT1,FGGY,REEP2,CAMK2N1,TNXA,TCF7,TMEM155

Downregulated:
PCDHB2,PCDHGA12,DBP,ENC1,DDIT4,LAMC2,COL5A2,COBLL1,NMNAT2,NETO2,PRSS23,PHLDB2,APBB2,ARHGAP26,MEI1,LRRC32,FLT1,MTUS1,JPH2,SLC6A9,AC093724.2,TMEM52B,TNS1,MFAP3L,FAM110B,SMYD3,CPA4,COL16A1,LRRN3,POU2F2,PKD2,MAMDC2,RASGRP1,CTD-2269F5.1,AC068522.4,SMCO4,LOXL4,TRIM58,C8orf4,ADARB1,ARRDC4,SHROOM2,AE000658.30,IGF2,ADAMTSL2,SLC39A14,PYCR1,GADD45B,KDM5D,RPL34P33,MEX3B,SPHK1,CDK15,TIPARP,SYNJ2,STXBP2,ALDH1B1,RP11-92C4.6,SPESP1,AFF3,IGFBP3,PCDHGB3,HLA-B,FAIM3,FOXD1-AS1,POLR2J2,ICAM1,VCAM1,TRNP1,KLF7,CCDC74A,TUFT1,TMEM154,LRRC15,SSTR1,NEK7,RP11-265D17.2,BCHE,STAC,ADAMTS4,LGALS9,RNaseP_nuc,RP11-175K6.1,LPXN,SLC16A3,PTER,GOLM1,RBM24,KCTD15,KCND2,GSTT2B,GPR68,GRIK2,DPP4,CAP2,COL7A1,RP11-234N17.1,TNFRSF6B,KLF9,AR,FAM13C,PEAR1,bP-21264C1.2,RP3-423B22.5,PCDHGA9,SGK1,RELN,CXCL8,TLR4,COL3A1,MAP3K7CL,CHRNE,PHGDH,TMEM2,CHIC2,RPLP0P2,STARD4-AS1,BX842568.1,CH507-154B10.1,RP11-715I4.1,AFAP1,PDGFRL,CD4,ITIH5,VAT1L,TPM1,EGFL7,SLC6A6,STEAP3,AMIGO2,LIMS2,AC000032.2,TENM3,FOXC2,ACSS3,NRXN3,CSRP2,LPIN3,STARD4,IL6,TXLNGY,RP11-212D3.2,LINC01133,SH3TC1,HMGA2,PCDH1,SIK1,RP11-599B13.6,FMOD,ADM2,FAP,ADAM19,CHST11,MFSD7,CRACR2A,RP11-758N13.1,ADAMTS6,CRNDE,PTPRF,SERPINB7,BAMBI,AMZ1,ADAMTSL1,SNHG18,NLRP10,KLF2,IL24,CMTM4,HLA-F,AC093850.2,CSTA,KRT19,PSAT1,NOX4,SNTB1,FGF1,PDGFRB,WISP2,SCG2,CD36,LINC00839,CORIN,TTTY15,CHI3L1,MTHFD2,SLC2A1,GREM1,STXBP6,IFITM1,ATP10A,MYO1D,BAALC,IFI27,RP5-1172A22.1,RP11-54A9.1,KRTAP2-3,NLGN4Y,APCDD1L-AS1,TPBG,TERT,CH17-472G23.2,SLC1A1,SEMA5A,PRSS3,SCN9A,HYI,SEPT2P1,THNSL2,WNT5A-AS1,AC079780.3,PLXDC2,G0S2,ITGA1,TNNT2,SEMA3C,MICAL2,CA12,MGP,MME,FOXE1,RP11-400N13.3,DMD,SPARC,THBS2,KCNE4,RP3-430N8.10,OLFM2,ADAM12,IL1RAP,STARD10,B3GALNT1,HSPB3,PTGS1,COL4A2,EIF1AY,ENPP2,CDK6,GATA6,FAM167A,MFAP5,GDF6,SDC2,FAM46A,UBL5P2,LPHN2,TWIST1,ADAMTS12,APBA2,RP11-1151B14.4,EBF1,TINAGL1,MMP1,NTN4,SYNPO2,AC002075.4,MIR210HG,VEGFA,CACNA1H,OLFML1,APBB1IP,LOXL2,TES,RHOJ,COL11A1,NXPH4,SLC12A8,B3GALT2,ANKRD1,NGF,GMFG,DDX3Y,BST2,LYN,NALCN,NTM,RP11-11N9.4,ANKH,COL12A1,OLR1,BST1,SEMA7A,PDGFA,RP11-480I12.2,HLA-DPB1,ST6GALNAC5,RP11-305L7.6,DSP,NUAK1,HES1,CHN1,FAM212B,WNT2,WNT5A,BHLHE40,BGN,LDHAP4,GPR116,TEKT4P2,BEX1,RP11-351I24.3,KCNG1,ARHGDIB,LOX,MEST,RAC2,COL5A1,KIF26B,KCNK2,FLI1,COL15A1,GPR1,TRPC4,CPE,COL4A1,CTHRC1,INHBA,RGS4,PAWR,DEPTOR,SLC38A1,PLOD2,NDUFA4L2,CTB-79E8.3,APCDD1L,CDC42EP3,IL32,MEDAG,NREP,RPS4Y1,TNFSF4,ALPK2,PTX3,COL5A3,IGFBP7,CARD16,FBN2,CSGALNACT1,SERPINE2,KRT8,RPS4Y1,CTA-276O3.4,OXTR,SERPINB2,SULF1,EDIL3,CDH13,ITGA11,SRGN,RP11-563H6.1,KRT18

CAF-B

Upregulated: TERT,RP11-545D22.1,CXCL8,COL11A1,APCDD1L-AS1,CSGALNACT1,RP11-323N12.5,APCDD1L,ITGA11,SERPINA9,AC079780.3,DSP,SHROOM2,NOX4,U3,TFPI2,PCDH10,SERPINE2,TFAP2A,IL24,LRRN3,CTB-79E8.3,CXCL1,POU2F2,AMZ1,COL15A1,BEX1,GRIK2,OPCML,SPHK1,FMN2,IRX3,AC093850.2,GPAM,PTGS1,Metazoa_SRP,EGR2,COL5A3,COL22A1,OXTR,MSR1,SNORA73B,RP11-328N19.1,SPDL1,AMIGO2,UBL5P2,CTHRC1,GPR116,BCHE,CTD-

2196E14.7,NREP,SLC6A6,BAALC,HMCN1,INHBA,GPR115,FOXE1,HLA-F,ANKRD20A5P,PRR5L,IL32,SHOX2,RP11-244F12.2,GREM2,STARD10,MYOCD,NLGN1,RAC2,DSG2,ADAMTS4,TNFSF4,EDIL3,FAM196B,NALCN,APBB1IP,KRT8,AC017002.1,PTX3,COL5A1,BHLHE40,DACT1,AC008746.5,ANKRD44,NETO2,NAMPT,CYB561A3,RP3-512B11.3,FAM13C,NDUFA4L2,ANKRD1,KCNK2,CD4,MEDAG,SOD2,RP11-395G17.1,CCL11,IGFBP7,C5orf46,LINC01119,OLFML1,FOXD1-AS1,AP000695.6,ELFN2,OLFM2,LOXL3,CDH2,SRGN,IFI6,ANKRD30B,SCARNA12,GPR68,IL1B,CSAG1,FBXO32,LIMS3L,STK38L,CHSY3,LIMS3,FER1L4,RP11-480I12.2,SCUBE3,ADAMTS6,IL11,CYP4F35P,CRNDE,ADCY4,ZC3H12A,PLOD2,C1QTNF6,RP11-474G23.2,ANKH,PTGFRN,IFI30,PAPPA-AS1,CTSS,LRRC15,LINC01021,FZD8,TLE4,FAM46A,UBL3,LPXN,PCDHB2,NEFL,COL16A1,KIAA1549L,SPOCK1,SNRPGP15,PLA2G4A,NAMPTL,RP11-65J21.3,AGTR1,LINC01444,AC003092.1,C11orf96,PPAPDC1A,TMEM2,WWC3,IER3,RP11-298I3.5,SAMD11,CCDC85A,STARD4,MYO1D,PCDHGA9,CA11,LDHAP4,GPR183,TLR4,PCDHB16,MME,KIF26B,TPM1,COL7A1,DNM3OS,KCNAB1,TRGV7,AC020571.3,RELN,C7orf60,EBF1,RN7SL659P,TNFAIP3,ADAMTSL2,SPESP1,STARD4-AS1,PDGFC,IFI27,TES,RP11-11N9.4,HEPH,AFAP1,AP000695.4,DOCK10,PTGS2,RP11-183C12.1,MMP1,SMCO4,RP13-608F4.5,SEMA3C,RP11-295P9.3,PCDHB8,TRIB2,MIR210HG,TIPARP,ARHGEF19,LDB2

Downregulated: ATP2B4,IL6R,NPC1,CSPG4,RP13-228J13.5,EHD1,AC007560.1,RP11-14N7.2,ARSJ,SCN4B,PRDM6,HMGA1,NFATC1,PTGES,RP11-423H2.3,FAM49A,MAP3K5,SORT1,SLC7A11,ELTD1,FAM132B,RPL39P3,CCDC113,ARHGEF34P,PCSK5,ATP9A,PDE9A,ARHGAP28,H19,ARVCF,ADM,LXN,BHMT2,WFS1,BAG2,HAAO,IRAK3,STMN3,FAM65B,TMTC2,ZFP36L2,CCDC8,HIGD1AP1,MFGE8,BAIAP2,SDC3,LRP3,CYB5A,PLAU,WISP2,PRKG2,GPC1,PMP22,AE000658.30,PSEN2,SLC7A8,FAHD2B,ABCG1,IL15RA,KDM5D,NEDD4L,C4B,BDKRB2,PLAT,MYH10,MRGPRF,ID4,TPD52L1,ENSAP2,AKR1C1,MT1M,DNASE1L1,HHEX,IGFBP6,MIPEP,PMAIP1,SCARA3,ENDOD1,IGFBP5,TRHDE,D4S234E,VCAM1,HLA-DMA,CDK18,NPEPL1,LTBP4,FBXO27,GRASP,PSG1,COL4A5,IGF2,MT1A,MXRA5,CLDN23,SH2D5,KCNF1,STC2,SPON1,ABCC4,STXBP2,TINAGL1,CHST15,AC002398.12,TSPYL5,HBD,PPAPDC3,ADAMTS5,SMAD3,CTD-3157E16.2,DIRAS1,ME1,PDLIM3,RARRES3,CLIC3,ADPRH,ATF5,MALL,SLC12A7,DENND3,C1QTNF5,POSTN,ZFPM2,ADAM23,HAPLN3,CYSTM1,SLCO3A1,FYCO1,TUBA4A,BX842568.1,C10orf54,RP11-715I4.1,CPNE7,PCDHGA11,MEIS3P1,MDGA1,TRIB3,SLC43A2,CLEC2B,CDKN1C,CAMK2N1,ANGPT1,RPS10-NUDT3,TCF21,CTD-3157E16.1,PDPN,FOXF1,FAM65C,ARHGEF35,LRCH2,MPHOSPH6,LYNX1,ADH1B,RP4-545C24.1,FMO2,ANKRD29,ETS2,RND3,RASSF2,STK32C,SNORD17,RP11-212D3.2,ARHGEF5,PPL,GPR126,PLXNC1,ACKR4,PCDHGB5,RGN,BMP2,TXLNGY,HSD17B2,AGT,ACEA_U3,SERINC2,SOCS2,FAM46C,CRIP1,DENND2A,CCND2,ERAP2,AC109642.1,SEMA3F,ITGA6,HHIPL1,PRUNE2,SLIT3,RBM38,SUSD1,PRSS35,PGM5P4-AS1,GSTM5,MFSD6,EPHB2,GFRA1,CKB,SDC1,WARS,ECHDC3,MMP23B,DBNDD1,QSOX1,ADAMTSL4,MYEF2,NXN,IL13RA2,KISS1,DTX4,PODN,CDIP1,CCBE1,RAB11FIP1,CPPED1,OR2A20P,SLC2A8,TTTY15,DAPK1,MEST,SHANK2,SYBU,FIBIN,IMPA2,EFNB2,EIF4EBP3,PCSK2,ZNF702P,NLGN4Y,PTGER2,EDNRB,MATN2,PRICKLE1,DKK1,PGD,SNCG,C4A,SLC40A1,PCBP3,OR7E47P,NDUFA4,MAF,RPS27P29,FZD6,TXNRD1,AP1S3,SEPT2P1,CEACAM19,SLC29A1,SOCS2-AS1,SLC25A4,SPINT2,IL12A,PLA2G5,KREMEN1,SEMA3B,RGCC,PLXDC2,FAM150A,AHNAK2,TP73-AS1,RP11-318C24.1,TMTC1,RASL12,GSTM1,TNC,AC092066.1,PCBD1,TNFRSF6B,HSPB3,VAT1,CASS4,ADAM33,C10orf10,C9orf64,EIF1AY,SESN3,FHL1,EYA4,CHI3L1,CHAC1,ACOT7,CH17-13I23.3,CREB5,CTD-2033D15.2,CPA4,CHRM2,CYP2S1,OR2A1-AS1,FGFR4,GDF10,CD36,ACVRL1,APOE,PVT1_1,LRRN4CL,SLC7A5,RP13-582O9.7,IGFBP2,TNXA,CLU,ANK2,GNG2,OR2A9P,CTSH,MAOA,MAN1C1,GALNT6,SULF2,PTPRN,CES1,ACAN,RP11-2N1.2,LSAMP,CLEC3B,FAM129A,COL14A1,PPARG,DDX3Y,FHOD3,LINC01436,ITIH5,BCAM,GALNT15,PITX1,FXYD1,TOR4A,KRTAP1-5,DOK5,PDE5A,COLEC12,C1QTNF9B-AS1,SOX9,RRAD,CYP27A1,TMEM35,OCIAD2,UCP2,RNase_MRP,FGL2,SYNPO,LAMA5,RASL11A,SLC38A5,RP11-384F7.2,ALDH1A3,FABP5,PCDHGB4,PVR,PTGIS,VLDLR,KCNJ2,LIMCH1,GAL,RARRES1,BDKRB1,FENDRR,CECR1,MT2P1,PSG4,OLFM1,BMP4,SYNGR2,NAALADL1,ELN,ATP6V0E2,CTD-2540B15.13,RHOD,CRABP2,TNXB,RP11-270C12.3,RN7SL3,SLC43A3,ZSCAN18,GJA1,TIMP3,CSDC2,SLC39A4,TBX4,ALDH1A1,EPDR1,ISLR,RP11-307O1.1,RDH10,EPB41L3,ITGA7,DHRS3,PAX8-AS1,RPS4Y1,GPRC5A,TMEM176A,GPR133,CPZ,TMSB4XP2,S100A4,FBLN2,FBLN1,SGCD,TMEM176B,FAM180A,LINC00578,CFD,INMT,BACE2,PDLIM4,ACTG2,ASS1,ALDH2,ADAMTS8,RAMP1,USMG5P1,NDN,MTATP8P1,SEPP1,GPNMB,GPX3,SERPINF1,CAPG,RPS4Y1,ADIRF,WFDC1,A2M,PTGDS,ITGBL1,FGF7

CAF-C

Upregulated: IGF2,PSG4,RP11-307O1.1,KISS1,AC132217.4,CPXM2,MT1XP1,GNG5P2,RGCC,S100A4,RPS4Y1,GSTM1,LRRC15,C7,SEPT2P1,FGF7,ST7-OT4_1,GPNMB,PDLIM4,RP11-212D3.2,FAM167A,FBN2,COL10A1,RP11-110I1.5,RP11-563H6.1,EFNB2,FHOD3,ITIH5,LINC00578,AC134873.1,ALDH1A1,SULF1,PLCB4,CAPG,GAL,TRBV12-4,AC138623.1,AE000658.30,RP3-430N8.10,PVT1,WNT5A,C5orf38,CLIC6,MXRA5,RPS4Y1,IL24,ITGBL1,USMG5P1,WFDC1,RP11-566K11.5,RP4-765C7.2,TMEM176B,PSG5,CLEC14A,PLA2G5,FAM180A,MMP3,MT2P1,LRRN4CL,RP11-498E2.9,CTB-79E8.3,ST6GALNAC5,LINC00460,TFAP2C,CORIN,CHN1,HIST2H3PS2,SERPINF1,RP11-585F1.2,FAM105A,AC092299.6,RP11-772E11.1,DIO2,BHMT2,GABBR2,TRBC2,SNRPGP2,RP11-90D4.4,SCG2,RN7SL738P,GFRA1,PAX8-AS1,DUXAP8,FAM46C,FMO3,ISLR,MME,RP11-480I12.2,RP3-423B22.5,HMGN1P18,MCTP2,RDH10,TRHDE,FAM225A,TMEM176A,RUNX3,FENDRR,ACTG2,FAM84A,IL32,CHRNA1,NTF3,NFE2L3,DLEU1_1,RP11-392P7.6,PTGDS,NTN4,NLGN4Y,SEMA6A,BST2,RP11-131M6.1,PRICKLE1,TMEM178B,LGALS9,DCHS1,SCARA3,CTSK,CH17-

472G23.2,RASGRP2,POSTN,IGDCC4,COL15A1,INMT,FAIM3,GALNT15,DDX3Y,CRISPLD2,RP4-669L17.4,APCDD1,FBLN1,RP11-982M15.2,ICAM5,GSTM5,PLXDC2,COL8A2,USP44,TNFRSF6B,LINC00565,SLC7A11,SGCD,SMAD5-AS1_1,THNSL2,F2RL2,TENM3,EMB,SCARNA10,WNT2,SERINC2,RN7SL3,SLC38A1

Downregulated: FGF18,RSRC1,MEF2D,CTA-268H5.12,CDK16,IL6R,RP1-130H16.18,RP5-878I13.2,AC007041.2,RP11-927P21.1,RPL34P6,B3GNT4,RP11-152N13.5,RP11-33E12.2,LINC01011,EEF1A1P12,ATP6V0A2,PA2G4P4,TTLL7,RP11-33N14.3,RP11-160E2.17,RP11-508N22.13,SDCCAG8,PLEKHA4,PARN,H3F3A,RP11-334L9.1,ZBTB45,ERCC4,HNRNPKP4,AC005077.9,PER2,CRELD2,PAPSS2,POU2F1,PHF8,RPL34P18,TMEM194B,SLC16A13,CCNE1,CSF1R,AC010761.6,RP11-856F16.2,PARD6A,KIFC1,PPIP5K1,NEK1,KLHL7-AS1,C5orf17,HIST1H1B,KIAA1107,FBXW7,NPHP3,SUN1,RP11-548B3.3,RPL13,RP11-49I4.3,RP5-999L4.2,RP11-432J24.5,MCF2L,RN7SKP78,PPP1R9B,STAT3,RP11-169K17.3,TUBD1,NPHP4,LSM11,MAP4K5,TG,DBH,CRYGN,PDK4,C6orf57,NAB1,RP11-288L9.1,LINC01091,PTPRD-AS1,RP11-95F22.1,COL17A1,KDELC2,MOXD1,PUS3,ELMSAN1,RPL7P47,UBE3B,PCSK5,MEIS3,RAB24,FAM96A,RP11-187A9.3,PKMP1,TDO2,CLASP2,RP11-395A13.2,C15orf38-AP3S2,AHI1,HOXB4,IQGAP3,TYSND1,AC007879.2,ALDH8A1,ADIRF-AS1,RP11-529H20.3,RP11-543D5.2,BMP5,LRRC34,AC093627.12,PAM,C22orf46,CECR5,RP11-230C9.4,XKR9,LINC00526,GNG10,ING4,BTBD8,RP11-337C18.10,ATRNL1,GOLGA8H,RP11-575L7.8,KLHDC7B,ARHGAP6,MTHFSD,ATXN1L,LINC01106,LGALS3BP,SYVN1,LINC00920,RP11-342K6.2,ADCY5,CYP51A1P1,CBR3,MAP3K2,PRMT6,MXD3,VEGFB,HMGN2P5,HSP90B2P,ST13P15,SIN3A,CNTLN,GPR89B,RP11-34P13.8,RP11-112L6.2,HAUS6P1,PRKAR2A-AS1,C10orf35,ZNF224,RP11-490H24.5,FAM102A,CTD-2537I9.18,CNN2P9,AGPAT5,CTD-2561B21.7,ALPK1,RNPC3,BCL2L15,EEF1A1P4,HNRNPF,SPIN4,RP11-615J4.4,RP11-159G9.5,RP11-384K6.2,C1orf228,GCC2,RP11-517I3.2,RP11-391L3.1,PLA2G6,IL18BP,ICK,RUFY2,NCK2,ZNF525,GP1BB,RP11-661A12.5,MADD,RPS2P55,ITPRIP,ZNF718,RFC2,PRTFDC1,PCIF1,COG2,TOB1-AS1,DDX11-AS1,TREX2,TXLNB,SMARCD2,ERAP1,WWTR1-AS1,ADAMTS7P1,RP4-550H1.7,RBP4,LINC01431,AP1G2,RP11-384C4.3,COL4A2-AS1,MMP16,PSMG3,MOB3C,RP3-417G15.1,LLNLR-284B4.1,RP11-34P1.2,VASH2,AC002310.12,LINC01266,RPS6KA5,LXN,RP11-94I2.4,CTC-512J12.7,GAPDHP1,CTD-3105H18.16,CEPT1,ALPK3,FN1,C4orf3,YEATS2,RP11-109N23.6,RP6-105D16.1,RN7SKP150,RP3-465N24.6,RP11-867G23.13,WDR91,LAMC1,LL0XNC01-116E7.5,TMEM164,UHRF2,CSRP2,RP11-738E22.3,RMND5B,PRKAR1B,C11orf57,ZDHHC23,AP003068.12,RP11-123K3.4,FAM8A1,C14orf1,TTC19,CNTN5,DAPL1,AC016577.1,LRTOMT,ABHD5,FCHSD2,ZNF700,CTC-436P18.3,RP11-401N16.2,RP11-353N14.7,BACH2,ATP8B3,NEO1,XX-FW83128A1.2,CCDC36,RP11-2C24.3,RP11-331F9.4,RP4-584D14.6,SFRP4,DNHD1,FAM168A,P2RY1,Metazoa_SRP,ZBTB8OSP2,ZNF140,KPTN,RP11-624D11.2,RP11-79P5.9,KIAA1683,APOBEC3G,SLC38A2,AGAP6,FAM151B,ZCCHC2,PLCB3,AC004076.9,RP11-347C12.12,PARP8,SYT16,MIR6080,AC015987.1,CTC-340A15.2,ULK4P2,GORAB,KBTBD3,PCMTD1,DBNDD2,OR7E7P,AC073130.3,BX470102.3,RP11-972P1.11,RP11-84A14.5,ADO,CH507-42P11.8,RP11-222K16.1,RP11-320A16.1,RP11-5O17.1,RP11-529H2.2,EEF1A1P6,KLRG1,SERTAD4,ST3GAL1,LINC00662,SLX4IP,RP1-178F10.1,BAG1,CNBD2,PBX1,C16orf70,KIAA2018,CHCHD2P2,CPQ,NRSN2-AS1,WDR86,RP11-20J15.5,SEC24B-AS1,SNX25P1,ARHGEF1,LDHA,TBC1D2B,RP11-532L16.1,MESP2,KATNBL1,DDX17,ZNF571-AS1,CTD-2207P18.1,RXRB,MTHFR,FAF1,RP4-545C24.1,RP11-103H7.5,TFAP2A-AS1,LINC00342,HAND2,CEP63,FAM208A,NUCB1,RP11-799B12.4,LMBRD2,RP11-697E2.11,FANCA,SULT4A1,STS,P4HA1,RP11-967K21.1,RP11-34P13.14,DKFZP586I1420,NUSAP1,MBD4,NBL1,RPP21,ATP10A,AACS,ZNF646,RP1-59D14.1,PCDHB12,IL4I1,CEP162,CTC-332L22.1,ANXA10,PIN4P1,RP11-244H3.1,CTD-2382E5.6,CARD8,KCNH1-IT1,ERP29P1,HEY1,TOPORS-AS1,PDIA2,DRD4,RP11-723O4.9,CACNB4,RP11-603B24.2,GK-AS1,SMTNL2,FAM156B,WASH4P,RPL5P3,RP11-932O9.8,PYROXD2,FBXO42,IQCB1,C15orf57,PSMC1P1,CTD-2154I11.2,KCNN4,TUBGCP4,PAX6,RP11-268J15.5,BIN1,LRRC23,NFATC2,KLHL30,CTC-347C20.2,USP51,AC093106.5,WDR37,ABBA01017803.1,PLAG1,PLEKHH2,CCDC12,RP11-932O9.7,CTD-2587H24.5,USP31,ADAMTS7P3,MSRB2,NME5,RP11-131M11.2,RP11-923I11.8,FIGF,C2orf82,RNASE4,EEF1A1P19,RPL36AP45,MOK,LZTFL1,CCDC40,NDUFB5,ATG16L1,CUEDC2,SLFN11,RP11-420A23.1,HERC2P8,TRAF5,CCDC53,PRSS51,RP4-747G18.5,KB-431C1.4,FSTL3,PHF10,MESDC1,DLX1,NME2P1,CTC-559E9.8,RP1-224A6.3,MSH5,RP11-299H21.1,SMIM3,MAGI3,GABPB2,RP5-907D15.4,RP11-155D18.12,MLLT4,THUMPD1,EDA2R,MANF,CEP55,CXorf57,RP11-512M8.5,AC092155.1,LNX2,TDRD9,MARCH2,RANBP3,MBNL3,AC069155.1,CTB-33G10.6,EIF3LP3,EBP,BUB1B,CKLF-CMTM1,PPM1AP1,TBC1D3C,GPR89A,TMEM256,CALHM2,RP11-553P9.1,AP006216.10,DUSP2,ZNF250,CTD-3185P2.1,PGM5P2,RMND5A,CCDC107,PCYOX1L,PLA2G1B,Metazoa_SRP,DIO1,ZFX,EIF4A2,DCXR,UXT-AS1,IL31RA,GABBR1,ING1,GS1-257G1.1,RPS2P7,SRSF4,COMMD2,CTD-3193O13.1,FGD5,FKBP6,NDUFV2-AS1,RIMS3,GPSM3,EBI3,ZNF254,RP11-797A18.6,VEPH1,CTSA,DYNLT3,RP11-90H3.1,AC055876.1,SS18L1,SEPHS1,PHF3,ACAD11,AP000662.9,MRPS16,ZNF449,RP13-216E22.4,PTP4A2P2,PMS2P3,PRDM5,ANKRD55,MBD2,MFSD8,RP11-67L2.2,LRRC75A,AKAP13,SUCLG2,B3GNT9,JMJD8,RP11-158H5.2,TSC22D1,ANAPC4,CYP27B1,RP11-5C23.1,LINC01003,AC026271.5,STAU2,TNFRSF8,ATP6V0D2,VLDLR-AS1,JARID2,ZNF667,LIAS,AC074391.1,CSGALNACT2,RP1-90L14.1,C21orf49,RP3-395M20.12,RP11-395P16.1,IL1A,ZBTB14,TFAP2E,PEBP4,ABCB6,LRRC37A,EMR1,ZSCAN5A,FUT4,CTB-36H16.2,LINC00271,OARD1,RP11-321A17.3,TSLP,ELF2,CTSF,NLRX1,S1PR5,SRR,C4orf32,RP11-137H15.3,RP11-5A19.5,LURAP1L-AS1,AC005253.4,RP11-95I16.4,CDK11A,RP11-887P2.3,ZNF699,RP11-175I6.1,TMCC3,STX1A,HSD3B7,BCL2L11,LRFN3,RP11-644F5.11,RP11-295D4.1,AIM1L,ERI2,C1orf101,DKKL1,TRAM2-AS1,TRDMT1,IGLV5-52,LYPLA2P1,RP11-635N19.1,ZNF285,RP11-262A16.1,AC011530.4,TM2D1,RP11-338K17.10,AC107081.5,TARBP1,HSF2,RP11-577H5.1,RP11-342I1.2,SKI,ACTR3B,XRRA1,AP000254.8,LINC01347,RP11-537E18.1,CTC-336P14.1,CENPC,ADCY6,LRRC37A2,CDH11,RP11-155G14.6,FXYD6,RP11-332H14.1,KCNE1,RPS3AP5,PDE1A,LA16c-

313D11.12,EID3,SIK1,TLL1,DHRS12,GIPC3,PITX2,ZNF90,SUSD4,ZNF277,MAGI1,RP11-
347C12.4,GLOD4,AP000695.4,CYCSP52,TTC23L,PPARGC1A,CYTL1,MMP28,RP11-69L16.5,ZBTB25,ACBD5,CTB-
96E2.10,FOXP4-AS1,RP11-185E8.2,RN7SKP255,CHKB,SLC39A13,RASA4CP,MIR31HG,GEM,RP11-
140I16.3,RNF13,FAM209B,TBC1D8B,CTD-2547L24.4,HNRNPA3P10,SLC25A21,PGM2,AC007246.3,PCDHB16,RP3-
425P12.4,PHKA2-AS1,RP11-96C23.10,TSPAN14,EPHB3,ABCA7,RP13-1039J1.4,KRTAP1-1,MARCH3,CTC-
756D1.2,SMAP2,ATP7B,ENPP6,MAST4-AS1,RP11-798K3.2,CTC-246B18.8,TPCN1,MYC,AC007229.3,RP11-23N2.4,RP11-
755F10.3,CH507-145C22.1,RP11-231C14.4,MDP1,NUDT4,CTC-534A2.2,PFN4,GUSBP3,CATSPERG,RP11-574K11.29,RP3-
331H24.7,RSPO1,H1FX,METTL23,OGFOD3,NT5DC1,MAPK7,C19orf33,RP11-46H11.12,SNHG20,NFIL3,CTC-
429P9.4,LRRC57,ERV3-1,AP000320.6,ABCC6P1,RP11-33A14.1,MMS22L,TRMT11,RP11-449P15.2,PAXBP1,ULK3,STK19,RP11-
110I1.14,OSGEPL1,RN7SL130P,LINC01341,MIPEPP3,C9orf72,SYT15,RP11-
575F12.3,TMEM38A,TOP3BP1,AKT3,MCL1,LYRM4,RP13-128O4.3,LINC00324,RP11-308D16.2,RP11-
1055B8.8,NTSR1,ZNF420,DSN1,IBA57,KCTD18,FAM179B,GALNT1,C17orf49,LINC00339,FAM149B1,DAB2IP,CTD-
2207O23.10,RP11-131L23.2,NPHP3-ACAD11,UIMC1,NEK6,PIGL,CASC2,RP11-
130L8.2,GPX7,MAP3K3,LINC00087,C19orf57,GUCY1A3,IRAK2,PEX1,OXR1,CIRBP-AS1,AC138649.1,PGK1P2,RP1-
40E16.12,ESYT3,SKIDA1,RP3-508I15.9,ARHGEF10,AC012487.2,PACS1,OLFM2,DPYSL2,RP11-626G11.4,RP11-
388C12.1,EPB41L4A,CHST15,MAGIX,CTB-55O6.10,RP11-
599B13.8,ZNF697,GSTM3,GTPBP3,INTS3,ZBTB45P2,CCNI2,RPS3AP49,MAST1,ZNF548,RHOQP2,ABL1,RP11-
638I8.1,SH3BP2,MIR155HG,PKMYT1,RP11-221J22.2,DNAJC25-GNG10,IFFO1,HTRA2,L2HGDH,ACSL5,RP11-787I22.3,RP11-
326C3.7,TNFSF18,TRIM66,RP11-61L23.2,SEPSECS,WDFY2,BTAF1,THEGL,PTPRJ,ASF1B,CTD-2007H13.3,RP11-
516A11.1,RP11-736K20.5,BMI1,ZNRF2,ANKRD30BP1,CTD-2643K12.1,KANK2,PHACTR1,UNC13D,KCNC1,ZNF414,ZFP69,CTC-
548K16.2,KLC4,TMPO,AC008063.2,Metazoa_SRP,RP11-
681H18.2,ELP5,AC009299.5,DIEXF,ADCK1,SPEG,TENC1,NNMT,S100PBP,RP11-769O8.2,RP11-
555M1.3,SFI1,SPTBN4,FBXO21,CTD-
2260A17.2,MAST4,CHST14,CYGB,ZNF81,TMEM175,RALGDS,RAB33A,CYCSP34,HIST1H2AL,SEC14L6,ASPSCR1,RP11-
218M22.1,WDR76,LPCAT3,THG1L,TAMM41,TRIM69,RP11-885N19.6,DPY19L4,MYO19,UFL1,SMPDL3A,AC005519.4,RP11-
335O4.3,TRMT10B,LYSMD3,MAFG-AS1,PHACTR2,CFL1P1,RP11-482H16.1,CTA-363E19.2,CCDC121,FAM118A,CTD-
2035E11.3,CTD-3195I5.5,NR3C1,GLTSCR2,PTN,ANKRD49,RRP8,SEL1L2,PRKG1-AS1,ZNF625,CLDN12,RP11-
264I13.2,VCPKMT,GPR150,RP11-677M24.1,TRIB2,PXMP4,UBXN7-
AS1,CENPJ,RAD17,RGS11,METTL21A,CDC45,CRYAB,GAD1,ARHGAP26,PLEKHM1P,RBBP8,RNF38,HLCS,ADA,HELLS,CA9,C
CDC74A,MIDN,C21orf67,RP11-104G3.7,AC067940.1,UPRT,GRTP1,MT-ND1,WDR5B,CHST2,SMAP1,RP11-
498C9.3,NEFH,PGM2L1,AC069368.3,PDPN,DIAPH2,DOPEY2,KBTBD8,RP11-
706P11.2,AC019181.3,SIM2,PCDHGC5,SPATA5L1,PLA2G4A,MEPCE,ADAMTS4,EGLN3,ZNF804A,RP11-
598F7.6,C1QTNF3,RP11-104N10.2,SLC6A15,ZNF236,RP11-795F19.5,RP11-613M10.6,CTD-2201E18.5,CREM,RP11-
796E2.4,EFCC1,CGRRF1,P2RX1,RND2,TXNP4,AC005609.19,RP4-798A10.4,RP11-793H13.8,NOL3,SVILP1,RP5-
875H18.9,AC022201.5,RP11-283G6.3,RHOF,CTC-518P12.6,KANSL1L,RAET1G,RNF167,EVI2A,RPL14P3,PSAP,SWSAP1,RP11-
175P19.2,ITGB7,CLPB,UGGT2,RPSAP15,RP11-299L17.1,RP11-536C5.7,AL672183.2,JADE3,BAMBI,HOOK2,RP11-
480I12.5,RP11-888D10.4,HNRNPA1P8,RP11-501C14.7,RP11-430E17.1,RP1-117B12.4,PCGF6,SETD6,HAUS6P3,CTD-
2334D19.1,SLC25A36,NUDT18,ADCK3,CCL20,RP11-
110I1.12,INAFM1,LPAR3,KRT86,ZNF540,KLF9,RPL17P50,LRRC45,ITPR1,JUN,RAB40B,CASP9,COG3,HESX1,AP000568.2,XPN
PEP2,RP11-297N6.4,IFIH1,SLC2A14,ADAMTS10,SEC14L2,KIAA1324,ACACB,LINC01002,C6orf136,FEZ1,RP11-
161M6.6,TEF,OXER1,TRPC3,RP11-461A8.5,CTBP1,C19orf54,LEMD3,PTCD2,CRYM-AS1,ZNF281,ANKRD46,FBF1,LAG3,ZEB2-
AS1,CCNY,SOS2,ZNF175,PARPG1,SLC16A9,PTP4A1,MAN2C1,MYO1B,ZNF75A,PLXDC1,RPL7L1P8,RP11-
370A5.1,NRN1L,STAT5A,KLHL29,CCDC148,STK11IP,ZNF837,C9orf40,RPS15AP12,UPF3AP3,RP11-
341G23.4,QTRTD1,PABPC4L,ZNF845,AC074212.6,C11orf30,SPACA6P,TONSL,C18orf32,CDC7,AC007228.9,CATSPER2,LMO2,
AF131217.1,RP11-66N24.3,CROCCP3,SPOPL,CTC-559E9.4,ZNF133,GNLY,RP11-57H14.4,SCMH1,LSM3P3,RP11-
680F20.12,GPX1P2,UNC5C,TRAF6,ZAK,OLFML3,LINC00969,BBS2,PKD1P5,GCOM2,RN7SL471P,LRRC4,BMS1P4,ANKRD6,OL
FML2A,DSCC1,RP4-607I7.1,RP11-104N10.1,CDAN1,FAM3A,GXYLT2,FAM60CP,CH507-
236L23.1,PF4,KIF20B,LPCAT4,SYT7,LINC00619,GGCT,LINC01081,RP13-
270P17.2,AC019097.7,ARHGEF39,ZNF672,TRIM62,AC010980.2,AC090617.1,RMI2,MSMO1,RELL1,TMEM81,RN7SL664P,RP11-
200A1.1,IZUMO4,CELSR3,CNOT8,MRPS18B,WDTC1,CH507-338C24.1,LSM2,GBGT1,RP11-588H23.3,RP11-
458F8.4,STON1,RP5-1198O20.4,PCNA,TPI1,SPOP,RP3-
425C14.4,ACTRT3,DNASE1,STAG3,MIR6723,TCF7L2,PTPN20A,ZNF185,RP11-
315D16.2,SCARNA13,RAB2B,COMMD3,KRIT1,NUDT4P2,NFIA,RP11-344E13.3,RP11-603J24.5,RP11-
204M4.2,KLHL3,ABHD14A,UBAC2,RP11-316M1.12,TAB1,CHCHD7,SGPL1,TOPBP1,TMEM18,HSPA4L,CTD-
3199J23.6,MAP3K6,DROSHA,AC024592.12,Metazoa_SRP,RP11-337C18.9,RN7SL268P,IRF7,CTB-63M22.1,DNAJC22,RP11-
274B21.12,PLCD1,HIST2H3A,IFNGR1,PMS2P5,RP11-454L9.2,RP11-
65L3.4,BCL10,KNDC1,GNAT2,RPL7P26,ITGAV,SERGEF,RTN4RL2,HSPA8P8,CTD-2349P21.12,KBTBD11,MUC20,M1AP,RP3-
428L16.2,SEMA4A,PTGES3P4,RIMS1,CRHBP,EEF1A1P38,NAV2,CTD-
2319I12.4,ZNF19,PRPF18,TRIP10,TMEM260,ARHGEF19,PKIG,PRELID2,ISCA1P6,RP11-
505P4.6,GAPDHP38,RNF215,AP000662.4,EFHD1,CYB561A3,RP11-
3B7.1,GAPDHP60,C17orf100,BLOC1S2,AURKC,UBE2W,NBPF2P,EEF1B2P1,RP5-
855D21.1,RPS11P5,CSRP2BP,MZT2A,RN7SKP275,RP11-254F7.3,TMEM70,AGGF1,FAM133A,PPIL3,PCF11,GRK5-
IT1,SLC2A4RG,CCDC146,CFAP58,C14orf79,NMRK1,KIAA1841,RP11-417E7.1,PTGIS,PHKG1,RP11-
227G15.10,ATAD2,SP4,RP11-64K12.4,RP11-373D23.3,RP11-514P8.7,MSMP,STRN3,WDR63,RP11-53I6.1,RP11-
326C3.11,RP11-64P14.7,CTD-2270N23.1,WDR60,RP11-66D17.5,PITPNM3,C1orf131,SLC35E2,PLEKHA3P1,RP11-
321N4.4,RP11-597D13.7,SH3D21,SAMD13,NYAP1,NRBF2,GALNT11,ZNF219,KLF6,TMEM161B,GAP43,ZCCHC14,RP11-
225H22.4,PTCSC3,DYX1C1-
CCPG1,BIVM,TFDP2,ANP32AP1,FERMT3,KIFC2,AKAP8,FAM102B,ST20,RPL21P11,IFNWP2,PIK3CA,PEX7,SIRPA,NCOR1P2,C
TB-40H15.4,REL,FAM50B,CCNG2,ZNF121,CEP128,TRAF3IP2-AS1,ADAMTS16,RP11-422P24.10,RP11-158K1.3,RP11-
265N6.2,ZNF471,EEF1A1P13,TESK1,SNX5,OSER1-AS1,NHLRC3,APLF,BRI3P1,RP11-

274H2.5,HIVEP3,DHFR,PIGF,KIAA1328,RP11-1246C19.1,LDHAP3,RP11-407N17.4,RP11-3D4.2,CTD-
2083E4.6,AC009404.2,AC073063.10,ZNF660,EFCAB14P1,AC105760.2,ZNF843,RAB31,ZFP36L1,MAP3K4,C3orf14,XXbac-
B476C20.10,AP000351.3,OXCT1-AS1,TPT1-AS1,KCNRG,TMPO-AS1,RP11-
762H8.4,HMGB3P22,AC009302.2,NYNRIN,CCDC30,RP11-2L8.1,MEIS1-
AS2,PRKD3,DRAM2,SNX13,SLCO2A1,RPL12P33,RP13-
516M14.1,CRIPAK,YIPF4,CEP70,ARTN,VILL,RASSF1,RN7SL535P,RN7SL262P,ECM2,ARHGAP1,MEAF6,NNT,ARSI,RP11-
446H18.5,ARMC4,RP11-575F12.2,KAT6B,DYNLT1,FAM223A,RHBDD1,SPARCL1,IL17RE,SPTLC3,AP000295.10,RP11-
567J20.2,FZD8,TMEM106B,HAGHL,UTY,TCEANC,COL13A1,HIF1A-AS2,RPS7P11,AC007283.5,ZNF226,RP11-
321F8.4,NOD1,CTD-2575K13.6,AMY2B,RPL34P31,RP11-88I18.2,FANCC,DISP1,RASA4DP,SMG1P1,PXMP2,FRMD3,C1S,RP11-
146N23.1,CTD-2619J13.23,AK8,CTC-435M10.12,AC005062.2,RPL24P8,KIAA1161,NUP85,GLRX3P2,WRB,ATG4C,SOS1-
IT1,ASIC2,CDC6,CTD-
2651B20.1,HIP1,CREB3L4,BTF3P7,SYN2,RUNX1,GPSM2,DCAF4,ZBTB43,LDHAP2,ZNF768,TUBAP2,MAP2,LINC00910,UNC13
A,HLA-DMB,RP3-339A18.6,HMGN1P4,TCP11L2,MMS19,CASP7,FANCG,RP11-
696N14.1,ERMAP,ZNF284,RAB11FIP2,TMTC4,ARPC3P5,DYM,DOCK6,FOXRED1,RP1-93H18.7,TRPV1,CTD-2553L13.9,SCOC-
AS1,AP000442.1,RP11-290D2.6,LLGL2,CENPP,TTC28,POLD1,RN7SL138P,RP11-524F11.2,AC002056.3,DNAJC5B,ZNF41,RP1-
283E3.4,AC079354.5,CTD-2620I22.7,MCM3,ZNF34,RP4-612B15.3,RP11-386M24.4,MED4,ADAM10,CPOX,RPL10AP2,XXbac-
BPG249D20.9,HSD17B11,DRAM1,PPP1R3F,GBE1,SCN1B,CDH1,TTC32,RPL9P29,BMS1P1,PAXIP1OS,RP11-342M1.3,RP11-
291L22.6,RP11-646I6.5,RP11-467L13.7,COQ7,RN7SL477P,JAKMIP2,LINC01057,RP11-329A14.1,RP11-582E3.6,TMCC2,RP11-
757O6.6,ZNF701,TMEM63B,NAV2-AS1,TMEM209,SH3TC1,CLDN14,RP11-157P1.4,TMEM133,CRTC3,TMEM45A,GFOD1-
AS1,RP11-160E2.16,SPATA20,RP11-2B6.2,KANK3,CTD-2530H12.4,KIAA0391,IPO9,KHNYN,RP5-857K21.7,RP11-
642A1.3,RP11-
88H9.2,ZBTB3,TMCO6,KRBA1,C1orf192,LINC01265,Metazoa_SRP,COLGALT1,C1orf21,LRRC20,AP001471.1,PCDHB9,RP11-
367E12.4,SESN1,USP1,RP5-991G20.1,SLITRK5,PRR4,ARMC1,SLC40A1,ZNF419,SLU7,RN7SL76P,TARS2,RP11-266K4.1,RP5-
991C6.2,CTD-2562J17.6,AC092610.12,RGS16,NSUN5P1,LA16c-
390E6.4,CHIC1,MARVELD2,TMEM42,COX15,GAPDHP65,MPZ,WSB1,PRKX,LINC01372,RP11-384O8.1,CH507-
254M2.1,OCEL1,PVRL1,RP11-576I22.2,RP11-793H13.10,PLCE1,FGD5-AS1,RP11-307C12.12,RP11-104G3.2,RP11-
513O13.1,WASH1,C1orf52,HLF,GAB2,RN7SL610P,ZNF844,HAUS5,FLG-AS1,NSFP1,MICALCL,HIGD1AP14,RP4-740C4.5,RP11-
589C21.6,ADAMTSL3,PIGW,APOM,CH507-
145C22.4,ZNF223,CETP,LDHAP5,AC006157.2,N4BP2,RGS14,DLL1,AGAP10,ZDHHC6,TMEM161B-AS1,GUCY1A2,CTD-
2054N24.1,TUBG2,RP4-669L17.1,Metazoa_SRP,LA16c-380F5.3,LINC00909,NDUFB8,RP11-
449G16.1,PRUNE,ZNF638,PLEKHA2,RP3-508I15.21,RP11-286H15.1,CPEB3,RP11-305B6.1,CCL13,RNF138,LDLRAP1,RP11-
420L9.2,RN7SL573P,AC009237.17,AC009238.7,CDIPT-AS1,RPSAP14,MCOLN3,UST,NRP1,RP11-115L11.1,TRGV5,RP11-
250B2.4,RP11-293I14.2,ENSAP2,TMEFF1,LINC01119,APOBEC3D,RNMTL1,ARRDC3,LRCOL1,MLLT6,CDKN1B,CTD-
2184D3.6,BRWD1-AS2,NPM1P39,AC064834.2,PLEKHA7,RP11-478C6.6,RP11-345P4.10,CTD-
2555O16.4,YWHAZP6,RSL24D1P1,B3GALT4,TYW1B,FRS3,ZNF25,GLT8D1,NIPSNAP3B,RP11-
464F9.20,TMEM217,BHLHE40,TRAPPC9,PGAM4,KDELC1,TMED10P1,CAMLG,RP11-680H20.2,CTB-
50L17.16,LRRC8B,SLC12A6,HIF3A,ASXL1,DUT,FCRLB,SNX32,GIGYF1,ARHGDIG,TBRG1,CAMK1G,HCFC1-AS1,RP11-
265N6.3,SNHG22,RP11-529K1.2,ANG,VDAC1P1,AC011330.13,SLC41A2,CHPF,RP11-354M1.2,OSTN,RP11-
802O23.3,WBSCR27,ZBED6,CLK2,MUC1,LRRFIP1,RP11-
373L24.1,RPL12L3,CDH12P1,CDH12P3,Metazoa_SRP,ADRBK2,ASPA,DNAJC28,FSD1L,RPL36A-HNRNPH2,TRMT5,RP11-
263K19.6,SPAG8,RP11-
523H24.3,ARMC2,CLASRP,BMS1P7,ZNF766,ST13P5,RNF114,CEP44,RSL24D1P2,LINC00882,RNFT1,RBBP4P1,TTC33,FBXL1
4,RP11-356I2.4,RP11-389O22.5,MCF2L2,KCNH1,PPP1R3C,CTA-
445C9.15,ANAPC16,BCL2A1,ALG10B,MTCP1,KRTCAP3,LDHAP7,PDCD7,KLF11,ZNF846,EREG,RAB27A,RP11-
434C1.4,KIAA1377,COL16A1,RP11-350N15.6,SMAD9,NDUFA6-AS1,AP001372.2,USP37,ETV1,RP11-323J4.1,HIST1H3C,RP11-
314C16.1,EIF4HP2,RP11-214K3.25,PRMT9,IRAK4,RP11-121A8.1,RP11-234G16.4,CHRDL1,RP11-824M15.3,CTD-
2186M15.3,GALNT7,TMEM200B,RP11-426K3.1,RP11-105N14.1,RP11-553P9.3,SGCE,IRF2BP2,CTD-
2544N14.3,FURIN,RBL2,MARC1,CHKB-CPT1B,CLGN,RP11-572O6.1,CCR1,TXNDC16,GLI2,DUSP16,RP11-
712B9.2,IFI44,NAPA-AS1,CH507-236L23.2,PRSS36,TBC1D3,A1BG,IL21R,NADK2,ADAT1,LYRM7,AC010894.3,ZNF628,RP11-
499E18.1,RP4-717I23.3,ARL10,NFKBIL1,RP11-266L9.8,PSIP1,AC004980.7,PDXP,RP3-395M20.8,RP11-802E16.3,CTD-
2532K18.2,ENTPD7,CCT8P1,BAHCC1,SMOC1,RP11-417E7.2,RP11-41O4.1,RP11-
546D6.3,SCHIP1,MIR4500HG,ZNF18,AHSA2,CHD4,DYRK4,ELOVL3,POGLUT1,GPR137C,TFIP11,TSKU,KB-
1410C5.5,SH2D3A,ANKRD36B,EIF4EBP2,RP11-97C16.1,C3orf67,BATF3,RP11-
261C10.7,FRG1B,CYP4V2,MAPK1IP1L,ZCWPW2,AC144652.1,KIT,ZNF688,AC090587.5,RPL29P12,PAK3,RP4-
668J24.2,EFNB1,RP11-571L19.8,CTA-253N17.1,SEMA3C,UQCRBP1,ABCA9,DNAJC9,RP11-
135A24.4,DNAJB5,MSTN,PLIN2,RP11-574K11.26,RSG1,DBH-AS1,GNPTAB,RPL12P1,RP11-
535M15.1,RN7SL614P,AL133168.3,CD14,MAML3,RORB,USP41,TRAPPC11,GPATCH1,APOBEC3H,DMC1,PARD3-
AS1,JAK3,DUSP19,IL17B,CDT1,CUTC,LINC01160,AC010879.1,TTLL3,RAB17,TAGLN2P1,EGR3,RP11-
113C12.2,UBQLN4P1,RP11-74J13.9,RN7SL368P,PDLIM3,ABCG4,FRAT2,SH2B2,RP11-301M17.1,CTD-
2006H14.2,GAB3,UFSP2,AC010226.4,CTD-2245F17.3,RP11-522B15.3,ZNF418,RAD51AP1,ASIC3,STC1,MAGEC2,CTB-
13L3.1,MYL4,TOR2A,ADARB1,TBC1D22B,HSPB1P1,FAM66B,TIPIN,FRRS1,RP11-349N19.2,WDHD1,RP11-
397P13.7,CD68,RPS20P14,RP3-510D11.1,THSD4,RP11-78J21.7,RP11-156K23.3,LINC00312,RP11-
107F6.3,CCDC183,RN7SL209P,RP5-1057I20.6,XXbac-B33L19.4,LETMD1,ZNF566,TSNAXIP1,CTD-
3105H18.18,BAZ2B,PHLDB2,SYNJ1,ELL2P1,ATRN,MMD,NDUFA5P11,LYPD8,DNAJC12,ETV2,ZNF559,CREB1,WDR90,AC0000
67.1,ELP4,PPT1,SLC35A1,ATL1,GUSB,RPL23AP32,KNTC1,NEK11,SYCE2,DOK3,RP11-517P14.2,C2orf40,BTF3P5,RP11-
669E14.6,RP5-967N21.11,RP11-67P15.1,HECA,BCL6,NSUN3,HERC6,CUX1,RP11-
529K1.3,LINC00643,TRIQK,TSTD3,HECTD2,RAB11B,RP11-
681N23.1,AC007952.4,PDE4DIP,MTND2P28,AC068533.7,MUTYH,CTD-2031P19.5,PAPPA2,AC026202.3,RIBC2,CTB-
13F3.1,SPIDR,KMT2A,HERC2P5,COL21A1,RP11-316O14.1,RP11-385F5.4,TIRAP,RPS15AP1,KBTBD7,RP11-849F2.9,RP11-
700J17.2,FAM66D,HDAC10,RP11-109G10.1,RNASEL,SLC41A3,C2orf72,RP11-359K18.4,CCDC85B,SSBP3,RP11-27I1.6,RP11-

49K24.5,ZNF266,MITD1,ZFAND6,ITGA10,PROSER3,RP11-139J15.2,ADCK5,AQP1,PRPSAP2,CFAP44,RP11-
426C22.5,HAPLN1,ZNF518A,RTN2,CASP8,RP11-110I1.13,KIAA1644,RP11-579D7.2,RP11-440L14.1,CTD-
2376I4.1,C17orf70,ZC3H6,RP11-864N7.2,RP5-850O15.4,TMEM254-AS1,FAM57A,RP11-77H9.2,RP11-
95P2.1,RPL21P120,HSPA2,NQO2,ZNF747,PSTK,NAT6,TRIM65,RP11-366M4.1,HMGB2,RP11-
575H3.1,LINC01023,PTPRH,MAP2K5,RP11-822E23.6,C17orf59,LBX2,RPL15P20,GUSBP11,VGLL4,CHST11,RP11-
404P21.9,RP11-89C3.3,RP11-464D20.2,EML3,C8orf58,P4HA2,SPSB1,PTMAP8,BOK,TMEM242,C19orf40,FGF11,IGLV1-
51,DHRS4-AS1,RPS13P2,UBL7-AS1,ACKR3,IGSF10,CTGLF10P,ZNF815P,GAA,P2RX4,CH507-
338C24.2,CENPU,LINC01068,RP5-890O3.9,RP1-198K11.5,CH507-145C22.3,KIAA1551,RP11-404P21.8,FMO5,RP11-
548P2.2,AKNAD1,CTC-492K19.4,CTD-2240J17.3,RELL2,TCEAL6,CEP112,C17orf58,RP11-
473M20.7,ZNF678,AC108488.4,NPAS2,TAPBPL,EAF1,DCUN1D4,IL18,CISH,RP11-367N14.2,TSPAN2,CTC-
444N24.8,HERC2P2,RP11-313J2.1,COLEC11,TCEB1P19,GOLGA6L4,NDRG1,HOMER1,LINC00963,ANO8,RP11-
455O6.8,CAMK2B,PDIA3,PTPLB,TMED8,MAGEA12,LINC01336,RPL37AP8,RP11-351I24.1,TPI1P1,RP11-
2C24.4,RNF7P1,RPS4XP16,PAQR8,F8A3,ZNF37BP,CTC-
250I14.1,WASH7P,STARD8,HSPE1P5,MDM4,RN7SL81P,AP003068.18,RP4-613B23.1,ANKMY1,RP11-21L23.3,PCDHB10,RP11-
434E6.4,CBLB,ZNF785,IRF2,RP11-497H16.7,CLCA2,CYFIP2,ABCG2,RP5-1120P11.4,CEP72,PRKCDBP,UCN,RP11-
867G23.10,AC006014.7,NDUFV2P1,NATD1,CTD-2207P18.2,RPS3P6,RP11-462G12.2,RP11-
884K10.7,SAT1,F8,HIST2H3D,RP11-47A8.5,HERC2P2,BLNK,LA16c-316G12.2,TEN1-
CDK3,PTCD1,C19orf81,CYBRD1,LDLRAD3,MYCBP2-AS1,PGK1,C1QTNF9B-AS1,LINC01004,ADAM8,OSBPL7,DTNB,RP11-
359B12.2,MCM6,SLC25A28,PCED1A,RPL23AP3,PRRT1,RPL10P1,TNFAIP3,SYTL5,RP11-
151H2.3,STAT4,PIP4K2A,AC016292.3,RP11-848G14.2,PCDHA7,CTC-510F12.6,ZNF292,SPATA6,CA12,CTC-241N9.1,RP11-
24H1.1,NMNAT2,R3HDM2,NUDT2,MTMR9LP,AGAP4,BOLA1,LRCH4,C1QTNF2,ACTA2-
AS1,LZTS2,HIST1H2BO,BARD1,HLTF,LINC00674,HIST1H4E,MEX3B,ERICH5,RP11-736K20.6,ZNF503-AS2,CYTH1,RP11-
3K16.1,PRH2,AC005363.9,IL23A,KLHDC8B,KCNC3,SNAI3-
AS1,ARHGEF3,E2F1,NR2C2AP,TAP2,TOB1,NPY4R,RPH3AL,ANKRA2,LYSMD4,MMP23A,CH507-
254M2.2,INO80C,DNM3,AC020594.5,ATP2A3,SCARNA10,EFNA4,COL9A2,SNCA,CTD-2619J13.14,HOXB7,LAMA5,CTD-
2337A12.1,RP11-367G18.2,THAP7-AS1,NPIPA2,CREG2,MED30,RP11-
477H21.2,GPR135,ARAP3,FAHD2B,MEI1,RPS4XP3,CCDC110,RP11-196G18.24,CTD-
2124B8.2,CRACR2B,FAM24B,GADD45B,CYP1B1-AS1,RPL9P28,NPM2,PTGER3,P4HA2-
AS1,GON4L,GLDC,RAPGEF5,EFCAB5,SENP7,PDXDC2P,ZNF490,MARVELD1,SPTSSA,ADH1B,AOC3,INSR,SLC39A8,ZNF808,
MCM10,RP11-118K6.3,AC005306.3,DENND5B-AS1,PLD2,TMEM67,RP4-773N10.4,RP11-171I2.5,LINC00933,ARHGEF40,CTD-
2530N21.4,RP11-61K9.3,GMNC,NUTM2D,PIPOX,COMP,ZDHHC11,GUSBP9,PFKL,INHA,ZNF692,RP11-
54C4.1,ALDH1A3,FAM66E,LL0XNC01-240C2.1,SDK2,DAK,UPK1A,RNF212,RP11-5G9.6,UBE2NP1,RP11-
1000B6.7,AC005822.1,ABHD10,KRR1,TNXB,HTR2B,DCSTAMP,SCARNA2,GMCL1,RARB,RPRM,CABLES1,RP11-
302B13.5,SKIL,SLC38A9,C1orf198,MYOZ1,HILPDA,ANXA8,TIA1,ENPP7P12,RP11-345K20.2,PTMAP2,CTD-
2647L4.5,SPG20OS,YWHAEP5,RP11-492E3.2,RP11-383H13.1,COL22A1,TMX2-
CTNND1,HOXA2,ZBTB8A,ACTC1,AC073621.2,RP11-15A1.7,C5orf63,CDK19,ZNF653,FILIP1,URGCP-
MRPS24,STON2,HAVCR2,CACFD1,AP001434.2,RP11-712L6.5,MFSD6,AC009120.6,RP11-
831H9.3,ZNF221,PANK1,SRPX,RP11-343B18.2,SDAD1P1,SH3BGRL,AC012065.5,ZNF571,RP11-
461A8.1,ZNF491,CGB7,LINC00702,HNRNPA1P4,RP11-2N1.3,RP11-
1198D22.1,TBC1D4,AP000783.1,PRR15,WNT2B,DDX50,BMF,SMAD1,FPGT-TNNI3K,PRKG1,RPS4XP6,LINC01444,CH507-
154B10.2,HEIH,CDK1,DPY19L1,PRELP,RPL9P25,GIMAP2,SPATA1,RP11-77K12.1,ZNF709,RP11-
96B5.3,CLEC3B,ACVR2A,SPC24,TPT1P6,PLEKHA1,CAMK1D,AC079250.1,KATNBL1P6,RP11-
464F9.1,FAM66A,DOT1L,NR4A3,CMTM1,RP5-
940J5.9,JUND,GRIK4,CCDC117,TBC1D16,SUMO2P17,ELL3,PARP16,PNRC1,C19orf83,RCAN1,RP11-
214K3.22,SNX30,RHOBTB2,HEPH,NPNT,USP6NL,POLR3GP1,ABLIM2,DCK,AC025750.5,ZNF776,CXorf40B,AC010890.1,RP11-
973H7.3,RNF182,RP11-458J1.1,HSF2BP,CTD-2024P10.2,RP11-485G7.5,CH17-472G23.4,RP11-334A14.5,RP11-
127B20.3,MIR210HG,H3F3C,AC009133.21,TRNAU1AP,TMPRSS5,RP3-
445N2.1,NAPEPLD,AC002456.2,PTMA,MIF,MECR,SMARCD3,PAGE5,LAT,FAM21FP,ANKRD36C,RP11-
284H19.1,CHRNB1,RP11-434H6.6,LZTS1,CTD-
2260A17.1,C14orf28,OSBPL3,DFNB31,LIME1,C4orf33,AKAP3,NPR1,SNAI1,SUMO2P1,RP1-
140K8.5,PTMAP5,ABTB1,TCEA3,ARRB1,CKMT2,TM2D3,SFR1,C12orf73,PAN2,RP3-
509I19.1,PHOSPHO1,ZNF169,CCDC81,AB019441.29,CCDC28A,KLHL24,RP11-20B24.4,ITIH3,SAMD14,KANSL1-AS1,RP5-
890E16.4,LRRCC1,PFN1P1,AC003088.1,S100A1,METTL25,RP11-
362A9.3,FAM228B,C1orf233,PRPS2,HSPB2,ACBD7,OAS1,RPS15AP36,TMEM198,RP11-
325L12.6,WBP1L,ZSWIM8,SAPCD1,UMPS,FRS2,RAB40C,ZNF696,AC005606.15,RP11-
360L9.8,H3F3AP6,LINC00997,OMA1,FAM72B,RP11-585P4.6,P4HA3,SYNGR3,RP11-206L10.5,GCNT2,SRGAP2B,GDAP1,RP11-
379B18.1,HACE1,VWCE,XX-C2158C6.2,SMAD6,RP11-
216B9.6,LSP1P3,RPL12P8,NIM1K,CROCCP2,ZNF211,TPT1P9,FOXO1,RNF170,POMC,MEF2C,RP5-1050D4.4,DYRK2,RP3-
486I3.5,Metazoa_SRP,TRPC1,AC138035.2,SLC44A3,RHOU,STAC3,KLF8,LINC01060,RP11-249L21.4,RP1-96H9.5,RP11-
299J3.8,PLSCR1,HLX,ALDH6A1,PTPRZ1,RPL5P12,SERINC5,GNRHR2P1,ALDH3A2,GPR183,RP11-
112J1.1,CBR4,F8A2,IL6STP1,C11orf80,RAB3IP,PCDHB7,CDK18,CRTC2,TBC1D12,ZNF862,PAQR4,NT5M,DNM1P46,AC017002.
1,CARHSP1,P2RY6,DDR1,RP11-820L6.1,ANO7,DHRS7B,RP11-806H10.4,RP1-
292B18.1,NUTM2A,HSPA12B,SNHG6,MCHR1,HSF4,ABHD3,SLMO1,HSPE1P3,RP11-473C18.3,AMN1,OGFRP1,RP11-
83J21.3,SMCO3,HSD17B7,AC016753.1,RP11-1280N14.3,ZRANB2-AS2,RP11-87H9.2,RNF5P1,HTRA1,RP11-274H2.3,RP11-
627G18.1,RP1-170O19.22,CTGF,RP5-884G6.2,RP11-396F22.1,KLHL38,TSGA10,CACNA1C,TMEM37,FOXC2,CTD-
2020K17.1,HS2ST1,KLF13,ARHGAP20,RP11-
566K11.4,ERCC6,SSR4P1,RABGAP1L,PPT2,FAS,PRH1,SBNO2,PCED1B,PTEN,EEF1DP1,ASMTL-
AS1,AC018755.16,LINC01279,ZNF324,ZNF462,BDH2P1,PFKFB3,ITGA7,SLC2A13,ZNF431,JAM2,ARHGAP19,SDR42E1,HMGN1
P36,GPR146,RP11-192H23.8,GPR160,TMEM240,AC010879.2,ZNF827,MT1G,ZNF503-AS1,TSPAN15,MAN1C1,RP5-
1180E21.5,TAPT1,AKR1C3,HSPE1P6,TIFA,TMEM107,PTPRB,NALCN,LINC01089,OBFC1,SDR39U1,LDLRAD2,RP11-

653B10.1,RP3-462E2.5,ZSWIM4,GMNN,SEC22B,LRRC37BP1,FBXO24,NSMCE4A,RNVU1-
14,PPP1R3E,DHRS4L1,SLC22A1,PCDHB14,AC093642.5,RP3-486I3.4,PIK3IP1,JPH2,CTC-429C10.2,STARD4,GPR21,RP11-
152H18.3,ZNF23,POT1,RP11-15A1.8,RP11-531F16.4,FMNL3,TCF4,RP11-136H19.1,SNX18,STARD10,SYT12,ACSM3,RP11-
253E3.1,GPCPD1,TGFB3,CTD-2026K11.1,UBE2MP1,OPA3,Metazoa_SRP,RP11-53O19.1,RP4-
796I17.5,MIR99AHG,LRBA,LL22NC03-80A10.6,TNXA,ADAMTSL1,FBLN7,SEC11B,INPP5A,PPL,ISY1-
RAB43,HMBOX1,ANGPTL2,GTF2H2B,CH17-360D5.1,CNN1,CH17-478G19.2,SLX1B-SULT1A4,DARS-AS1,FAT3,RP11-
346C20.4,NRTN,ZNF558,NAIP,FAM193B,ST7-OT4,ZFP36,LINC01006,AC005534.6,IGSF23,RP4-
647C14.2,CEACAMP10,TRAF3IP2,LINC01415,EPB41L3,PTENP1,RP11-248J18.3,RP1-
273G13.2,ZNF710,LAMA3,CD163L1,ZNF607,RN7SL657P,DNAJC1,SIRT4,AC004538.3,RPL21P134,FKBP5,HSD11B1L,CYP3A7,
MRAP,ANKZF1,EPGN,ZNF10,NR2F2,ITGB1,ABC7-42391500H16.2,FABP5P7,RIMKLB,RPL36AP41,HMGCLL1,C10orf11,CH507-
513H4.1,RP11-732A19.8,SYS1-DBNDD2,EMR3,CTC-451P13.1,GPR157,EP400NL,RP11-
513D4.1,FERMT1,AL132709.8,LINC01139,RP11-837J7.4,LINC01515,AC003002.4,PDXDC2P,RP5-899B16.1,GHR,RP11-
739P1.2,CCDC174,SEPT7P9,AC013271.3,RP11-697E22.1,CH507-528H12.1,RAB6B,RPS21P4,HPRT1,C1RL,RP11-
497H16.5,PLA2G2A,BDNF-AS,ATP6V1B1,NUDT8,OTUD7A,CCDC80,SGCG,RP11-166B2.1,PRCD,RP11-
144G6.12,ESCO2,SOD2,AC012354.8,RP13-104F24.3,IL6ST,ELFN1,CTD-2630F21.1,C8orf46,LFNG,RP11-477I4.4,RP11-
46C24.6,LIMD1,ABCA6,RP11-35G9.3,NPR3,DDX26B,ACAD10,PTPRG-AS1,SPRYD3,RP11-264B14.1,PPARG,RP11-
417L19.6,CEP83,PROCA1,MT1M,HSPA9,TEX41,AF213884.2,SYNPO2,KLF3,RP11-38C17.1,CYP2R1,ZNF713,FLJ37035,RP11-
19G24.3,HDAC6,TMEM79,RGL3,TLCD2,C1R,SIAE,AP001062.8,EPS8,MYLPF,ADCK2,MIER3,CEMP1,XXbac-B476C20.9,RP5-
933K21.3,RP11-
420L9.5,PROS1,SHOX2,HRH1,TEP1,KCNMB3P1,KALRN,CENPK,DDX60,ITPK1,F11R,TEX2,LINC01197,TMOD1,AC078883.3,CH
I3L2,ANO1,NEFL,CTD-2616J11.11,C6orf52,SSPO,DTWD1,HIST2H2BD,CH507-42P11.1,CDC37L1-AS1,ADAMTSL2,RAB4B-
EGLN2,AC020571.3,RSPO2,EFEMP1,MTFP1,KCNJ2-AS1,SOX13,CEBPD,HIST2H3DP1,RP11-
390P24.1,MDC1,AK4P1,CCNL1,RP11-717F1.2,ATHL1,ZNF852,CTC-487M23.5,LINC01301,RTCA-AS1,NETO2,NOP14-
AS1,HECW2,RPL23AP60,VMO1,SPDL1,IER2,CBLN3,RP5-1116H23.4,RP3-449M8.6,CACNA2D4,TSC22D1-
AS1,PKIB,THOC6,PCDHB8,AC138031.1,C5orf34,NKAPP1,MPC1,H2AFY2,HCST,ELMOD2,ZNF467,LINC01376,RPS3AP25,MYB
PH,TMEM100,CNNM3,RIN3,ZNF879,HMGB1P1,SIRT3,IL34,CCDC186,IQSEC3,CCR10,CD3EAP,RP13-941N14.1,CABP1,RP11-
385F5.5,RP11-95H3.1,MACROD2,RAC1P4,RP11-54O7.3,LYRM9,AMACR,LL21NC02-21A1.1,RPL9P18,SLC13A3,RP11-
697E2.7,RNF122,AC007383.3,RP11-
832N8.1,CCDC85A,DHX32,DSP,FGGY,AGT,HEYL,PTCHD4,HIST1H2AI,SERPINE1,FAM89A,ITGB1P1,RP11-
746M1.1,PAPLN,FCGR2A,RP11-76H14.2,NFKBIZ,AC005795.1,RP11-149I23.3,ABCC6,RP11-
338K17.8,SSPN,MROH6,PIWIL4,RP11-109P14.9,RP11-544M22.13,SH2D4A,YEATS4,LYN,GTPBP10,HSPB2-
C11orf52,AC009005.2,HLA-C,MEIS2,LIF,IL4R,PALD1,SOCS3,RNaseP_nuc,HAS3,PPP1R2P3,TMEM110-
MUSTN1,CLTCL1,FRA10AC1,RRNAD1,RP11-210N13.4,NDNF,MALAT1,TOMM20P4,RP11-817O13.9,GSDMB,FAM160B1,RP11-
663P9.2,NKD2,GAS8,TLR6,ZFYVE16,RP11-863P13.1,RP11-98J23.2,APBB1IP,AP000295.9,AC007566.10,RP11-
1415C14.4,ZNF503,TMEM150C,SNORA76C,ID1,ABHD16B,SERPING1,FBLL1,AUH,ATG16L2,GAB1,PDE4C,ANPEP,FMOD,SWT
1,RP11-686O6.2,IMMP2L,HIST1H4C,RP11-20J15.3,ERO1LB,MRPS31P4,FAM122C,ENPP5,RP11-
680G24.4,CDH12P2,AC091492.2,C11orf65,GABRE,ASAH2,RP11-231G3.1,IFT122,RGS4,ZNF337-AS1,SAMD1,KB-
1027C11.4,DUSP28,BTG1,CTD-2571L23.9,RP11-686D22.3,RPS28P7,MFAP2,C1orf213,IGFBP3,CETN3,CTC-
250I14.6,METTL20,USP2,RP1-
43E13.2,SMARCA2,WASH5P,WDR19,ABHD17AP1,AP1S3,RPL31P49,CACNA1A,IL1B,FAM27B,PRSS53,ZBED3,NOP56P1,ANK
RD7,RTKN2,AMZ2P1,ANKHD1-EIF4EBP3,SPSB3,PFKP,KIAA1586,UPF3AP2,CHSY1,CH507-154B10.1,RP11-
301O19.1,CFI,RP11-690I21.1,TNFRSF25,CHURC1-FNTB,NHP2P1,FAM132B,SLX1A,RP11-
343C2.12,C5orf66,KLF10,WDR53,HRSP12,MBD5,PCDHGB2,PEG3,RP11-166P13.3,STXBP5-AS1,CTA-963H5.5,RP13-
104F24.1,MYO15B,IQCH-AS1,PDK1,AGTPBP1,GSTZ1,ADAMTS7,LARGE,CTB-55B8.1,RPS15AP38,AC004381.6,SLX1B,RP11-
474G23.2,RP11-379K17.12,MFAP3L,CD72,NAMPT,NLRP1,RP11-79P5.10,RP11-
361L15.3,ANKRD20A5P,SLC14A1,CFB,MYOM2,CTD-2286N8.2,SEPT6,SESTD1,RP11-656D10.5,PC,RP11-
12M9.3,CYB5R4,EMC9,MCOLN2,ITGA3,RAET1E-AS1,RFX3-AS1,ITPR3,AC009133.12,RP11-572M11.4,EVL,JUP,RP13-
401N8.1,VIM-AS1,RP3-327A19.5,AC098831.4,KCNC4,ID2,PELI1,SLC24A1,RP11-626H12.1,SEMA4B,RP11-
184M15.1,BCL9,N4BP2L1,MIPEP,RPL7P19,RP11-318E3.9,INSIG1,DPY19L3,STK38L,RP11-758H9.2,STARD5,RP4-
816N1.6,PLCD4,PZP,ERO1L,CCDC150,EPOR,RP11-1319K7.1,RP11-352E6.2,LGALSL,ADAMTS1,RP11-
1000B6.5,LAMC2,CSAG1,RP5-1087E8.3,PNP,HOXA4,BNC2,ZNF517,SCARNA12,SRGAP2C,ALDOC,FRAT1,RP1-
182O16.1,CTD-3203P2.3,RPS15AP11,AC005540.3,CYP4F35P,ATP5LP2,THAP9,BNIP3L,CTB-147N14.6,ISG20,KB-
1732A1.1,BRICD5,LINC00941,CTD-2555O16.2,RP11-342D11.2,APLN,PF4V1,PPP1R3B,ABC7-43041300I9.1,RP11-
809N8.2,AEBP2,BCL7A,CRHR1-IT1,LIN7A,LOXL1,FAM72A,CRYZ,CH17-140K24.5,GPHN,RP11-134K1.2,AC074212.5,RP11-
815M8.1,INSIG2,SUCLG2P2,RP11-745A24.2,PROSER2,MED14,RN7SL23P,RP11-305M3.2,KDM4C,MYOC,COPG2,RP11-
345J4.3,P2RX7,EGR1,bP-21264C1.1,TP53TG3D,ARRDC2,ORC4,RP11-274B21.4,TGFBI,RP11-134G8.6,RP5-
930J4.4,KRT34,GS1-124K5.4,RP11-150O12.1,FAM196B,ZNF626,HMGN1P38,LMCD1,PRRX1,TOP3A,RP11-
395G17.1,SLC27A3,LIPA,AC003002.6,H19,C11orf71,PDIA5,HSPE1P7,TNIK,HSD17B6,SFXN2,BNIP3P1,LCAT,RPL36AP21,PIBF
1,B4GALNT4,PTGFRN,HSPE1-MOB4,TFEB,HOPX,AC005785.2,TGFBR1,CDKN1C,PTGIR,RPS6KA2,FOXQ1,PPFIA4,RP11-
73M18.7,GPER1,C1orf54,MPP2,RPS26P31,CTC-
296K1.4,GCH1,ATOH8,PLAC9,ANXA2R,ABLIM1,ENO2,HIST2H2BA,RASL11A,MIS18BP1,FHL1,LIMD1-
AS1,AC015933.2,COMTD1,MEF2A,RP11-126K1.2,HIST1H2AJ,VAMP8,ZRANB3,SEPT5,CTC-507E2.2,LL0XNC01-
237H1.2,ANKRD30B,RP11-83J16.1,ENO3,PFKFB4,RP11-100N21.1,TPK1,AC008746.5,ST20-
MTHFS,ENDOD1,FBXL15,ZNF395,SNX25,RP1-
241P17.4,HOXA7,TMEM246,DMKN,CERS6,HMGN1P3,FTX_5,RTN3P1,FUT11,SDK1,AP001046.5,C8orf4,XXbac-
BPG252P9.9,ROR2,CAMK2A,ZNF33A,ODF3B,DIO3OS,SYN1,ADAMTSL5,POMZP3,RN7SL689P,CTD-2256P15.2,MST1,LA16c-
359F1.1,SKAP2,FAM162A,ST6GALNAC2,IL1R1,RP11-603B24.1,GPR115,PRKG2,RP3-512B11.3,MAN1A1,DSG2,PCDHB5,RP11-
1348G14.8,TIMM8BP2,CTC-367J11.1,FAM19A2,RP11-350J20.5,MAP3K8,CDH2,EIF1P3,RP11-815J21.4,RP11-
347C12.3,AC112229.4,FAM47E-STBD1,MIR3916,RP11-173M11.2,RP11-597M12.1,SAP30,TRPC4,ZC3H12A,RP11-
33B1.1,PDE3A,HMGN2P27,ATP6AP1L,RP11-334A14.2,AC156455.1,MFI2-AS1,SHMT1,RP11-

27I1.4,TMEM189,DPP4,NR4A2,MBOAT2,AC073072.7,SMAD7,FMO2,CCDC77,BEST1,BEX1,CD4,TANGO6,HRCT1,AFAP1L2,CHSY3,OSBPL9,PDE3B,CIART,ADCY4,RN7SKP106,HCFC1R1,RNF128,RP11-295P9.3,SDHAP1,ERBB3,ANGPTL1,RP11-45P15.4,CTD-2003C8.2,CHCHD2P6,CLSTN3,GJC2,CDKL5,MSC,OSBPL8,KRT14,CARF,HNRNPUP1,IER5L,PAPPA-AS1,POLM,FAM207BP,KCNJ12,GLIPR2,AC005339.2,SLC12A5,KLHL35,ZSCAN23,RASGRP3,ZNF567,IKZF5,RPL35P2,FAM212A,C1orf53,SESN3,MLXIP,NLGN1,ALDH1A2,RASL12,DACT1,BNIP3,RARRES1,RP11-574K11.24,FAM115C,FRMD4A,IGF1,AP006621.5,XKR6,USP32P1,INO80B-WBP1,RP11-72M17.1,C10orf10,RP11-893F2.6,SLC2A5,LOXL4,ADSSL1,FLRT3,HOXA5,PODXL,RP11-399O19.9,LINC00663,RP11-262H14.3,RASSF4,ABCA8,LDHD,FOS,SNORA73B,MAF,TMEM187,CREB5,RWDD4P2,DHX58,LINC01503,RP11-33N14.5,CCDC109B,ACP6,RP11-666O2.2,SEL1L3,RP11-796G6.1,RP11-798M19.6,ENPP4,MXI1,CORO6,IRX3,RP11-500G22.4,ID4,RP11-488C13.7,PLXND1,UBE2E2,RENBP,LGMN,PCDHGB1,WI2-1896O14.1,RP11-150O12.6,LIMS3L,AC027612.6,CLDN23,RNF112,NAPRT,TBX4,RP11-11N9.4,PLAGL1,CCL7,PGM5-AS1,LYNX1,POU6F1,FAM131B,PRSS35,NXPH3,KSR1,GALNT16,TMEM178A,RP1-278E11.3,RPL23P8,AGTR1,SLC22A23,RP11-783K16.13,ARHGAP44,RASGRP1,RN7SL659P,TNFAIP8L3,ACSS1,RN7SL674P,OTUD1,AC005618.8,ARID5A,ZNF213-AS1,RP11-328N19.1,CADPS2,UCP2,PEG10,PLXNC1,CADPS,ITPKB,RPS26P13,PCDHGB7,TNFRSF1B,APCDD1L-AS1,STAG3L5P-PVRIG2P-PILRB,RP5-1009N12.1,FOXC2-AS1,RP11-325K4.2,FER1L4,AP000580.1,FES,GFPT2,PKNOX2,LAMB3,PAGR1,MIF4GD,CTC-435M10.3,GRAMD4,TFAP2A,DACT3,SORBS2,RP11-1023L17.1,SMYD3,DFNB59,BMPER,PKMP4,NTN1,AP000695.6,SCUBE3,RP11-402J6.3,ZFPM2-AS1,RP4-583P15.14,IFI6,RP11-366M4.11,RPS18P12,RAB20,SPATC1L,TNFSF13,OMG,IER3,PAIP2,PODNL1,MTL5,DLGAP1,D4S234E,RP13-20L14.6,CTD-2017C7.2,CTD-2269F5.1,FOXC1,RP11-10K16.1,GPAM,FAM115D,RP11-508N12.4,MATN2,MYH11,H3F3BP1,CA11,LIG1,RP11-3P17.5,GTF2H2,CTD-2514C3.1,AC092933.3,RP11-467L13.5,RPS20P10,SAMD11,HSPB6,C5orf46,NOVA1,SNED1,TRIM61,RP11-384K6.4,TBCAP1,RP11-10C24.1,C11orf54,PRR5L,LDHAP4,PTP4A2P1,MMP23B,U3,UPK1A-AS1,PDGFB,AP000936.1,AP003419.11,JUNB,SMCO4,WDR27,RPL30P4,NAMPTL,CCK,SCUBE1,CTD-3131K8.2,RP4-761J14.8,AC159540.1,GPRC5C,SNORA74A,KGFLP1,LPHN1,RP11-293A21.1,TCTEX1D2,MTND1P23,ANGPTL4,CTC-429P9.2,OAS3,RP11-291L22.7,AC003092.1,LIMCH1,HOXA-AS2,DPH3P1,RAD52,LINC00545,RP11-96H19.1,RP11-95I19.3,RP11-140K17.3,RNASE4,RPL32P29,RP11-475I24.1,CELF2,RPL35P5,NFIB,SNRPGP10,RP11-229P13.23,AD001527.4,RP11-758N13.3,GPC3,KIF26B,ABCA3,FIBCD1,PARK2,CTD-2192J16.22,ANKRD44,SNRPGP15,RP13-608F4.5,MTND6P4,FAM149A,BCHE,CTD-3222D19.11,CTB-33G10.1,GMDS-AS1,RP11-333E13.2,C2,CXCL6,COX17P1,FBXO32,AMZ1,RPS26P15,RP11-603J24.9,PRUNE2,TTC28-AS1_3,COX7CP1,AC005884.1,RP1-159A19.3,AJ011932.1,ADAM12,RP11-1100L3.8,SPAG4,ANKRD1,FANK1,RP1-199J3.5,NCAM2,ZP3,CD36,AC011933.2,CPM,ABI3BP,RP5-1021I20.1,APOC1,GPR128,GDF6,CMAHP,SOBP,RP11-1000B6.3,ADAP1,RP1-122P22.2,RP11-734J24.1,EGR2,RP11-259G18.3,HOXA6,FHIT,C8orf37-AS1,AK4,SERPINA9,KCNF1,NTNG1,ERHP1,PCSK2,CTC-425F1.4,UNC5B-AS1,RHOT1P1,TIMM8AP1,CXCL12,RP11-500M8.7,AC093850.2,AL022328.1,IL33,SNORA23,AC133528.2,ID3,ANO4,AC005838.2,ATP8B4,HSPB7,SLC4A4,FP236383.5,ADORA1,SPRY1,C11orf96,SOD3,GGACT,NDUFB1P1,SPON1,RP11-323N12.5,MTSS1,AQP3,PLAT,TMED7-TICAM2,CTD-2207O23.11,TCEB1P2,PCOLCE2,RP11-265N6.1,RP11-545D22.1,RCAN2,ZNF444P1,PALM,RP11-40C6.2,MSR1,AC093627.8,OPCML,FGL2,COL14A1,RP1-170O19.23,G0S2,CTC-260E6.2,HOXA3,PDIA3P2,DES,PKIA,DPYSL4,RP11-1148L6.8,PGM5,RNF185-AS1,AC016708.2,TRGV7,SSC5D,GDF10,RP11-192N10.2,APOE,RP5-882O7.1,AC007560.1,RN7SL731P,RPL39P3,C3,PTGS2,RP11-715I4.1,AC000032.2,MYOCD,TERT,AC079780.3,RP11-1100L3.7,RP11-649E7.5,CH17-13I23.3,CENPBD1,PVT1_1

CAF-D

<u>Upregulated:</u> ACAN,TINAGL1,KRT18,NDUFA4L2,RP11-40C6.2,TNNT2,FP236383.5,FHIT,PCDH1,SORBS2,H19,NTN4,C8orf37-AS1,COL15A1,GDF6,SLIT3,FAM212B,PTX3,CACNA1H,CDH13,ANKRD1,EFHD1,MEST,KRT34,NGF,TNFSF4,AC018647.3,RP11-92C4.6,OXTR,COL5A3,RGS4,SEPT2P1,AC079780.3,SIK1,SNORA74A,GPR116,KCND3,AP003419.11,ITGA11,TPD52L1,SERPINB2,CH507-42P11.8,SGCA,EDIL3,GPR1,LRRC32,LINC01133,PDGFA,RPS4Y1,KIAA1324L,RP11-212D3.2,CTA-276O3.4,COL4A1,PVT1_1,SULF1,FLT1,NXPH4,DSP,LIMS2,KCNG1,FAM212B-AS1,NALCN,ELN,CDA,RGS7BP,CTD-2269F5.1,CSGALNACT1,MBP,RP11-33N14.5,KCNE4,BST1,BST2,FOXS1,GPR133,KRT8,RASGRP1,HCLS1,CDC42EP3,TRIB3,MEX3B,LDHAP4,WNT2,MIR210HG,ST6GAL1,KRT19,EBF1,FOXC2,PRSS3,COBLL1,IGFBP7,NOTCH3,PSAT1,NREP,SDC2,CTC-425F1.4,SYNPO2L,CLEC3B,CPE,MEDAG,WISP2,MFAP3L,HES1,DEPTOR,SEPT5,GP1BB,PRELP,AK4,PCK2,JAG1,TES,SCRG1,NUAK1,NRXN3,COL4A5,TIMM8BP2,SERPINE2,SYNPO,BHLHE40,ALDH1A2,RP11-175K6.1,BGN,ARHGDIB,HSD17B6,CA12,ADM2,AK4P1,SLC6A9,PTK2B,JPH2,TRPC4,ACEA_U3,PTGIS,DMD,DDIT4,OLFML1,RPLP0P2,KLF2,TM6SF1,RPS4Y1,FOXC2-AS1,KLHL30,LINC01279,ATP10A,SLC2A5,DYSF,SH3TC1,PAWR,OLR1,PTPRZ1,ARHGAP26,ASPN,RNase_MRP,SLC38A1,NEO1,SCN9A,MTHFD2,ADAMTS15,SYT15,GATA6,MGARP,PHGDH,IGFBP2,PRSS23,STXBP2,CMAHP,COL4A2,CH17-13I23.3,ASNS,ADAMTSL2,WFDC3,KLF4,CHRNE,CRNDE,DCLK1,ROR1,GPR157,TSC22D3,PEAR1,EBI3,CPA4,SLC1A4,PDE3A,SLC2A1,SERTAD4,TMEM52B,B3GALT2,AC005838.2,PLAC9,HAPLN3,BX842568.1,RAB20,KRBOX1,NPPB,OLFM2,NLRP10,CACNB4,WFDC21P,AMZ1,PLEKHG3,C11orf87,ITGBL1,TRGV7,MGP,PTPRH,BAMBI,RN7SL731P,CORIN,RP11-115L11.1,DDX3Y,UNC5B,FLI1,CTD-3222D19.11,CTD-2571L23.9,RP3-423B22.5,RP5-1172A22.1,GEM,MALL,RP11-603J24.9,COL5A1,EPB41L4A-AS1,CSRP2,RP11-88H9.2,PDLIM3,HECW2,RP5-1050D4.3,SYBU,LPPR4,ERBB3,PALM,WWP2,INHBA,SLC7A5,FOXD1-AS1,ITGA8,AC007560.1,CARD9,TNFSF18,RP11-508N12.4,TGFB2,IFI27,ACTA2,DBNDD2,LURAP1L,ABLIM2,PDGFRB,CYFIP2,NEK7,SLC12A8,PTER,RP11-291L22.7,FRAS1,PKD2,SULT1A1,PAPPA2,TNXB,ANKRD6,LINC01197,PPP1R14A,UBL5P2,ECM2,ADAM12,AL022328.1,SYNPO2,MN1,VEGFA,FBN1,SYT15,PDK1,SAMD12,ERCC6,NDRG1,SFTA1P,PIM1,CTD-3131K8.2,TEX41,ANO1,MFAP5,LACC1,RP11-732A19.8,STARD4,RNaseP_nuc,CCDC3,TUFT1,RIMS3,ABHD4,LFNG,RP11-893F2.6,CDH2,NCOA7,FAM46B

Downregulated: HIST2H2AA4,DLL4,ANKRD29,RP1-232L22__B.1,RAET1G,SCN4B,RP11-513I15.6,CASS4,AHNAK2,SOCS2,RPL39P3,CLDN23,MECOM,CXCL8,NKD2,RASSF2,C3,ASPHD1,STC1,HIST1H2BJ,MPHOSPH6,DNM1,AC069368.3,GSTM5,TM4SF1,POPDC3,DAPK1,NABP1,SSC5D,IQGAP2,C1QTNF5,AE000658.30,HMGA1P8,QPRT,IFNWP19,TNFRSF1B,AKR1C2,SLC38A5,RASGRF2,MMD,SPON2,RP4-765C7.2,PDPN,TCF21,MT1A,KCNF1,MAOA,USP18,D4S234E,SLC16A6,STAMBPL1,SLC14A1,VAT1L,PTPRN,ALDH1A3,TBX2,HIST2H2AA4,SPON1,RGS2,LIF,HMGA1,FGL2,RND3,APOE,KIAA1217,CLEC2B,RP11-715I4.1,PDE7B,TBX2-AS1,NR4A1,PCDH10,CRLF1,MFAP2,SNRPGP2,IGF2,HSD17B2,AK5,TMTC1,FAM167A,RP11-82L18.4,CCL7,SNORD17,AKR1C3,ITGA2,RP11-746M1.1,KCNG2,WFDC1,NPTX1,DNASE1L1,RP11-2N1.2,RASL12,CLU,FAM46C,CDCP1,GALNT5,CYP27A1,PTGER2,CTSK,PPAP2B,CXCL1,LPXN,LRRC15,SDC1,SHC3,SOX9,TENM4,FENDRR,TRPA1,OR7E47P,IL13RA2,AMPD3,MIPEP,CCL11,TGM2,CYP2S1,HGF,IL24,AC109642.1,NR4A2,EDNRB,PLA2G5,ABCC4,FAM20A,SVEP1,TERT,MT2A,SGIP1,SCARA3,SNAP25,LINC00856,EYA4,TOR4A,STEAP1,DCHS1,IGJ,PSG5,ERAP2,ABCC3,CABLES1,F2RL1,CYGB,GSTM1,OLFML2A,ALPL,RP11-649E7.5,TRHDE,GAL,SLC40A1,CHI3L1,PCSK2,PRICKLE1,BMP4,F2RL2,C1QTNF9B-AS1,HS3ST3B1,ITIH5,TMEM35,FAM65C,GDF10,DUSP6,AC006449.2,GK,NCAM2,FGFR4,DENND2A,ETV1,S100A4,COL10A1,HIST1H4J,HS3ST3A1,TNFRSF21,LSAMP,LIPE-AS1,LRRC17,IL11,LINC01436,IL33,RARRES1,LRRN4CL,RP11-480I12.2,MOXD1,PRKG2,PAMR1,SEMA3A,RP11-384F7.2,PDLIM4,FBLN1,CECR1,KCNJ2,MT2P1,COLEC12,C1QTNF1,PSG4,BDKRB1,CSDC2,PLAU,AKR1C1,GALNT15,FAM180A,CD82,ACKR4,HSD11B1,MDK,ALDH1A1,MT1L,GREM2,GPNMB,BDKRB2,TFPI2,TNFRSF19,CAPG,CPM,CTB-79E8.3,RP11-307O1.1,SERPINF1,CFD,TNC,TMEM176A,MMP3,MME,TMEM176B,LINC00578,A2M,ADAMTS8,TMEM158,SFRP1,USMG5P1,SEPP1,RGCC,FGF7,PTGDS

CAF-E

Upregulated: RP11-715I4.1,CHI3L1,RP5-882O7.1,CD36,SEPP1,PTGDS,NDUFB1P1,ITIH5,SNORA23,HSPB3,RPS4Y1,FGF7,USMG5P1,OMG,GPR128,A2M,RP1-159A19.3,COX7CP1,GPRC5C,ENPP2,SCN4B,MLPH,TNFRSF6B,CRABP2,ATP2A3,RPS4Y1,HTR2B,RP11-384K6.4,CFI,GPNMB,PDPN,SPINT2,SERPINF1,LINC00578,ADAMTS8,CSDC2,CFD,VCAM1,CECR1,MME,TMEM158,IL13RA2,CES1,GALNT6,TMSB4XP2,SEMA3F,PSG5,SNCA,PDGFB,SLC40A1,ALDH1A3,IL12A,CCDC8,AE000658.30,RPL7AP28,EPB41L3,RP11-384F7.2,EPDR1,APOE,RAMP1,FAM180A,PLXDC2,AHNAK2,EYA4,LAMC2,SFRP1,RP11-2N1.2,RNF212,MT1L,RARRES1,FBN2,FIGF,EIF1AY,BDKRB2,FAM167A,KRTAP1-5,NLGN4Y,MOXD1,GPX3,F2RL1,PRKG2,USP32P1,AC106869.2,G0S2,MT1A,AC000032.2,FTX_5,COLEC12,CLGN,SOCS2-AS1,MAOA,PCDHGA3,PRSS35,PTPRN,LSAMP,C1QTNF9B-AS1,MT2P1,TNFRSF19,CTB-79E8.3,TOR4A,SCG2,CAPG,MAN1C1,CADPS,MMP3,HMGA1,TMTC1,FAM20A,CH17-13I23.3,ELTD1,FBLN2,PPARG,CPZ,CDCP1,DMKN,PDE5A,LRRC17,RNF128,CDK18,NPTXR,IL7R,BDKRB1,APBB1IP,RGCC,TNFRSF1B,KCNJ2,MAF,TXLNGY,AGT,TMEM37,AC092651.1,AC109642.1,RP5-930J4.4,SERINC2,TNFRSF21,NTNG1,DDX3Y,SEMA3A,SPON2,CDKN2A,PKIB,PLAU,CCDC69,GALNT15,RP11-480I12.2,FAM27B,NES,MYEF2,C16orf89,AC005785.2,LYNX1,AC091492.2,SOCS2,SDC1,TMTC2,CALB2,HSD11B1,AC010879.2,ASS1,OSTN-AS1,IGJ,RRAD,INMT,MIPEP,PNMAL1,SULF2,KREMEN1,NET1,RP11-563H6.1,HMGA1P3,NXN,MYBPH,TTTY15,ADIRF,CES1P1,SOX9,ANGPTL1,KRTAP1-1,SRGN,CCBE1,DHRS3,RP11-82L18.2,TTTY14,SLC7A8,SLC22A4,FAM49A,AC112229.4,GPC3,GAL,WFDC1,C1QTNF1,CLDN23,SLC38A5,CSMD2,PDLIM4,EVI2A,METRN,FMO2,ERAP2,MTATP8P1,NEDD4L,PDE9A,HSPB7,ATP6V0E2,MMP23B,SLC16A6,GJA1,BMP2,FAM149A,FLRT2,ITGBL1,FAM155A,STK32C

Downregulated:FBN1,TCF7L1,ARHGAP31,FAM212B,MFAP3L,LRRC15,RPL39P3,TLE4,RASSF2,FOSB,ITGA11,RP5-1172A22.1,RNASE4,AC253572.1,RP11-686D22.8,FOS,CHRNE,AL162151.3,SPESP1,CH17-472G23.2,PTGS2,SERPINE2,ABI3BP,NGF,ASPN,NALCN,TRIM58,PLA2G4A,RP11-175K6.1,LINC00702,CORIN,TES,NAP1L3,DACT1,ABCC9,ID3,GP1BB,CXCL1,SLC6A6,OSR2,MTUS1,RP3-423B22.5,PCOLCE2,IFI27,CRLF1,KCNE4,AMZ1,SNRPGP2,PCDH1,RP1-56K13.3,SCUBE3,RP11-488C13.1,RP11-212D3.2,TEK,MCAM,GDF6,FOXD1,MGARP,GBP2,ACEA_U3,PTGS1,PLAC9,PRSS3,RP4-765C7.2,ANKRD1,RP13-401N8.3,C11orf96,AMIGO2,CDH2,EBF1,RP11-686D22.7,CRNDE,TERT,OLFM1,SEPT2P1,MYOCD,AC079780.3,PPAPDC1A,HMCN1,OLFML1,FOXE1,LRRC32,IFI30,GSTM1,RP11-166D19.1,MN1,UBL5P2,RP11-92C4.6,TINAGL1,COL5A3,SHROOM2,WFDC21P,CACNA1H,BST2,PTX3,SLFN12,HTATSF1P2,CCL11,TNFSF4,ACAN,FOXD1-AS1,DSP,LIMS2,GPR116,HEPH,PSG4,CSGALNACT1,NTF3,CDH6,RP11-307O1.1,NTN4,NDUFA4L2,COL15A1

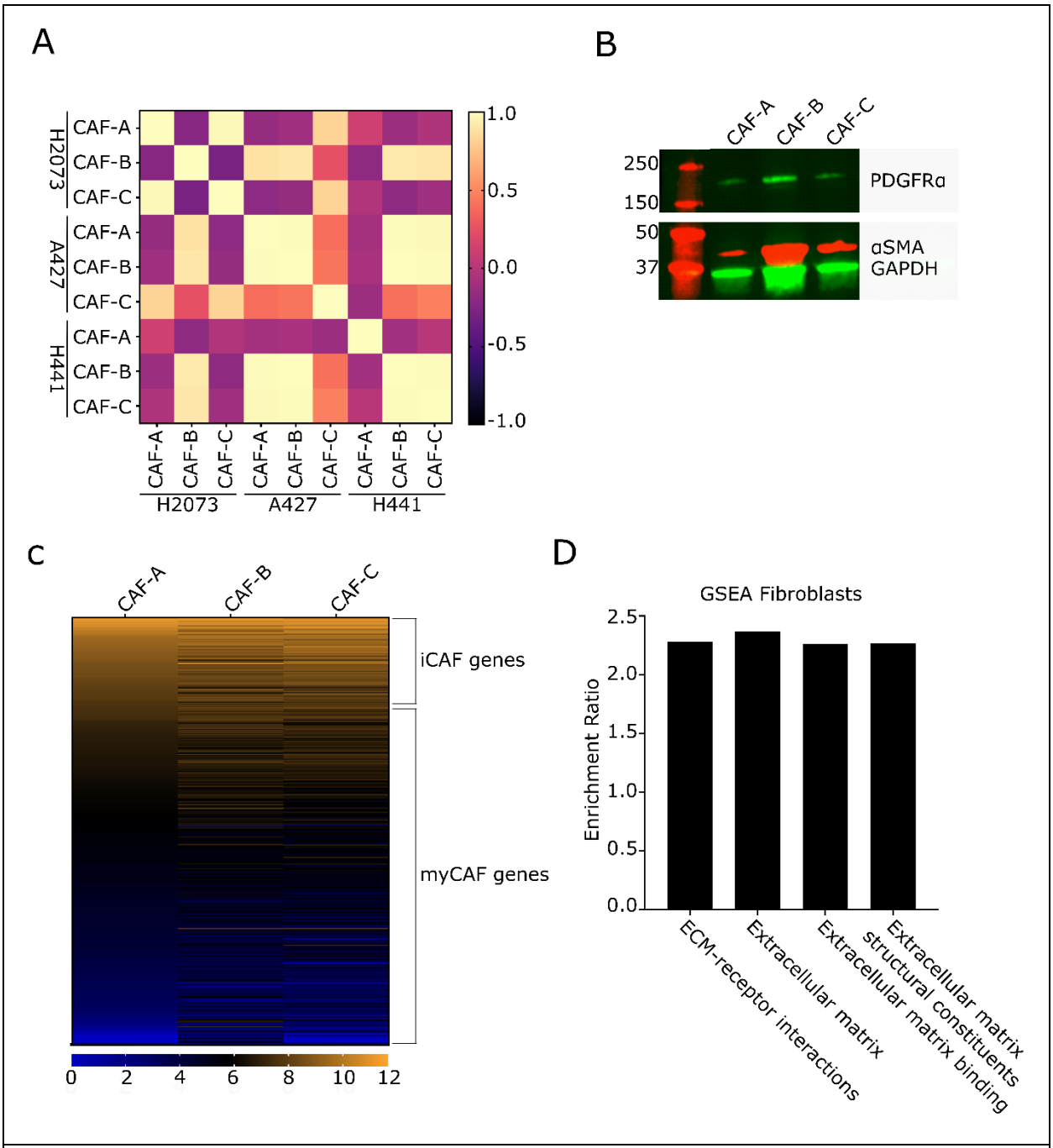

Figure 10: Cancer-associated Fibroblast interrogation assays. A) Five different patient-derived CAF lines were used in three different NSCLC co-cultures. Macrophage polarity was accessed by qPCR and compared by Pearson correlation analysis. The heatmap is the Pearson correlation values, n = 3. B) CAFs were cultured independently for 72 hrs and harvested for western blot analysis. PDGFRα and αSMA were used to determine iCAF vs

myCAF fibroblast phenotypes, respectively. C) RNA sequencing data illustrating both iCAF and myCAF genes are expressed in all CAF lines, gene list determined from [212]. D) RNA expression pathways upregulated identified by gene set enrichment analysis, FDR < 1.0, Enrichment Ratio > 1.5.

3.3 Lung cancer cells induce heterogeneous macrophage phenotypes in a multicellular co-culture panel

Utilizing the platform described, we interrogated 84 distinct cell lines (81 NSCLC, 2 SCLC, 1 immortalized Human Bronchial Epithelial Cell line) for their impact on macrophage polarization (Figure 11A). We discovered that the panel of lung cancer cell lines polarized macrophages into three highly reproducible phenotypes: High Arg1, High Socs3 and High Il-1β. These data were corroborated through non-biased affinity propagation mapping to cluster the macrophage qPCR dataset (Figure 11B). We additionally performed one-way ANOVA analysis comparing the expression of *Arginase-1* (*Arg1*), *Socs3* and *Il-1β* between the clusters to indicate strong expression of *Arg1*, *Socs3* and *Il-1β* mRNA expression in each individual cluster (Figure 11C). The induced macrophage phenotypes were highly reproducible (small standard deviations), regardless of passage number in any one NSCLC line (Figure 11D).

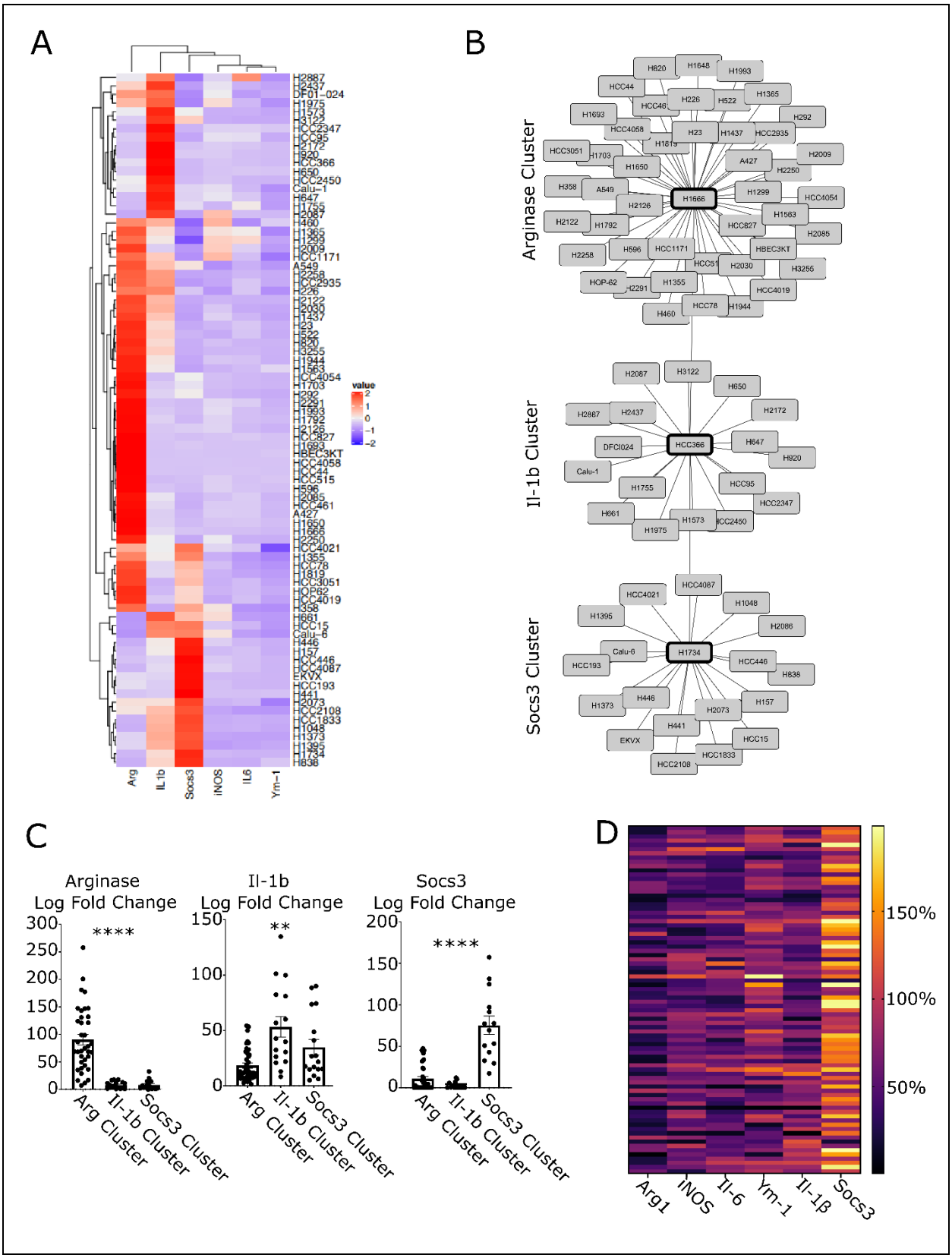
A
B
C
D
Arginase Cluster
Il-1b Cluster
Socs3 Cluster
Arginase
Log Fold Change
Il-1b
Log Fold Change
Socs3
Log Fold Change
Arg Cluster
Il-1b Cluster
Socs3 Cluster
Arg1
iNOS
Il-6
Ym-1
Il-1β
Socs3
150%
100%
50%

Figure 11: NSCLC cells induce heterogeneous macrophage phenotypes in a novel multicellular co-culture panel. A) Heatmap of mRNA expression of macrophages isolated from NSCLC, CAF, macrophage co-cultures reflecting three major inducible phenotypes (Arg, Socs3, Il-1β) B) Affinity propagation clustering of macrophage qPCR dataset with three induced phenotypes (Arg, Socs3, Il-1β). C) RT-qPCR gene expression analysis of differential expression of Arg, Socs3, Il-1β. Each dot represents a NSCLC co-culture transcriptional activity, which is segregated by affinity propagation clusters. Fisher exact tests were used for comparative analysis of gene expression between macrophage clusters. n = 84, Mean ± SD, ** P=0.0016, **** P <0.0001 D) A heatmap illustrating the coefficients of variation between LC co-cultures was used to determine reproducibility. Each LC co-culture had between 2-7 biological replicates. Every biological replicated had four technical replicates. The average coefficient of variation across all genes and co-cultures was 69%.

Additionally, we examined a limited panel of co-cultures at the protein level by immunofluorescence staining. We found that macrophages cultured with NSCLC from the high Arg1 cluster were ARG1, CD163 and CD206 positive. Macrophages cultured with NSCLC from the high Socs3 cluster expressed high levels of CD206 only. Whereas, macrophages clustered with NSCLC from the high Il-1β cluster expressed high levels of HLA. These findings demonstrate significant heterogeneity in macrophage receptor expression in response to NSCLC co-culture, corroborating our RT-qPCR findings (Figure 12A). To determine if, our *in vitro* co-culture model represented *in vivo* macrophage polarization, we evaluated macrophage phenotype in human NSCLC xenografts. We found that NSCLC cells that drove high macrophage expression of *Arg1* in the co-culture model also induced elevated macrophage expression of ARG1 protein *in vivo* (Figure 12B). Conversely, NSCLC lines associated with high *Socs3* expression *in vitro* induced a balanced expression of $SOCS3^{+}$ and $ARG1^{+}$ macrophages

in vivo. For further comparison, we explored RNA expression and mutation data from NSCLC cells and used this information to perform molecular match analysis with deposited expression and mutation data from The Cancer Genome Atlas (TCGA) (Figure 12C). Through this approach, we demonstrated a quantitative correlation between any one NSCLC line and TCGA tumor samples. We then took the bulk RNAseq expression data from the TCGA and used CIBERSORT [213] to quantitate M1-like and M2-like macrophages. We investigated how the macrophage-induced phenotypes in our co-culture model related to the ratio of M2:M1 macrophages in TCGA NSCLC tumor specimens. We found that our Arg1 phenotype data correlated significantly with TCGA tumor expression data (Figure 12D). These findings indicate that the co-culture system generates reproducible data on induced macrophage phenotypes that are represented *in vivo* and in clinical NSCLC deposited mRNA datasets.

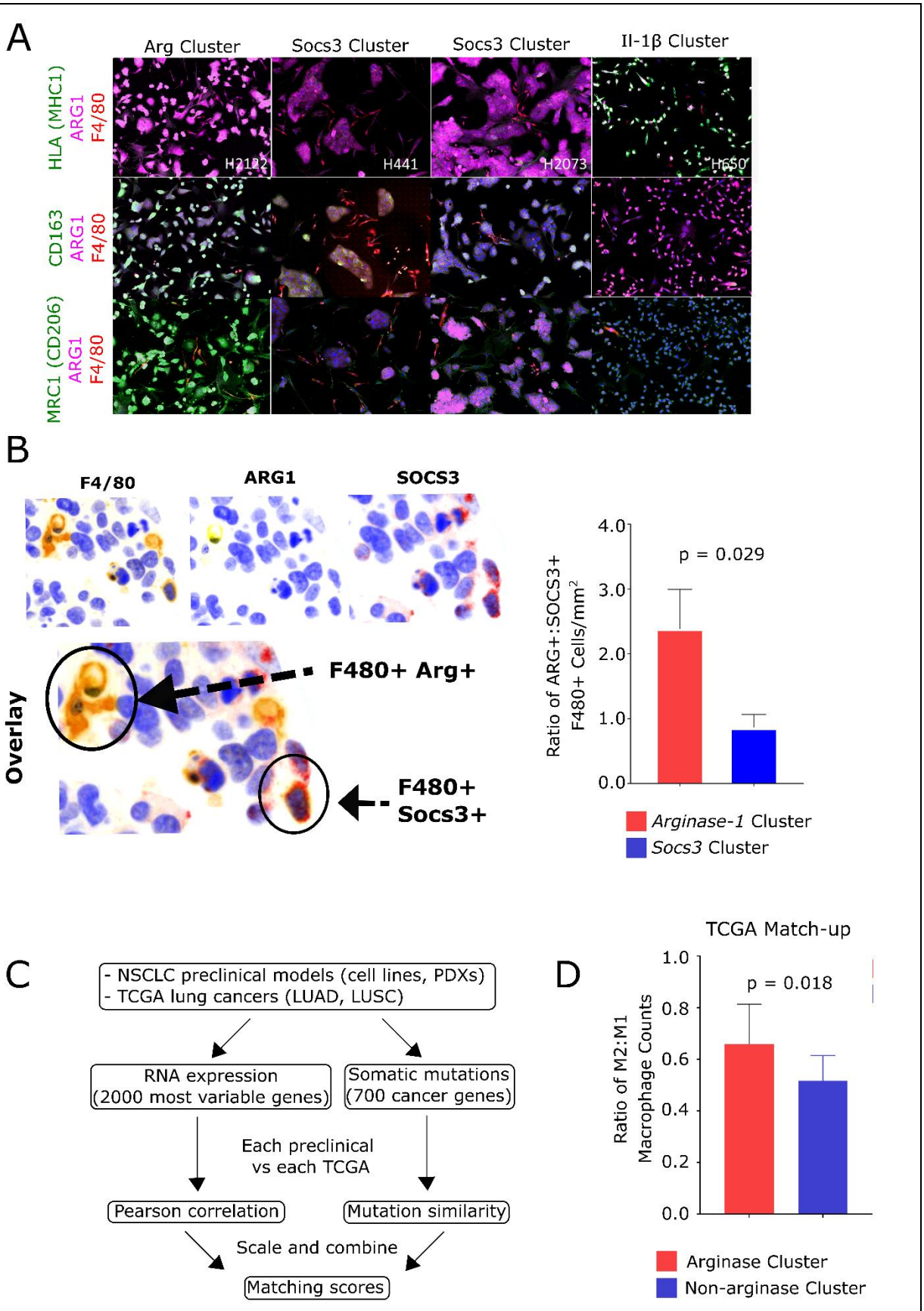
A
Arg Cluster
Socs3 Cluster
Socs3 Cluster
Il-1β Cluster
HLA (MHC1) ARG1 F4/80
CD163 ARG1 F4/80
MRC1 (CD206) ARG1 F4/80
H2122
H441
H2073
H650
B
F4/80
ARG1
SOCS3
Overlay
F480+ Arg+
F480+ Socs3+
Ratio of ARG+:SOCS3+ F480+ Cells/mm2
4.0
3.0
2.0
1.0
0.0
p = 0.029
Arginase-1 Cluster
Socs3 Cluster
C
- NSCLC preclinical models (cell lines, PDXs)
- TCGA lung cancers (LUAD, LUSC)
RNA expression (2000 most variable genes)
Somatic mutations (700 cancer genes)
Each preclinical vs each TCGA
Pearson correlation
Mutation similarity
Scale and combine
Matching scores
D
TCGA Match-up
Ratio of M2:M1 Macrophage Counts
1.0
0.8
0.6
0.4
0.2
0.0
p = 0.018
Arginase Cluster
Non-arginase Cluster

Figure 12: Corroboration of macrophage polarization demonstrating preclinical and clinical relevance. A) Four different NSCLC co-cultures representing different macrophage clusters were stained with F4/80, ARG1 and HLA, CD163, or MRC1. B) NSCLC xenograft panel stained and quantified for macrophage expression of ARG1 and SOCS3. C) An illustration of the pipeline used for the TCGA match up. D) CIBERSORT quantifications of macrophage populations in NSCLC cell lines matched to TCGA patient data by transcriptome and mutation similarity. Mean ± SD, * P = 0.018.

3.4 Overview of the discovery approach and macrophage characterization platform

To examine the contribution of specific cancer cell characteristic to macrophage polarity within the TME, we utilized archival molecular and clinicopathologic data on our extensive cell line repository, and corroborated these findings with publicly available data from The Cancer Genome Atlas (Figure 13) [214]. Whole exome and RNA sequencing from NSCLC (n = 79) and SCLC (n = 2) cell lines were used to characterize total mutation burden, copy number variants, and somatic mutations. These data were then used to perform our TCGA matchup and gene set enrichment analyses (GSEA). CIBERSORT software was used to estimate immune cell populations within the TCGA patient-derived tumor specimens [213]. From the CIBERSORT analysis, we used M1-like and M2-like macrophage cell counts for further analyses. Additionally, we assessed the contribution of clinicopathologic covariates including: pathologic subtype, sex, age, smoking status, clinical stage, anatomic origin of cell line (i.e. primary tumor, metastatic lymph node, distant metastasis) to macrophage polarity in lung cancer co-culture and TCGA samples.

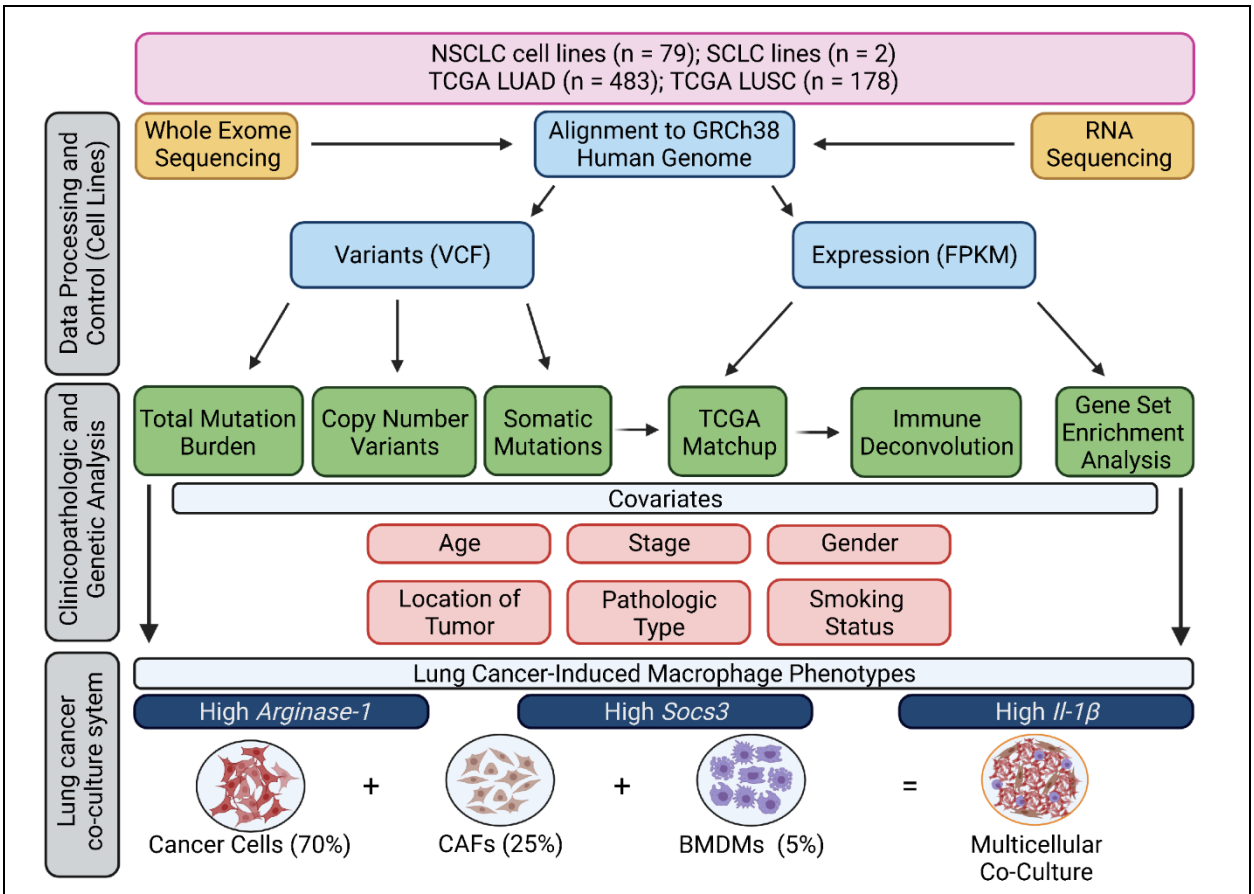

Figure 13: Overview of discovery approach

Flowchart showing analytic workflows, source of molecular and clinicopathologic characteristics, and lung cancer multicellular co-culture model.

3.5 Traditional clinicopathologic characteristics of NSCLC cell lines do not correlate with induced macrophage phenotype

We performed a comprehensive interrogation of demographic and molecular characterization of the cancer cells used in the *in vitro* screen to determine if macrophage phenotype correlated with discernable cell line characteristics. It was reasonable to query demographics of the patients from which the lung cancer cell lines were derived as others have shown the efficacy of immunotherapy can vary between male and female patients [215]. Additionally, studies have

found that in breast cancer the immune landscape, particularly macrophages, can vary between Caucasian and Black patients [216]. We leveraged archival demographical data on the patient-derived cancer cell and found that there was no correlation between patient gender, ethnicity, age or smoking status with our macrophage clusters identified through the *in vitro* platform (Figure 14B,D). Moreover, studies have shown significant differences in immune cell profiling in tumors with different histological lung cancer subtypes [203, 217]. Equally important tumor mutation burden has been linked to immune profiling and response to PD-L1 blockade [218]. Patients with higher mutation burden are more prone to develop neo-antigens that can be recognized by APCs, thus leading to an immune response against cells constraining these neo-antigens. However, after comparing the macrophage clustering results from the *in vitro* platform with clinicopathological data on the cell line panel. We found that anatomic origin of cell line, tumor subtype and the magnitude of tumor mutation burden were not predictive of macrophage clusters (Figure 14A,C). Additionally, we assessed the M1-like and M2-like macrophage phenotypes in TCGA patient samples using CIBERSORT. We found no correlation with M2:M1 macrophage counts to pathologic subtype, gender, age, total mutation burden or oncogene/tumor suppressor status in the TCGA lung cancer patient data (Figure 14E).

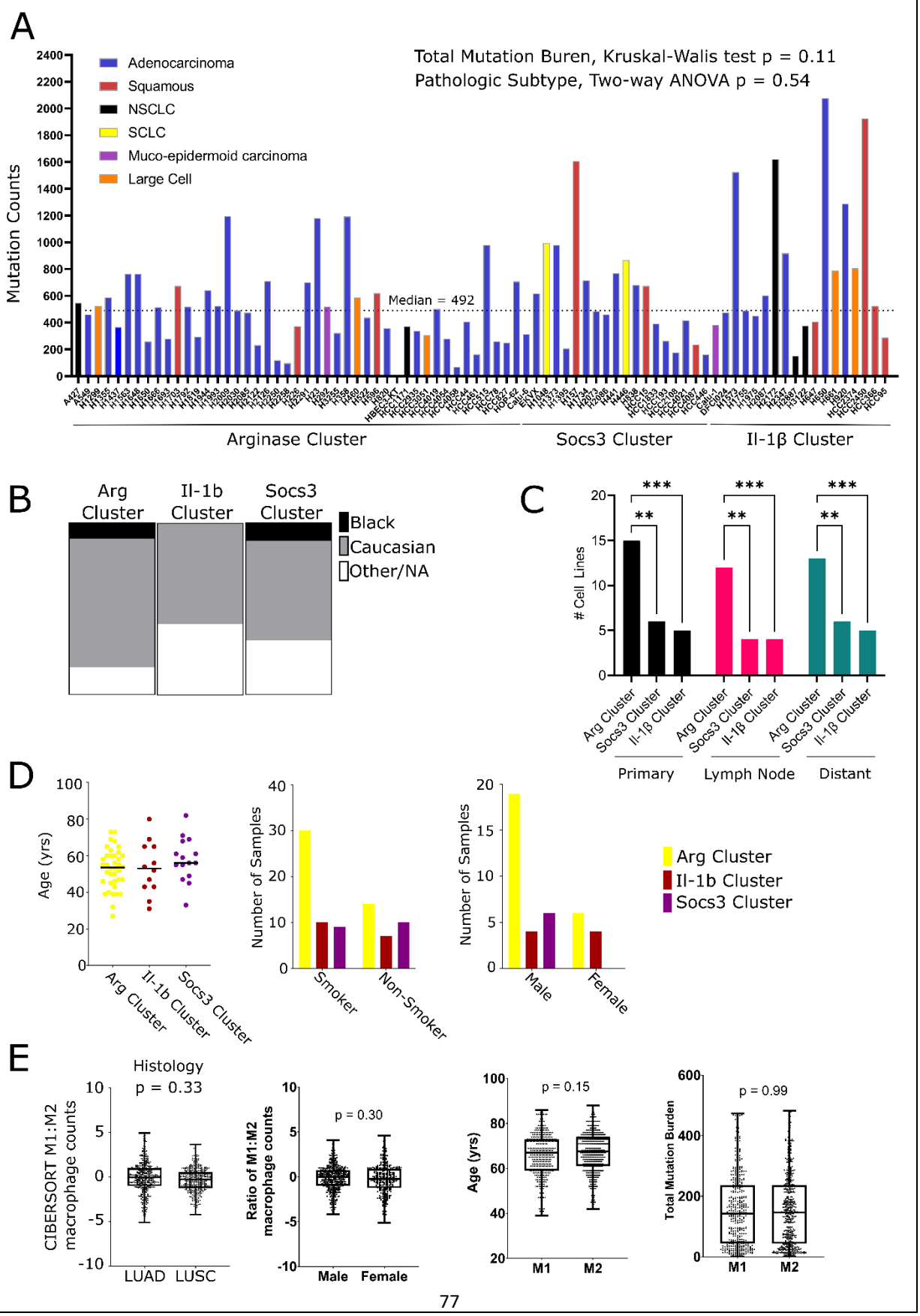
A
Total Mutation Buren, Kruskal-Walis test p = 0.11
Pathologic Subtype, Two-way ANOVA p = 0.54
Adenocarcinoma
Squamous
NSCLC
SCLC
Muco-epidermoid carcinoma
Large Cell
Mutation Counts
Median = 492
Arginase Cluster
Socs3 Cluster
Il-1β Cluster
B
Arg Cluster
Il-1b Cluster
Socs3 Cluster
Black
Caucasian
Other/NA
C
Cell Lines
Primary
Lymph Node
Distant
D
Age (yrs)
Number of Samples
Smoker
Non-Smoker
Male
Female
Arg Cluster
Il-1b Cluster
Socs3 Cluster
E
Histology
p = 0.33
CIBERSORT M1:M2 macrophage counts
LUAD
LUSC
p = 0.30
Ratio of M1:M2 macrophage counts
p = 0.15
p = 0.99
Total Mutation Burden
M1
M2

Figure 14: Traditional clinicopathologic characteristics of NSCLC cell lines do not correlate with induced macrophage phenotype. Demographic data from cancer cell lines was used for comparative analyses between the three macrophage clusters in regard to A) Patient Tumor Subtypes & Total Mutation B) Ethnicity C) Anatomical Origin D) Age & Smoking Status & Gender. Fisher exact tests were used for comparative analysis. n = 84, n.s. E) TCGA macrophage deconvoluted M1:M2 counts in cross referenced with TCGA patient gender, age and total mutation burden. Paired T-test were used for comparative analyses and no significant differences were found. **: <0.005; ***: <0.001.

Oncogenes are quintessential to cancer biology and there is, extensive research linking poor prognosis to mutations in genes such as KRAS, EGFR and KEAP1. Studies have shown loss of TP53 leads to increased cytokine production by cancer cells, resulting in recruitment of macrophages [219, 220]. Additionally, mutant KRAS tumor cells increase secretion of GM-CSF, facilitating M2 macrophage polarization. Moreover, loss of tumor suppressor LKB1 can increase neutrophil recruitment resulting in inhibition of cytotoxic T-cell and poor response to immune checkpoint blockade therapies [221]. Similarly, overexpression of MYC can lead to upregulation of PD-L1 and CD47 which subvert cytotoxic T-cell activity [222]. To that end, we compared the oncogenotype information and RNA-seq data from the panel of lung cancer cell lines employed in the co-culture platform and found that no solitary gene mutation was predictive of macrophage phenotypes (Table 4). Furthermore, we segregated EGFR mutants by exon mutations, KRAS mutants by codon mutations and LKB1 mutants by the type of individual mutations (Figure 15A-C). We found that presence of major driver oncogenes/tumor suppressor genes (such as mutant KRAS (p=0.66), TP53 (0.73), STK11 (p=0.48), EGFR (p=0.99), KEAP1 (p=0.12), or various combinations (Figure 15D) did not correlate significantly with the three induced macrophage phenotypes.

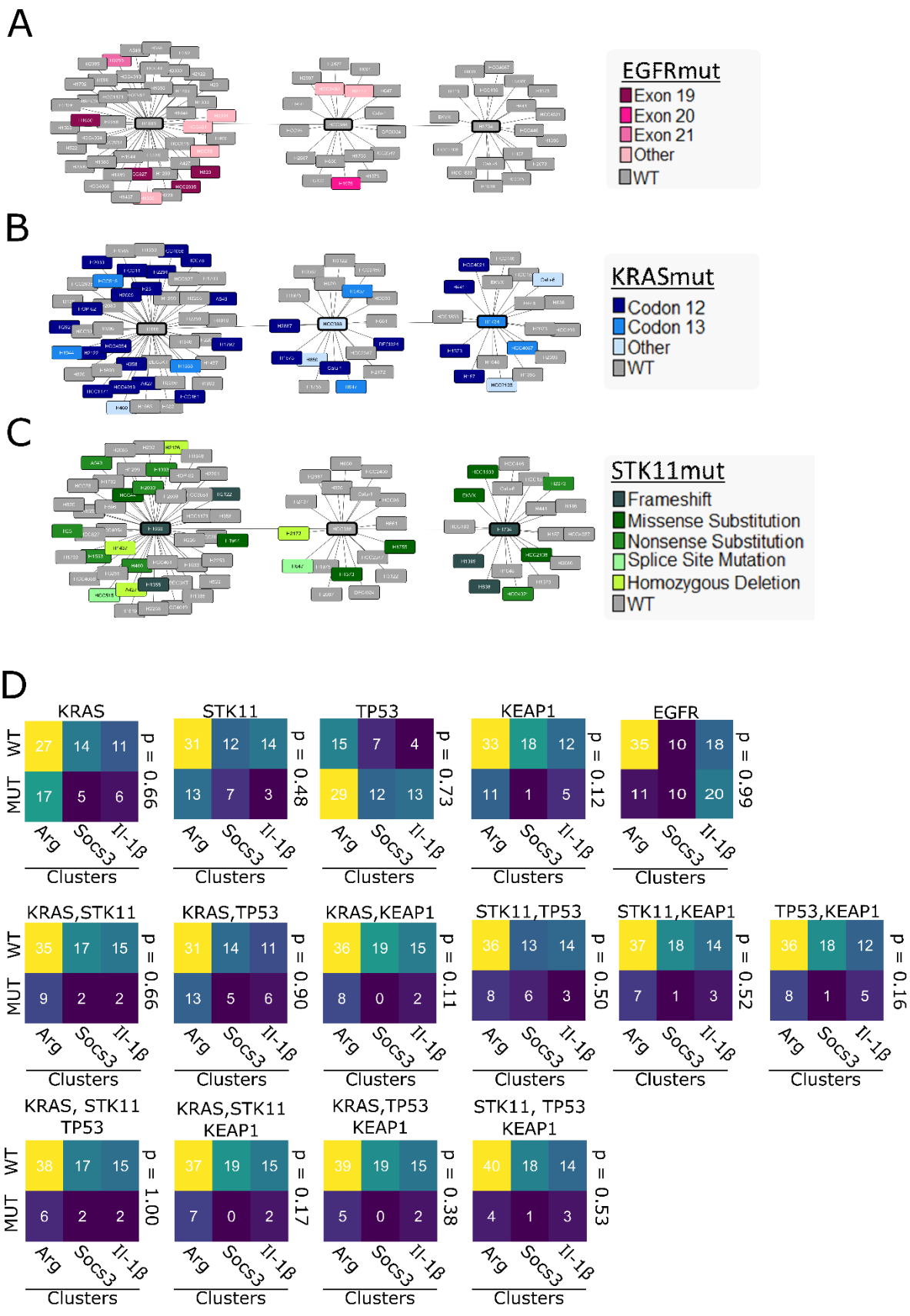
A
EGFRmut
Exon 19
Exon 20
Exon 21
Other
WT
B
KRASmut
Codon 12
Codon 13
Other
WT
C
STK11mut
Frameshift
Missense Substitution
Nonsense Substitution
Splice Site Mutation
Homozygous Deletion
WT
D
KRAS
27 14 11
17 5 6
p = 0.66
STK11
31 12 14
13 7 3
p = 0.48
TP53
15 7 4
29 12 13
p = 0.73
KEAP1
33 18 12
11 1 5
p = 0.12
EGFR
35 10 18
11 10 20
p = 0.99
KRAS,STK11
35 17 15
9 2 2
p = 0.66
KRAS,TP53
31 14 11
13 5 6
p = 0.90
KRAS,KEAP1
36 19 15
8 0 2
p = 0.11
STK11,TP53
36 13 14
8 6 3
p = 0.50
STK11,KEAP1
37 18 14
7 1 3
p = 0.52
TP53,KEAP1
36 18 12
8 1 5
p = 0.16
KRAS, STK11 TP53
38 17 15
6 2 2
p = 1.00
KRAS,STK11 KEAP1
37 19 15
7 0 2
p = 0.17
KRAS,TP53 KEAP1
39 19 15
5 0 2
p = 0.38
STK11, TP53 KEAP1
40 18 14
4 1 3
p = 0.53
WT
MUT
Arg
Socs3
Il-1β
Clusters

Figure 15: Hallmark genetic alterations do not correlate with induced macrophage phenotype. Cancer cell lines with individual mutations in A) EGFR B) KRAS and C) LKB1 genes in regards to macrophages cluster. D) qPCR co-culture mouse RNA transcriptional data cross referenced with cancer cell lines with individual or synchronous mutations in TP53, KRAS, STK11 and KEAP1 genes in regards to macrophage clusters. Paired T-test and Fisher exact were used for comparative analyses for each synchronous condition. n.s.

We also assessed oncogenic mutation status in relation to qPCR expression of each of the 6 macrophage genes (Arg1, Il-1β, Socs3, iNos, Il-6, Ym-1). We found that qPCR expression of macrophage genes did not correlate with any single or synchronous mutations in major oncogenes/tumor suppressors (Figure 16A). Furthermore, Additionally, we assessed the M1-like and M2-like macrophage phenotypes in TCGA patient samples using CIBERSORT. We found no correlation with M2:M1 macrophage counts to oncogene/tumor suppressor status in the TCGA lung cancer patient data (Figure 16B).

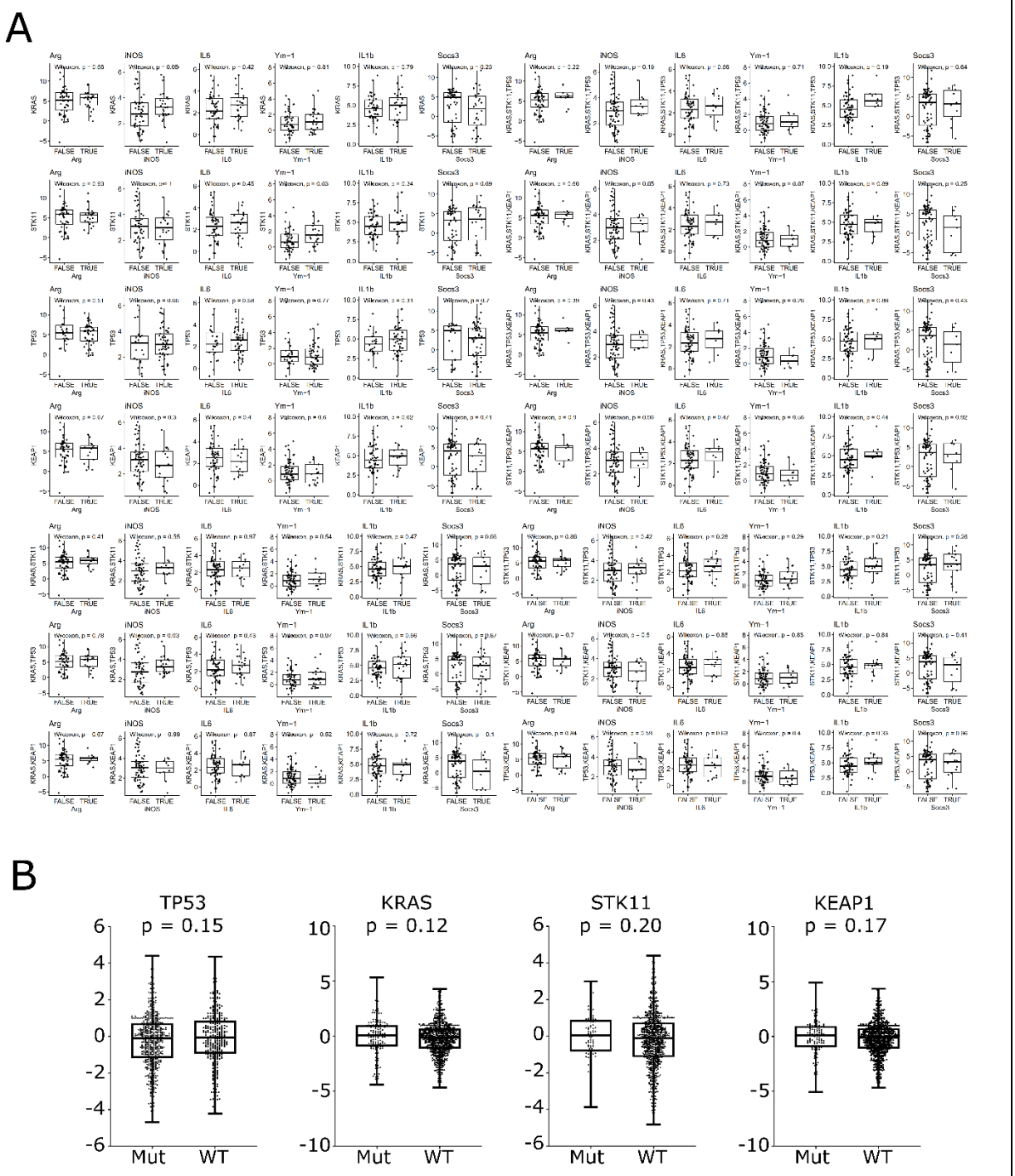

Figure 16: Hallmark genetic alterations do not correlate with induced macrophage phenotype, continued…

A) qPCR co-culture mouse RNA transcriptional data for macrophage relevant genes (Arg1, Il-1β, Socs3, iNOS, Il-6, Ym-1) cross referenced with cancer cell lines with synchronous mutations in TP53, KRAS, STK11 and KEAP1. B) Macrophage M1:M2 ratio determined by CIBERSORT with TCGA lung cancer patient samples in correlation to Histology and mutation status for TP53, KRAS, STK11 and KEAP1.

Table 4: Correlation of single genetic alterations with macrophage clusters

	pval	pval.adj
SPTA1	0.001485	0.780822
PTPRB	0.021341	0.780822
SMPD1	0.043947	0.780822
KAT6B	0.017254	0.780822
ZNF66P	0.011255	0.780822
TG	0.044031	0.780822
C15orf2	0.039132	0.780822
LAMB4	0.012081	0.780822
NAV3	0.030806	0.780822
CNTNAP5	0.021805	0.780822
AJAP1	0.029972	0.780822
F5	0.042273	0.780822
KCNMA1	0.042273	0.780822
MYH13	0.042273	0.780822
MYO3A	0.042273	0.780822
NLRP8	0.042273	0.780822
SIGLEC12	0.042273	0.780822
AHNAK	0.008988	0.780822
OCA2	0.009473	0.780822
COL4A2	0.012929	0.780822
F13A1	0.012929	0.780822
NADSYN1	0.012929	0.780822
PAPPA	0.012929	0.780822
RP1	0.012929	0.780822

PLCL1	0.016781	0.780822
ADAMTSL3	0.016871	0.780822
LRP5	0.022364	0.780822
OR4C15	0.02697	0.780822
SALL1	0.02697	0.780822
TRPV6	0.02697	0.780822
AC027369	0.040156	0.780822
ADCY8	0.040156	0.780822
ARFGAP1	0.040156	0.780822
BOC	0.040156	0.780822
CADPS	0.040156	0.780822
CASC5	0.040156	0.780822
CD163L1	0.040156	0.780822
DHX16	0.040156	0.780822
FLT4	0.040156	0.780822
FRYL	0.040156	0.780822
KIF26A	0.040156	0.780822
MEFV	0.040156	0.780822
OR4A5	0.040156	0.780822
OR6K2	0.040156	0.780822
OR8I2	0.040156	0.780822
PCMTD1	0.040156	0.780822
SOGA1	0.040156	0.780822
TRPA1	0.040156	0.780822
ANK3	0.043788	0.780822
FANCM	0.001372	0.780822
CDH9	0.002683	0.780822
KCNU1	0.002683	0.780822
HLX	0.004823	0.780822
KIAA0889	0.004823	0.780822
OPRM1	0.004823	0.780822
PRUNE	0.004823	0.780822
XYLT1	0.004823	0.780822
TRIO	0.006638	0.780822
DMBT1	0.008309	0.780822
SRRM2	0.014008	0.780822
CASS4	0.014037	0.780822
CNST	0.014037	0.780822
FAM83C	0.014037	0.780822
GRIN3A	0.014037	0.780822
ZNF521	0.014037	0.780822

PROX1	0.021003	0.780822
ZNF329	0.021327	0.780822
GON4L	0.025536	0.780822
RB1	0.025536	0.780822
ASXL2	0.03427	0.780822
ADAMTS3	0.040843	0.780822
EVC2	0.040843	0.780822
KCNC1	0.040843	0.780822
PRKCG	0.040843	0.780822
TRRAP	0.040843	0.780822
CNTN4	0.043311	0.780822
ENPP2	0.043311	0.780822
FRMPD4	0.043311	0.780822
IGSF22	0.043311	0.780822
MGAT4C	0.043311	0.780822
OR10Z1	0.043311	0.780822
PRR12	0.043311	0.780822
RFPL4A	0.043311	0.780822
RTN3	0.043311	0.780822
SLC14A2	0.043311	0.780822
SS18	0.043311	0.780822
TBX3	0.043311	0.780822
TMPRSS3	0.043311	0.780822
TOPORS	0.043311	0.780822
ZNF658	0.043311	0.780822
SCN7A	0.046541	0.816264
KIAA1211	0.047803	0.825407
BAZ2B	0.051641	0.825407
CACNA1C	0.051641	0.825407
DYSF	0.051641	0.825407
FCRL5	0.051641	0.825407
MCF2	0.051641	0.825407
BAI3	0.052234	0.825407
FAM55B	0.052234	0.825407
KCNB2	0.052234	0.825407
SCN1A	0.052234	0.825407
CSMD1	0.113104	0.837448
XIRP2	0.061064	0.837448
NEB	0.090602	0.837448
ZFHX4	0.084395	0.837448
LPA	0.087044	0.837448

DST	0.132893	0.837448
GPR98	0.094559	0.837448
SVEP1	0.136544	0.837448
FAT3	0.055905	0.837448
ANK2	0.056442	0.837448
CDH8	0.069208	0.837448
LOXHD1	0.069208	0.837448
ATP8B4	0.070023	0.837448
HERC1	0.070023	0.837448
ZNF208	0.070023	0.837448
CDKN2A	0.092437	0.837448
CRIPAK	0.096741	0.837448
KCNT2	0.06255	0.837448
SCN3A	0.06255	0.837448
DNAH8	0.094415	0.837448
HEATR7B2	0.094415	0.837448
MYH1	0.094415	0.837448
FRAS1	0.103753	0.837448
MUC6	0.103753	0.837448
POM121L2	0.103753	0.837448
PRDM9	0.103753	0.837448
FLRT2	0.113897	0.837448
KIF21B	0.113897	0.837448
POLE	0.113897	0.837448
PTPN13	0.113897	0.837448
ROBO3	0.113897	0.837448
OBSCN	0.127708	0.837448
ABCA5	0.130716	0.837448
ABCC6	0.130716	0.837448
BPTF	0.130716	0.837448
EPHA3	0.130716	0.837448
KCNN3	0.130716	0.837448
KCNV1	0.130716	0.837448
CIT	0.133725	0.837448
PRIC285	0.059368	0.837448
SLCO1B1	0.080089	0.837448
TMEM131	0.080089	0.837448
IGFN1	0.104315	0.837448
MMP16	0.104315	0.837448
MYH6	0.104315	0.837448
PAK7	0.104315	0.837448

PCDH7	0.104315	0.837448
TCHH	0.104315	0.837448
C3orf30	0.114872	0.837448
CALB1	0.114872	0.837448
DCAF12L1	0.114872	0.837448
GPR112	0.061202	0.837448
MYH7	0.061202	0.837448
CSMD2	0.078539	0.837448
ASTN2	0.094215	0.837448
BZRAP1	0.112074	0.837448
C9orf174	0.112074	0.837448
CDH11	0.112074	0.837448
DGKB	0.112074	0.837448
DPP10	0.112074	0.837448
MYH8	0.112074	0.837448
PCSK5	0.112074	0.837448
SNTG1	0.112074	0.837448
THBS2	0.112074	0.837448
TNRC18	0.112074	0.837448
ZIC1	0.112074	0.837448
ZNF418	0.112074	0.837448
AKAP9	0.118867	0.837448
DNAH3	0.118867	0.837448
EP400	0.118867	0.837448
MLL4	0.130548	0.837448
WDR44	0.130548	0.837448
FCRL3	0.088837	0.837448
MCM3AP	0.088837	0.837448
SLC9A2	0.088837	0.837448
AUTS2	0.094589	0.837448
FAM75C1	0.094589	0.837448
IGSF10	0.094589	0.837448
IRS4	0.094589	0.837448
KIF14	0.094589	0.837448
MAPK8IP3	0.094589	0.837448
PCDHGA12	0.094589	0.837448
PTPRQ	0.094589	0.837448
ST6GAL2	0.094589	0.837448
STAB2	0.094589	0.837448
TMEM132B	0.094589	0.837448
ZBTB40	0.094589	0.837448

DUSP27	0.12492	0.837448
FBN2	0.12492	0.837448
ADAMTS16	0.140873	0.837448
KCNH7	0.140873	0.837448
ODZ3	0.140873	0.837448
RTL1	0.140873	0.837448
PCDHB5	0.056558	0.837448
COL6A5	0.074144	0.837448
LYST	0.074144	0.837448
NBAS	0.074144	0.837448
ZNF257	0.074144	0.837448
C5orf42	0.091	0.837448
OR4A15	0.091	0.837448
RLTPR	0.111613	0.837448
VPS13B	0.124995	0.837448
EPB41L2	0.134439	0.837448
GNAS	0.134439	0.837448
KCNH2	0.134439	0.837448
KCNH5	0.134439	0.837448
NBN	0.134439	0.837448
OR8G2	0.134439	0.837448
POM121L12	0.134439	0.837448
ACACA	0.141673	0.837448
ATP2C2	0.141673	0.837448
CASC1	0.141673	0.837448
CHD2	0.141673	0.837448
COL17A1	0.141673	0.837448
FAM186B	0.141673	0.837448
FAM198B	0.141673	0.837448
FRY	0.141673	0.837448
INTU	0.141673	0.837448
KANK4	0.141673	0.837448
KCNJ12	0.141673	0.837448
KCNJ16	0.141673	0.837448
KIDINS220	0.141673	0.837448
LACRT	0.141673	0.837448
LILRA2	0.141673	0.837448
LRRTM1	0.141673	0.837448
MGA	0.141673	0.837448
MIB2	0.141673	0.837448
MON2	0.141673	0.837448

MYT1	0.141673	0.837448
NOM1	0.141673	0.837448
NOTCH3	0.141673	0.837448
NRCAM	0.141673	0.837448
OLFML2B	0.141673	0.837448
OR8H3	0.141673	0.837448
PLCB2	0.141673	0.837448
POLA1	0.141673	0.837448
RPTN	0.141673	0.837448
SORCS2	0.141673	0.837448
SPAG17	0.141673	0.837448
SPATA16	0.141673	0.837448
ST18	0.141673	0.837448
SYCP1	0.141673	0.837448
TMC2	0.141673	0.837448
TRIM42	0.141673	0.837448
TTC12	0.141673	0.837448
UBE2O	0.141673	0.837448
WDR33	0.141673	0.837448
ZNF462	0.141673	0.837448
ZNF573	0.141673	0.837448
CARD6	0.057355	0.837448
FAM131B	0.057355	0.837448
GRM6	0.057355	0.837448
NFASC	0.057355	0.837448
SDK1	0.057355	0.837448
ADAMTSL4	0.064139	0.837448
COL4A4	0.064139	0.837448
DIP2C	0.064139	0.837448
KCNC2	0.064139	0.837448
NLRP11	0.064139	0.837448
NTRK1	0.064139	0.837448
ANO7	0.080251	0.837448
ARFGEF2	0.080251	0.837448
ARID1A	0.080251	0.837448
GRID1	0.080251	0.837448
MKI67	0.080251	0.837448
MYOM1	0.080251	0.837448
NCAPD3	0.080251	0.837448
PARP4	0.080251	0.837448
PCNXL2	0.080251	0.837448

CACNA1E	0.151959	0.861959
MXRA5	0.151959	0.861959
CR1	0.152017	0.861959
HEATR8	0.151376	0.861959
SLCO1B3	0.151376	0.861959
DNAH10	0.152301	0.861959
SORCS3	0.152301	0.861959
C7orf63	0.14983	0.861959
CORIN	0.14983	0.861959
DIP2B	0.14983	0.861959
KIF2B	0.14983	0.861959
ROBO1	0.14983	0.861959
FAT2	0.176787	0.864089
LRRIQ1	0.157042	0.864089
PLXNA4	0.181918	0.864089
ANK1	0.173786	0.864089
CCDC108	0.173786	0.864089
CLSTN2	0.173786	0.864089
KLHL1	0.173786	0.864089
LRRTM4	0.173786	0.864089
OR2W3	0.173786	0.864089
PIK3C2B	0.173786	0.864089
TRANK1	0.173786	0.864089
AHNAK2	0.155446	0.864089
GRM8	0.17965	0.864089
LOC51059	0.17965	0.864089
PCDHGA8	0.17965	0.864089
ADAM29	0.183538	0.864089
APC	0.183538	0.864089
ATP2B1	0.183538	0.864089
ATP7B	0.183538	0.864089
EGFLAM	0.183538	0.864089
ELAVL4	0.183538	0.864089
GPR148	0.183538	0.864089
LRGUK	0.183538	0.864089
MTA1	0.183538	0.864089
MYOM2	0.183538	0.864089
NLRP14	0.183538	0.864089
NRAP	0.183538	0.864089
NTM	0.183538	0.864089
OBSL1	0.183538	0.864089

PARK2	0.183538	0.864089
PCDH19	0.183538	0.864089
PIK3CG	0.183538	0.864089
PYHIN1	0.183538	0.864089
RABGEF1	0.183538	0.864089
SCYL2	0.183538	0.864089
SMC5	0.183538	0.864089
TRIM48	0.183538	0.864089
TRPV4	0.183538	0.864089
UGT2B28	0.183538	0.864089
ZNF135	0.183538	0.864089
THSD7B	0.166312	0.864089
ABLIM2	0.170833	0.864089
AMBRA1	0.170833	0.864089
C20orf26	0.170833	0.864089
C8A	0.170833	0.864089
DENND1B	0.170833	0.864089
ERBB4	0.170833	0.864089
FAM179A	0.170833	0.864089
FSHR	0.170833	0.864089
GAB4	0.170833	0.864089
IQGAP2	0.170833	0.864089
MEGF8	0.170833	0.864089
PDLIM3	0.170833	0.864089
RNF17	0.170833	0.864089
SEMA5A	0.170833	0.864089
TGFBI	0.170833	0.864089
UBE4B	0.170833	0.864089
ABCA10	0.193887	0.90111
RYR3	0.202775	0.90111
COL24A1	0.204226	0.90111
ARHGAP32	0.206058	0.90111
MSH2	0.206058	0.90111
MSH4	0.206058	0.90111
OR6N2	0.206058	0.90111
PDE4D	0.206058	0.90111
PLEKHG4B	0.206058	0.90111
ROBO4	0.206058	0.90111
SLC5A11	0.206058	0.90111
SLCO1C1	0.206058	0.90111
TTC7B	0.206058	0.90111

YTHDC2	0.206058	0.90111
MYH15	0.206743	0.90111
ABCA3	0.208904	0.90111
ACE	0.208904	0.90111
COL5A3	0.208904	0.90111
INPP4B	0.208904	0.90111
KIF13A	0.208904	0.90111
OR10G7	0.208904	0.90111
PCDHA4	0.208904	0.90111
RECQL4	0.208904	0.90111
SLC8A3	0.208904	0.90111
TIAM1	0.208904	0.90111
TMPRSS9	0.208904	0.90111
DNAH1	0.196452	0.90111
DSCAML1	0.196452	0.90111
NF1	0.196452	0.90111
NLRP12	0.196452	0.90111
HECW1	0.201536	0.90111
FLG	0.222287	0.912691
STK11	0.322652	0.912691
RP1L1	0.342291	0.912691
GRIA1	0.260503	0.912691
DNAH14	0.271024	0.912691
UNC5D	0.271024	0.912691
RYR1	0.35579	0.912691
TRPV5	0.247026	0.912691
MUC17	0.255382	0.912691
MGAM	0.279011	0.912691
NLRP5	0.281585	0.912691
HMCN1	0.300668	0.912691
UNC80	0.300668	0.912691
ASPM	0.311681	0.912691
ZNF536	0.311681	0.912691
CDH12	0.348061	0.912691
EYS	0.237496	0.912691
HERC2	0.237496	0.912691
RALYL	0.238743	0.912691
SGCD	0.238743	0.912691
ZNF142	0.238743	0.912691
PEX5L	0.273021	0.912691
VPS13C	0.273021	0.912691

OTOF	0.286529	0.912691
ZFPM2	0.286529	0.912691
UNC13C	0.216013	0.912691
AIPL1	0.222285	0.912691
EPPK1	0.222285	0.912691
FUT5	0.222285	0.912691
KMT2C	0.222285	0.912691
NUP155	0.222285	0.912691
PCDHA2	0.222285	0.912691
PRDM15	0.222285	0.912691
SHANK3	0.222285	0.912691
AFF2	0.263274	0.912691
ALK	0.263274	0.912691
COL23A1	0.270923	0.912691
DPCR1	0.270923	0.912691
DSP	0.270923	0.912691
EPHB1	0.270923	0.912691
EYA4	0.270923	0.912691
FAM120B	0.270923	0.912691
GRID2	0.270923	0.912691
LMTK2	0.270923	0.912691
NOTCH4	0.270923	0.912691
RGPD4	0.270923	0.912691
STXBP5L	0.270923	0.912691
UNC5C	0.270923	0.912691
RELN	0.328045	0.912691
THSD7A	0.328045	0.912691
ENSG00000215407	0.221396	0.912691
GLI3	0.221396	0.912691
GOLGB1	0.221396	0.912691
PTCH2	0.221396	0.912691
DMD	0.222709	0.912691
PCDH11X	0.222709	0.912691
ASXL1	0.228792	0.912691
TRHDE	0.228792	0.912691
WDR49	0.228792	0.912691
COQ2	0.243927	0.912691
DYRK4	0.243927	0.912691
NDE1	0.243927	0.912691
PCDHB2	0.243927	0.912691
PKP2	0.243927	0.912691

RALY	0.243927	0.912691
TACC2	0.243927	0.912691
FAT4	0.30236	0.912691
LAMA1	0.30236	0.912691
SSPO	0.30236	0.912691
ACTRT1	0.317161	0.912691
ANKS1B	0.317161	0.912691
ATP10A	0.317161	0.912691
CACNA2D4	0.317161	0.912691
CARD11	0.317161	0.912691
CTNND2	0.317161	0.912691
EIF3A	0.317161	0.912691
EP300	0.317161	0.912691
FAM169A	0.317161	0.912691
FAM170A	0.317161	0.912691
FAM46D	0.317161	0.912691
GLB1L3	0.317161	0.912691
IFT88	0.317161	0.912691
KLHL14	0.317161	0.912691
MTMR8	0.317161	0.912691
OTOL1	0.317161	0.912691
PCDHB3	0.317161	0.912691
PRRC2C	0.317161	0.912691
RIMBP2	0.317161	0.912691
TGFBR1	0.317161	0.912691
TOX2	0.317161	0.912691
TRPC4	0.317161	0.912691
UBR1	0.317161	0.912691
UGT2B11	0.317161	0.912691
ZNF454	0.317161	0.912691
FAM135B	0.318276	0.912691
ACAN	0.353735	0.912691
ADAM23	0.353735	0.912691
ADAMTS19	0.353735	0.912691
AMOTL1	0.353735	0.912691
CDH7	0.353735	0.912691
DGKI	0.353735	0.912691
DIP2A	0.353735	0.912691
EFCAB4B	0.353735	0.912691
EHBP1	0.353735	0.912691
FER1L6	0.353735	0.912691

VWA5B1	0.353735	0.912691
CMYA5	0.23902	0.912691
MUC19	0.23902	0.912691
PEG3	0.23902	0.912691
CEP350	0.251799	0.912691
EPHA5	0.251799	0.912691
RANBP2	0.251799	0.912691
DOCK4	0.290116	0.912691
ADAMTS2	0.318147	0.912691
CDH18	0.318147	0.912691
CLCN1	0.318147	0.912691
FHOD3	0.318147	0.912691
GRM1	0.318147	0.912691
ITGA8	0.318147	0.912691
KIF19	0.318147	0.912691
MAGEC1	0.318147	0.912691
NIN	0.318147	0.912691
PDGFRA	0.318147	0.912691
PODN	0.318147	0.912691
REG3G	0.318147	0.912691
SLITRK3	0.318147	0.912691
SPEG	0.318147	0.912691
TLR4	0.318147	0.912691
ZNF292	0.318147	0.912691
SLC44A5	0.350943	0.912691
SLC8A1	0.350943	0.912691
SPTBN5	0.350943	0.912691
SDK2	0.353936	0.912691
CAGE1	0.355588	0.912691
CCDC88C	0.355588	0.912691
CHD5	0.355588	0.912691
CHD7	0.355588	0.912691
CNGB1	0.355588	0.912691
CRNN	0.355588	0.912691
CUL9	0.355588	0.912691
DAB2	0.355588	0.912691
EFCAB5	0.355588	0.912691
ESRP1	0.355588	0.912691
FBLN2	0.355588	0.912691
GPR115	0.355588	0.912691
GPR63	0.355588	0.912691

GRIA2	0.355588	0.912691
IGDCC4	0.355588	0.912691
KCNB1	0.355588	0.912691
LILRA6	0.355588	0.912691
MAGEA12	0.355588	0.912691
MAP3K9	0.355588	0.912691
MAST4	0.355588	0.912691
MYH9	0.355588	0.912691
MYPN	0.355588	0.912691
OR11G2	0.355588	0.912691
PARP14	0.355588	0.912691
PCDHB16	0.355588	0.912691
PDZRN4	0.355588	0.912691
PER1	0.355588	0.912691
PLXNC1	0.355588	0.912691
POU6F2	0.355588	0.912691
PTPRF	0.355588	0.912691
Q8N8K0	0.355588	0.912691
QSOX2	0.355588	0.912691
R3HDM2	0.355588	0.912691
RAB11FIP1	0.355588	0.912691
RAG1	0.355588	0.912691
RERGL	0.355588	0.912691
RGS22	0.355588	0.912691
RSPH10B2	0.355588	0.912691
RXFP3	0.355588	0.912691
SMG1	0.355588	0.912691
SPEN	0.355588	0.912691
SPP1	0.355588	0.912691
SSC5D	0.355588	0.912691
TDP1	0.355588	0.912691
TKTL2	0.355588	0.912691
TTC37	0.355588	0.912691
TTLL6	0.355588	0.912691
UACA	0.355588	0.912691
WWP2	0.355588	0.912691
ZFYVE9	0.355588	0.912691
ZNF239	0.355588	0.912691
ZNF407	0.355588	0.912691
ZNF423	0.355588	0.912691
KEL	0.251221	0.912691

MYOM3	0.251221	0.912691
PAPPA2	0.251221	0.912691
TMEM132A	0.251221	0.912691
ABL2	0.267847	0.912691
AGC1	0.267847	0.912691
ANKRD26	0.267847	0.912691
AP1G2	0.267847	0.912691
C14orf39	0.267847	0.912691
CAMK4	0.267847	0.912691
CDH2	0.267847	0.912691
CDON	0.267847	0.912691
COL1A2	0.267847	0.912691
COL25A1	0.267847	0.912691
DOCK8	0.267847	0.912691
ELMO1	0.267847	0.912691
FAM47A	0.267847	0.912691
FBXL7	0.267847	0.912691
GRIK4	0.267847	0.912691
KCNJ3	0.267847	0.912691
KRT6A	0.267847	0.912691
MYF5	0.267847	0.912691
NLRP7	0.267847	0.912691
OR4N2	0.267847	0.912691
SHROOM4	0.267847	0.912691
SNTG2	0.267847	0.912691
SUN1	0.267847	0.912691
TMEM132E	0.267847	0.912691
TRPC6	0.267847	0.912691
USO1	0.267847	0.912691
ZFC3H1	0.267847	0.912691
ZNF638	0.267847	0.912691
ZSCAN12	0.267847	0.912691
BAI2	0.291265	0.912691
DROSHA	0.291265	0.912691
IGF2R	0.291265	0.912691
KRT2	0.291265	0.912691
STARD9	0.291265	0.912691
SYCP2L	0.291265	0.912691
SYTL2	0.291265	0.912691
TNC	0.291265	0.912691
VAV3	0.291265	0.912691

ZNF507	0.291265	0.912691
ADCY2	0.357414	0.912691
ANAPC1	0.357414	0.912691
ARFGEF1	0.357414	0.912691
BCORL1	0.357414	0.912691
BDP1	0.357414	0.912691
C3orf77	0.357414	0.912691
CD86	0.357414	0.912691
COL14A1	0.357414	0.912691
CREBBP	0.357414	0.912691
IGSF21	0.357414	0.912691
KIF17	0.357414	0.912691
MS4A14	0.357414	0.912691
MYCBP2	0.357414	0.912691
MYH3	0.357414	0.912691
NINL	0.357414	0.912691
OR2L13	0.357414	0.912691
OR2M2	0.357414	0.912691
OR5T2	0.357414	0.912691
PDE10A	0.357414	0.912691
PDZRN3	0.357414	0.912691
SACS	0.357414	0.912691
TECTA	0.357414	0.912691
TMEM132D	0.357414	0.912691
TNNI3K	0.357414	0.912691
UTP20	0.357414	0.912691
WDR87	0.357414	0.912691
AGL	0.369232	0.919335
ATP1A4	0.369232	0.919335
ENSG00000121031	0.369232	0.919335
GAK	0.369232	0.919335
GRIN2A	0.369232	0.919335
MYO5A	0.369232	0.919335
PIK3CA	0.369232	0.919335
PTCH1	0.369232	0.919335
SBF1	0.369232	0.919335
SLC9A4	0.369232	0.919335
VPS13D	0.369232	0.919335
VWF	0.369232	0.919335
WDR64	0.369232	0.919335
WNK1	0.369232	0.919335

ZNF485	0.369232	0.919335
ZNF814	0.369232	0.919335
MUC16	0.381604	0.946737
FBN1	0.382017	0.946737
NRXN3	0.382017	0.946737
LRP1B	0.424584	0.952527
KRAS	0.39817	0.952527
HRNR	0.390042	0.952527
HYDIN	0.398851	0.952527
USH2A	0.393653	0.952527
HLA-C	0.410884	0.952527
PRUNE2	0.410884	0.952527
KEAP1	0.4148	0.952527
CNTN6	0.393134	0.952527
GRM5	0.429711	0.952527
KIAA0040	0.429711	0.952527
NBEA	0.429711	0.952527
POLQ	0.429711	0.952527
POTEC	0.429711	0.952527
TEP1	0.429711	0.952527
UNC79	0.429711	0.952527
WDFY4	0.429711	0.952527
DSEL	0.409083	0.952527
PIEZO2	0.409083	0.952527
ADAM12	0.426036	0.952527
ALPI	0.426036	0.952527
ARHGEF11	0.426036	0.952527
ATAD5	0.426036	0.952527
C15orf42	0.426036	0.952527
CDHR2	0.426036	0.952527
CKAP2L	0.426036	0.952527
COL4A6	0.426036	0.952527
CSF1R	0.426036	0.952527
CUX2	0.426036	0.952527
DOCK5	0.426036	0.952527
EPB41L3	0.426036	0.952527
FAM123C	0.426036	0.952527
FAM55D	0.426036	0.952527
FIG4	0.426036	0.952527
FLT3	0.426036	0.952527
GABRB3	0.426036	0.952527

KIF23	0.426036	0.952527
KIF26B	0.426036	0.952527
LPPR4	0.426036	0.952527
LZTR1	0.426036	0.952527
MATN2	0.426036	0.952527
MCC	0.426036	0.952527
MCM2	0.426036	0.952527
MMP8	0.426036	0.952527
MYOF	0.426036	0.952527
NCAM2	0.426036	0.952527
NIPBL	0.426036	0.952527
OR4P4	0.426036	0.952527
OR8U1	0.426036	0.952527
PABPC4L	0.426036	0.952527
PASK	0.426036	0.952527
PCDHB13	0.426036	0.952527
PER2	0.426036	0.952527
PHLDB1	0.426036	0.952527
SAGE1	0.426036	0.952527
SDHA	0.426036	0.952527
SERPINA9	0.426036	0.952527
SIPA1L2	0.426036	0.952527
SLC9A10	0.426036	0.952527
TOP2B	0.426036	0.952527
UNC45B	0.426036	0.952527
C10orf71	0.389289	0.952527
CNTNAP2	0.389289	0.952527
COL19A1	0.389289	0.952527
CTNNA2	0.389289	0.952527
DYNC1H1	0.389289	0.952527
CNTN5	0.396682	0.952527
HSPG2	0.396682	0.952527
ADAMTS5	0.426036	0.952527
DCLK1	0.426036	0.952527
DYNC1I1	0.426036	0.952527
HHLA1	0.426036	0.952527
LRFN5	0.426036	0.952527
SETD2	0.426036	0.952527
STK32B	0.426036	0.952527
TUBA3C	0.426036	0.952527
SMARCA4	0.530574	0.952911

PCDH15	0.456931	0.952911
LRP2	0.492989	0.952911
CCDC144NL	0.45793	0.952911
FMN2	0.484885	0.952911
C1orf129	0.438407	0.952911
RET	0.438407	0.952911
C2orf71	0.490045	0.952911
COL7A1	0.490045	0.952911
MUC12	0.490045	0.952911
NCAM1	0.490045	0.952911
SORCS1	0.490045	0.952911
OR2T33	0.516939	0.952911
POTEE	0.516939	0.952911
ABCA4	0.46592	0.952911
DSCAM	0.46592	0.952911
ENSG00000174501	0.46592	0.952911
GLP1R	0.46592	0.952911
OR4K17	0.46592	0.952911
PCDHA11	0.46592	0.952911
PCDHGB1	0.46592	0.952911
MYH4	0.478679	0.952911
AQR	0.485918	0.952911
AR	0.485918	0.952911
FBN3	0.485918	0.952911
HIVEP1	0.485918	0.952911
KIAA1324	0.485918	0.952911
LRP1	0.485918	0.952911
LRRTM3	0.485918	0.952911
MDC1	0.485918	0.952911
QRICH2	0.485918	0.952911
SHPRH	0.485918	0.952911
SYNPO2	0.485918	0.952911
WBSCR17	0.485918	0.952911
GPRIN2	0.514924	0.952911
ADAMTS12	0.451335	0.952911
PTPRD	0.451335	0.952911
SCN10A	0.451335	0.952911
ABCB5	0.471807	0.952911
ATM	0.471807	0.952911
ARAP2	0.507003	0.952911
COL20A1	0.507003	0.952911

DOCK10	0.507003	0.952911
FREM1	0.507003	0.952911
GTF3C1	0.507003	0.952911
KALRN	0.507003	0.952911
KIAA1409	0.507003	0.952911
LRBA	0.507003	0.952911
NBEAL1	0.507003	0.952911
PRRC2B	0.507003	0.952911
SULF2	0.507003	0.952911
TNXB	0.507003	0.952911
WNK2	0.507003	0.952911
ANKRD17	0.530788	0.952911
ATN1	0.530788	0.952911
CENPF	0.530788	0.952911
COL4A5	0.530788	0.952911
DACT1	0.530788	0.952911
DLG2	0.530788	0.952911
DSPP	0.530788	0.952911
ERN2	0.530788	0.952911
FRMD6	0.530788	0.952911
GALNT13	0.530788	0.952911
GIMAP8	0.530788	0.952911
GREB1	0.530788	0.952911
GUCY1A3	0.530788	0.952911
IRS1	0.530788	0.952911
ITPR2	0.530788	0.952911
KCNH8	0.530788	0.952911
LAMA3	0.530788	0.952911
LAMB1	0.530788	0.952911
MMRN1	0.530788	0.952911
NBEAL2	0.530788	0.952911
NCOR2	0.530788	0.952911
NUP210L	0.530788	0.952911
PREX1	0.530788	0.952911
PXDN	0.530788	0.952911
RBM19	0.530788	0.952911
ROBO2	0.530788	0.952911
SCN5A	0.530788	0.952911
SH3TC2	0.530788	0.952911
SIK3	0.530788	0.952911
SLC5A10	0.530788	0.952911

SLIT3	0.530788	0.952911
TRPC5	0.530788	0.952911
A2ML1	0.517161	0.952911
ABCC9	0.517161	0.952911
ADAMTS18	0.517161	0.952911
AGBL1	0.517161	0.952911
ATRNL1	0.517161	0.952911
BRAF	0.517161	0.952911
C12orf26	0.517161	0.952911
CADM3	0.517161	0.952911
CAPN14	0.517161	0.952911
CCDC136	0.517161	0.952911
CD1E	0.517161	0.952911
CLNK	0.517161	0.952911
COL6A1	0.517161	0.952911
COL6A2	0.517161	0.952911
CSNK2A1	0.517161	0.952911
CTNNA3	0.517161	0.952911
CXCR4	0.517161	0.952911
DENND1A	0.517161	0.952911
DMBX1	0.517161	0.952911
DNA2	0.517161	0.952911
DNER	0.517161	0.952911
DPYS	0.517161	0.952911
DSG3	0.517161	0.952911
EXD3	0.517161	0.952911
EXT2	0.517161	0.952911
F9	0.517161	0.952911
FAM48B1	0.517161	0.952911
FNIP2	0.517161	0.952911
FOLH1	0.517161	0.952911
FOLH1B	0.517161	0.952911
FPGT-TNNI3K	0.517161	0.952911
GALNT9	0.517161	0.952911
GPR124	0.517161	0.952911
GPR179	0.517161	0.952911
HEATR1	0.517161	0.952911
HERC6	0.517161	0.952911
IL18RAP	0.517161	0.952911
KDM4C	0.517161	0.952911
KIAA0232	0.517161	0.952911

KIAA1671	0.517161	0.952911
KIAA2022	0.517161	0.952911
KPNA7	0.517161	0.952911
LEMD3	0.517161	0.952911
LGR5	0.517161	0.952911
MAGEB18	0.517161	0.952911
MIA3	0.517161	0.952911
MRVI1	0.517161	0.952911
MYT1L	0.517161	0.952911
NACAD	0.517161	0.952911
NLRP1	0.517161	0.952911
NRAS	0.517161	0.952911
NSD1	0.517161	0.952911
NUP210	0.517161	0.952911
OR2T3	0.517161	0.952911
OR6C75	0.517161	0.952911
OR6X1	0.517161	0.952911
PCDHB10	0.517161	0.952911
PDCD6IP	0.517161	0.952911
PDE1A	0.517161	0.952911
PNMA5	0.517161	0.952911
PRCP	0.517161	0.952911
PRSS55	0.517161	0.952911
PTDSS1	0.517161	0.952911
PTPRU	0.517161	0.952911
RBMXL3	0.517161	0.952911
REG1A	0.517161	0.952911
RPP40	0.517161	0.952911
RUFY4	0.517161	0.952911
SEC16B	0.517161	0.952911
SF1	0.517161	0.952911
SPATC1	0.517161	0.952911
SVIL	0.517161	0.952911
SYT6	0.517161	0.952911
TAS2R5	0.517161	0.952911
TNS3	0.517161	0.952911
TRIP11	0.517161	0.952911
TUSC3	0.517161	0.952911
UMODL1	0.517161	0.952911
VLDLR	0.517161	0.952911
VSTM1	0.517161	0.952911

VWA3A	0.517161	0.952911
ZNF160	0.517161	0.952911
ZNF234	0.517161	0.952911
ZNF451	0.517161	0.952911
RNF213	0.534733	0.958915
DNAH11	0.555654	0.964186
FLNC	0.558386	0.964186
MACF1	0.539035	0.964186
BAI1	0.546554	0.964186
C11orf41	0.546554	0.964186
INTS1	0.546554	0.964186
KDR	0.546554	0.964186
LAMA2	0.546554	0.964186
MYBPC1	0.546554	0.964186
PTPRT	0.546554	0.964186
ADAMTS7	0.558817	0.964186
AKAP6	0.558817	0.964186
ATP10D	0.558817	0.964186
CACNA1I	0.558817	0.964186
CLCA2	0.558817	0.964186
DPP6	0.558817	0.964186
FAM188B	0.558817	0.964186
FAM83B	0.558817	0.964186
JMJD1C	0.558817	0.964186
11-Mar	0.558817	0.964186
NLRP9	0.558817	0.964186
OR12D3	0.558817	0.964186
OR1C1	0.558817	0.964186
OR5W2	0.558817	0.964186
RFX6	0.558817	0.964186
TAF2	0.558817	0.964186
TGM6	0.558817	0.964186
TYR	0.558817	0.964186
USP6NL	0.558817	0.964186
WWOX	0.558817	0.964186
ZIM2	0.558817	0.964186
ZNF365	0.558817	0.964186
ZNF534	0.558817	0.964186
ZNF665	0.558817	0.964186
ZP1	0.558817	0.964186
BIRC6	0.560655	0.966313

Q9Y6V0-3	0.581866	0.97311
CSMD3	0.598836	0.97311
MUC4	0.613448	0.97311
NRXN1	0.608699	0.97311
COL12A1	0.568	0.97311
SRCAP	0.568	0.97311
C12orf51	0.583454	0.97311
COL6A3	0.583454	0.97311
DNAH7	0.583454	0.97311
MED12L	0.583454	0.97311
SLIT2	0.583454	0.97311
SPEF2	0.583454	0.97311
TEX15	0.603742	0.97311
ASXL3	0.609397	0.97311
CDH10	0.609397	0.97311
LRRC7	0.566686	0.97311
ASH1L	0.588888	0.97311
ZFHX3	0.588888	0.97311
C7orf10	0.604923	0.97311
DAGLA	0.604923	0.97311
FCRL2	0.604923	0.97311
GRIK3	0.604923	0.97311
INTS2	0.604923	0.97311
KIF1A	0.604923	0.97311
MED12	0.604923	0.97311
NCKAP1L	0.604923	0.97311
NOTCH2	0.604923	0.97311
PRG4	0.604923	0.97311
ROS1	0.604923	0.97311
SEC16A	0.604923	0.97311
SLC12A5	0.604923	0.97311
TBRG4	0.604923	0.97311
VWA3B	0.604923	0.97311
ADAM22	0.621302	0.97311
ANKRD50	0.621302	0.97311
ANO6	0.621302	0.97311
APLP2	0.621302	0.97311
ATP13A2	0.621302	0.97311
BEND2	0.621302	0.97311
BNC1	0.621302	0.97311
C11orf9	0.621302	0.97311

CTAGE1	0.621302	0.97311
FASN	0.621302	0.97311
FRMPD3	0.621302	0.97311
GADL1	0.621302	0.97311
GALNT14	0.621302	0.97311
GOLGA5	0.621302	0.97311
GPR149	0.621302	0.97311
HHAT	0.621302	0.97311
HIVEP2	0.621302	0.97311
HYOU1	0.621302	0.97311
KDM5B	0.621302	0.97311
KIAA0317	0.621302	0.97311
KIAA0947	0.621302	0.97311
KIAA1109	0.621302	0.97311
KIAA1244	0.621302	0.97311
KIF3B	0.621302	0.97311
KIRREL	0.621302	0.97311
MAN1A1	0.621302	0.97311
MAP9	0.621302	0.97311
MET	0.621302	0.97311
MN1	0.621302	0.97311
MYO10	0.621302	0.97311
MYO5C	0.621302	0.97311
NCOA1	0.621302	0.97311
NCOA7	0.621302	0.97311
NFATC1	0.621302	0.97311
NOS2	0.621302	0.97311
PARP1	0.621302	0.97311
PCDHGB4	0.621302	0.97311
PCNXL3	0.621302	0.97311
PKP4	0.621302	0.97311
POLR3B	0.621302	0.97311
PPL	0.621302	0.97311
RBL1	0.621302	0.97311
RIN3	0.621302	0.97311
SCAF11	0.621302	0.97311
SCAPER	0.621302	0.97311
SH3PXD2A	0.621302	0.97311
SIPA1L1	0.621302	0.97311
SIPA1L3	0.621302	0.97311
SLC45A1	0.621302	0.97311

SLC6A6	0.621302	0.97311
SP3	0.621302	0.97311
TCF20	0.621302	0.97311
TCHHL1	0.621302	0.97311
TULP4	0.621302	0.97311
UGT2A1	0.621302	0.97311
UHRF1BP1	0.621302	0.97311
USP40	0.621302	0.97311
VIT	0.621302	0.97311
ZEB1	0.621302	0.97311
ZNF512	0.621302	0.97311
XIRP1	0.622154	0.973489
LPHN3	0.637616	0.979845
SI	0.645251	0.979845
TNN	0.628912	0.979845
DCAF8L1	0.645918	0.979845
FAM47B	0.645918	0.979845
FTMT	0.645918	0.979845
HUWE1	0.645918	0.979845
INF2	0.645918	0.979845
POTEH	0.645918	0.979845
RASGRP3	0.645918	0.979845
SCN11A	0.645918	0.979845
SLC5A7	0.645918	0.979845
SYMPK	0.645918	0.979845
TLL2	0.645918	0.979845
TTC28	0.645918	0.979845
UGT1A7	0.645918	0.979845
WDR52	0.645918	0.979845
CRB1	0.647684	0.979845
DBC1	0.647684	0.979845
LRRK2	0.647684	0.979845
ATP8B3	0.65016	0.979845
C2CD3	0.65016	0.979845
CCDC141	0.65016	0.979845
COL2A1	0.65016	0.979845
DCC	0.65016	0.979845
DOCK7	0.65016	0.979845
IQGAP3	0.65016	0.979845
ITPKB	0.65016	0.979845
KIAA1210	0.65016	0.979845

KIAA1731	0.65016	0.979845
KMT2D	0.65016	0.979845
LTBP1	0.65016	0.979845
MYH11	0.65016	0.979845
NLGN1	0.65016	0.979845
PDE1C	0.65016	0.979845
PKD1	0.65016	0.979845
PLCB1	0.65016	0.979845
SORBS1	0.65016	0.979845
TNRC6B	0.65016	0.979845
ANKRD36	0.663312	0.985704
C1orf173	0.663312	0.985704
CEP250	0.663312	0.985704
CXorf22	0.663312	0.985704
DOCK2	0.663312	0.985704
MYO7A	0.663312	0.985704
NTRK3	0.663312	0.985704
SEZ6L	0.663312	0.985704
SLITRK2	0.663312	0.985704
TMPRSS15	0.663312	0.985704
TPR	0.663312	0.985704
UBR4	0.663312	0.985704
ZDBF2	0.663312	0.985704
ZNF469	0.663312	0.985704
ZNF804B	0.663312	0.985704
PKHD1	0.668069	0.990007
SETBP1	0.668069	0.990007
TSHZ3	0.668069	0.990007
COL3A1	0.678267	0.991077
DYNC2H1	0.678267	0.991077
CECR2	0.683073	0.991077
DDX11	0.683073	0.991077
EGFR	0.683073	0.991077
FAM38B	0.683073	0.991077
FAT	0.683073	0.991077
FRMPD2	0.683073	0.991077
OR2T34	0.683073	0.991077
PCDHA8	0.683073	0.991077
SLC4A10	0.683073	0.991077
UNC13D	0.683073	0.991077
USP6	0.683073	0.991077

ZEB2	0.683073	0.991077
CEP192	0.680951	0.991077
CUBN	0.680951	0.991077
ENGASE	0.680951	0.991077
LAMC3	0.680951	0.991077
ODZ4	0.680951	0.991077
PTPRN2	0.680951	0.991077
SCN2A	0.680951	0.991077
SHANK1	0.680951	0.991077
TNR	0.680951	0.991077
LOC652153	0.7108	0.99538
ABCA13	0.746463	0.99538
COL22A1	0.687671	0.99538
DNAH9	0.687671	0.99538
SYNE1	0.740502	0.99538
NCKAP5	0.715905	0.99538
SPHKAP	0.715905	0.99538
ABCA9	0.752435	0.99538
ALMS1	0.752435	0.99538
STAB1	0.752435	0.99538
MAP2	0.707255	0.99538
MKRN3	0.725616	0.99538
PCDH17	0.725616	0.99538
PCDHA3	0.725616	0.99538
PDHA2	0.725616	0.99538
RIMS2	0.731147	0.99538
KIAA1107	0.731392	0.99538
NALCN	0.742811	0.99538
ADCY6	0.730178	0.99538
AKAP13	0.730178	0.99538
ATAD3B	0.730178	0.99538
ATF7IP	0.730178	0.99538
BTK	0.730178	0.99538
C14orf135	0.730178	0.99538
CCDC88A	0.730178	0.99538
CDH20	0.730178	0.99538
CHL1	0.730178	0.99538
CPXM2	0.730178	0.99538
CRISP2	0.730178	0.99538
DHRS2	0.730178	0.99538
DMXL2	0.730178	0.99538

EZR	0.730178	0.99538
FAM75D4	0.730178	0.99538
GRM7	0.730178	0.99538
JAKMIP3	0.730178	0.99538
KIAA0240	0.730178	0.99538
LRIT1	0.730178	0.99538
MAEL	0.730178	0.99538
NCOA2	0.730178	0.99538
NOX5	0.730178	0.99538
NRP2	0.730178	0.99538
PCDHB11	0.730178	0.99538
PCDHB14	0.730178	0.99538
PCM1	0.730178	0.99538
PCNX	0.730178	0.99538
PDZD7	0.730178	0.99538
PPFIA3	0.730178	0.99538
PRAMEF10	0.730178	0.99538
RGPD3	0.730178	0.99538
RGS6	0.730178	0.99538
RTEL1	0.730178	0.99538
SGOL2	0.730178	0.99538
SLC24A4	0.730178	0.99538
SLC2A14	0.730178	0.99538
SLITRK4	0.730178	0.99538
SPAG16	0.730178	0.99538
TGM7	0.730178	0.99538
TTLL5	0.730178	0.99538
USP13	0.730178	0.99538
XDH	0.730178	0.99538
ZC3H12B	0.730178	0.99538
ZNF670	0.730178	0.99538
ZNF724P	0.730178	0.99538
ABCA1	0.755267	0.99538
AKAP12	0.755267	0.99538
AOAH	0.755267	0.99538
ATP2B2	0.755267	0.99538
BAZ2A	0.755267	0.99538
BRCA1	0.755267	0.99538
C10orf81	0.755267	0.99538
C7orf72	0.755267	0.99538
CELSR3	0.755267	0.99538

CHD8	0.755267	0.99538
CLCA4	0.755267	0.99538
CNGA3	0.755267	0.99538
COL1A1	0.755267	0.99538
DACH2	0.755267	0.99538
DNHD1	0.755267	0.99538
FREM2	0.755267	0.99538
GUCY2F	0.755267	0.99538
HPSE2	0.755267	0.99538
INPPL1	0.755267	0.99538
ITGB4	0.755267	0.99538
KNTC1	0.755267	0.99538
KSR2	0.755267	0.99538
LRIT2	0.755267	0.99538
MAN2A1	0.755267	0.99538
MYLK	0.755267	0.99538
NEBL	0.755267	0.99538
OR4N4	0.755267	0.99538
OR51A4	0.755267	0.99538
OR8B4	0.755267	0.99538
PCDHGB5	0.755267	0.99538
PPP4R4	0.755267	0.99538
PREX2	0.755267	0.99538
PTCHD2	0.755267	0.99538
PTPRM	0.755267	0.99538
S1PR1	0.755267	0.99538
SEMA3D	0.755267	0.99538
SLC30A10	0.755267	0.99538
SLC39A12	0.755267	0.99538
SLX4	0.755267	0.99538
SRGAP3	0.755267	0.99538
TET2	0.755267	0.99538
TONSL	0.755267	0.99538
TRPM6	0.755267	0.99538
XRN1	0.755267	0.99538
ZFP64	0.755267	0.99538
ZNF607	0.755267	0.99538
ZNF676	0.755267	0.99538
ZPLD1	0.755267	0.99538
TAS2R30	0.758084	0.998269
TP53	0.925968	1

TTN	1	1
PCLO	0.807234	1
RYR2	0.948004	1
APOB	0.945404	1
COL11A1	1	1
PKHD1L1	0.786028	1
MYO18B	0.934343	1
ANKRD30B	1	1
SYNE2	1	1
CDH23	0.870053	1
FCGBP	0.870053	1
MLL3	0.870053	1
VCAN	0.878946	1
CACNA1B	0.930239	1
MYH2	0.930239	1
CASR	0.782521	1
CTTNBP2	0.782521	1
DNAH17	0.782521	1
ODZ2	0.782521	1
PTPRZ1	0.782521	1
AGRN	0.9149	1
WDFY3	0.9149	1
ZNF831	0.9149	1
MLL2	0.931607	1
HDAC9	1	1
PDE4DIP	1	1
PXDNL	1	1
FAT1	1	1
GGT1	1	1
TRPS1	1	1
USP34	1	1
GRIN2B	1	1
CDK5RAP2	0.771931	1
MDN1	0.771931	1
MUC5AC	0.771931	1
SEMA3E	0.771931	1
TRPM2	0.771931	1
ANKRD30A	0.79284	1
CPS1	0.79284	1
NLRP3	0.79284	1
ODZ1	0.79284	1

PKD1L1	0.79284	1
CACNA1G	0.84871	1
MYO7B	0.84871	1
ABCA12	0.890246	1
ADGB	0.890246	1
BCOR	0.890246	1
MAGI2	0.890246	1
OC90	0.890246	1
PCNT	0.890246	1
THADA	0.890246	1
CNTNAP4	0.920573	1
DCHS2	0.920573	1
MUC5B	0.920573	1
OVCH1	0.920573	1
TMEM132C	0.920573	1
DNAH5	1	1
DNAH6	1	1
DNAJC13	1	1
ITGAD	1	1
AC010872	1	1
MDGA2	1	1
NID1	1	1
NOTCH1	1	1
SCN4A	1	1
C4orf21	1	1
CACNA1H	1	1
COBL	1	1
COL6A6	1	1
HTT	1	1
MAP2K3	1	1
NOBOX	1	1
OR4M2	1	1
PDE3A	1	1
PDPR	1	1
TLN2	1	1
TRIOBP	1	1
TRPM8	1	1
ZP4	1	1
CAMTA1	0.782538	1
DLG5	0.782538	1
EPRS	0.782538	1

FAM171B	0.782538	1
FAM75D1	0.782538	1
GRIK1	0.782538	1
HCN1	0.782538	1
HOMEZ	0.782538	1
ITGA2B	0.782538	1
NDST4	0.782538	1
NRG3	0.782538	1
OR10J1	0.782538	1
PDE4B	0.782538	1
PLXNA2	0.782538	1
PPFIA2	0.782538	1
PPP1R3A	0.782538	1
SLC2A13	0.782538	1
STARD8	0.782538	1
TPTE	0.782538	1
VPS13A	0.782538	1
DDX60L	0.804011	1
HEATR5A	0.804011	1
NLRP4	0.804011	1
OR2T6	0.804011	1
SCN9A	0.804011	1
WDR90	0.804011	1
ZBBX	0.804011	1
FLG2	0.829799	1
KIAA1549	0.829799	1
LCT	0.829799	1
LPHN2	0.829799	1
MYO15A	0.829799	1
ABCB11	0.87503	1
ATP1A2	0.87503	1
C19orf44	0.87503	1
C6orf103	0.87503	1
CACNA1S	0.87503	1
CACNB2	0.87503	1
CAMSAP1	0.87503	1
CHIT1	0.87503	1
COL21A1	0.87503	1
DNAH12	0.87503	1
ENAM	0.87503	1
ERBB2IP	0.87503	1

FAM171A1	0.87503	1
GPR50	0.87503	1
HCFC1	0.87503	1
HTR3A	0.87503	1
INHBA	0.87503	1
JAKMIP1	0.87503	1
KCNH1	0.87503	1
KIF13B	0.87503	1
KIF21A	0.87503	1
LOC652737	0.87503	1
MYO16	0.87503	1
MYO19	0.87503	1
NEK1	0.87503	1
OR2G2	0.87503	1
OR2T4	0.87503	1
OR52A1	0.87503	1
OR52K1	0.87503	1
PCDHA5	0.87503	1
PCDHB8	0.87503	1
PLCH1	0.87503	1
PRX	0.87503	1
PTPN14	0.87503	1
RFTN2	0.87503	1
SCUBE1	0.87503	1
SNRPN	0.87503	1
SON	0.87503	1
TAF5L	0.87503	1
TANC2	0.87503	1
TRIM49	0.87503	1
UNC5A	0.87503	1
USH1C	0.87503	1
WDR63	0.87503	1
ASTN1	0.904688	1
BCLAF1	0.904688	1
CACNA2D1	0.904688	1
CD1B	0.904688	1
COL15A1	0.904688	1
COL5A1	0.904688	1
FAM193A	0.904688	1
FAM5C	0.904688	1
GLI2	0.904688	1

ITPR3	0.904688	1
LILRB2	0.904688	1
NEFH	0.904688	1
OR5T3	0.904688	1
POSTN	0.904688	1
RTTN	0.904688	1
TENM2	0.904688	1
VWDE	0.904688	1
YLPM1	0.904688	1
ADAMTS20	1	1
CHD6	1	1
CKAP5	1	1
DCAF4L2	1	1
ELTD1	1	1
FNDC1	1	1
FREM3	1	1
LILRB1	1	1
NES	1	1
UBR5	1	1
UTRN	1	1
WDR17	1	1
ZNF804A	1	1
AC007731	1	1
ADCY10	1	1
ALPK2	1	1
BRWD1	1	1
CAPN6	1	1
CEP290	1	1
DIDO1	1	1
FMNL3	1	1
FOXP2	1	1
FYB	1	1
GRIA4	1	1
HEPACAM2	1	1
HEPH	1	1
MEF2A	1	1
NOS1	1	1
PLEC	1	1
SLC4A2	1	1
TTC40	1	1
AADACL4	0.843787	1

ABCD4	0.843787	1
ADM2	0.843787	1
ASNS	0.843787	1
C9	0.843787	1
CDK11B	0.843787	1
CNDP1	0.843787	1
COBLL1	0.843787	1
FMN1	0.843787	1
FSTL5	0.843787	1
GK2	0.843787	1
GLRA2	0.843787	1
IFT122	0.843787	1
IGSF3	0.843787	1
INSRR	0.843787	1
ITFG1	0.843787	1
KCNT1	0.843787	1
KIAA0226L	0.843787	1
KIAA1404	0.843787	1
KIAA2026	0.843787	1
LRRC15	0.843787	1
MVP	0.843787	1
OR5B12	0.843787	1
OR6Y1	0.843787	1
OTOG	0.843787	1
PAXIP1	0.843787	1
PCDHGA1	0.843787	1
PCK1	0.843787	1
PDE9A	0.843787	1
PHKA1	0.843787	1
PIK3R5	0.843787	1
PSG6	0.843787	1
RBM10	0.843787	1
SIGLEC5	0.843787	1
SLC2A4	0.843787	1
SLC32A1	0.843787	1
SLC38A8	0.843787	1
SLC4A4	0.843787	1
SUPT6H	0.843787	1
TTLL7	0.843787	1
UNC5B	0.843787	1
ZNF251	0.843787	1

ZNF516	0.843787	1
ZNFX1	0.843787	1
ABCC11	0.886327	1
ADAM19	0.886327	1
AMPH	0.886327	1
ATR	0.886327	1
BAT2D1	0.886327	1
DNAH2	0.886327	1
GABRE	0.886327	1
GUCY1A2	0.886327	1
ITGA4	0.886327	1
KCTD3	0.886327	1
KIAA1462	0.886327	1
MICAL3	0.886327	1
OGDHL	0.886327	1
OR2C3	0.886327	1
PCDHGA9	0.886327	1
PCF11	0.886327	1
PTGER3	0.886327	1
PZP	0.886327	1
TRIM64C	0.886327	1
ABCB1	1	1
ABI3BP	1	1
ABLIM3	1	1
ADAM21	1	1
AGBL3	1	1
APAF1	1	1
ARHGAP15	1	1
ARHGAP6	1	1
ATRN	1	1
CD300C	1	1
CEP78	1	1
CFTR	1	1
CHRM2	1	1
COL28A1	1	1
COL4A1	1	1
CPPED1	1	1
CYP11B2	1	1
DACH1	1	1
EIF5B	1	1
FAM47C	1	1

FAM48B2	1	1
FANCD2	1	1
FCER1A	1	1
GIMAP1	1	1
GPR144	1	1
GRIK2	1	1
HTR7	1	1
ITGAM	1	1
ITPR1	1	1
KIAA0319	1	1
KIAA0907	1	1
KIF16B	1	1
KIF27	1	1
LAMB3	1	1
LCORL	1	1
LEPR	1	1
LRP12	1	1
LRRC43	1	1
MARK4	1	1
MLL	1	1
MSR1	1	1
MYH14	1	1
MYO3B	1	1
NID2	1	1
NLRP13	1	1
NLRP2	1	1
NOX3	1	1
OPA1	1	1
OR14K1	1	1
OR2AK2	1	1
OR2M5	1	1
OR56A5	1	1
P2RY10	1	1
PAN2	1	1
PCDHA1	1	1
PDE11A	1	1
PDE2A	1	1
PDILT	1	1
PIGN	1	1
PLCB4	1	1
PLD5	1	1

POP1	1	1
PPARGC1A	1	1
PSG2	1	1
Q96MC4	1	1
RADIL	1	1
RASGRF1	1	1
RBFOX1	1	1
RGL2	1	1
RNF112	1	1
SELP	1	1
SNRNP200	1	1
SNX29	1	1
SPATA17	1	1
SV2A	1	1
SV2B	1	1
TNS1	1	1
TPO	1	1
TRIM64B	1	1
UGT1A8	1	1
USP36	1	1
WDR27	1	1
WDR96	1	1
ZNF33B	1	1
ZNF341	1	1
ZNF582	1	1
ZNF600	1	1
ABP1	1	1
AEBP1	1	1
BRIP1	1	1
BRWD3	1	1
CELSR2	1	1
CHD1	1	1
CNGB3	1	1
COL18A1	1	1
COL5A2	1	1
DDX26B	1	1
DNMT3A	1	1
DPY19L4	1	1
EMR2	1	1
ENSG00000093100	1	1
FGA	1	1

GHR	1	1
JMY	1	1
KIAA0556	1	1
LIMCH1	1	1
LRRC4C	1	1
NDST3	1	1
PKD1L2	1	1
POTEF	1	1
RUNX1T1	1	1
SAMD9L	1	1
TAF1L	1	1
TAP1	1	1
TENM1	1	1
TRPC7	1	1

To further corroborate our findings, we used human epithelial cells with concurrent gene mutations commonly seen in lung cancer. Human bronchial epithelial cells (HBECs) and Human Small Airway Epithelial cells (HSEAC) were previously immortalized with the over-expression of mouse Cyclin D kinase 4 (*Cdk4*) and human telomerase reverse transcriptase (*hTERT*) [200]. The combination of these two manipulations bypass p16/Rb cell cycle checkpoint pathway and override replicative senescence allowing the cells to proliferative similar to that of lung cancer cell lines. Retroviral vector-mediated RNAi technology was used to create stable human epithelial cell clones with p53 knocked down. Next, a pBabe-hyg-KRAS2-V12 retroviral vector was introduced into p53 knock-down human epithelial cells in order to overexpress $KRAS^{v12}$ [223]. Stably $p53_{KD}$ + $KRAS^{v12}$ clones were isolated for genetic manipulations. The addition of c-MYC to $p53_{KD}$ + $KRAS^{v12}$ clones was achieved by introducing a c-MYC overexpressing retroviral vector [224]. Additionally, LKB1 was knocked down using a shRNA pLKO-Hyg construct in $p53_{KD}$ + $KRAS^{v12}$ clones. We found that the loss of TP53 did not alter macrophage polarization. Moreover, loss of TP53 and introduction of $KRAS^{V12}$ mutation in human epithelial cells did not subvert the strong *Arg1* phenotype. Furthermore, c-MYC over-expression or knock-down of

LKB1 with concurrent TP53 and KRAS mutations did not change macrophage polarization (Figure 17A-C). Recent studies on tumor microarrays from colorectal patients demonstrated that comparison of M1:M2 macrophage presence in patient tumors only correlated to microsatellite instability (MSI) and not clinicopathologic characteristics or alterations from main cancer driver genes (KRAS, TP53, BRAF, SMAD4, CDKN2A, PIK3CA) [225, 226]. Therefore, it is our conclusion that our findings, corroborated by multiple systems preclinical and clinical, suggest clinicopathologic markers or genetic alterations of NSCLC do not predict macrophage polarization in the co-culture system.

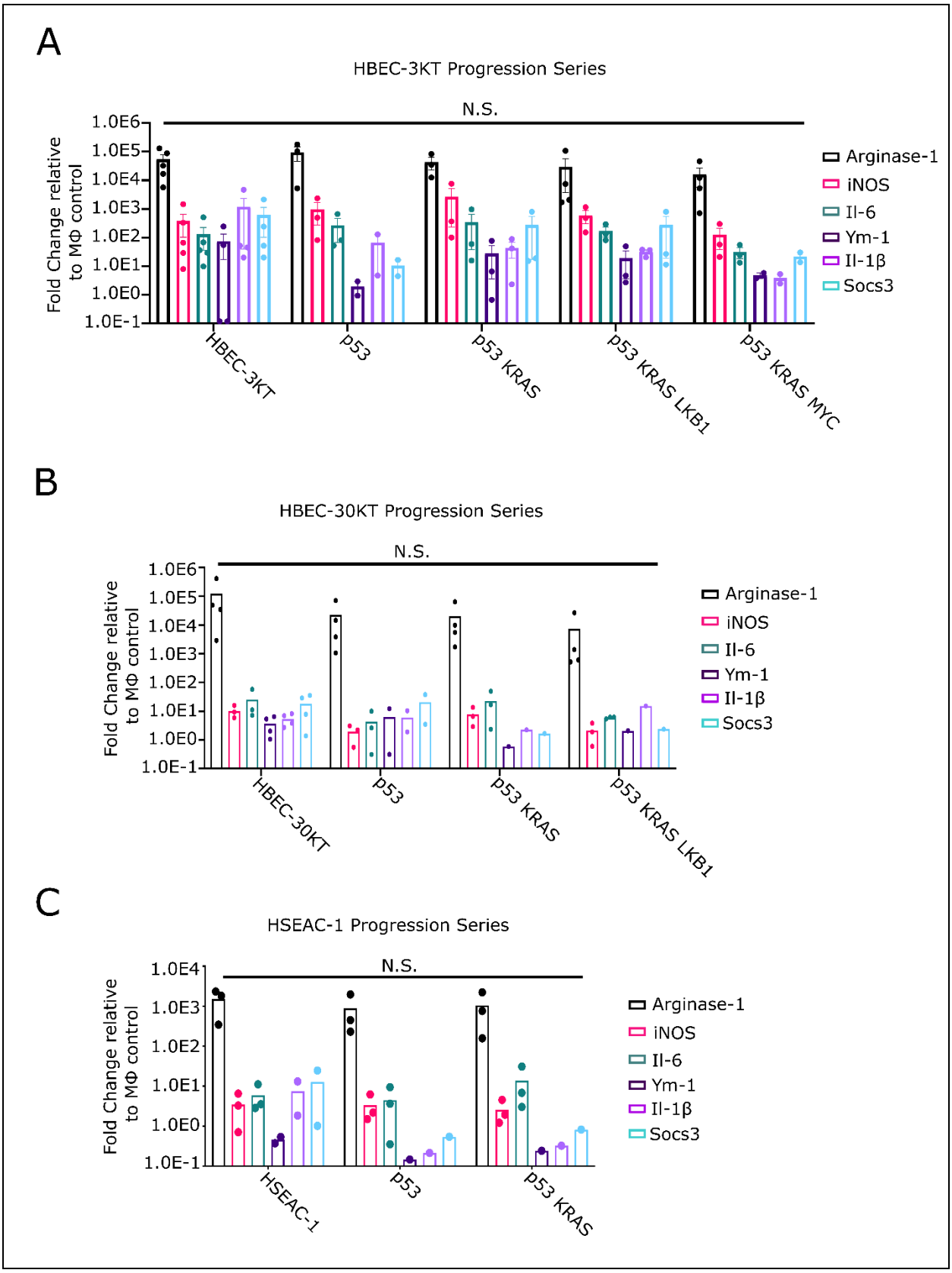
A
HBEC-3KT Progression Series
N.S.
Fold Change relative to MΦ control
1.0E6
1.0E5
1.0E4
1.0E3
1.0E2
1.0E1
1.0E0
1.0E-1
HBEC-3KT
p53
p53 KRAS
p53 KRAS LKB1
p53 KRAS MYC
Arginase-1
iNOS
Il-6
Ym-1
Il-1β
Socs3
B
HBEC-30KT Progression Series
N.S.
Fold Change relative to MΦ control
1.0E6
1.0E5
1.0E4
1.0E3
1.0E2
1.0E1
1.0E0
1.0E-1
HBEC-30KT
p53
p53 KRAS
p53 KRAS LKB1
Arginase-1
iNOS
Il-6
Ym-1
Il-1β
Socs3
C
HSEAC-1 Progression Series
N.S.
Fold Change relative to MΦ control
1.0E4
1.0E3
1.0E2
1.0E1
1.0E0
1.0E-1
HSEAC-1
p53
p53 KRAS
Arginase-1
iNOS
Il-6
Ym-1
Il-1β
Socs3

Figure 17: Controlled genetic alterations confirm that macrophage polarity does not correlate with tumor suppressor or oncogenic drivers. A) HBEC-3KT, B) HBEC-30KT and C) HSEAC-1 immortalized normal human bronchial epithelial cell lines were established by introducing mouse *Cdk4* and human h*TERT.* Both LKB1 and TP53 genes were knocked down with RNAi probes, $KRAS^{v12}$ and cMYC were overexpressed in bronchial cells [223, 224]. Co-cultures with the bronchial cells were performed to determine macrophage polarization in the presence of isolated genetic alterations. RT-qPCR was used to determine macrophage polarity, n = 3-4, two-way ANOVA with Tukey's *post-hoc* analysis for multiple comparisons, n.s.

3.6 Macrophages are modulated by paracrine, autocrine and juxtacrine cancer cell processes

In light of our discovery, cancer cell line transcriptome data was utilized to interrogate cancer cell gene signatures that could potentially contribute to macrophage polarization. Cancer cell RNA expression was segregated based on macrophage expression (*Arg1, iNOS, Il-6, Ym-1, Il-1β, Socs3*) in the co-culture. Our analysis found that several immune signaling genes were up-regulated in NSCLC that induced the high Arg1 phenotype in macrophages (Figure 18A). We then preformed GSEA on genes identified to be upregulated in cancer cells found to induce high *Arg1* expression in macrophages. From the GSEA analysis we found several cytokine signaling pathways upregulated, in particular IL-20 family signaling and IL-4 signaling (Figure 18B). As mentioned previously, cancer cells secrete IL-4 to polarize macrophages into the M2 phenotype. IL-20 family cytokines are commonly associated with cardiovascular biology and included family members IL-19, IL-20, IL-22, and IL-24. IL-20 family cytokines bind IL-20 receptors and consequently activate JAK/STAT3 signaling. As mentioned previously, activation of JAK/STAT3 signaling leads to M2 polarization in macrophages. Additionally, IL-20 secretion is commonly upregulated in endothelial cells and promotes proliferation, angiogenic tube formation, and

angiogenesis in hypoxic tissue [227]. To decipher transcriptional changes in macrophage RNA expression, we submitted a small panel of 15 different co-cultures for RNA sequencing. RNA expression data was then filtered for mouse transcripts (macrophage transcripts). We then analyzed transcriptional differences between the 15 different co-culture samples. We segregated samples by macrophages clusters and by RT-qPCR expression of *Arg1, Il-1β,* and *Socs3.* From these segregated groups we found genes significantly increased in co-cultures associated with the *Arg1* macrophage expression. GSEA identified cytokine-receptor genes that were significantly upregulated in NSCLC co-cultures (Figure 18C). This gene list included: *Il4rα, Ccr1, Ccr5, Gpr35, Cx3cr1, Ccr2, Cmklr1, Il31rα, Il21rα* and *Il17rα*. Genetic and chemical perturbations of IL-4 receptor-α (IL-4rα) have shown that IL-4rα is the primary receptor for IL-4 binding and is vital for M2 polarization in mice [228]. Monocyte chemotactic protein 1 (MCP-1/CCL2) binds CC chemokine receptor 1&5 (CCR1, CCR5). These interactions regulate the migration of monocytes and their differentiation into macrophages [229]. Additionally, activation of CCR1 and CCR5 can lead to STAT3 signaling [230, 231]. Furthermore, IL-31r*α* and IL-21rα have been shown to activate JAK/STAT signaling and consequently M2 polarization [232, 233]. $Cx3CR1^{+}$ macrophages have been characterized as long-term tissue-resident macrophages that reside in the M2 polarization state [234]. Additionally, GPR35, a receptor for IL-17, maintains TNF-mediated metabolic homeostasis in $Cx3CR1^{+}$ macrophages [235]. Opposing these findings, macrophages in co-culture also express high levels of CCR2. CCR2 is the receptor for chemoattractant CCL2, which recruits macrophages. Macrophage nomenclature largely dictates $Cx3CR1^{+}$ macrophages are residential and $CCR2^{+}$ macrophages are monocytes recruited from circulation [236]. Upregulation of chemokine-like receptor 1 (CMKLR1) expression on macrophages has been associated with fibroblast-assisted maturation of tumor-infiltrating macrophages [237]. This heterogeneity in RNA expression argues that our co-culture model has heterogeneous macrophage populations that are represented in human lung cancer.

A

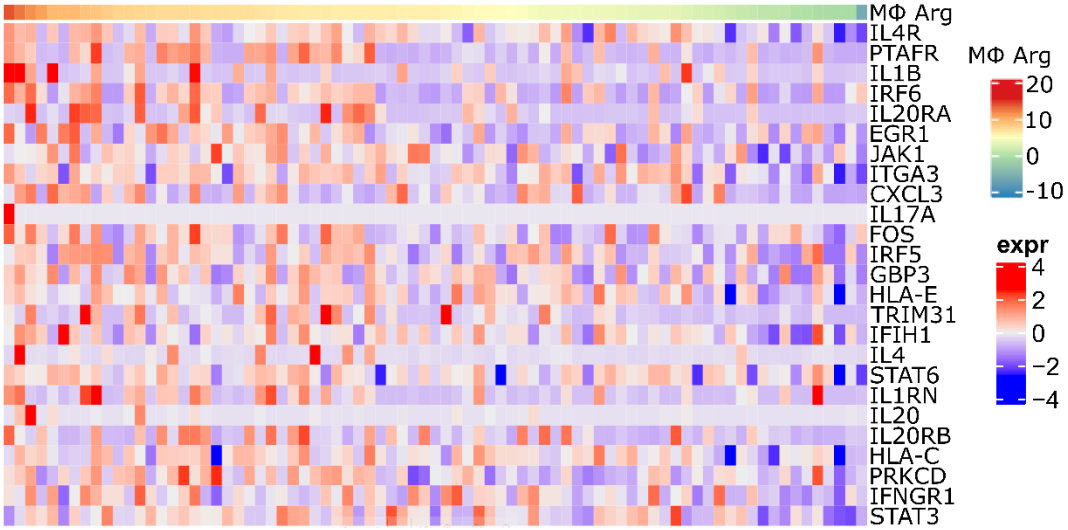
MΦ Arg
IL4R
PTAFR
IL1B
IRF6
IL20RA
EGR1
JAK1
ITGA3
CXCL3
IL17A
FOS
IRF5
GBP3
HLA-E
TRIM31
IFIH1
IL4
STAT6
IL1RN
IL20
IL20RB
HLA-C
PRKCD
IFNGR1
STAT3
MΦ Arg
20
10
0
-10
expr
4
2
0
−2
−4

B

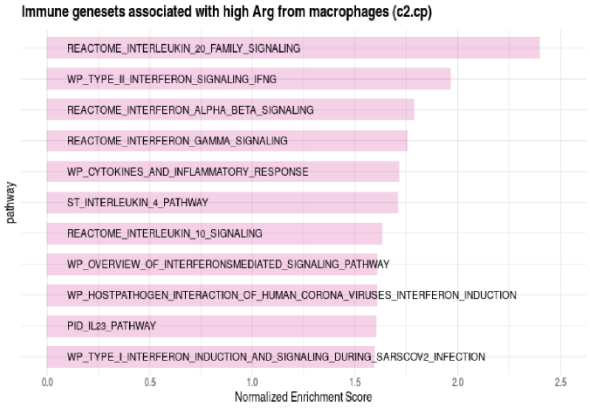
Immune genesets associated with high Arg from macrophages (c2.cp)
REACTOME_INTERLEUKIN_20_FAMILY_SIGNALING
WP_TYPE_II_INTERFERON_SIGNALING_IFNG
REACTOME_INTERFERON_ALPHA_BETA_SIGNALING
REACTOME_INTERFERON_GAMMA_SIGNALING
WP_CYTOKINES_AND_INFLAMMATORY_RESPONSE
ST_INTERLEUKIN_4_PATHWAY
REACTOME_INTERLEUKIN_10_SIGNALING
WP_OVERVIEW_OF_INTERFERONSMEDIATED_SIGNALING_PATHWAY
WP_HOSTPATHOGEN_INTERACTION_OF_HUMAN_CORONA_VIRUSES_INTERFERON_INDUCTION
PID_IL23_PATHWAY
WP_TYPE_I_INTERFERON_INDUCTION_AND_SIGNALING_DURING_SARSCOV2_INFECTION
pathway
0.0
0.5
1.0
1.5
2.0
2.5
Normalized Enrichment Score

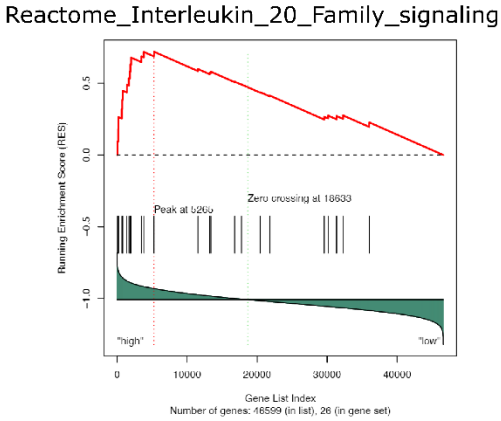
Reactome_Interleukin_20_Family_signaling
Running Enrichment Score (RES)
0.5
0.0
−0.5
−1.0
Peak at 5266
Zero crossing at 18633
"high"
"low"
0
10000
20000
30000
40000
Gene List Index
Number of genes: 16599 (in list), 26 (in gene set)

C

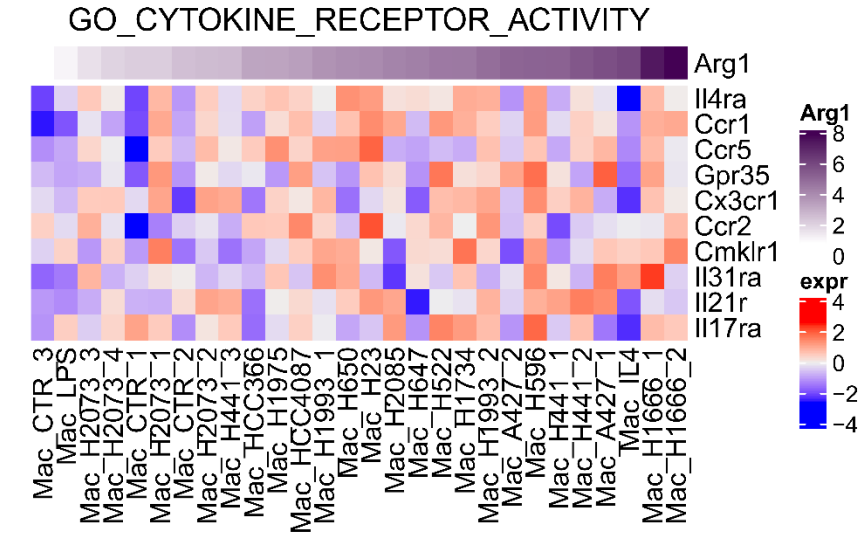
GO_CYTOKINE_RECEPTOR_ACTIVITY
Arg1
Il4ra
Ccr1
Ccr5
Gpr35
Cx3cr1
Ccr2
Cmklr1
Il31ra
Il21r
Il17ra
Arg1
8
6
4
2
0
expr
4
2
0
−2
−4
Mac_CTR_3
Mac_LPS
Mac_H2073_3
Mac_H2073_4
Mac_CTR_1
Mac_H2073_1
Mac_CTR_2
Mac_H2073_2
Mac_H441_3
Mac_HCC366
Mac_H1975
Mac_HCC4087
Mac_H1993_1
Mac_H650
Mac_H23
Mac_H2085
Mac_H647
Mac_H522
Mac_H1734
Mac_H1993_2
Mac_A427_2
Mac_H596
Mac_H441_1
Mac_H441_2
Mac_A427_1
Mac_IL4
Mac_H1666_1
Mac_H1666_2

Figure 18: NSCLC and macrophages upregulated suppressor cytokine-receptor signaling for high Arg1 polarization. A) Top 20 genes upregulated in human cancer cell RNA expression immune panel. B) Gene set enrichment analysis of genes upregulated in NSCLC that induce the high Arginase macrophage phenotype, FDR < 1.0, Enrichment Ratio > 1.5. C) RNA sequencing from NSCLC co-cultures and filtered for mouse transcripts show upregulation of suppressive cytokine receptors that promote M2 polarization in macrophages, n=15.

We then sought to understand how cancer cells polarize macrophages. Studies have shown cancer cells will secrete IL-4, IL-6, G-CSF and GM-CSF that can influence macrophage polarity, with this in mind we performed a series of transwell assays. Cancer cells and fibroblasts with a stable GFP reporter were plated on top of a transwell that was placed in a well with macrophages cultured on the plate. These conditions ensured cancer cells and CAFs cannot physically touch the macrophages (Figure 19A). RNA was isolated from the macrophages for qPCR analysis. We found that macrophage transcription in the transwell assay was similar to that of the normal co-culture, arguing that macrophages are largely polarized by secreted proteins (Figure 19B). To reinforce this data, a series of cytokine arrays were performed to investigate the cytokines that are secreted by mouse and human cells within the co-culture. We found that human cells were secreting IL-6, IL-8 and MCP-1 (Figure 19C). Stimulation of macrophages with IL-6 leads to M2 polarization and upregulation of the IL-4 receptor [238]. Endothelial cells secrete IL-8 in response to injury or in this case tumor, this causes cancer cell proliferation, survival, angiogenesis, neutrophil recruitment as well as epithelial-to-mesenchymal transition (EMT) [239]. Additionally, macrophages stimulated by IL-8 can deplete extracellular L-arginase by upregulating arginase expression (M2 macrophage marker) causing inhibition of T-cell activation and proliferation [240]. Furthermore, studies have shown that through tumor-

stromal interactions MCP-1 is upregulated resulting in increased M2-like macrophage recruitment which leads to tumor progression [241, 242]. Correspondingly, within the co-culture, macrophages upregulated IL-4 secretion (Figure 19D), arguing macrophages reinforce M2 polarization.

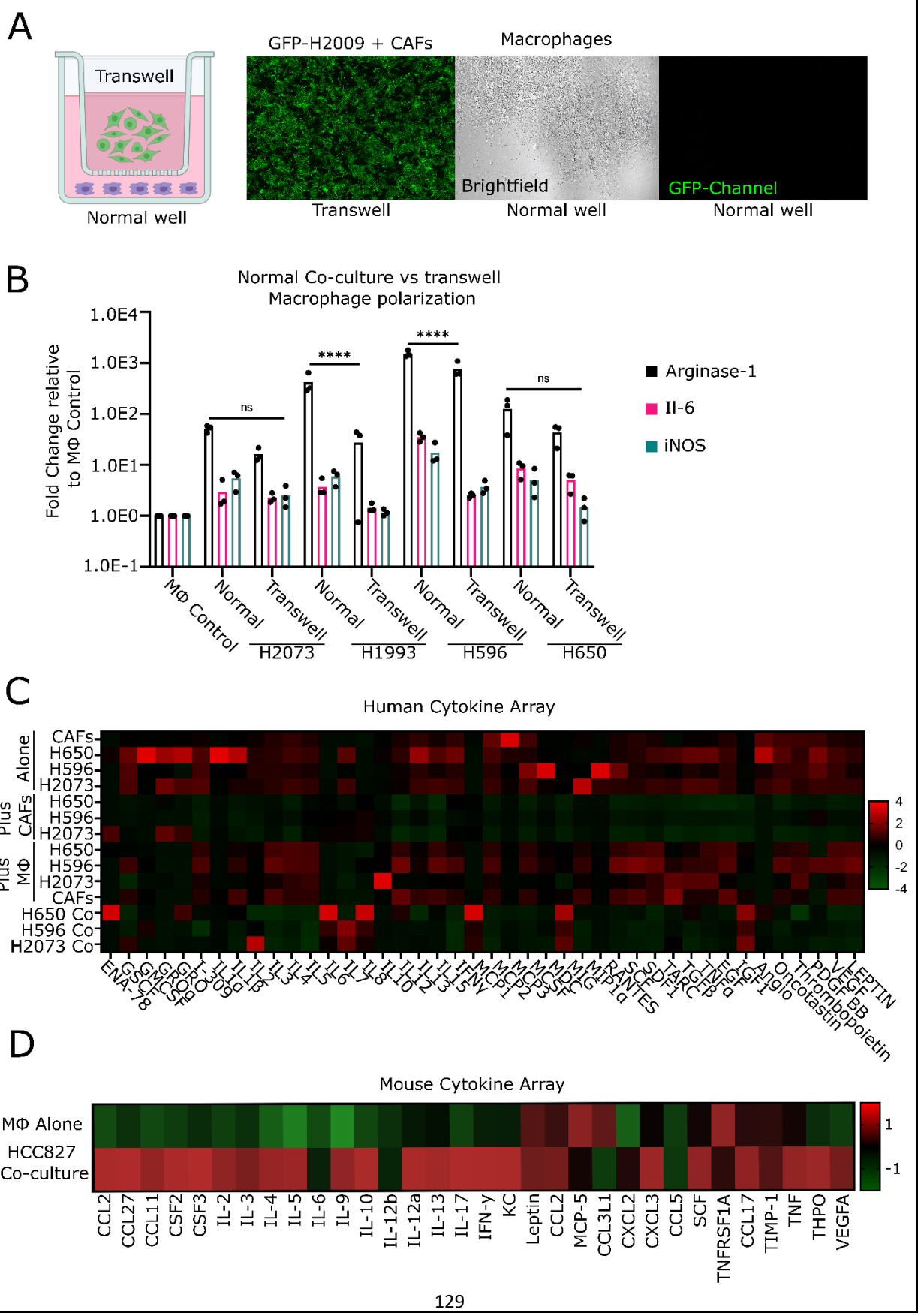
A
Transwell
Normal well
GFP-H2009 + CAFs
Macrophages
Brightfield
GFP-Channel
Transwell
Normal well
Normal well
B
Normal Co-culture vs transwell
Macrophage polarization
Fold Change relative to MΦ Control
1.0E4
1.0E3
1.0E2
1.0E1
1.0E0
1.0E-1
****
****
ns
ns
Arginase-1
Il-6
iNOS
MΦ Control
Normal
Transwell
Normal
Transwell
Normal
Transwell
Normal
Transwell
H2073
H1993
H596
H650
C
Human Cytokine Array
CAFs
H650
H596
H2073
Alone
Plus CAFs
H650
H596
H2073
Plus MΦ
H650
H596
H2073
CAFs
H650 Co
H596 Co
H2073 Co
4
2
0
-2
-4
ENA-78
GCSF
GMCSF
GRO
GRO a
IL-10
IL-1a
IL-1b
IL-1
IL-3
IL-4
IL-5
IL-6
IL-7
IL-8
IL-10
IL-12
IL-13
IL-15
IFNγ
MCP1
MCP2
MCP3
MCSF
MDC
MIG
MIP1a
RANTES
SCF
SDF1
TARC
TGFβ
TNFa
EGF
IGF1
Angio
Oncostatin
Thrombopoietin
PDGF BB
VEGF
LEPTIN
D
Mouse Cytokine Array
MΦ Alone
HCC827 Co-culture
1
-1
CCL2
CCL27
CCL11
CSF2
CSF3
IL-2
IL-3
IL-4
IL-5
IL-6
IL-9
IL-10
IL-12b
IL-12a
IL-13
IL-17
IFN-γ
KC
Leptin
CCL2
MCP-5
CCL3L1
CXCL2
CXCL3
CCL5
SCF
TNFRSF1A
CCL17
TIMP-1
TNF
THPO
VEGFA

Figure 19: Macrophage polarity modulated by NSCLC through paracrine signaling and reinforced by macrophage autocrine signaling. A) GFP-tagged H2009 and CAF cells were plated on the transwell as shown in the far left image. Macrophages were plated in the 6 well plate. Brightfield (Middle image) and GFP (Far right image) images were taken after 48 hours of culture to ensure cancer cells or fibroblast had not extravagated through the transwell. B) Macrophages from transwell assays cultured with four cell lines were harvested for qPCR. Two-way ANOVA with Tukey's *post-hoc* analysis for multiple comparisons, significance was only found between normal and transwell arginase expression in H1993 and H596, n=3. C) Human cells (CAFs, H650, H596, H2073) were cultured alone or in combination with CAFs, Mφ or both for 72hrs. Supernatant from these cultures were collected and used for human cytokine arrays, all signals were normalized to internal controls and expression between blots were normalized. Mφ cells were cultured alone and used to dismiss signal from mouse proteins binding. IL-6, IL-8, and MCP-1 proteins were significantly higher in NSCLC co-cultures, Paired T-test, $p < 0.05$. D) Macrophages were cultured alone or in NSCLC co-culture with HCC827 cells for 72 hrs and supernatant was collected for mouse cytokine array. HCC827 cells were cultured alone and used to dismiss signal from human proteins binding. IL-4 protein was significantly high in co-culture compared to Mφ alone, T-test, $p < 0.0001$.

We wanted to understand whether the macrophages within the co-culture were functionally M2 polarized. Previous studies have shown that M2 macrophages endocytose dextran with greater efficacy due to the increased expression of CD206 (mannose receptor that binds dextran molecules). Therefore, we introduced dextrans conjugated with Alexa Flour 647 into the co-cultures. We found that IL-4 treated macrophages (M2) had increased signal in comparison to LPS-treated and baseline control macrophages (Figure 20A). Surprisingly, we found that within

lung cancer co-cultures macrophages have no signal, suggesting that these M2 macrophages are unable to endocytose dextran within the co-culture (Figure 20B).

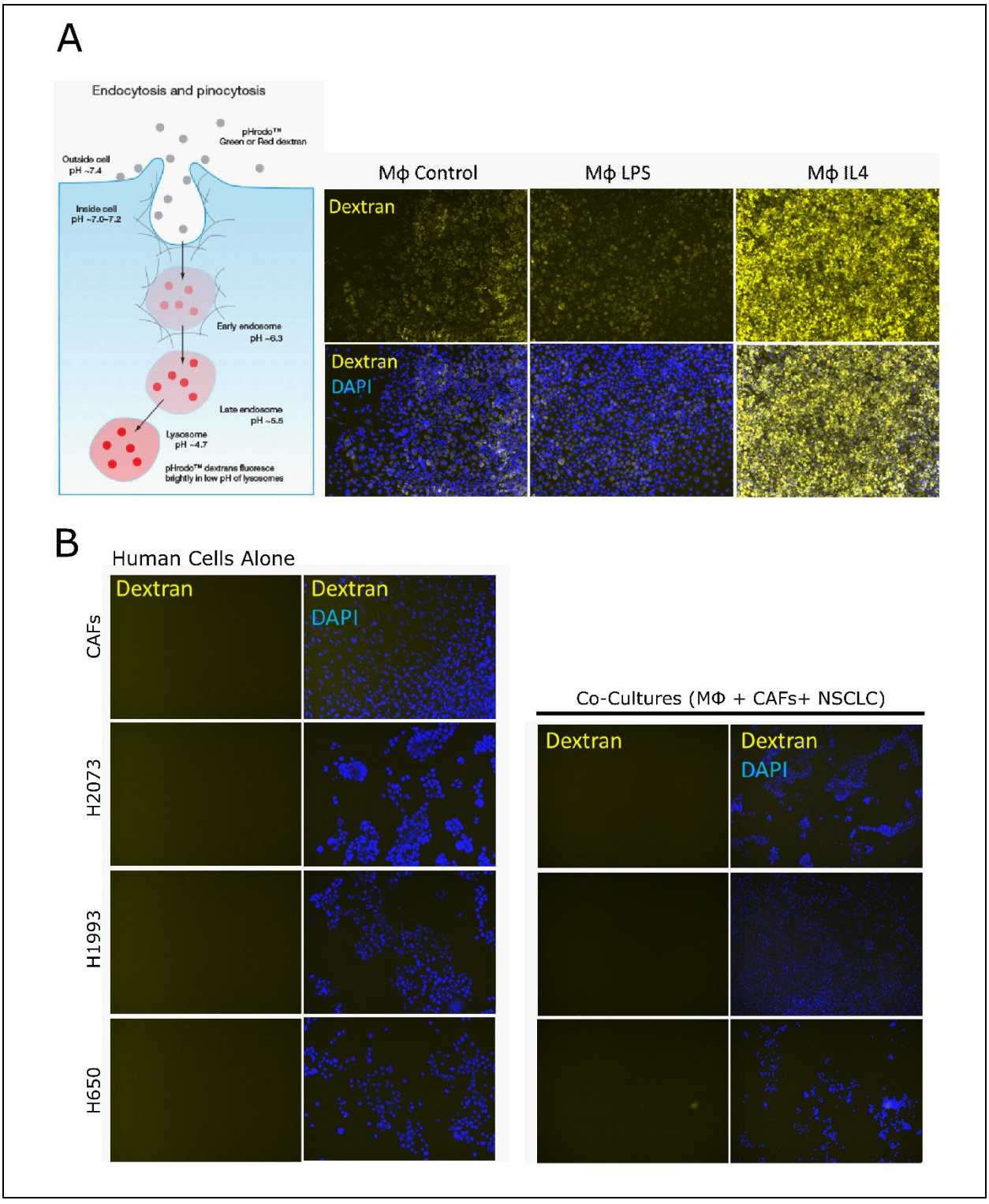

Figure 20: NSCLC suppress macrophage functionality. Dextrans were added to cultures of macrophages alone, human cells alone or NSCLC co-cultures. Endocytosis was analyzed by epiflourescence microscopy for alexa fluor 647 expression. A) Macrophages polarized with LPS and IL-4 were accessed for endocytosis activity. B) Human cells were cultured with dextrans and no endocytosis was detected (Left panel). NSCLC co-cultures were cultured with dextrans and macrophages were found to no longer be able to endocytose dextrans (Right panel).

3.7 Epithelial-high, neuroendocrine-low LC cells contribute to high arginase macrophage phenotype

Transcriptome data from NSCLC cell lines prior to co-culture were stratified as mesenchymal or epithelial using an established signature metric assay [243]. GSEA identified that epithelial and mesenchymal related pathways were elevated in cancer cells that induced the high Arg1 macrophage phenotype in the co-culture model (Figure 21A). We found that NSCLC cell lines with high epithelial gene expression induced higher macrophage expression of Arg1 (log2-fold change 6.27 vs 4.15, p=0.002) (Figure 21B, right panel). To confirm these findings, tissues from the *in vivo* panel were stained for epithelial cadherins (E-cadherins) and Vimentin. E-cadherin is expressed on the cell surface as a cell-cell junction and is a classical marker for epithelial cells. Vimentin is a type III intermediate filament protein used to anchor organelles in the cytosol and expressed in mesenchymal cells and sarcomas. These proteins are used to assess if the stem cell status of cancer cells, as well as prognostic markers for cancer [37,38] [244].We confirmed that cell lines enriched for epithelial features displayed significantly higher in vivo expression of E-cadherin (an epithelial marker) compared to cell lines enriched for mesenchymal features (79 vs. 11%, p=0.03) (Figure 21C). In summary, we found that epithelial NSCLCs correlate to the high Arg-1 macrophage phenotype.

Concordantly, NSCLC cells with mesenchymal RNA signatures expressed higher Vimentin than epithelial NSCLC. EMT is a mechanism cancers cells use to gain mobility to migrate from the primary tumor. Cancer metastasis has been highly associated with a mesenchymal signature as well as disease progression [245-248]. After undergoing EMT, cancer cells migrate and invade the basal membrane of blood and lymphatic vessels. The majority of cells will reside in the vessels and continue to circulate, but few will escape and establish secondary tumor sites [249, 250]. Additionally, studies have shown that EMT promotes resistance to chemotherapy and reduces apoptotic cell death [246, 251-253]. Current studies demonstrate that various myeloid derived immune cells secrete TGF-β, which activates transcription factors SMAD and NFkβ, leading to EMT and initiation of metastasis [254]. Our data was surprising given that the Arginase phenotype is typically associated with mesenchymal status in NSCLC. However, higher density of tumor-associated macrophage in the TME have been correlated with: worse prognosis, expression of mesenchymal markers, activation of NFkβ signaling, decrease of E-cadherin expression, and ultimately cancer cell invasion [255]. Therefore, we could be capturing early stages of EMT and prolonged cultures may give insight into macrophage induce EMT in cancer cells.

Additionally, we used the NSCLC transcriptome data to assess neuroendocrine features (NE) in the cancer cells in relation to macrophage expression. Neuroendocrine tumors tend to follow a prolonged clinical course and are less likely to metastasis in comparison to aggressive carcinomas [256]. In relation to our study, we found that NSCLC that induced high *Arg1* expression in macrophages had low-NE features, whereas NSCLC with neuroendocrine features (NSCLC-NE) and small-cell lung cancer cell lines (derived from APUD cells and classically enriched for neuroendocrine features) caused low *Arg1* expression in macrophages (Figure 21D). The extent of high-NE lung cancers is limited therefore these findings need to be further investigated. However, despite the limitations of this analysis, our findings are in line the

observations that a higher density of M2 macrophages are commonly found in aggressive carcinomas and associated with poor prognosis [257-259]. The summation of these findings conclude that epithelial lung cancers with low NE-scores induce high Arg1 macrophages and these are potential biomarkers for prognosis and macrophage polarization in NSCLC.

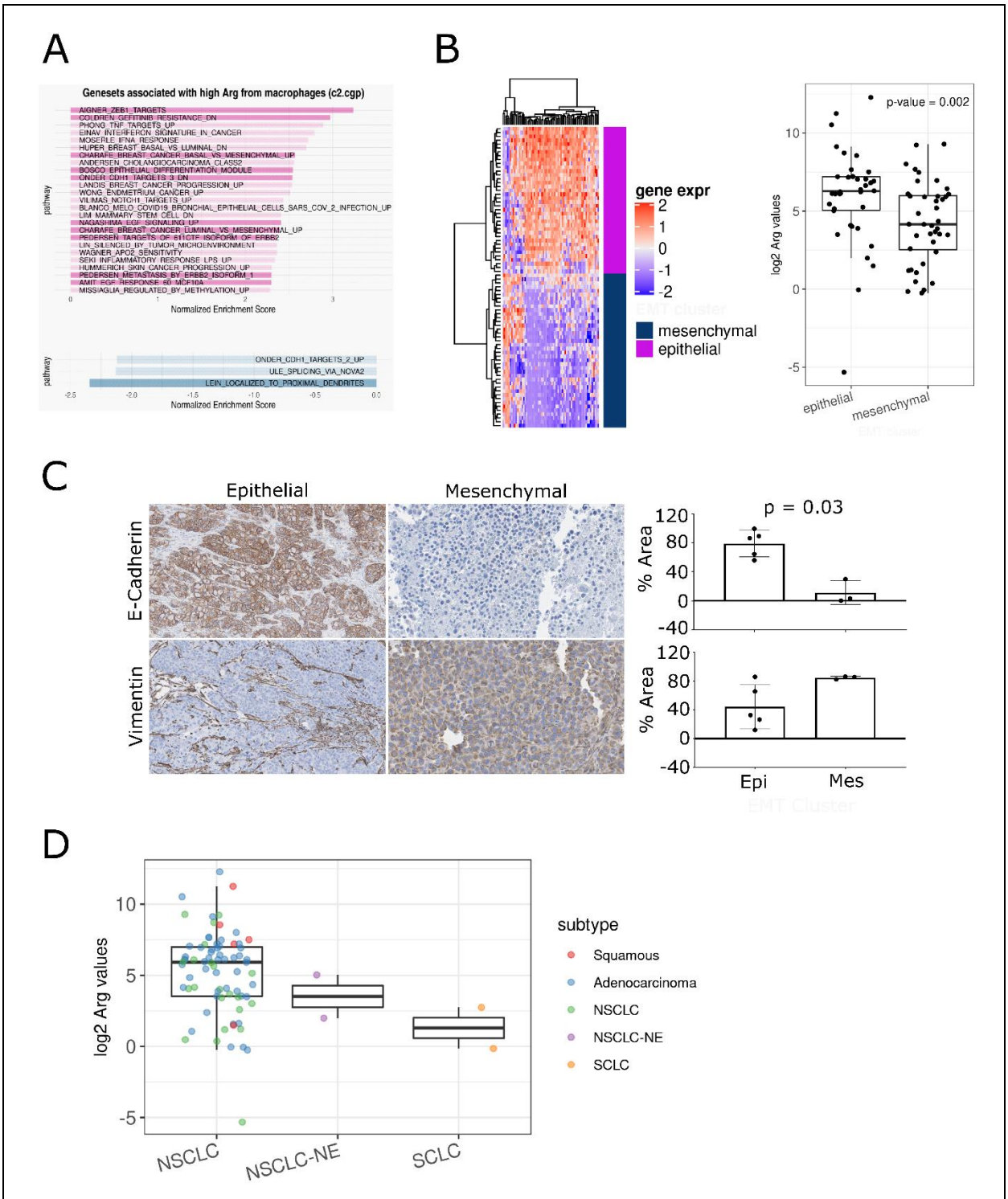

Figure 21: Epithelial-high, neuroendocrine-low LC cells contribute to high arginase macrophage phenotype. Gene set enrichment analysis with cancer cell line RNA

sequencing data segregated based on Arg expression in co-culture models. A) All genesets. B) Classification of lung cancer cell lines by an epithelial-mesenchymal transition (EMT) gene signature. An EMT signature metric previously established was used to classify lung cancer cell lines into epithelial (purple) and mesenchymal (dark blue) clusters by hierarchical clustering with Ward's method [243]. Comparison of macrophage *Arg1* expression by EMT status of co-cultured lung cancer cell line as determined from the EMT heatmap. P-value is determined by two-sided Mann-Whitney U test. C) Representative images and quantification of E-cadherin and Vimentin-stained tumors from EMT clusters, n = 5 D) Macrophage *Arg1* expression levels by subtype of co-cultured lung cancer cell lines. NSCLC, non-small cell lung cancer; NSCLC-NE, NSCLC with neuroendocrine differentiation; SCLC, small cell lung cancer.

3.8 Modulation of arginase transcription in macrophages

$Arg1^+$ macrophages have traditionally been characterized as immunosuppressive and have been shown to contribute to tumor progression and immune evasion [260]. Therefore, reducing the M2-like macrophages density within the TME could reshape the tumor microenvironment. Additionally, repolarizing macrophages to the M1 state, may alter the immune landscape to a more immunostimulatory state, enhancing the efficacy of immune checkpoint inhibitors. In light of this, the pursuit for macrophage modulating therapies has potential therapeutic value.

Macrophage colony stimulating factor 1 (MCSF-1/CSF-1) recruits' monocytes to the tumor and causes M2 polarization. Several groups are targeting the CSF1 receptor on macrophages to prevent the recruitment of macrophages to the site of the tumor. Most of these studies are in early-stage clinical trials [261]. Other groups focused on toll-like receptors of which preliminary data has shown TLR inhibitors can influence the immune response resulting in tumor reduction

[262, 263]. Most notably are therapeutics specifically targeting M2 polarization. Several therapeutic are in development that target $CD206^+$ macrophages and cause apoptosis in the macrophages [264]. Additionally, in some scenarios M1 macrophages can slow the growth of tumor cells as well as increase drug susceptibility [265]. Therefore, we sought to target M2 macrophages by killing the cancer cells through a process that would stimulate repolarization of macrophages.

Immunogenic cell death (ICD) is a cell death process that is inflammatory. Unlike apoptosis, ICD induces the release of microorganism-associated molecular patterns (MAMPs) or damage-associated molecular patterns (DAMPS) that interact with pattern recognition receptors on APCs to elicit an innate immune response. To test this process, mice were inoculated with tumors and then treated with mitoxantrone. In response to treatment, dendritic cells were activated, initiating an adaptive immune response, which subsequently led to resistance against additional cancer cell inoculation attempts. Therefore, ICD induction provided tumor cell specific immunity [266]. We exploited this feature of mitoxantrone to determine if we could use the *in vitro* multicellular co-culture platform to identify compounds that induce a change in macrophage phenotype (Figure 22C). We found mitoxantrone was effective in killing cells, as well as reducing *Arg1* expression in macrophages. Additionally, paclitaxel is a taxane that has been shown to not induce ICD, in line with these previous findings we found that paclitaxel did not reduce *Arg1* transcription in macrophages. Therefore, we used U-2 OS cells to confirm that treatment with mitoxantrone increased exposure of calreticulin on the membrane, a hallmark of ICD (Figure 22A). Then we tested the sensitivity of our lung cancer lines to mitoxantrone treatment (Figure 22B). However, we could not confirm ICD was occurring in our lung cancer cells. Despite this, we found mitoxantrone to be effective at reducing macrophage *Arg1* transcription in isolation and with select NSCLC cell lines in the co-culture model (Figure 22D). These data suggest that mitoxantrone acts on macrophages directly and its activity may be

differentially impacted by specific NSCLC cell lines in co-culture. Macrophage *Arg1* expression from co-culture with H441 cells did not significantly differ with mitoxantrone therapy vs. placebo, while a significant reduction in macrophage *Arg1* expression was observed in co-culture with H2073 cells. To investigate this further, we submitted H441 and H2073 co-culture treated with mitoxantrone for RNA sequencing. We then filtered the RNA expression data for mouse transcripts. RNA expression data from non-treated and mitoxantrone treated macrophages was then compared. From this comparison, genes were identified for being > 2-fold change in response to mitoxantrone. We found that cancer cells, CAFs and macrophages treated with mitoxantrone separately showed little changes at the transcriptional level. However, we found that macrophages within the co-culture down-regulated cell cycle and gluconeogenesis pathways in response to mitoxantrone (Figure 22E). These findings suggest that in the context of NSCLC treatment with mitoxantrone causes senescence in *Arg1*$^{+}$ macrophages.

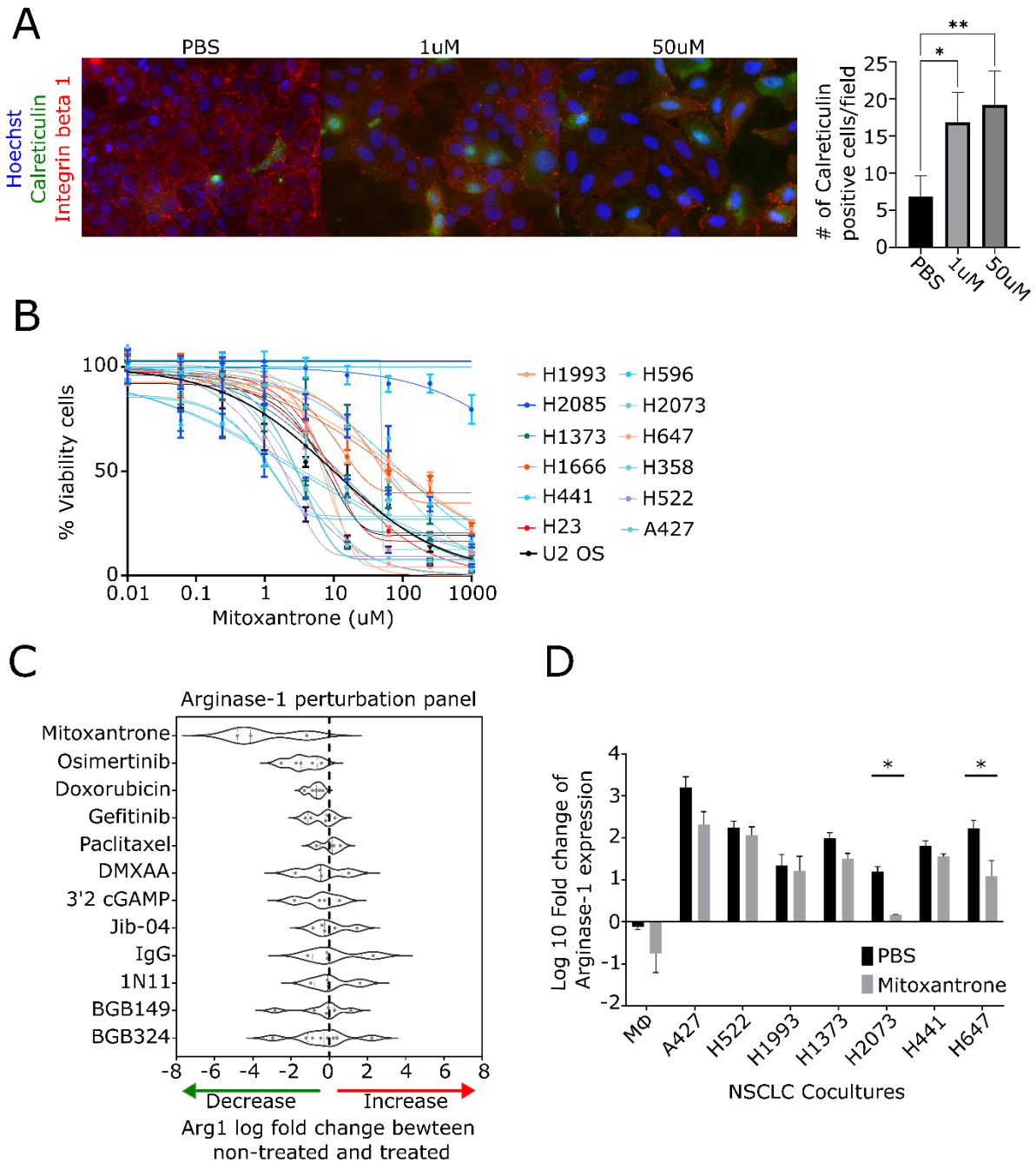
A
PBS
1uM
50uM
Hoechst
Calreticulin
Integrin beta 1
# of Calreticulin positive cells/field
B
% Viability cells
Mitoxantrone (uM)
H1993
H2085
H1373
H1666
H441
H23
U2 OS
H596
H2073
H647
H358
H522
A427
C
Arginase-1 perturbation panel
Mitoxantrone
Osimertinib
Doxorubicin
Gefitinib
Paclitaxel
DMXAA
3'2 cGAMP
Jib-04
IgG
1N11
BGB149
BGB324
Decrease
Increase
Arg1 log fold change bewteen non-treated and treated
D
Log 10 Fold change of Arginase-1 expression
PBS
Mitoxantrone
MΦ
A427
H522
H1993
H1373
H2073
H441
H647
NSCLC Cocultures
E
Mac_1
Mac_2
Mac_mito_1
Mac_mito_2
Mac_H2073_1
Mac_H2073_2
Mac_H2073_mito_1
Mac_H2073_mito_2
Mac_H441_1
Mac_H441_2
Mac_H441_mito_1
Mac_H441_mito_2
HALLMARK_E2F_TARGETS

Figure 22: Mitoxantrone modulates arginase expression in macrophages. A) U2 OS cells were treated with mitoxantrone (1uM or 50uM) and strained for calreticulin translocation to the cell membrane (Integrin beta 1). Nuclei were stained with Hoechst and six images were taken of the cell cultures for quantification (far right bar graph), n = 6, two-way ANOVA with Tukey's *post-hoc* analysis for multiple comparisons, mean ± SD, * $p < 0.05$, * $p < 0.01$. B) U2 OS (Black) and NSCLC lines were tested for dose dependent toxicity to mitoxantrone treatment, n=16/concentration. C) Arginase transcription in response to chemical perturbations. A shift to the left indicates a decrease in arginase expression and to the right an increase in response to treatment. D) RT-qPCR of Arginase-1 expression of a small panel of NSCLC co-cultures in response to mitoxantrone treatment. E) Mφ alone or NSCLC co-culture RNA sequencing filtered for mouse transcripts. In response to mitoxantrone (Mito) treatment no significant changes in human or mouse transcripts in mono cultures. In response to treatment in NSCLC co-cultures, macrophages downregulated cycle and glycogenesis pathways, n = 2.

To investigate the effect of mitoxantrone *in vivo*, we utilized two NSCLC adenocarcinoma cell lines (H441 and H2073) which both induced mouse macrophage *Arg1* expression in the co-cultures. Mice bearing H441 or H2073 xenografts were randomized to mitoxantrone or placebo therapy at 2.5 mg/kg which did not significantly impact tumor volume. H2073 tumors demonstrated a slight increase in $SOCS3^+$ macrophages and a reduction in $ARG1^+$ macrophages in response to mitoxantrone, while H441 tumors, showed significantly decreased $SOCS3^+$ macrophages and a moderate decrease in $ARG1^+$ macrophages (Figure 23A-C). Furthermore, because macrophage density in the tumor stroma significantly impacts tumor behavior and prognosis in NSCLC [2], we analyzed macrophages in relation to stromal regions. In doing so, we found that H2073 tumors, the distance between $ARG1^+$ macrophages and the

stroma increased significantly in response to mitoxantrone treatment, while H441 tumors showed no change in spatial distribution (Figure 23D). Nanostring analysis of RNA from H2073 tumors revealed that the innate and inflammatory pathways were enriched in response to mitoxantrone. In tumors from H441 xenografts, adhesion pathways were also enriched while antigen processing were decreased in response to mitoxantrone (Figure 23E). These data suggest that mitoxantrone weakens macrophage-to-stromal interactions and increases innate and inflammatory signaling in responsive tumors.

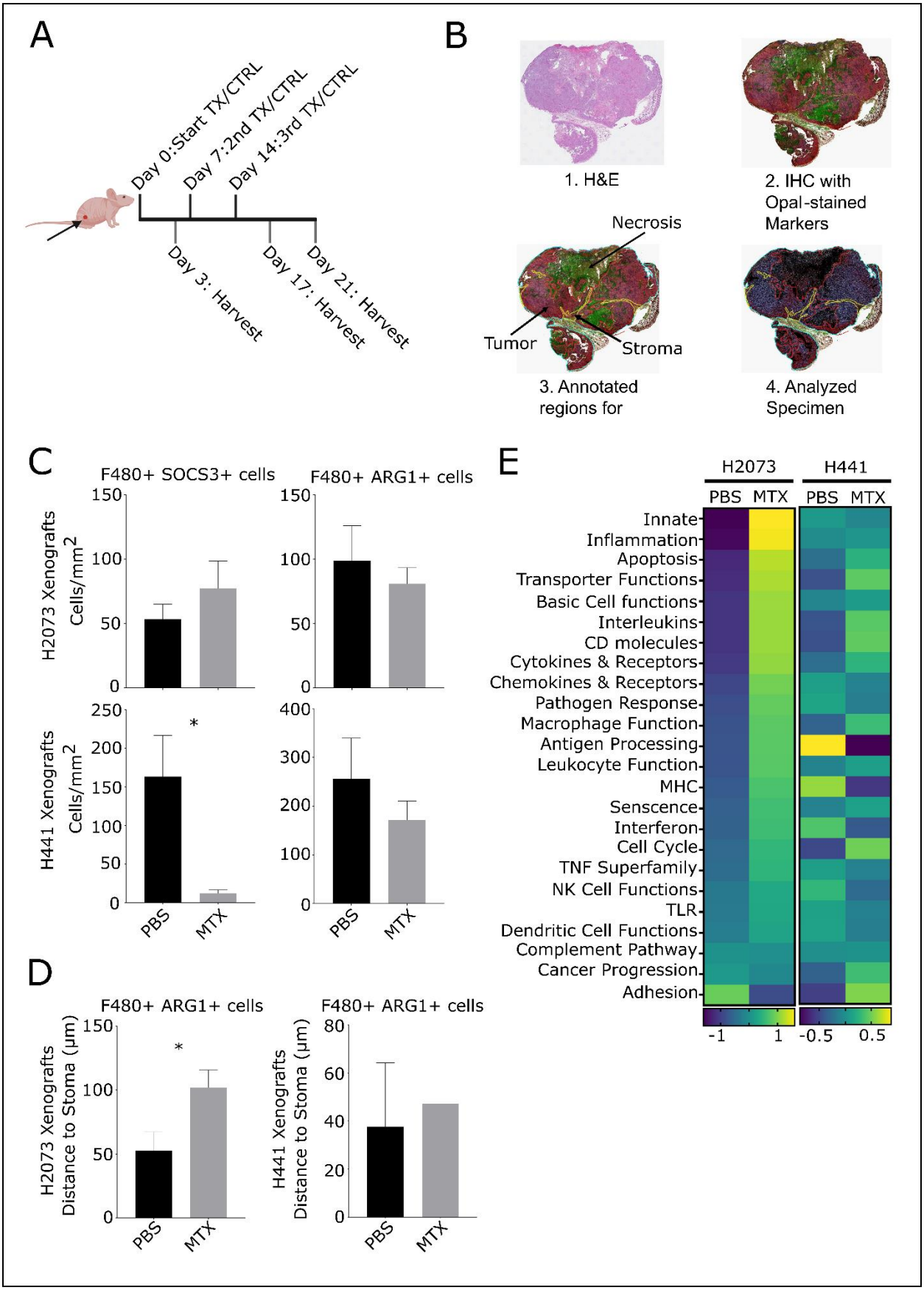
A
Day 0:Start TX/CTRL
Day 7:2nd TX/CTRL
Day 14:3rd TX/CTRL
Day 3: Harvest
Day 17: Harvest
Day 21: Harvest
B
1. H&E
2. IHC with Opal-stained Markers
Necrosis
Tumor
Stroma
3. Annotated regions for
4. Analyzed Specimen
C
F480+ SOCS3+ cells
F480+ ARG1+ cells
H2073 Xenografts Cells/mm2
H441 Xenografts Cells/mm2
PBS
MTX
D
F480+ ARG1+ cells
F480+ ARG1+ cells
H2073 Xenografts Distance to Stoma (µm)
H441 Xenografts Distance to Stoma (µm)
E
H2073
H441
PBS MTX PBS MTX
Innate
Inflammation
Apoptosis
Transporter Functions
Basic Cell functions
Interleukins
CD molecules
Cytokines & Receptors
Chemokines & Receptors
Pathogen Response
Macrophage Function
Antigen Processing
Leukocyte Function
MHC
Senscence
Interferon
Cell Cycle
TNF Superfamily
NK Cell Functions
TLR
Dendritic Cell Functions
Complement Pathway
Cancer Progression
Adhesion
-1 1 -0.5 0.5

Figure 23: Mitoxantrone alters macrophage polarization in the TME of NSCLC. A) Timeline for the mitoxantrone *in vivo* study (n = 16/cell line, mitoxantrone (2.5 mg/kg). H441 and H2073 tumors were established in nude mice. Treatment started when tumors were well established and subsequent treatments followed every seven days. Multiple harvest timepoints were taken to look at effects of mitoxantrone treatment. B) IHC quantification pipeline. Sequential sections at four microns thick were used for H&E and IHC staining. H&E and IHC scans were overlaid using the Halo software to articulate areas of stroma and necrosis. Using the Halo software tumors were quantified for respective macrophage phenotypes. Spatial analyzes were performed in regards to regions of interests. C) IHC quantification of $F480^{+}$ $SOCS3^{+}$ and $F480^{+}$ ARG^{+} cells in response to mitoxantrone treatment. D) Distance of $F480^{+}$ ARG^{+} macrophages to stroma regions. Mean ± SD, * $P < 0.05$. E) Tumors were sent for nCounter PanCancer Immune Profiling Panel gene expression nanostring analysis, n=3.

In contrast to mitoxantrone, we identified two novel therapeutics that are more effective at selectively killing lung cancer, reducing *Arg1* and increasing *Socs3* expression in macrophages. Previously the Minna lab in collaboration with the White and Roth laboratories screened a chemical library of ~250,000 small molecules. These compounds were screened for selective lung cancer lethality in comparison to HBEC cells. The consortium identified the “precision oncology probe set (POPS)” a group of 222 selective compounds that effectively killed lung cancer [267]. We utilized our co-culture platform to assess several of the POPS compounds for the ability to reduce *Arg1* transcription across a small panel of co-cultures (Figure 24A). We then expanded this study to a larger panel of co-cultures for SW141407 and SW022906 (Figure 24C-D). In comparison, mitoxantrone was found to reduce *Arg1* transcription, but not to increase *Socs3* transcription (Figure 24B). We found that in some co-cultures these POPS

compounds reduce *Arg1* expression and increase *Socs3* expression in a reproducible manner. The group that identified the POPS compounds utilized extensive molecular annotations of cancer cells to identify biomarkers for antitumor activity of the compounds. Previously SW022906 was reported to be associated with the expression TTC21B, which regulates cancer cell motility. Also, SW022906 was identified to selectively kill LKB1 mutant lung cancers. Currently this molecule is under active investigation by the consortium. Contrary to these data, SW141407 currently has no mechanism of action or biomarkers associated with it, therefore further investigation of our two selected compounds is needed. In a broader sense, we demonstrated the efficacy of our co-culture system to monitor *Arg1* transcription in response to treatment which coincided with findings *in vivo*. To this end, we propose that this *in vitro* co-culture model functions as a physiologically consistent platform from which to identify potential therapeutic compounds that impact macrophage polarization.

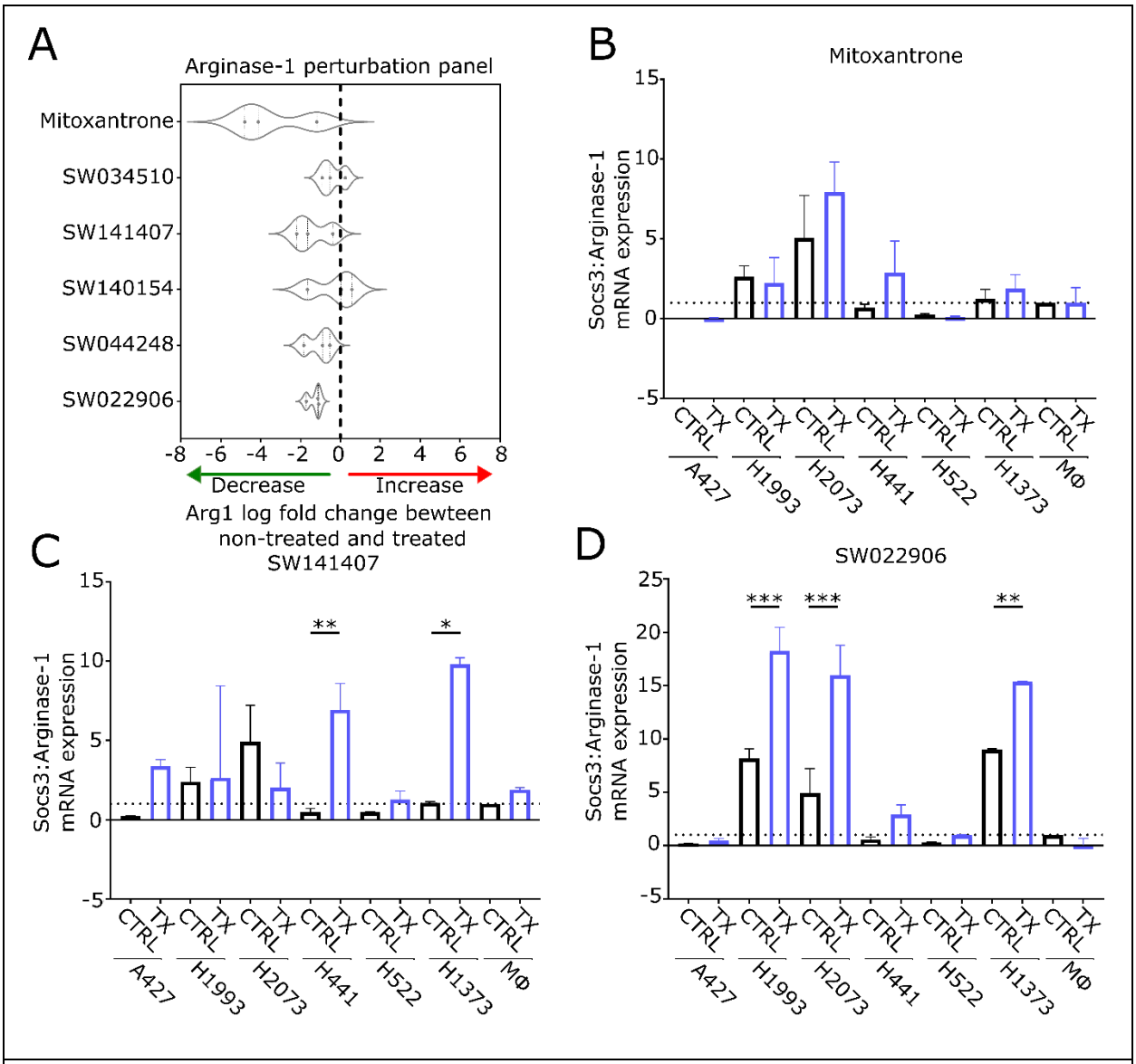

Figure 24: POPS compound selectively repolarize macrophages. A) Arginase transcription in response to chemical perturbations. A shift to the left indicates a decrease in arginase expression and to the right an increase in response to treatment. Transcriptional fold change between Socs3 (M1) and Arginase-1 (M2) markers were compared to infer polarization states of the macrophages in response to treatment. Mφ alone or NSCLC co-cultures were treated with chemical agents B) Mitoxantrone C) SW141407 D) SW022906 and RNA was harvested for RT-qPCR analysis, n=5, mean ± SD, Two-way ANOVA with Tukey's *post-hoc* analysis for multiple comparisons, * $p < 0.05$, ** $p < 0.01$, *** $p < 0.001$.

Chapter 4: Discussion

In our studies, we established a novel co-culture system that integrated macrophages, CAFs, and NSCLC cell lines. We found that communication between CAF and cancer cells is important for macrophage polarization. We used this platform to investigate 83 different patient-derived lung cancers and one human bronchial epithelial cell line. We identified three robust macrophage phenotypes (high Arg1, high Socs3 and high Il-1β). The high Arg phenotype was corroborated by other preclinical and clinical data. In relation to these data, we found that the traditional clincopathological and molecular characteristics of NSCLC cell lines do not correlate with the induced phenotypes identified. However, using our extensive cancer cell RNA expression library, we found that NSCLC lines that polarize the Arg macrophage phenotype upregulate suppressive immune pathways. In line with these findings, macrophages in the NSCLC co-culture upregulated receptors for M2 polarization. These findings were also corroborated at the protein level by cytokine arrays. The data indicates that, in the context of NSCLC, macrophages are largely polarized by cytokine secretion and not through direct cell-cell contacts. Moreover, macrophages reinforce M2 polarization by upregulating IL-4 secretion. Furthermore, dextran assay demonstrated that M2-like macrophages lacked the ability to endocytose in the presence of CAFs and NSCLC. Additionally, we found EMT and NE features that may be predictive biomarkers of M2-like macrophage polarization in NSCLC patients. To combat the suppressive macrophage phenotype, we developed a chemical perturbation approach to target arginase in macrophages in the context of NSCLC. We found that mitoxantrone was effective in reducing arginase expression in macrophages, both in the co-cultures and in the *in vivo* setting. We also identified two novel compounds that can reduce *Arg1* expression and increase *Socs3* transcription. Taken together, these findings demonstrate the utility of our platform for investigating macrophage polarity in the context of cancer, as well as a drug discovery tool for macrophage-targeted therapies.

Our study has certain limitations. One limitation is human-derived macrophages were not studied. Cytokines such as IL-6 are known to be species-specific; therefore, one could argue that many cell-to-cell communications were not evaluated in this system due to the differences between species. Several attempts were made to establish human-derived macrophages from cord blood using various protocols. We also contacted two labs that had previously established human macrophages. However, these attempts were unsuccessful, macrophage presence was confirmed by flow cytometry using CD68, CD206 and HLA for markers. We did, however, evaluate a few mouse lung cancers and fibroblasts using the transwell assay with *Arg1* and *iNOS* as markers and found that these co-culture conditions polarized the strong *Arg1* expression. Interspecific differences notwithstanding this allowed for us to use mouse-specific primers to evaluate the macrophage phenotype in the context of NSCLC. This is the first model of its kind, and while simplistic in nature, it proved to be effective.

Another limitation is, most of these findings were based on RT-qPCR, for which standards were put in place to ensure robustness. Despite these standards, it is still a weakness that should be addressed by utilizing alternative methods. Moreover, RT-qPCR is a slow process compared to other screening methods. If used for screening, this platform should utilize different technologies to improve standardization and speed. Integration of fluorescent or absorbance reporters into genes that characterize macrophage polarity can enable high-throughput screening. This was attempted using YARG mice from the Jackson Laboratory, which had eYFP inserted downstream of the Arg1 gene. We generated BMDMs from these mice and found that they were transcriptionally similar to C57BL/6J BMDMs. However, the YFP signal was too weak to detect using the high-throughput microscope at the UT Southwestern screening core, even after IL-4 stimulation. Generation of reporter mice or reporter macrophages would dramatically improve the speed of this assay and make it more generalizable.

We also investigated the presence of the high Arg1 and Socs3 phenotype *in vivo*, the effects found were not statistically significant although we saw clear trends, therefore the *in vivo* panel should be expanded to include more mice per cell line. The current panel of cell lines tested range from two to seven tumors per NSCLC. Eight mice were used per cell line, but the failure to form tumors was higher in some cell lines than others. Expanding this panel to better forming xenograft models is necessary. Additionally, these data were generated from xenografts established in athymic nude mice, which lack adaptive immunity. We mitigated these weaknesses using the TCGA matchup analysis to establish clinical relevance, however further studies should include orthotropic models to better represent the lung biology found in lung cancer. This study should also be expanded to in humanized mice, because nude mice lack alternative stimuli from T cells that could alter macrophage biology. Additionally, a collaboration with MD Anderson to evaluate macrophage polarity on its extensive tumor microarrays would allow an in-depth characterization of clinical macrophage biology in relation to our system. The combination of these studies would strengthen the platform and possibly corroborate the TCGA matchup findings. In line with capturing multiple immune components of the TME, additional immune cells should be introduced into the co-cultures. The transwell assay could be used to introduce T cells into these cultures and T cell activation state could be evaluated by flow cytometry.

Throughout our studies, we focused on the high Arg1 phenotype due to its robustness. We found that the high Socs3 and Il-lβ clusters were too small and not as robust as the Arg1 cluster. Therefore, we speculate that Socs3 and Il-lβ may not be the best markers for these phenotypes. To identify new markers, more co-cultures should be RNA-sequenced, or single-cell RNA sequencing could be used to identify better markers and perhaps articulate multiple macrophage phenotypes within the co-culture setting instead of relying on the most prominent phenotype. Moreover, as these clusters were small in comparison to the Arg1 cluster, they

lacked power for statistical analyses to identify NSCLC features that correlate with each of the three induced macrophage phenotype classes. The panel of lung cancers should be further expanded to overcome these two limitations.

A further limitation is, small-cell lung cancer was barely present in our screen (only two lines). This was due to the irregular floating phenotype and the difficulty obtaining cell counts for small cells. A new 3D co-culture method would need to be developed specifically for small-cell lung cancer. Integration of more SCLC cell lines would also improve the neuroendocrine analysis.

In these studies, we only hint at the mechanism of mitoxantrone-induced changes in the co-cultures. RNA expression data from these conditions suggest that macrophages in cultures with NSCLC may be dying or senescing in response to therapy. This phenotype and mechanism should be further investigated by examining cell cycle checkpoints.

Using NSCLC transcriptome data, we found EMT features that correlate with the high Arg1 phenotype in macrophages. For further investigation, several EMT modulation studies should be considered. As our RNA expression data were from cancer cells alone (i.e., prior to co-culture), we were able to determine whether the EMT status of the cell lines. This evidence suggests that the EMT state of cancer cells, may dictate macrophage polarization. Therefore, inducing EMT in NSCLCs that are epithelial by default might provide insight as to whether the EMT status determines macrophage polarity. We would expect to see a shift from the high Arg1 phenotype. Additionally, suppression of SMAD-signaling may alter macrophage phenotypes in mesenchymal NSCLC co-cultures.

We found evidence at the RNA and protein levels that macrophages are polarized by cytokines secreted into the extracellular milieu. The human cytokine array showed heterogeneity between the three NSCLCs tested, as well as commonalities in proteins secreted in the co-culture that should be exploited. We attempted to use CRISPR-Cas9 technology to knock out MCP-1, IL-6 and IL-8, but these efforts were mitigated because these genes are essential for cell survival.

Given these findings, future studies should utilize conditional knock-down technology to suppress these other genes of interest. Additionally, antibodies could be used to inhibit the effects of selected cytokines on macrophage polarity in our co-cultures. Furthermore, genetically engineered mouse models (GEMMs) could be used to examine the effects of specific cytokines on macrophage polarity in NSCLC. However, these may prove to be formidable tasks due to the complexity of cytokine signaling and macrophage polarization.

Our studies; provide evidence of the possible mechanism of M2-like polarization of macrophages in NSCLC. We used our platform to chemically modulate *Arg1* transcription in these macrophages. In addition to a chemical approach, genetic manipulation could be utilized to investigate reduction of *Arg1* expression in macrophages in the context of NSCLC. In previous studies, GEMM models were used to study lung cancer growth when *arginase* transcription is reduced in myeloid cells. They found that reduction in *arginase* expression led to slowed lung cancer growth [268]. Expanding upon such studies by utilizing immune checkpoint inhibitors in these mice would provide a context for combination therapy with arginase modulation.

In my studies I screened a handful of POPS compounds for their ability to reduce *Arg1* expression in macrophages. The Minna lab currently has access to 66 of the 222 POPS compounds identified and they have been screened for toxicity across a few cell lines. To identify more novel chemicals that can reeducate macrophages from the M2-like phenotype, an expansion of POPS compounds in the co-culture is warranted. A clear limitation of this chemical library is that these compounds are not optimized and will need additional structural adaptations to be effective *in vivo*. Furthermore, NSCLC co-cultures treated with SW141407 and SW022906 should be submitted for RNA sequencing to determine mechanisms of action on cancer cells, CAFs and macrophages. Considerable efforts to modulate macrophages in the TME of solid tumors are currently underway. Most therapeutics currently in clinical trials target the entire

macrophage population instead of modulating only M2-like macrophages. However, a couple of therapies aimed at modulating this population by inhibition of CD206 are currently in the preclinical testing stage. These efforts are remarkable and may prove to be effective as monotherapies. However, most immunotherapies in solid tumors are used in combination regimens. Therefore, it is necessary to investigate the effects of macrophage repolarization in combination with chemotherapies or immune-checkpoint inhibitors. The POPS compounds should be evaluated in humanized mice with parallel studies combining anti-PD1 or doxorubicin with the investigated POPS compounds. Doxorubicin reduces arginase transcription and has been shown to repolarize macrophages [269]. Therefore, it could offer additional benefits for macrophage re-education and tumor cell cytotoxicity.

In conclusion, this work provides insights into macrophage polarization in the context of NSCLC. We found that NSCLC induces three distinct macrophage phenotypes that are independent of major clinical demographic and molecular oncogenotype related features. Instead, we discovered that macrophage polarization largely takes place through cytokine-receptor communication pathways. These *in vitro* findings were corroborated by xenografts *in vivo*, and also in tumor datasets deposited in TCGA. Our findings suggest that this co-culture model can be used to investigate the finite mechanism of macrophage polarization in the context of NSCLC. In addition to this mechanism, we provide evidence of arginase-1 modulation *in vitro* and *in vivo* by mitoxantrone. Furthermore, we demonstrate the utility of this platform for discovering macrophage repolarization chemical agents by identifying two novel compounds. This platform is the first to incorporate NSCLC, CAFs and macrophages. The large dataset generated from our NSCLC co-culture screen can be used as a resource for future studies predicting response to therapeutics. Lastly, this platform provides the foundational elements to build a more immune-inclusive preclinical NSCLC TME model for extensive immune characterization and precision medicine discovery.

Chapter 5: Bibliography

1. Flaming, J., et al., *746 Non small-cell lung cancer cells and cancer-associated fibroblasts drive macrophage polarization in a novel co-culture model.* Journal for ImmunoTherapy of Cancer, 2020. **8**: p. A447-A448.
2. Flaming, J., et al., *Abstract PO021: Lung cancer cells and cancer-associated fibroblasts drive macrophage polarization in a co-culture model.* Cancer Immunology Research, 2021. **9**(2 Supplement): p. PO021.
3. Kalaitzoglou, E., et al., *TLR4 Promotes and DAP12 Limits Obesity-Induced Osteoarthritis in Aged Female Mice.* JBMR plus, 2018. **3**(4): p. e10079-e10079.
4. Yenerall, P., et al., *RUVBL1/RUVBL2 ATPase Activity Drives PAQosome Maturation, DNA Replication and Radioresistance in Lung Cancer.* Cell Chemical Biology, 2020. **27**(1): p. 105-121.e14.
5. *IARC Globocan 2008. Cancer Fact Sheet: Lung Cancer Mortality Worldwide in 2008*. 2008; Available from: http://globocan.iarc.fr/factsheets/cancers/lung.asp.
6. I. Adler, A.M., M. D., *Primary malignant growths of the lungs and bronchi—A pathological and clinical study.* The Laryngoscope. 1912. 325.
7. Ochsner, A., *Corner of history. My first recognition of the relationship of smoking and lung cancer.* Prev Med, 1973. **2**(4): p. 611-4.
8. CS, C. *Lung Cancer and Smoking: What We Really Know*. 1956; Available from: https://www.researchandmarkets.com/reports/4535763/tobacco-packaging-market-growth-trends-and?utm_source=GNOM&utm_medium=PressRelease&utm_code=dfpccs&utm_campaign=1267420+-+Global+Tobacco+Packaging+Market+Forecasts+2019-2024+-+Secondary+Packaging+to+Witness+Significant+Demand&utm_exec=joca220prd.
9. M, R. *Global Tobacco Packaging Market Forecasts 2019-2024*. Research and Markets - Market Research Reports 2019; Available from: https://www.researchandmarkets.com/reports/4535763/tobacco-packaging-market-growth-trends-and?utm_source=GNOM&utm_medium=PressRelease&utm_code=dfpccs&utm_campaign=1267420+-+Global+Tobacco+Packaging+Market+Forecasts+2019-2024+-+Secondary+Packaging+to+Witness+Significant+Demand&utm_exec=joca220prd.
10. *Cancer Facts & Figures 2015*. American Cancer Society 2016 May 25, 2016]; Available from: http://www.cancer.org/research/cancerfactsstatistics/cancerfactsfigures2015/index.
11. Siegel, R., et al., *Cancer statistics, 2014.* CA Cancer J Clin, 2014. **64**(1): p. 9-29.
12. Govindan, R., et al., *Changing epidemiology of small-cell lung cancer in the United States over the last 30 years: analysis of the surveillance, epidemiologic, and end results database.* J Clin Oncol, 2006. **24**(28): p. 4539-44.
13. George, J., et al., *Comprehensive genomic profiles of small cell lung cancer.* Nature, 2015. **524**(7563): p. 47-53.
14. Herbst, R.S., et al., *Pembrolizumab versus docetaxel for previously treated, PD-L1-positive, advanced non-small-cell lung cancer (KEYNOTE-010): a randomised controlled trial.* Lancet, 2016. **387**(10027): p. 1540-1550.

15. Travis, W.D., E. Brambilla, and G.J. Riely, *New pathologic classification of lung cancer: relevance for clinical practice and clinical trials.* J Clin Oncol, 2013. **31**(8): p. 992-1001.

16. Dela Cruz, C.S., L.T. Tanoue, and R.A. Matthay, *Lung cancer: epidemiology, etiology, and prevention.* Clin Chest Med, 2011. **32**(4): p. 605-44.

17. Hanna, J.M. and M.W. Onaitis, *Cell of origin of lung cancer.* J Carcinog, 2013. **12**: p. 6.

18. Larsen, J.E. and J.D. Minna, *Molecular biology of lung cancer: clinical implications.* Clin Chest Med, 2011. **32**(4): p. 703-40.

19. Shimosato, Y., et al., *Prognostic implications of fibrotic focus (scar) in small peripheral lung cancers.* Am J Surg Pathol, 1980. **4**(4): p. 365-73.

20. Russell, P.A., et al., *Correlation of mutation status and survival with predominant histologic subtype according to the new IASLC/ATS/ERS lung adenocarcinoma classification in stage III (N2) patients.* J Thorac Oncol, 2013. **8**(4): p. 461-8.

21. Network, C.G.A.R., *Comprehensive molecular profiling of lung adenocarcinoma.* Nature, 2014. **511**(7511): p. 543-50.

22. Travis, W.D., et al., *Introduction to The 2015 World Health Organization Classification of Tumors of the Lung, Pleura, Thymus, and Heart.* J Thorac Oncol, 2015. **10**(9): p. 1240-1242.

23. Network, C.G.A.R., *Comprehensive genomic characterization of squamous cell lung cancers.* Nature, 2012. **489**(7417): p. 519-25.

24. Skoulidis, F. and J.V. Heymach, *Co-occurring genomic alterations in non-small-cell lung cancer biology and therapy.* Nat Rev Cancer, 2019. **19**(9): p. 495-509.

25. Sanchez-Vega, F., et al., *Oncogenic Signaling Pathways in The Cancer Genome Atlas.* Cell, 2018. **173**(2): p. 321-337 e10.

26. Ellrott, K., et al., *Scalable Open Science Approach for Mutation Calling of Tumor Exomes Using Multiple Genomic Pipelines.* Cell Syst, 2018. **6**(3): p. 271-281 e7.

27. Hoadley, K.A., et al., *Cell-of-Origin Patterns Dominate the Molecular Classification of 10,000 Tumors from 33 Types of Cancer.* Cell, 2018. **173**(2): p. 291-304 e6.

28. Kadara, H., et al., *Whole-exome sequencing and immune profiling of early-stage lung adenocarcinoma with fully annotated clinical follow-up.* Ann Oncol, 2017. **28**(1): p. 75-82.

29. Imielinski, M., et al., *Mapping the hallmarks of lung adenocarcinoma with massively parallel sequencing.* Cell, 2012. **150**(6): p. 1107-20.

30. Jordan, E.J., et al., *Prospective Comprehensive Molecular Characterization of Lung Adenocarcinomas for Efficient Patient Matching to Approved and Emerging Therapies.* Cancer Discov, 2017. **7**(6): p. 596-609.

31. Frampton, G.M., et al., *Activation of MET via diverse exon 14 splicing alterations occurs in multiple tumor types and confers clinical sensitivity to MET inhibitors.* Cancer Discov, 2015. **5**(8): p. 850-9.

32. Lince, L. and D.J. Lulu, *Carcinoma of the lung. A comparative series of 687 cases.* Arch Surg, 1971. **102**(2): p. 103-7.

33. Host, H., *Cyclophosphamide (NSC-26271) as adjuvant to radiotherapy in the treatment of unresectable bronchogenic carcinoma.* Cancer Chemother Rep 3, 1973. **4**(2): p. 161-4.

34. Hoeltgen, T.M., et al., *Adriamycin and Cytoxan in the treatment of inoperable lung cancer.* Cancer, 1983. **51**(11): p. 2005-12.

35. Livingston, R.B., *Combination chemotherapy of bronchogenic carcinoma. I. Non-oat cell.* Cancer Treat Rev, 1977. **4**(3): p. 153-65.

36. Cortes, E.P., H. Takita, and J.F. Holland, *Adriamycin in advanced bronchogenic carcinoma.* Cancer, 1974. **34**(3): p. 518-25.

37. Casper, E.S., et al., *Phase II study of high-dose cis-dichlorodiammineplatinum(II) in the treatment of non-small cell lung cancer.* Cancer Treat Rep, 1979. **63**(11-12): p. 2107-9.

38. Gralla, R.J., et al., *Cisplatin and vindesine combination chemotherapy for advanced carcinoma of the lung: A randomized trial investigating two dosage schedules.* Ann Intern Med, 1981. **95**(4): p. 414-20.

39. Ruckdeschel, J.C., et al., *Chemotherapy for metastatic non-small-cell bronchogenic carcinoma: EST 2575, generation V--a randomized comparison of four cisplatin-containing regimens.* J Clin Oncol, 1985. **3**(1): p. 72-9.

40. *Chemotherapy in non-small cell lung cancer: a meta-analysis using updated data on individual patients from 52 randomised clinical trials. Non-small Cell Lung Cancer Collaborative Group.* BMJ, 1995. **311**(7010): p. 899-909.

41. Burkes, R.L., et al., *Induction chemotherapy with mitomycin, vindesine, and cisplatin for stage III unresectable non-small-cell lung cancer: results of the Toronto Phase II Trial.* J Clin Oncol, 1992. **10**(4): p. 580-6.

42. Rosell, R., et al., *A randomized trial comparing preoperative chemotherapy plus surgery with surgery alone in patients with non-small-cell lung cancer.* N Engl J Med, 1994. **330**(3): p. 153-8.

43. Dillman, R.O., et al., *A randomized trial of induction chemotherapy plus high-dose radiation versus radiation alone in stage III non-small-cell lung cancer.* N Engl J Med, 1990. **323**(14): p. 940-5.

44. Le Chevalier, T., et al., *Randomized study of vinorelbine and cisplatin versus vindesine and cisplatin versus vinorelbine alone in advanced non-small-cell lung cancer: results of a European multicenter trial including 612 patients.* J Clin Oncol, 1994. **12**(2): p. 360-7.

45. Cullen, M.H., et al., *Mitomycin, ifosfamide, and cisplatin in unresectable non-small-cell lung cancer: effects on survival and quality of life.* J Clin Oncol, 1999. **17**(10): p. 3188-94.

46. Lee, E.Y. and W.J. Muller, *Oncogenes and tumor suppressor genes.* Cold Spring Harb Perspect Biol, 2010. **2**(10): p. a003236.

47. Kempf, E., et al., *KRAS oncogene in lung cancer: focus on molecularly driven clinical trials.* Eur Respir Rev, 2016. **25**(139): p. 71-6.

48. Jänne, P.A., et al., *Selumetinib plus docetaxel for KRAS-mutant advanced non-small-cell lung cancer: a randomised, multicentre, placebo-controlled, phase 2 study.* Lancet Oncol, 2013. **14**(1): p. 38-47.

49. Dingemans, A.M., et al., *A phase II study of sorafenib in patients with platinum-pretreated, advanced (Stage IIIb or IV) non-small cell lung cancer with a KRAS mutation.* Clin Cancer Res, 2013. **19**(3): p. 743-51.

50. Blumenschein, G.R., et al., *A randomized phase II study of the MEK1/MEK2 inhibitor trametinib (GSK1120212) compared with docetaxel in KRAS-mutant advanced non-small-cell lung cancer (NSCLC)†.* Ann Oncol, 2015. **26**(5): p. 894-901.

51. Sholl, L.M., *Biomarkers in lung adenocarcinoma: a decade of progress.* Arch Pathol Lab Med, 2015. **139**(4): p. 469-80.

52. Ying, M., et al., *KRAS Mutation as a Biomarker for Survival in Patients with Non-Small Cell Lung Cancer, A Meta-Analysis of 12 Randomized Trials.* Asian Pac J Cancer Prev, 2015. **16**(10): p. 4439-45.

53. Pao, W., et al., *KRAS mutations and primary resistance of lung adenocarcinomas to gefitinib or erlotinib.* PLoS Med, 2005. **2**(1): p. e17.

54. Fujimoto, J. and I.I. Wistuba, *Current concepts on the molecular pathology of non-small cell lung carcinoma.* Semin Diagn Pathol, 2014. **31**(4): p. 306-13.

55. Mok, T.S., *Personalized medicine in lung cancer: what we need to know.* Nat Rev Clin Oncol, 2011. **8**(11): p. 661-8.

56. Shaw, A.T., et al., *Clinical features and outcome of patients with non-small-cell lung cancer who harbor EML4-ALK.* J Clin Oncol, 2009. **27**(26): p. 4247-53.

57. Solomon, B.J., et al., *First-line crizotinib versus chemotherapy in ALK-positive lung cancer.* N Engl J Med, 2014. **371**(23): p. 2167-77.

58. Choi, Y.L., et al., *EML4-ALK mutations in lung cancer that confer resistance to ALK inhibitors.* N Engl J Med, 2010. **363**(18): p. 1734-9.

59. Sasaki, T., et al., *The neuroblastoma-associated F1174L ALK mutation causes resistance to an ALK kinase inhibitor in ALK-translocated cancers.* Cancer Res, 2010. **70**(24): p. 10038-43.

60. Sullivan, I. and D. Planchard, *ALK inhibitors in non-small cell lung cancer: the latest evidence and developments.* Ther Adv Med Oncol, 2016. **8**(1): p. 32-47.

61. Cardarella, S., et al., *Clinical, pathologic, and biologic features associated with BRAF mutations in non-small cell lung cancer.* Clin Cancer Res, 2013. **19**(16): p. 4532-40.

62. Planchard, D., et al., *Dabrafenib in patients with BRAF(V600E)-positive advanced non-small-cell lung cancer: a single-arm, multicentre, open-label, phase 2 trial.* Lancet Oncol, 2016. **17**(5): p. 642-50.

63. Hyman, D.M., et al., *Vemurafenib in Multiple Nonmelanoma Cancers with BRAF V600 Mutations.* N Engl J Med, 2015. **373**(8): p. 726-36.

64. Hill, R., et al., *Targeting nucleocytoplasmic transport in cancer therapy.* Oncotarget, 2014. **5**(1): p. 11-28.

65. Karlsson, A., et al., *Mutational and gene fusion analyses of primary large cell and large cell neuroendocrine lung cancer.* Oncotarget, 2015. **6**(26): p. 22028-37.

66. Barbie, D.A., L.A. Conlan, and B.K. Kennedy, *Nuclear tumor suppressors in space and time.* Trends Cell Biol, 2005. **15**(7): p. 378-85.

67. Ogawara, K., et al., *Allelic loss of chromosome 13q14.3 in human oral cancer: correlation with lymph node metastasis.* Int J Cancer, 1998. **79**(4): p. 312-7.

68. Sanchez-Cespedes, M., et al., *Inactivation of LKB1/STK11 is a common event in adenocarcinomas of the lung.* Cancer Res, 2002. **62**(13): p. 3659-62.

69. Hawley, S.A., et al., *Complexes between the LKB1 tumor suppressor, STRAD alpha/beta and MO25 alpha/beta are upstream kinases in the AMP-activated protein kinase cascade.* J Biol, 2003. **2**(4): p. 28.

70. Corradetti, M.N., et al., *Corrigendum: Regulation of the TSC pathway by LKB1: evidence of a molecular link between tuberous sclerosis complex and Peutz-Jeghers syndrome.* Genes Dev, 2019. **33**(7-8): p. 477.

71. Koh, H.J., et al., *Skeletal muscle-selective knockout of LKB1 increases insulin sensitivity, improves glucose homeostasis, and decreases TRB3.* Mol Cell Biol, 2006. **26**(22): p. 8217-27.

72. Shaw, R.J., et al., *The tumor suppressor LKB1 kinase directly activates AMP-activated kinase and regulates apoptosis in response to energy stress.* Proc Natl Acad Sci U S A, 2004. **101**(10): p. 3329-35.

73. Baker, S., et al., *A critical review of recent developments in radiotherapy for non-small cell lung cancer.* Radiat Oncol, 2016. **11**(1): p. 115.

74. Wei, S.C., C.R. Duffy, and J.P. Allison, *Fundamental Mechanisms of Immune Checkpoint Blockade Therapy.* Cancer Discov, 2018. **8**(9): p. 1069-1086.

75. Bardhan, K., T. Anagnostou, and V.A. Boussiotis, *The PD1:PD-L1/2 Pathway from Discovery to Clinical Implementation.* Front Immunol, 2016. **7**: p. 550.

76. Herbst, R.S., D. Morgensztern, and C. Boshoff, *The biology and management of non-small cell lung cancer.* Nature, 2018. **553**(7689): p. 446-454.

77. Lin, H., et al., *Host expression of PD-L1 determines efficacy of PD-L1 pathway blockade-mediated tumor regression.* J Clin Invest, 2018. **128**(4): p. 1708.

78. Poggio, M., et al., *Suppression of Exosomal PD-L1 Induces Systemic Anti-tumor Immunity and Memory.* Cell, 2019. **177**(2): p. 414-427.e13.

79. Parry, R.V., et al., *CTLA-4 and PD-1 receptors inhibit T-cell activation by distinct mechanisms.* Mol Cell Biol, 2005. **25**(21): p. 9543-53.

80. Vitaly Vasilevko 1, A.G., Mark J Holterman, Michael G Agadjanyan, *CD80 (B7-1) and CD86 (B7-2) are functionally equivalent in the initiation and maintenance of CD4+ T-cell proliferation after activation with suboptimal doses of PHA.* DNA AND CELL BIOLOGY. **21**.

81. Qureshi, O.S., et al., *Trans-endocytosis of CD80 and CD86: a molecular basis for the cell-extrinsic function of CTLA-4.* Science, 2011. **332**(6029): p. 600-3.

82. Kong, K.F., et al., *Protein kinase C-η controls CTLA-4-mediated regulatory T cell function.* Nat Immunol, 2014. **15**(5): p. 465-72.

83. Maruhashi, T., et al., *LAG-3 inhibits the activation of CD4.* Nat Immunol, 2018. **19**(12): p. 1415-1426.

84. E Baixeras , B.H., C Miossec , S Jitsukawa , M Martin , T Hercend , C Auffray , F Triebel , D Piatier-Tonneau, *Characterization of the lymphocyte activation gene 3-encoded protein. A new ligand for human leukocyte antigen class II antigens.* Journal of Experimental Medicine, 1992. **176**: p. 327-337.

85. Celis-Gutierrez, J., et al., *Quantitative Interactomics in Primary T Cells Provides a Rationale for Concomitant PD-1 and BTLA Coinhibitor Blockade in Cancer Immunotherapy.* Cell Rep, 2019. **27**(11): p. 3315-3330.e7.

86. Yu, X., et al., *The surface protein TIGIT suppresses T cell activation by promoting the generation of mature immunoregulatory dendritic cells.* Nat Immunol, 2009. **10**(1): p. 48-57.

87. Borghaei, H., et al., *Nivolumab versus Docetaxel in Advanced Nonsquamous Non-Small-Cell Lung Cancer.* N Engl J Med, 2015. **373**(17): p. 1627-39.

88. Brahmer, J., et al., *Nivolumab versus Docetaxel in Advanced Squamous-Cell Non-Small-Cell Lung Cancer.* N Engl J Med, 2015. **373**(2): p. 123-35.

89. Reck, M., et al., *Pembrolizumab versus Chemotherapy for PD-L1-Positive Non-Small-Cell Lung Cancer.* N Engl J Med, 2016. **375**(19): p. 1823-1833.

90. Socinski, M.A., et al., *Atezolizumab for First-Line Treatment of Metastatic Nonsquamous NSCLC.* N Engl J Med, 2018. **378**(24): p. 2288-2301.

91. Gandhi, L., et al., *Pembrolizumab plus Chemotherapy in Metastatic Non-Small-Cell Lung Cancer.* N Engl J Med, 2018. **378**(22): p. 2078-2092.

92. Chen, Q., T. Li, and W. Yue, *Drug response to PD-1/PD-L1 blockade: based on biomarkers.* Onco Targets Ther, 2018. **11**: p. 4673-4683.

93. Skoulidis, F., et al., *Mutations and PD-1 Inhibitor Resistance in.* Cancer Discov, 2018. **8**(7): p. 822-835.

94. Mazieres, J., et al., *Immune checkpoint inhibitors for patients with advanced lung cancer and oncogenic driver alterations: results from the IMMUNOTARGET registry.* Ann Oncol, 2019. **30**(8): p. 1321-1328.

95. Müller-Quernheim, U.C., et al., *Tumor-cell co-culture induced alternative activation of macrophages is modulated by interferons in vitro.* J Interferon Cytokine Res, 2012. **32**(4): p. 169-77.

96. Michael P Smith, H.Y., Adam Hurlstone, and Claudia Wellbrock*, *Differentiation of THP1 Cells into Macrophages for Transwell Coculture Assay with Melanoma Cells.* PMC Bio Protocals, 2015. **21**(5).

97. Shen, Z., et al., *Macrophage coculture enhanced invasion of gastric cancer cells via TGF-beta and BMP pathways.* Scand J Gastroenterol, 2013. **48**(4): p. 466-72.

98. Hanahan, D. and L.M. Coussens, *Accessories to the crime: functions of cells recruited to the tumor microenvironment.* Cancer Cell, 2012. **21**(3): p. 309-22.

99. Altorki, N.K., et al., *The lung microenvironment: an important regulator of tumour growth and metastasis.* Nat Rev Cancer, 2019. **19**(1): p. 9-31.

100. Balkwill, F.R., M. Capasso, and T. Hagemann, *The tumor microenvironment at a glance.* J Cell Sci, 2012. **125**(Pt 23): p. 5591-6.

101. Schneider, T., et al., *Non-small cell lung cancer induces an immunosuppressive phenotype of dendritic cells in tumor microenvironment by upregulating B7-H3.* J Thorac Oncol, 2011. **6**(7): p. 1162-8.

102. Dumitriu, I.E., et al., *Human dendritic cells produce TGF-beta 1 under the influence of lung carcinoma cells and prime the differentiation of CD4+CD25+Foxp3+ regulatory T cells.* J Immunol, 2009. **182**(5): p. 2795-807.

103. Erdogan, B. and D.J. Webb, *Cancer-associated fibroblasts modulate growth factor signaling and extracellular matrix remodeling to regulate tumor metastasis.* Biochem Soc Trans, 2017. **45**(1): p. 229-236.

104. Brittan, M., et al., *Bone marrow derivation of pericryptal myofibroblasts in the mouse and human small intestine and colon.* Gut, 2002. **50**(6): p. 752-7.

105. Spaeth, E.L., et al., *Mesenchymal stem cell transition to tumor-associated fibroblasts contributes to fibrovascular network expansion and tumor progression.* PLoS One, 2009. **4**(4): p. e4992.

106. Wu, X., et al., *IL-6 secreted by cancer-associated fibroblasts promotes epithelial-mesenchymal transition and metastasis of gastric cancer via JAK2/STAT3 signaling pathway.* Oncotarget, 2017. **8**(13): p. 20741-20750.

107. Fridman, W.H., et al., *The immune contexture in human tumours: impact on clinical outcome.* Nat Rev Cancer, 2012. **12**(4): p. 298-306.

108. Choi, H., et al., *Transcriptome analysis of individual stromal cell populations identifies stroma-tumor crosstalk in mouse lung cancer model.* Cell Rep, 2015. **10**(7): p. 1187-201.

109. Qin, Z., et al., *B cells inhibit induction of T cell-dependent tumor immunity.* Nat Med, 1998. **4**(5): p. 627-30.

110. Mauri, C. and A. Bosma, *Immune regulatory function of B cells.* Annu Rev Immunol, 2012. **30**: p. 221-41.

111. Nishida, N., et al., *Angiogenesis in cancer.* Vasc Health Risk Manag, 2006. **2**(3): p. 213-9.

112. Jeong, H., et al., *Tumor-Associated Macrophages Enhance Tumor Hypoxia and Aerobic Glycolysis.* Cancer Res, 2019. **79**(4): p. 795-806.

113. Wang, R., et al., *Tumor-associated macrophages provide a suitable microenvironment for non-small lung cancer invasion and progression.* Lung Cancer, 2011. **74**(2): p. 188-96.

114. Swartz, M.A. and A.W. Lund, *Lymphatic and interstitial flow in the tumour microenvironment: linking mechanobiology with immunity.* Nat Rev Cancer, 2012. **12**(3): p. 210-9.

115. Gao, D., et al., *Endothelial progenitor cells control the angiogenic switch in mouse lung metastasis.* Science, 2008. **319**(5860): p. 195-8.

116. Minami, T., et al., *The calcineurin-NFAT-angiopoietin-2 signaling axis in lung endothelium is critical for the establishment of lung metastases.* Cell Rep, 2013. **4**(4): p. 709-23.

117. Frantz, C., K.M. Stewart, and V.M. Weaver, *The extracellular matrix at a glance.* J Cell Sci, 2010. **123**(Pt 24): p. 4195-200.

118. Weigelt, B. and M.J. Bissell, *Unraveling the microenvironmental influences on the normal mammary gland and breast cancer.* Semin Cancer Biol, 2008. **18**(5): p. 311-21.

119. Edovitsky, E., et al., *Heparanase gene silencing, tumor invasiveness, angiogenesis, and metastasis.* J Natl Cancer Inst, 2004. **96**(16): p. 1219-30.

120. Lerner, I., et al., *Heparanase powers a chronic inflammatory circuit that promotes colitis-associated tumorigenesis in mice.* J Clin Invest, 2011. **121**(5): p. 1709-21.

121. Cheng, H., Z. Zheng, and T. Cheng, *New paradigms on hematopoietic stem cell differentiation.* Protein Cell, 2020. **11**(1): p. 34-44.

122. Palframan, R.T., et al., *Inflammatory chemokine transport and presentation in HEV: a remote control mechanism for monocyte recruitment to lymph nodes in inflamed tissues.* J Exp Med, 2001. **194**(9): p. 1361-73.

123. Wynn, T.A., A. Chawla, and J.W. Pollard, *Macrophage biology in development, homeostasis and disease.* Nature, 2013. **496**(7446): p. 445-55.

124. Jantsch, J., et al., *Macrophages in homeostatic immune function.* Front Physiol, 2014. **5**: p. 146.

125. Solinas, G., et al., *JNK1 in hematopoietically derived cells contributes to diet-induced inflammation and insulin resistance without affecting obesity.* Cell Metab, 2007. **6**(5): p. 386-97.

126. Krzyszczyk, P., et al., *The Role of Macrophages in Acute and Chronic Wound Healing and Interventions to Promote Pro-wound Healing Phenotypes.* Front Physiol, 2018. **9**: p. 419.

127. Falanga, V., *Wound healing and its impairment in the diabetic foot.* Lancet, 2005. **366**(9498): p. 1736-43.

128. Italiani, P. and D. Boraschi, *New Insights Into Tissue Macrophages: From Their Origin to the Development of Memory.* Immune Netw, 2015. **15**(4): p. 167-76.

129. Epelman, S., K.J. Lavine, and G.J. Randolph, *Origin and functions of tissue macrophages.* Immunity, 2014. **41**(1): p. 21-35.

130. Haldar, M. and K.M. Murphy, *Origin, development, and homeostasis of tissue-resident macrophages.* Immunol Rev, 2014. **262**(1): p. 25-35.

131. Arango Duque, G. and A. Descoteaux, *Macrophage cytokines: involvement in immunity and infectious diseases.* Front Immunol, 2014. **5**: p. 491.

132. Martinez, F.O. and S. Gordon, *The M1 and M2 paradigm of macrophage activation: time for reassessment.* F1000Prime Rep, 2014. **6**: p. 13.

133. Hu, X. and L.B. Ivashkiv, *Cross-regulation of signaling pathways by interferon-gamma: implications for immune responses and autoimmune diseases.* Immunity, 2009. **31**(4): p. 539-50.

134. Kayagaki, N., et al., *Noncanonical inflammasome activation by intracellular LPS independent of TLR4.* Science, 2013. **341**(6151): p. 1246-9.

135. Hagar, J.A., et al., *Cytoplasmic LPS activates caspase-11: implications in TLR4-independent endotoxic shock.* Science, 2013. **341**(6151): p. 1250-3.

136. Ravikumar, B., et al., *Mammalian macroautophagy at a glance.* J Cell Sci, 2009. **122**(Pt 11): p. 1707-11.

137. Brough, D. and N.J. Rothwell, *Caspase-1-dependent processing of pro-interleukin-1beta is cytosolic and precedes cell death.* J Cell Sci, 2007. **120**(Pt 5): p. 772-81.

138. Marty, V., et al., *ATP binding cassette transporter ABC1 is required for the release of interleukin-1beta by P2X7-stimulated and lipopolysaccharide-primed mouse Schwann cells.* Glia, 2005. **49**(4): p. 511-9.

139. Ben-Sasson, S.Z., et al., *IL-1 acts directly on CD4 T cells to enhance their antigen-driven expansion and differentiation.* Proc Natl Acad Sci U S A, 2009. **106**(17): p. 7119-24.

140. Carmi, Y., et al., *The role of macrophage-derived IL-1 in induction and maintenance of angiogenesis.* J Immunol, 2009. **183**(7): p. 4705-14.

141. Barkhausen, T., et al., *Selective blockade of interleukin-6 trans-signaling improves survival in a murine polymicrobial sepsis model.* Crit Care Med, 2011. **39**(6): p. 1407-13.

142. Hurst, S.M., et al., *Il-6 and its soluble receptor orchestrate a temporal switch in the pattern of leukocyte recruitment seen during acute inflammation.* Immunity, 2001. **14**(6): p. 705-14.

143. Scheller, J., et al., *The pro- and anti-inflammatory properties of the cytokine interleukin-6.* Biochim Biophys Acta, 2011. **1813**(5): p. 878-88.

144. Wilson, H.M., *SOCS Proteins in Macrophage Polarization and Function.* Front Immunol, 2014. **5**: p. 357.

145. Lang, R., et al., *SOCS3 regulates the plasticity of gp130 signaling.* Nat Immunol, 2003. **4**(6): p. 546-50.

146. Croker, B.A., et al., *SOCS3 negatively regulates IL-6 signaling in vivo.* Nat Immunol, 2003. **4**(6): p. 540-5.

147. Yasukawa, H., et al., *IL-6 induces an anti-inflammatory response in the absence of SOCS3 in macrophages.* Nat Immunol, 2003. **4**(6): p. 551-6.

148. Liu, X., et al., *SOCS3 promotes TLR4 response in macrophages by feedback inhibiting TGF-beta1/Smad3 signaling.* Mol Immunol, 2008. **45**(5): p. 1405-13.

149. Arnold, C.E., et al., *A critical role for suppressor of cytokine signalling 3 in promoting M1 macrophage activation and function in vitro and in vivo.* Immunology, 2014. **141**(1): p. 96-110.

150. Liu, Y., et al., *Unique expression of suppressor of cytokine signaling 3 is essential for classical macrophage activation in rodents in vitro and in vivo.* J Immunol, 2008. **180**(9): p. 6270-8.

151. Qin, H., et al., *Correction: SOCS3 Deficiency Promotes M1 Macrophage Polarization and Inflammation.* J Immunol, 2016. **197**(1): p. 387-9.

152. Vannini, F., K. Kashfi, and N. Nath, *The dual role of iNOS in cancer.* Redox Biol, 2015. **6**: p. 334-343.

153. Xue, Q., et al., *Regulation of iNOS on Immune Cells and Its Role in Diseases.* Int J Mol Sci, 2018. **19**(12).

154. Rodriguez, P.C., A.C. Ochoa, and A.A. Al-Khami, *Arginine Metabolism in Myeloid Cells Shapes Innate and Adaptive Immunity.* Front Immunol, 2017. **8**: p. 93.

155. Ignarro, L.J., et al., *Endothelium-derived relaxing factor produced and released from artery and vein is nitric oxide.* Proc Natl Acad Sci U S A, 1987. **84**(24): p. 9265-9.

156. Ignarro, L.J., C. Napoli, and J. Loscalzo, *Nitric oxide donors and cardiovascular agents modulating the bioactivity of nitric oxide: an overview.* Circ Res, 2002. **90**(1): p. 21-8.

157. Alderton, W.K., C.E. Cooper, and R.G. Knowles, *Nitric oxide synthases: structure, function and inhibition.* Biochem J, 2001. **357**(Pt 3): p. 593-615.

158. Liu, H., et al., *Redox-dependent transcriptional regulation.* Circ Res, 2005. **97**(10): p. 967-74.

159. Geller, D.A. and T.R. Billiar, *Molecular biology of nitric oxide synthases.* Cancer Metastasis Rev, 1998. **17**(1): p. 7-23.

160. Quinn, A.C., A.J. Petros, and P. Vallance, *Nitric oxide: an endogenous gas.* Br J Anaesth, 1995. **74**(4): p. 443-51.

161. Bogdan, C., *Nitric oxide and the immune response.* Nat Immunol, 2001. **2**(10): p. 907-16.

162. Rath, M., et al., *Metabolism via Arginase or Nitric Oxide Synthase: Two Competing Arginine Pathways in Macrophages.* Front Immunol, 2014. **5**: p. 532.

163. Bronte, V., et al., *L-arginine metabolism in myeloid cells controls T-lymphocyte functions.* Trends in Immunology, 2003. **24**(6): p. 301-305.

164. Ash, D.E., *Structure and Function of Arginases.* American Society for Nutritional Sciences, 2004.

165. Gray, M.J., et al., *Induction of arginase I transcription by IL-4 requires a composite DNA response element for STAT6 and C/EBPbeta.* Gene, 2005. **353**(1): p. 98-106.

166. Pauleau, A.L., et al., *Enhancer-mediated control of macrophage-specific arginase I expression.* J Immunol, 2004. **172**(12): p. 7565-73.

167. Vasquez-Dunddel, D., et al., *STAT3 regulates arginase-I in myeloid-derived suppressor cells from cancer patients.* J Clin Invest, 2013. **123**(4): p. 1580-9.

168. Rőszer, T., *Understanding the Mysterious M2 Macrophage through Activation Markers and Effector Mechanisms.* Mediators Inflamm, 2015. **2015**: p. 816460.

169. Yu, T., et al., *Modulation of M2 macrophage polarization by the crosstalk between Stat6 and Trim24.* Nat Commun, 2019. **10**(1): p. 4353.

170. Dupasquier, M., et al., *The dermal microenvironment induces the expression of the alternative activation marker CD301/mMGL in mononuclear phagocytes, independent of IL-4/IL-13 signaling.* J Leukoc Biol, 2006. **80**(4): p. 838-49.

171. Bellón, T., et al., *Alternative activation of macrophages in human peritoneum: implications for peritoneal fibrosis.* Nephrol Dial Transplant, 2011. **26**(9): p. 2995-3005.

172. Medbury, H.J., et al., *Differing association of macrophage subsets with atherosclerotic plaque stability.* Int Angiol, 2013. **32**(1): p. 74-84.

173. Stütz, A.M., et al., *The Th2 cell cytokines IL-4 and IL-13 regulate found in inflammatory zone 1/resistin-like molecule alpha gene expression by a STAT6 and CCAAT/enhancer-binding protein-dependent mechanism.* J Immunol, 2003. **170**(4): p. 1789-96.

174. Pesce, J.T., et al., *Retnla (relmalpha/fizz1) suppresses helminth-induced Th2-type immunity.* PLoS Pathog, 2009. **5**(4): p. e1000393.

175. Nair, M.G., et al., *Alternatively activated macrophage-derived RELM-{alpha} is a negative regulator of type 2 inflammation in the lung.* J Exp Med, 2009. **206**(4): p. 937-52.

176. Liu, T., et al., *Regulation of found in inflammatory zone 1 expression in bleomycin-induced lung fibrosis: role of IL-4/IL-13 and mediation via STAT-6.* J Immunol, 2004. **173**(5): p. 3425-31.

177. Raes, G., et al., *Arginase-1 and Ym1 are markers for murine, but not human, alternatively activated myeloid cells.* J Immunol, 2005. **174**(11): p. 6561; author reply 6561-2.

178. Raes, G., et al., *Differential expression of FIZZ1 and Ym1 in alternatively versus classically activated macrophages.* J Leukoc Biol, 2002. **71**(4): p. 597-602.

179. Welch, J.S., et al., *TH2 cytokines and allergic challenge induce Ym1 expression in macrophages by a STAT6-dependent mechanism.* J Biol Chem, 2002. **277**(45): p. 42821-9.

180. Arora, S., et al., *Role of IFN-gamma in regulating T2 immunity and the development of alternatively activated macrophages during allergic bronchopulmonary mycosis.* J Immunol, 2005. **174**(10): p. 6346-56.

181. Waern, I., et al., *Accumulation of Ym1 and formation of intracellular crystalline bodies in alveolar macrophages lacking heparanase.* Mol Immunol, 2010. **47**(7-8): p. 1467-75.

182. Osborne, L.C., et al., *Coinfection. Virus-helminth coinfection reveals a microbiota-independent mechanism of immunomodulation.* Science, 2014. **345**(6196): p. 578-82.

183. de Sousa, J.R., P.F. Da Costa Vasconcelos, and J.A.S. Quaresma, *Functional aspects, phenotypic heterogeneity, and tissue immune response of macrophages in infectious diseases.* Infect Drug Resist, 2019. **12**: p. 2589-2611.

184. Wang, L.X., et al., *M2b macrophage polarization and its roles in diseases.* J Leukoc Biol, 2019. **106**(2): p. 345-358.

185. Curren Smith, E.W., *Macrophage Polarization and Its Role in Cancer.* Journal of Clinical & Cellular Immunology, 2015. **06**(04).

186. Derlindati, E., et al., *Transcriptomic analysis of human polarized macrophages: more than one role of alternative activation?* PLoS One, 2015. **10**(3): p. e0119751.

187. Mantovani, A., et al., *The chemokine system in diverse forms of macrophage activation and polarization.* Trends Immunol, 2004. **25**(12): p. 677-86.

188. Colin, S., G. Chinetti-Gbaguidi, and B. Staels, *Macrophage phenotypes in atherosclerosis.* Immunol Rev, 2014. **262**(1): p. 153-66.

189. De Paoli, F., B. Staels, and G. Chinetti-Gbaguidi, *Macrophage phenotypes and their modulation in atherosclerosis.* Circ J, 2014. **78**(8): p. 1775-81.

190. Wynn, T.A. and K.M. Vannella, *Macrophages in Tissue Repair, Regeneration, and Fibrosis.* Immunity, 2016. **44**(3): p. 450-462.

191. Chanmee, T., et al., *Tumor-associated macrophages as major players in the tumor microenvironment.* Cancers (Basel), 2014. **6**(3): p. 1670-90.

192. Mosser, D.M. and J.P. Edwards, *Exploring the full spectrum of macrophage activation.* Nat Rev Immunol, 2008. **8**(12): p. 958-69.

193. Yue, Y., et al., *Corrigendum to "M2b macrophages reduce early reperfusion injury after myocardial ischemia in mice: A predominant role of inhibiting apoptosis via A20" [Int. J. Cardiol. 245 (2017) 228-235].* Int J Cardiol, 2019. **278**: p. 311.

194. Lu, J., et al., *Discrete functions of M2a and M2c macrophage subsets determine their relative efficacy in treating chronic kidney disease.* Kidney Int, 2013. **84**(4): p. 745-55.

195. Martinez, F.O., et al., *Macrophage activation and polarization.* Front Biosci, 2008. **13**: p. 453-61.

196. Shapouri-Moghaddam, A., et al., *Macrophage plasticity, polarization, and function in health and disease.* J Cell Physiol, 2018. **233**(9): p. 6425-6440.

197. Lurier, E.B., et al., *Transcriptome analysis of IL-10-stimulated (M2c) macrophages by next-generation sequencing.* Immunobiology, 2017. **222**(7): p. 847-856.

198. Cortez-Retamozo, V., et al., *Origins of tumor-associated macrophages and neutrophils.* Proc Natl Acad Sci U S A, 2012. **109**(7): p. 2491-6.

199. West, R.B., et al., *A landscape effect in tenosynovial giant-cell tumor from activation of CSF1 expression by a translocation in a minority of tumor cells.* Proc Natl Acad Sci U S A, 2006. **103**(3): p. 690-5.

200. Ramirez, R.D., et al., *Immortalization of Human Bronchial Epithelial Cells in the Absence of Viral Oncoproteins.* Cancer Research, 2004. **64**: p. 9027-9034.

201. Gazdar, A.F., et al., *Lung Cancer Cell Lines as Tools for Biomedical Discovery and Research.* JNCI: Journal of the National Cancer Institute, 2010. **102**(17): p. 1310-1321.

202. Trouplin, V., et al., *Bone marrow-derived macrophage production.* Journal of visualized experiments : JoVE, 2013(81): p. e50966-e50966.

203. Banat, G.A., et al., *Immune and Inflammatory Cell Composition of Human Lung Cancer Stroma.* PLoS One, 2015. **10**(9): p. e0139073.

204. Kim, J., et al., *XPO1-dependent nuclear export is a druggable vulnerability in KRAS-mutant lung cancer.* Nature, 2016. **538**(7623): p. 114-117.

205. Zilionis, R., et al., *Single-Cell Transcriptomics of Human and Mouse Lung Cancers Reveals Conserved Myeloid Populations across Individuals and Species.* Immunity, 2019. **50**(5): p. 1317-1334.e10.

206. Poczobutt, J.M., et al., *Expression Profiling of Macrophages Reveals Multiple Populations with Distinct Biological Roles in an Immunocompetent Orthotopic Model of Lung Cancer.* J Immunol, 2016. **196**(6): p. 2847-59.

207. Mould, K.J., et al., *Single cell RNA sequencing identifies unique inflammatory airspace macrophage subsets.* JCI Insight, 2019. **4**(5).

208. Gensel, J.C., et al., *Predictive screening of M1 and M2 macrophages reveals the immunomodulatory effectiveness of post spinal cord injury azithromycin treatment.* Sci Rep, 2017. **7**: p. 40144.

209. Jablonski, K.A., et al., *Novel Markers to Delineate Murine M1 and M2 Macrophages.* PLoS One, 2015. **10**(12): p. e0145342.

210. Ji, X., et al., *Cancer-associated fibroblasts from NSCLC promote the radioresistance in lung cancer cell lines.* Int J Clin Exp Med, 2015. **8**(5): p. 7002-8.

211. Depke, M., et al., *Bone marrow-derived macrophages from BALB/c and C57BL/6 mice fundamentally differ in their respiratory chain complex proteins, lysosomal enzymes and components of antioxidant stress systems.* Journal of Proteomics, 2014. **103**: p. 72-86.

212. Huang, H. and R.A. Brekken, *Recent advances in understanding cancer-associated fibroblasts in pancreatic cancer.* Am J Physiol Cell Physiol, 2020. **319**(2): p. C233-C243.

213. Newman, A.M., et al., *Determining cell type abundance and expression from bulk tissues with digital cytometry.* Nat Biotechnol, 2019. **37**(7): p. 773-782.

214. Gazdar, A.F. and J.D. Minna, *NCI series of cell lines: an historical perspective.* J Cell Biochem Suppl, 1996. **24**: p. 1-11.

215. Ye, Y., et al., *Sex-associated molecular differences for cancer immunotherapy.* Nat Commun, 2020. **11**(1): p. 1779.

216. Abdou, Y., et al., *Racial differences in CD8(+) T cell infiltration in breast tumors from Black and White women.* Breast Cancer Res, 2020. **22**(1): p. 62.

217. Busch, S.E., et al., *Lung Cancer Subtypes Generate Unique Immune Responses.* J Immunol, 2016. **197**(11): p. 4493-4503.

218. Danaher, P., et al., *Pan-cancer adaptive immune resistance as defined by the Tumor Inflammation Signature (TIS): results from The Cancer Genome Atlas (TCGA).* Journal for ImmunoTherapy of Cancer, 2018. **6**(1).

219. Schwitalla, S., et al., *Loss of p53 in enterocytes generates an inflammatory microenvironment enabling invasion and lymph node metastasis of carcinogen-induced colorectal tumors.* Cancer Cell, 2013. **23**(1): p. 93-106.

220. Cooks, T., et al., *Mutant p53 prolongs NF-κB activation and promotes chronic inflammation and inflammation-associated colorectal cancer.* Cancer Cell, 2013. **23**(5): p. 634-46.

221. Koyama, S., et al., *STK11/LKB1 Deficiency Promotes Neutrophil Recruitment and Proinflammatory Cytokine Production to Suppress T-cell Activity in the Lung Tumor Microenvironment.* Cancer Res, 2016. **76**(5): p. 999-1008.

222. Casey, S.C., et al., *MYC regulates the antitumor immune response through CD47 and PD-L1.* Science, 2016. **352**(6282): p. 227-31.

223. Sato, M., et al., *Multiple oncogenic changes (K-RAS(V12), p53 knockdown, mutant EGFRs, p16 bypass, telomerase) are not sufficient to confer a full malignant phenotype on human bronchial epithelial cells.* Cancer Res, 2006. **66**(4): p. 2116-28.

224. Sato, M., et al., *Human lung epithelial cells progressed to malignancy through specific oncogenic manipulations.* Mol Cancer Res, 2013. **11**(6): p. 638-50.

225. Vayrynen, J.P., et al., *The Prognostic Role of Macrophage Polarization in the Colorectal Cancer Microenvironment.* Cancer Immunol Res, 2021. **9**(1): p. 8-19.

226. Vayrynen, S.A., et al., *Composition, Spatial Characteristics, and Prognostic Significance of Myeloid Cell Infiltration in Pancreatic Cancer.* Clin Cancer Res, 2021. **27**(4): p. 1069-1081.

227. Autieri, M.V., *IL-19 and Other IL-20 Family Member Cytokines in Vascular Inflammatory Diseases.* Front Immunol, 2018. **9**: p. 700.

228. Weng, S.Y., et al., *IL-4 Receptor Alpha Signaling through Macrophages Differentially Regulates Liver Fibrosis Progression and Reversal.* EBioMedicine, 2018. **29**: p. 92-103.

229. Andreas Kaufmann, R.S., * Diethard Gemsa,* and Hans Sprenger, *Increase of CCR1 and CCR5 expression and enhancedfunctional response to MIP-1 ⎵ during differentiation ofhuman monocytes to macrophages.* Journal of Leukocyte Biology, 2001. **69**.

230. Wong, M. and E.N. Fish, *RANTES and MIP-1α Activate Stats in T Cells.* Journal of Biological Chemistry, 1998. **273**(1): p. 309-314.

231. Lee, M.M., et al., *CCR1-mediated STAT3 tyrosine phosphorylation and CXCL8 expression in THP-1 macrophage-like cells involve pertussis toxin-insensitive Galpha(14/16) signaling and IL-6 release.* J Immunol, 2012. **189**(11): p. 5266-76.

232. Edukulla, R., et al., *Th2 Cytokines Augment IL-31/IL-31RA Interactions via STAT6-dependent IL-31RA Expression.* J Biol Chem, 2015. **290**(21): p. 13510-20.

233. Leonard, W.J., J.X. Lin, and J.J. O'Shea, *The gammac Family of Cytokines: Basic Biology to Therapeutic Ramifications.* Immunity, 2019. **50**(4): p. 832-850.

234. Burgess, M., et al., *Cx3CR1 Expression Identifies Distinct Macrophage Populations That Contribute Differentially to Inflammation and Repair.* ImmunoHorizons, 2019. **3**(7): p. 262-273.

235. Kaya, B., et al., *Lysophosphatidic Acid-Mediated GPR35 Signaling in CX3CR1+ Macrophages Regulates Intestinal Homeostasis.* Cell Reports, 2020. **32**(5).

236. Boniakowski, A.E., et al., *Murine macrophage chemokine receptor CCR2 plays a crucial role in macrophage recruitment and regulated inflammation in wound healing.* Eur J Immunol, 2018. **48**(9): p. 1445-1455.

237. Rama, D., G. Esendagli, and D. Guc, *Expression of chemokine-like receptor 1 (CMKLR1) on J744A.1 macrophages co-cultured with fibroblast and/or tumor cells: modeling the influence of microenvironment.* Cell Immunol, 2011. **271**(1): p. 134-40.

238. Braune, J., et al., *IL-6 Regulates M2 Polarization and Local Proliferation of Adipose Tissue Macrophages in Obesity.* J Immunol, 2017. **198**(7): p. 2927-2934.

239. Li, A., et al., *IL-8 directly enhanced endothelial cell survival, proliferation, and matrix metalloproteinases production and regulated angiogenesis.* J Immunol, 2003. **170**(6): p. 3369-76.

240. Rodriguez, P.C., et al., *Arginase I production in the tumor microenvironment by mature myeloid cells inhibits T-cell receptor expression and antigen-specific T-cell responses.* Cancer Res, 2004. **64**(16): p. 5839-49.

241. Fujimoto, H., et al., *Stromal MCP-1 in mammary tumors induces tumor-associated macrophage infiltration and contributes to tumor progression.* Int J Cancer, 2009. **125**(6): p. 1276-84.

242. Negus, R.P., et al., *The detection and localization of monocyte chemoattractant protein-1 (MCP-1) in human ovarian cancer.* J Clin Invest, 1995. **95**(5): p. 2391-6.

243. Byers, L.A., et al., *An epithelial-mesenchymal transition gene signature predicts resistance to EGFR and PI3K inhibitors and identifies Axl as a therapeutic target for overcoming EGFR inhibitor resistance.* Clin Cancer Res, 2013. **19**(1): p. 279-90.

244. Liu, C.-Y., et al., *Vimentin contributes to epithelial-mesenchymal transition cancer cell mechanics by mediating cytoskeletal organization and focal adhesion maturation.* Oncotarget, 2015. **6**(18): p. 15966-15983.

245. Micalizzi, D.S. and H.L. Ford, *Epithelial-mesenchymal transition in development and cancer.* Future Oncol, 2009. **5**(8): p. 1129-43.

246. Wang, Y. and B.P. Zhou, *Epithelial-mesenchymal Transition---A Hallmark of Breast Cancer Metastasis.* Cancer Hallm, 2013. **1**(1): p. 38-49.

247. Berrondo, C., et al., *Expression of the Long Non-Coding RNA HOTAIR Correlates with Disease Progression in Bladder Cancer and Is Contained in Bladder Cancer Patient Urinary Exosomes.* PLoS One, 2016. **11**(1): p. e0147236.

248. De Craene, B. and G. Berx, *Regulatory networks defining EMT during cancer initiation and progression.* Nat Rev Cancer, 2013. **13**(2): p. 97-110.

249. Yao, D., C. Dai, and S. Peng, *Mechanism of the mesenchymal-epithelial transition and its relationship with metastatic tumor formation.* Mol Cancer Res, 2011. **9**(12): p. 1608-20.

250. Tsai, J.H. and J. Yang, *Epithelial-mesenchymal plasticity in carcinoma metastasis.* Genes Dev, 2013. **27**(20): p. 2192-206.

251. Jing, L., et al., *Sema4C mediates EMT inducing chemotherapeutic resistance of miR-31-3p in cervical cancer cells.* Sci Rep, 2019. **9**(1): p. 17727.

252. Shi, Y., et al., *SMAD3 inducing the transcription of STYK1 to promote the EMT process and improve the tolerance of ovarian carcinoma cells to paclitaxel.* J Cell Biochem, 2019. **120**(6): p. 10796-10811.

253. Sale, M.J., et al., *MEK1/2 inhibitor withdrawal reverses acquired resistance driven by BRAF(V600E) amplification whereas KRAS(G13D) amplification promotes EMT-chemoresistance.* Nat Commun, 2019. **10**(1): p. 2030.

254. Labelle, M., S. Begum, and R.O. Hynes, *Direct signaling between platelets and cancer cells induces an epithelial-mesenchymal-like transition and promotes metastasis.* Cancer Cell, 2011. **20**(5): p. 576-90.

255. Bonde, A.K., et al., *Intratumoral macrophages contribute to epithelial-mesenchymal transition in solid tumors.* BMC Cancer, 2012. **12**: p. 35.

256. Zhang, W., et al., *Small cell lung cancer tumors and preclinical models display heterogeneity of neuroendocrine phenotypes.* Translational lung cancer research, 2018. **7**(1): p. 32-49.

257. Cao, L., et al., *M2 macrophage infiltration into tumor islets leads to poor prognosis in non-small-cell lung cancer.* Cancer Manag Res, 2019. **11**: p. 6125-6138.

258. Sumitomo, R., et al., *M2 tumor-associated macrophages promote tumor progression in non-small-cell lung cancer.* Exp Ther Med, 2019. **18**(6): p. 4490-4498.

259. Choi, S.H., et al., *Inhibition of NADPH oxidase promotes alternative and anti-inflammatory microglial activation during neuroinflammation.* J Neurochem, 2012. **120**(2): p. 292-301.

260. Petty, A.J. and Y. Yang, *Tumor-associated macrophages: implications in cancer immunotherapy.* Immunotherapy, 2017. **9**(3): p. 289-302.

261. Pathria, P., T.L. Louis, and J.A. Varner, *Targeting Tumor-Associated Macrophages in Cancer.* Trends Immunol, 2019. **40**(4): p. 310-327.

262. Wanderley, C.W., et al., *Paclitaxel Reduces Tumor Growth by Reprogramming Tumor-Associated Macrophages to an M1 Profile in a TLR4-Dependent Manner.* Cancer Res, 2018. **78**(20): p. 5891-5900.

263. Huang, L., H. Xu, and G. Peng, *TLR-mediated metabolic reprogramming in the tumor microenvironment: potential novel strategies for cancer immunotherapy.* Cell Mol Immunol, 2018. **15**(5): p. 428-437.

264. Lattimer, J., et al., *Retention and biodistribution of Sn-117m colloid in intra-articular injections.* Journal of Nuclear Medicine, 2016. **57**: p. 322-322.

265. Yuan, A., et al., *Opposite Effects of M1 and M2 Macrophage Subtypes on Lung Cancer Progression.* Sci Rep, 2015. **5**: p. 14273.

266. Sukkurwala, A.Q., et al., *Screening of novel immunogenic cell death inducers within the NCI Mechanistic Diversity Set.* Oncoimmunology, 2014. **3**: p. e28473.

267. McMillan, E.A., et al., *Chemistry-First Approach for Nomination of Personalized Treatment in Lung Cancer.* Cell, 2018. **173**(4): p. 864-878.e29.

268. Miret, J.J., et al., *Suppression of Myeloid Cell Arginase Activity leads to Therapeutic Response in a NSCLC Mouse Model by Activating Anti-Tumor Immunity.* Journal for ImmunoTherapy of Cancer, 2019. **7**(1): p. 32.

269. Huang, K., et al., *Glabridin Prevents Doxorubicin-Induced Cardiotoxicity Through Gut Microbiota Modulation and Colonic Macrophage Polarization in Mice.* Front Pharmacol, 2019. **10**: p. 107.